Stimulus-secretion coupling in L cells and factors affecting secretion of glucagon-like peptide 1



Małgorzata Cyranka

St. Catherine's College

University of Oxford

A thesis submitted for the degree of Doctor of Philosophy
to the Department of Physiology, Anatomy and Genetics, University of Oxford
Hilary Term 2023

Abstract

Glucagon-like peptide 1 (GLP-1) is a hormone released from gut endocrine L cells in response to the arrival of nutrients and plays an important role in regulating glucose homeostasis. However, factors and pathways modulating the stimulus-secretion coupling of GLP-1 are not fully understood. Our group previously reported a significant increase in GLP-1 plasma levels from an *Abcc5* knockout (*Abcc5*$^{-/-}$) mouse model, but the mechanism responsible for this effect remains unknown. Additionally, *Abcc5*$^{-/-}$ mice generated by other groups have reported an accumulation of various glutamate-conjugated compounds in the brain and other tissues, which could be responsible for driving the altered metabolic phenotype of the *Abcc5*$^{-/-}$ mice and also potentially affecting their behaviour.

In this study, we first characterised the neurobehavioural phenotype of mice lacking the *Abcc5* gene. We showed that *Abcc5*$^{-/-}$ mice displayed a neurobehavioural phenotype consistent with disruption of glutamatergic signalling such as increased startle reactivity, loss of pre-pulse inhibition, and a decreased conditioned fear response. Further electrophysiological evidence implicates that glutamate-gated ion channels, NMDA receptors, might be responsible for the neurobehavioural phenotype of the *Abcc5*$^{-/-}$ mice. We showed that inhibition of NMDA receptors in an L cell model cell line, GLUTag cells, by various methods resulted in a significant increase in the release of GLP-1.

Since native L cells are exposed to different pH conditions alongside the digestive tract, the effect of extracellular pH on GLP-1 secretion was also investigated using GLUTag and primary L cells. Stimulated release of GLP-1 was found to be pH sensitive and an extracellular acidic pH inhibited GLP-1 release in a proton concentration-dependent manner. The mechanism of pH-regulated GLP-1 secretion was explored further to identify the point of proton entry into the cell and possible proton targets within the cell. Importantly, the pH-dependent release of

GLP-1 in response to stimulation occurred irrespective of extracellular sodium levels, while chloride and calcium ions prove to be pivotal for GLP-1 secretion. Furthermore, while the production and processing of GLP-1 remained unaffected by an extracellular acidic pH, exocytosis of GLP-1 was inhibited and significantly more secretory granules containing active GLP-1 were shown to be retained intracellularly. Overall, results from this study showed that the activity of peripheral NMDA receptors expressed in L cells and the modulatory effect of extracellular pH plays an important role in the stimulus-secretion coupling of GLP-1 in response to nutrients. These findings provide new target possibilities to stimulate endogenous secretion of GLP-1, a much sought-after therapeutic strategy, for the treatment of obesity and diabetes.

Declaration of Authentication

The work presented in this thesis was performed under the supervision of Professor Heidi de Wet and Professor Lisa Heather, Department of Physiology, Anatomy and Genetics, Division of Medical Sciences, University of Oxford. This work is wholly my own, and any contribution to the thesis made by others has been acknowledged. The work submitted here does not form part of another thesis in this or any other university.

Małgorzata Cyranka,
December 2022

Acknowledgements

I am eternally grateful to my supervisor, Prof Heidi de Wet, for allowing me to take on this DPhil project and providing me with guidance, support, advice, and encouragement. I am also extremely grateful to my co-supervisor Prof Lisa Heather for the constructive feedback and for reviewing my thesis chapters.

I would like also to express my deepest gratitude to dr Natascia Vedovato (Tasha) for sharing her knowledge and experience, for always being available and advising on the experiments, for long scientific discussions and brain-storming about the results, and help in completing the work, but more than anything, for being a friend in the lab and outside. I'm truly thankful to dr Chelsea Larabee and dr Elizabeth Haythorne (Lizzie) for very insightful and invaluable feedback on my thesis chapters. Special thanks are in order to Lizzie for her great sense of humour, encouragement, and moral support near the end of my DPhil, which helped me to complete this thesis.

I am also grateful to all members of DPAG and de Wet group, past and present, for their continuous assistance and support, and for creating a friendly and welcome environment, especially to Jess Abele, dr Nelisa Tebeka, dr Rula Bany Bakar and dr Anna Veprik.

Finally, this thesis would not have been completed without the help and support from my parents and my dearest partner, dr Weiheng Su, who patiently look after our son Max while I was writing and was also an infinite source of encouragement and strength, challenging me to complete this work.

I dedicate this work to Max, my beloved son, who was born into this scientific journey, grew up with it and bravely endured it by my side. Hopefully, he can finally stop asking 'are you a doctor now?'.

Z dedykacją dla mojego kochanego syna, Maksia, który od urodzienia towarzyszył mi w tej naukowej podróży, dzielnie trwał przy mnie i rozwijał się razem z tym projektem. Teraz może już przestać pytać 'czy jesteś już doktorem?'.

Table of Contents

List of Abbreviations 1
Chapter 1: General Introduction 3
1.1 ABCC5, an ATP-binding cassette transporter from superfamily C 3
1.2 Expression patterns of ABCC5 5
1.3 ABCC5 physiological substrates in lower animal models 6
1.4 Substrates of ABCC5 transporter in mammals – *ex vivo* studies 8
1.4.1 *Abcc5* knock-out mouse model and transport studies 9
1.4.2 ABCC5 as multidrug resistance protein 5 (MRP5) 10
1.5 Metabolic phenotype of *Abcc5* knock-out mice – recent studies 10
1.5.1 Potential role of NAAG in driving *Abcc5* knock-out mice phenotype 12
1.6 Thesis overview 15
1.7 Aims of the study 18
Chapter 2: Methods 19
2.1 Generation of *Abcc5* knock-out mice (*Abcc5*$^{-/-}$) 19
2.2 Mice husbandry 19
2.3 Acoustic startle and pre-pulse inhibition (PPI) 20
2.4 Fear conditioning 21
2.5 Marble burying assay 23
2.6 Grip strength 23
2.7 Open field 24
2.8 Y-maze 25
2.9 Cell culture of GLUTag cells 26
2.10 Coating tissue culture dishes with Matrigel™ 28
2.11 Heat-inactivation of FBS 28
2.12 Glucagon-like peptide 1 (GLP-1) secretion experiments 28
2.13 Protein sample preparation and quantification 31
2.14 Glucagon-like peptide 1 (GLP-1) detection 32
2.15 SDS-PAGE and western blot 32
2.16 Reverse transcription (RT) and quantitative polymerase chain reaction (qPCR) 34
2.17 Murine primary small intestinal cultures – isolation and growth 35

2.18 siRNA knock-down of NMDAR (*Grin1)* in GLUTag cells 37
2.19 Secretory granules (SG) isolation from GLUTag cells 37
2.20 RNA sequencing of L cell model cell lines – GLUTag cells 41
2.21 Immunofluorescence 41
2.22 Statistical analysis 42
Chapter 3: Neurobehavioural phenotype of *Abcc5*$^{-/-}$ knockout (KO) mice 44
3.1 Introduction 44
3.1.1 Gene function studies on a mouse model 44
3.1.2 Behavioural phenotyping of mouse model 45
3.1.3 PPI as a neurological biomarker 45
3.1.4 Acoustic Startle Response (ASR) 46
3.1.5 Neuronal circuits driving ASR 47
3.1.6 ASR – methodological considerations 48
3.1.7 Pre-pulse inhibition (PPI) – modification of the ASR 49
3.1.8 PPI neuronal circuit 50
3.1.9 Receptors involved in PPI 51
3.1.10 Methodological caveats of measuring PPI in mice 52
3.1.11 Definition of fear 54
3.1.12 Fear conditioning – method 54
3.1.13 Anatomy of fear 55
3.1.14 Receptors involved in fear 56
3.1.15 *Abcc5* knockout mouse model 57
3.2 Results 60
3.2.1 *Abcc5*$^{-/-}$ mice have higher acoustic startle reactivity 60
3.2.2 *Abcc5* knockout mice display loss of pre-pulse inhibition 62
3.2.3 No gradient reactivity in *Abcc5*$^{-/-}$ mice to pre-pulse sound levels alone 65
3.2.4 *Abcc5*$^{-/-}$ mice display abnormal marble burying distribution patterns 66
3.2.5 *Abcc5*$^{-/-}$ mice retain learning ability in fear conditioning trial 68
3.2.6 Knock-out of *Abcc5* gene does not affect contextual fear 69
3.2.7 *Abcc5* gene plays a role in the expression of acquired fear in auditory-cued test ... 71
3.2.8 No change in grip strength 74
3.2.9 Absence of *Abcc5* has no effect in open field locomotor activity 75
3.2.10 *Abcc5*$^{-/-}$ females display enhanced exploratory behaviour in Y-maze assay 78
3.2.11 *Abcc5*$^{-/-}$ mice behavioural phenotype is driven by NMDA receptor transmission 80

3.3 Discussion 82
3.3.1 Locomotor activity is not affected by *Abcc5 k*nockout in Open field test 82
3.3.2 *Abcc5 k*nockout phenotype is not anxiety-related 82
3.3.3 Increased amplitude of ASR 83
3.3.4 Loss of PPI 84
3.3.5 Pre-pulse facilitation (PPF) 87
3.3.6 Fear Conditioning 88
3.3.7 Contextual fear 88
3.3.8 Auditory-cued fear expression 88
3.3.9 Mouse strain differences 90
3.4 Summary 91
Chapter 4: Role of NMDA receptor in GLP-1 secretion 92
4.1 Introduction 92
4.1.1 Gut as an endocrine organ 92
4.1.2 L cell – definition and distribution *in vivo* 94
4.1.3 Transcriptome profile of L cells 94
4.1.4 Experimental models for GLP-1 secretion studies 97
4.1.5 GLP-1 as an incretin – clinical relevance 98
4.1.6 Active GLP-1 in therapy of diabetes 99
4.1.7 Stimulus-secretion coupling of GLP-1 secretion 100
4.1.8 Glucose stimulated GLP-1 release 102
4.1.9 Role of neurotransmitters in stimulus-secretion coupling of GLP-1 secretion 104
4.1.10 Role of glutamate in GLP-1 secretion 105
4.1.11 Glutamate receptors 106
4.1.12 NMDA receptors 107
4.1.13 Peripheral tissues – role of NMDAR 108
4.2 Results 110
4.2.1 Expression of *Grin1* encoding GluN1 in primary small intestinal cell cultures of *Abcc5*$^{-/-}$ and wild-type mice 110
4.2.2 The NMDA receptor blocker MK-801 does not affect glucose-stimulated GLP-1 release from primary L cells 112
4.2.3 Expression of NMDA receptor subunits in GLUTag cells 114
4.2.4 The NMDA receptor blocker MK-801 does not affect glucose-stimulated GLP-1 release from GLUTag cells 115

4.2.5 siRNA knock-down of *Grin1* in GLUTag cells 117
4.2.6 Downregulation of NMDAR *Grin1* subunit expression in GLUTag cells increased glucose-stimulated GLP-1 secretion 118
4.2.7 NMDA receptor blocker MK-801 increases GLP-1 secretion in GLUTag cells stimulated with glycine and glutamate 119
4.2.8 Competitive NMDAR antagonist – D-AP5 showed no effect on GLP-1 secretion 121
4.3 Discussion 123
4.3.1 NMDAR expression in L cells 123
4.3.2 NMDAR inhibition 123
4.3.3 Different NMDAR antagonists 125
4.4 Summary 128
Chapter 5: Regulation of GLP-1 secretion by pH 129
5.1 Introduction 129
5.1.1 Secretion of gut hormones known to be affected by pH 129
5.1.2 pH profile of the gut 129
5.1.3 pH in the gut is disrupted in the pathology of obesity, diabetes and after bariatric surgery 131
5.1.4 pH-dependence of stimulus-secretion coupling in pancreatic β-cells 133
5.1.5 Exocytosis of GLP-1 134
5.1.6 Regulation of intracellular pH 136
5.1.7 Production of GLP-1 is pH-sensitive 138
5.1.8 Role of chloride in GLP-1 secretion from L cells 140
5.1.9 Glucose-sensing in L cells – the role of sodium ions 141
5.3 Results 143
5.3.1 Low pH does not affect the readout of the HTRF ELISA signal 143
5.3.2 Extracellular pH affects GLP-1 secretion 144
5.3.3 Acidic extracellular pH inhibits GLP-1 secretion primary L cell cultures 147
5.3.4 Decreased GLP-1 secretion in acidic pH is not caused by accelerated degradation of GLP-1 at low pH_o 149
5.3.5 Inhibition of V-ATPase proton pump mimics the effect of low pH_o on GLP-1 release 151
5.3.6 Acidity-induced inhibition of GLP-1 secretion occurs rapidly and is reversible 154
5.3.7 The role of calcium in the pH dependence of GLP-1 secretion 156

5.3.8 pH-sensitive GLP-1 secretion is independent of extracellular sodium levels 159
5.3.9 The role of chloride in the pH_o effect on GLP-1 secretion 163
5.3.10 Production of GLP-1 is not affected by pH_o 167
5.3.11 Acidic pH_o causes higher GLP-1 retention within the secretory granules 168
5.3.12 PC1/3 expression is not changed at acidic pH_o 171
5.4 Discussion 174
5.4.1 The effect of pH on GLP-1 secretion is not caused by the degradation of the hormone after release 174
5.4.2 The role of intracellular acidification in the regulation of GLP-1 exocytosis 175
5.4.3 The effect of pH on GLP-1 secretion is independent of glucose sensing 177
5.4.4 The role of calcium in pH-dependence of GLP-1 release remains unexplored 178
5.4.5 Extracellular chloride is essential for GLP-1 exocytosis 179
5.4.6 Expression and autocleavage of PC1/3 181
5.4.7 Acidic pH affects exocytotic machinery as more GLP-1 is retained in secretory granules at low pH 182
5.4 Summary 183
Chapter 6: Conclusions and future perspectives 185
Bibliography 189

List of Abbreviations

ABC	ATP-binding cassette transporter
AMPA	α-amino-3-hydroxy-5-methyl-4-isoxazole propionic acid
ASR	Acoustic startle response
ATP	Adenosine triphosphate
AUC	Area under the curve
BCA	Bicinchoninic acid assay
BCG	β-citrylglutamic acid
BSA	Bovine serum albumin (BSA)
cAMP	Cyclic adenosine monophosphate
CFTR	Cystic fibrosis transmembrane conductance regulator
cGMP	Cyclic guanosine monophosphate
CS	Conditioned stimulus
D-AP5	D-2-amino-5-phosphonopentanoate
DMEM	Dulbecco's Modified Eagle Medium
DPBS	Dulbecco's Phosphate-Buffered Saline (DPBS)
ECL	Enhanced chemiluminescence
EEC	Enteroendocrine cell
ELISA	Enzyme-linked immunosorbent assay
ENS	Enteric nervous system
FC	Fear conditioning
Fsk	Forskolin
FVB	Friend virus B-type
GI	Gastrointestinal
GISIS	Glucose-stimulated insulin secretion
Glc	Glucose
GLP-1	Glucagon-like peptide 1 (GLP-1)
HTRF	Homogeneous Time Resolved Fluorescence (HTRF)
i.v.	Intravenous
KO	Knockout
MRP	Multidrug resistance protein

MTX	Methotrexate
NAA	N-acetylaspartate
NAAG	N-acetylaspartylglutamate
NBD	Nucleotide-Binding Domain
NMDA	N-methyl-D-aspartic acid
NMDG	N-methyl-D-glucamine
OGTT	Oral glucose tolerance test
pH_i	Intracellular pH
pH_o	Extracellular pH
PIC	Protease Inhibitor Cocktail (PIC)
PPI	Pre-pulse inhibition
ROCK	Rho Kinase
SG	Secretory Granules
SNARE	Soluble N-ethylmaleimide-Sensitive Factor Attachment Proteins receptor
T2D	Type 2 Diabetes
US	Unconditioned Stimulus

Chapter 1: General Introduction

1.1 ABCC5, an ATP-binding cassette transporter from superfamily C

Type 2 diabetes (T2D) is a chronic, metabolic disease characterized by elevated blood glucose levels. Its development is primarily caused by a combination of two main factors: defective insulin secretion from pancreatic β-cells and the inability of insulin-sensitive tissues to respond to insulin [1]. T2D poses a serious public health problem. As it affects globally 462 million Statistical forecasting predicts that the prevalence of diabetes will increase on average from 6058 cases to 7862 per 100,000 by 2040 [2].

ABCC5 is an ATP-binding cassette transporter (ABC), member 5 of superfamily C of membrane transporters that has been linked to diabetes in humans by a genome-wide association study (GWAS) [3]. Upregulated expression of ABCC5 in subcutaneous adipose tissue was associated with reduced peripheral insulin sensitivity in nondiabetic individuals, increased visceral fat accumulation and a threefold increased risk of developing T2D with age [3]. The role of ABCC5 in diabetes and obesity remains unexplored, however studies on *Abcc5* knock-out mice model revealed that ABCC5 transporter plays a role in energy metabolism in mammals. *Abcc5*$^{-/-}$ mice show lower white and brown adipose tissue depots and increased GLP-1 release [4].

At present, there is no crystal structure for the ABCC5 protein. However, since genes for ABC transporters are highly conserved, ABC transporters are classified based on the sequence and organisation of their ATP-binding domains [5]. All members of the ABCC superfamily are structurally related and contain a common intracellular nucleotide-binding domain (NBD) motif that allows them to bind and hydrolyse ATP to mediate transport activity. The functional

protein also contains transmembrane domain(s) (TMD) that contribute to the substrate specificity, translocation and release of substrates [6-8].

ABCC5 is a large transmembrane protein (~190kDa) that contains two transmembrane domains (TMD1 and TMD2), each consisting of six membrane-spanning helices, with each TMD having an intracellular nucleotide-binding domain (NBD1 and NBD2, respectively) (Fig 1.1). The NBDs contain characteristic Walker A and Walker B motifs with the upstream signature C motif element [5].

Though structurally related, ABCC transporters fulfil many diverse functions such as regulation of insulin release from pancreatic β-cells by the ATP-sensitive potassium ion channel (K_{ATP}) that contains the regulatory subunit of sulfonylurea receptor SUR1 (ABCC8) [9], the conductance of chloride ions across epithelial membranes by cystic fibrosis transmembrane conductance regulator (CFTR, ABCC7) [10], transport of prostaglandin E2 by ABCC4 [11], chemoresistance of cancer cells and export of organic anions and drugs mediated by ABCC1 [12] or ABCC3 [13]. The physiological role of ABCC5 remains to be fully elucidated, but the evidence from our laboratory supports the genetic finding that ABCC5 may play a role in the pathophysiology of diabetes and obesity [4].

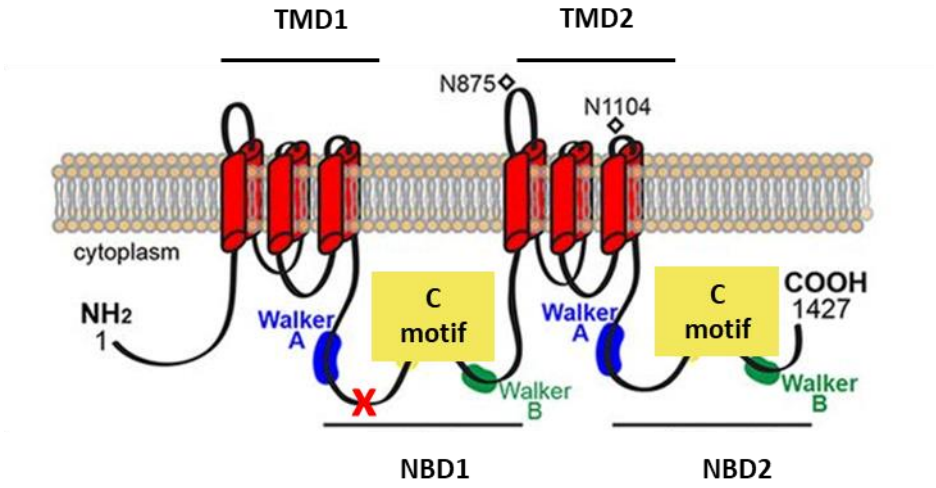


Figure 1.1 ATP-binding cassette transporter, ABCC5.

Topological overview of ABCC5 protein showing two transmembrane domains (TMD1 and TMD2) with their corresponding nucleotide-binding domains (NBD1 and NBD2). Adapted from [14]. The red cross is showing where the genetic disruption occurs in *Abcc5*$^{-/-}$ mice on C57BL/6N background reported in this dissertation.

1.2 Expression patterns of ABCC5

ABCC5 mRNA is ubiquitously expressed in all tissues of human origin with high expression scores in the brain, gastrointestinal (GI) tract, muscle, and heart [15, 16]. ABCC5 protein was detected by immunostaining in cardiovascular endothelium and smooth muscle cells [15], within the human placenta, and in and around foetal blood vessels [17]. Variable levels of ABCC5 protein were also detected in healthy human and mouse erythrocytes [18]. In rats, the brain, heart and skeletal muscles also show high expression of ABCC5 protein [19]. ABCC5 was found also to be highly expressed in the human brain, where it is mainly present in pyramidal neurons and astrocytes [20], but also in capillary endothelial cells [21]. There is also additional evidence of cell-specific enrichment within particular tissues, i.e. in the GI tract of the mouse, transcription of the mouse *Abcc5* gene is higher in the enteroendocrine cells (EECs) of the small intestine as compared to their non-endocrine neighbours [4]. Human *ABCC5* gene expression was also reported in adipose tissue, where its overexpression was found to confer a higher risk of developing type 2 diabetes [3].

The cellular localisation of ABCC5 within mammalian cells has been widely reported to be in the outer plasma membrane [19, 20, 22], but it was also found present in intracellular vesicles [4, 23]. Recombinant expression of human ABCC5 in mouse embryonic fibroblasts was shown to co-localise with Golgi and endosomal recycling organelles [24]. Most recently, natively expressed ABCC5 in mice testes was also shown to co-localise with the mitochondria-

associated membrane (MAM) markers, but was not present in purified mitochondrial fractions [22].

In *C. elegans* GFP-tagged expression of ABCC5 was shown to target the basolateral membrane of polarised intestinal cells, but also the intracellular compartments of intestinal cells where sorting of the vesicles occurs [24]. Basolateral location of ABCC5 was also found in polarised human intestinal cells of the jejunum [25] and syncytiotrophoblasts of pre-term human placenta [17], as well as *in vitro* in polarised Madin–Darby canine kidney II (MDCKII) cells transfected with ABCC5 [23].

The ambiguous reports of cellular localization may be due to the unreliable ABCC5 antibodies that are commercially available. This is likely due to sequence homology between ABC proteins. Additionally, multiple reports would use the same polyclonal anti-ABCC5 antibody (reviewed in [26, 27]) or monoclonal anti-ABCC5 (anti-MRP5 monoclonal antibody (mAb), NKI-12C5) [28]. None of these antibodies are commercially available and only limited validation studies exist for human and mice samples [18]. Currently, there is no conclusive, well-controlled evidence of the localization of ABCC5 protein expression in the literature.

1.3 ABCC5 physiological substrates in lower animal models

In addition to unclear cellular localisation of the ABCC5 protein, the physiological role of the ABCC5 transporter also largely remains a mystery. Studies in sea urchins provided evidence that ABCC5 is required for cAMP-mediated hindgut formation in sea urchin embryos [14]. The expression of ABCC5 here was shown to be time-dependent concerning the development of the sea urchins' digestive system. The waves of cAMP have been shown to appear together with increased expression of ABCC5 and preceding the body axis formation and invagination of the hindgut in these sea animals [14]. Despite some *ex vivo* evidence of ABCC5 indeed

transporting cyclic nucleotides (cAMP/cGMP), the physiological relevance of cyclic nucleotide transport by ABCC5 has not been confirmed in higher animals as yet [27].

Another physiologically relevant substrate of ABCC5 that has been reported is heme [24]. A study in *C. elegans* revealed that ABCC5 is pivotal for the development of the roundworm that when fed with RNAi against abcc5 shows no major developmental defects in the first generation, but 80% of the first generation (F1) offspring eggs failed to hatch, and those that did hatch failed to develop further past stage larvae 1 [24]. The lethal embryonic phenotype was found to be rescued by the addition of 500µM of exogenous heme into the growth media. Various *C. elegans* mutants for ABCC5 proved that fluorescent heme analogues enter the intestine and accumulate there, but the lack of functional ABCC5 makes that pool of heme inaccessible for other tissues [24]. Since intestinal ABCC5 expression proved to play a crucial role in heme homeostasis in *C. elegans,* Korolnek *et al.* used a vertebrate model of zebrafish to investigate this putative role of ABCC5 further. Genetic depletion of ABCC5 caused a significant reduction in red blood cell formation, followed by anaemia and heart enlargement in zebrafish, suggesting ABCC5 is also crucial for successful erythropoiesis in higher-order animals [24]. However, the exact mechanism of heme transport by ABCC5 remains unknown. In a different study using zebrafish embryos, an inactive ABCC5 transporter was overexpressed in addition to endogenous ABCC5 expression. Overexpression of inactive ABCC5 transporter caused developmental retardation of zebrafish embryos, which showed smaller eyes and heads and an overall reduction of body length and pigmentation. Zebrafish embryos overexpressing inactive ABCC5 display also increased cellular cGMP content and upregulated expression of Cyclin-dependent kinase inhibitor 1 (p21), signalling of which is known to mediate cell cycle arrest. Mechanistically it was suggested that ABCC5 plays a role in the embryonic development of zebrafish via association with cell cycle arrest but not apoptosis, and the

regulation of the cell cycle arrest is affected by the imbalance in cellular cGMP levels caused by overexpression of inactive ABCC5 [29].

1.4 Substrates of ABCC5 transporter in mammals – *ex vivo* studies

Although it is clear that ABCC5 plays an important role in the development of sea urchins and zebrafish, the role of ABCC5 in mammals is less clear, as *Abcc5*$^{-/-}$ mice show a mild phenotype, and have improved metabolic health [4]. To complicate matters, as previously discussed, it is ABCC5 overexpression which is associated with human pathology [3]. In mammals, ABC transporters are exporters and hydrolyses ATP to extrude substrates. There are multiple reports of potential ABCC5 substrates in mammalian cells [24, 27, 30, 31]. Generally, the fluorescent dye uptake assays suggest that ABCC5 in human embryonic kidney (HEK) cells exhibits a higher transport capacity for organic anions, with the notion that the increase in size or number of aromatic rings as well as a more positive charge results in decreased efflux [19]. Jedlitschky *et al*. reported cyclic nucleotides as native substrates of ABCC5. The function of the ABCC5 transporter as a cAMP and cGMP exporter was confirmed in *in vitro* transport assays using inside-out vesicles isolated from hamster fibroblasts transiently expressing human ABCC5 transporter, and assays returned very convincing Km values for cAMP (K_m = 379 µM) and cGMP (K_m = 2.1µM) [27]. An ATP-dependent transport of cGMP in human heart sarcolemma natively expressing ABCC5 has also been indirectly attributed to ABCC5 [15]. However, erythrocytes isolated from the first model of *Abcc5*$^{-/-}$ whole-body knock-out mice show no difference in cGMP transport between knockout samples and wild-type controls again suggesting that the role of ABCC5 in the murine model might be different to humans [18]. The role of ABCC5 in heme homeostasis was suggested by studies that used mouse embryonic fibroblasts generated from wild-type and *Abcc5*$^{-/-}$ mice. Fibroblast cultures from *Abcc5*$^{-/-}$ mice upon re-introduction of heme into the growth media showed diminished heme-dependent

horseradish peroxidase (HRP) activity when compared to wild-type cultures which managed to utilise heme [24].

1.4.1 *Abcc5* knock-out mouse model and transport studies

The first *Abcc5*$^{-/-}$ mouse model was established in 2007 using embryonic stem (ES) cell technology, and the homozygous mice were backcrossed to 100% Friend virus B-type (FVB) genetic background [18]. These mice were reported to accumulate several metabolic compounds in various tissues [31]. Notably, most of the accumulated metabolites were very similar structurally, containing glutamate or aspartate moieties at the C-terminal, and the highest fold changes presented in the whole brain of the *Abcc5*$^{-/-}$ mice. The potential *in vivo* substrates of ABCC5 included an endogenous neurotransmitter N-acetylaspartylglutamate (NAAG) [32] and its polyglutamated form $NAAG_2$ with an unknown physiological role [33], as well as β-citrylglutamic acid (BCG) shown to act as an iron carrier for mitochondrial aconitase in developing brains [34]. Vesicular transport assays confirmed that the inside-out membrane vesicles from HEK293 cells overexpressing ABCC5 can successfully efflux NAAG, $NAAG_2$ and the NAAG precursor N-acetylaspartate (NAA), as well as compounds with glutamate or aspartate moiety, i.e. NMDA or kainic acid [31]. The ATP-dependent transport by *ex vivo* vesicular ABCC5 expression has been also confirmed for NAAG with Km values of 3.5mM. However, the *in vitro* assays measuring the efflux into the media from whole-cell cultured HEK293 cells overexpressing ABCC5 showed only BCG, its analogue BCG_2 and NAA to be exported by ABCC5, but not NAAG [31]. These conflicting results between native vesicular and recombinant whole-cell transport assays could stem from the differential expression of ABCC5. As mentioned above, cellular localisation of ABCC5 was reported in both, plasma membrane and intracellular compartments.

1.4.2 ABCC5 as multidrug resistance protein 5 (MRP5)

There is also some evidence implicating the role of ABCC5 in the resistance to the chemotherapeutics used in cancer therapy, specifically antifolates [30, 35] and nucleotide analogues [23]. Interestingly, polyglutamated forms of methotrexate (MTX, 4-amino, 10-methyl pteroyl glutamic acid) showed higher transport rates by ABCC5 and lower cellular retention in cells overexpressing ABCC5. Also, the inhibition of cell growth by Raltitrexed, a drug that requires polyglutamylation to be fully active, was hampered in cells overexpressing ABCC5 (IC_{50} = 62nM versus IC_{50} = 7nM in control cells) [35]. However, there was no enhanced ABCC5-related resistance observed to the cytotoxic agents with a different mechanism of action such as cisplatin, daunomycin or vincristine that do not require polyglutamylation [19]. It would appear that the process of polyglutamylation is a common factor associated with the ABCC5 function. While overexpression of ABCC5 increases the efflux of glutamylated and polyglutamylated drugs, lack of ABCC5 decreases the efflux of these compounds causing the accumulation of glutamylated and polyglutamylated endogenous metabolites as shown in *Abcc5*$^{-/-}$ mice brains [31].

1.5 Metabolic phenotype of *Abcc5* knock-out mice – recent studies

Identified substrates of ABCC5 are well-defined physiological substrates of secondary messenger systems, such as cAMP/cGMP [27], neurotransmission (NAAG) and iron-dependent aconitase activation (BCG) [31]. Yet, the relevance of ABCC5 transporter involving these substrates remains elusive. Generation of the first model of homozygous *Abcc5*$^{-/-}$ mice on an FVB background returns no obvious phenotype [18]. Mice were viable and fertile, with no spontaneous differences observed in their behaviour [31]. The hint for the physiological role of ABCC5 in humans came from Direk *et. al*. who reported that increased expression of *ABCC5* in subcutaneous adipose tissue correlates with a higher risk of developing type 2 diabetes in

European and African American populations [3]. The role of the ABCC5 transporter in mammalian metabolism has been confirmed by our group in a newly generated CRISPR/Cas9 whole-body knockout (KO) model of *Abcc5*$^{-/-}$ mice on C57BL/6N background [4]. Our *Abcc5*$^{-/-}$ (*Abcc5* KO) mice are also healthy, viable and fertile, and show no symptoms of iron deficiency or anaemia by standard blood morphology markers. Work from our group showed that *Abcc5*$^{-/-}$ mice, both females and males, display a lean metabolic phenotype. The *Abcc5*$^{-/-}$ mice weighed less than wild-types and had lower visceral fat mass depots. They also display a higher level of general locomotor activity over 24hr period and are more insulin sensitive. A possible mechanism explaining the observed metabolic phenotype of *Abcc5*$^{-/-}$ mice was linked to the role of ABCC5 transporter in regulating incretin hormone secretion, namely glucagon-like peptide 1 (GLP-1) from enteroendocrine L cells in the gut. The increase of GLP-1 secretion in *Abcc5*$^{-/-}$ mice is possibly regulated by one of the ABCC5 substrates, the neurotransmitter, NAAG [4]. The exact mechanism and target receptor of NAAG in gut endocrine L cells, however, remains unknown (Fig. 1.2).

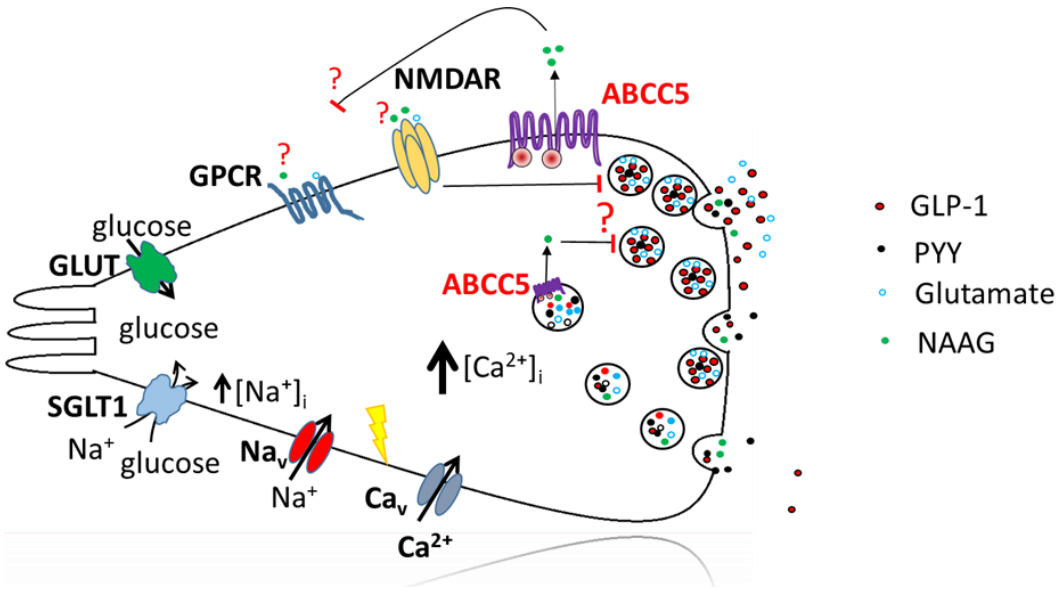


Figure 1.2 Schematic overview of an L cell.

L cell diagram showing the transporters (SGLT1) known to be involved in glucose-stimulated GLP-1 release. Marked in red is a possible role of ABCC5 via its glutamate analogue substrate(s), i.e. NAAG (green dot), acting through unknown target receptors or vesicular targets to inhibit GLP-1 secretion.

1.5.1 Potential role of NAAG in driving *Abcc5* knock-out mice phenotype

NAAG is enzymatically synthetized by NAAG synthases from NAA and glutamate [33]. The role of NAAG is best characterised within the central nervous system, where NAAG is the most abundant neuropeptide with a concentration *in vivo* in human brains ranging between 0.6-2.7mM, albeit region-dependent [32, 36]. Extracellularly, NAAG is hydrolysed by the NAAG peptidase (encoded by *FOLH1*) to release NAA and glutamate. NAAG peptidase is a membrane glycoprotein that, depending on the tissue expression, is known as GCPII (Glutamate carboxypeptidase II) in the brain, FOLH1 (folate hydrolase 1) in the small intestine or PSMA (prostate-specific membrane antigen) in the prostate [37]. Several studies suggested that NAAG plays a neuroprotective role in various neurological and psychiatric diseases such as epilepsy, schizophrenia or stroke [38]. Increased levels of NAAG resulting from the inhibition of GCPII were shown to be neuroprotective in traumatic brain injury [39]. NAAG has also been implicated in the pathophysiology of neurodegenerative diseases like Alzheimer's. Brain areas affected by Alzheimer's disease were shown to have lower NAAG levels in Alzheimer's patients compared to healthy controls [40]. Mechanistically, the neuroprotective properties of NAAG were attributed to the activation of metabotropic glutamate receptor 3 (mGluR3) [41]. NAAG was reported to be a highly selective agonist of the mGluR3 [42]. mGluR3 is a G-protein coupled receptor that primarily inhibits the glutamate release from presynaptic neurons [43]. Thus, the main physiological role of NAAG in the brain is to attenuate the excitotoxicity caused by excessive glutamate transmission. The proposed model of NAAG action assumes NAAG is released into the synaptic cleft from post-synaptic

neuron in the process mediated by activation of ionotropic glutamate receptors such as AMPA (α-amino-3-hydroxy-5-methyl-4-isoxazole propionic acid) or NMDA (N-methyl-D-aspartate) receptors. From there, NAAG activates mGluR3 and reduces the further release of glutamate (Fig 1.3) [38].

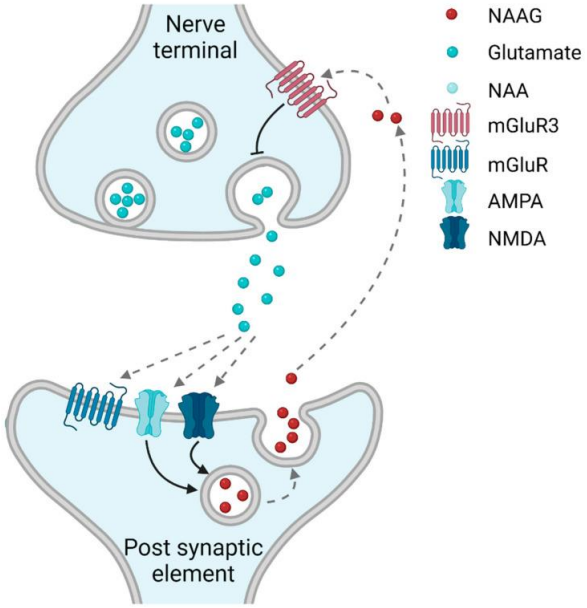


Fig 1.3 NAAG modulates glutamatergic signalling via mGluR3 activation. Adapted from [38].

The release of NAAG from neuronal cells was reported to occur in a Ca^{2+}-dependent manner from synaptic vesicles following membrane depolarisation [44]. The intracellular storage of NAAG in synaptic vesicles was reported to be mediated by sialin transporter SLC17A5 and occurs in an ATP-dependent manner [45]. Synaptic vesicles isolated from sialin-deficient mice were shown to be unable to perform the vesicular transport of NAAG and its glutamylated form $NAAG_2$, suggesting that in the brains of sialin-deficient mice, NAAG will be retained within the cytosol of the neuronal cell. Surprisingly, the total brain levels of NAAG in sialin-deficient mice were lower (rather than higher) when compared with control wild-type mice. The mRNA

encoding GCP-II expression on the other hand was increased two-fold [45]. The authors concluded that increased degradation of NAAG by GCP-II cannot be excluded, but it is unlikely to be the cause of lower NAAG levels in the brains of these mice. Firstly, without vesicular transport of NAAG by the sialin transporter into synaptic vesicles, there will be no NAAG released for GCP-II to degrade. And secondly, increased GCP-II gene expression does not necessarily translate into higher enzymatic activity. These data, therefore, indicate that SLC17A5 may not directly transport NAAG, but it mediates transport of NAAG in some way. Interestingly, Jansen et al. suggested that NAAG can be also constitutively released from the neuronal cells by the ABCC5 transporter, which would also occur in an ATP-dependent manner [31]. Unlike the sialin-deficient mice, brains from Abcc5-deficient mice display higher total levels of NAAG. Currently, there are no reports about the expression levels or enzymatic activity of GCP-II in the brains of *Abcc5*$^{-/-}$ mice.

mGluR3 is a confirmed receptor target for NAAG in the brain, but NAAG was also reported to bind to glutamate-gated ion channels, NMDA receptors, but with much lower affinity when compared to mGluR3 [46]. The effect of NAAG on NMDA receptors is also more complicated, as there are contradictory reports on whether NAAG functions as an agonist [47, 48] or an antagonist of NMDAR activity [49]. The effect of NAAG on the NMDA receptor was shown to be dependent on the subunit composition of the receptor, pH of the tissue or glycine presence [49, 50]. Thus, it has been suggested that the agonistic or antagonistic effect that NAAG has on NMDA receptors is a part of NAAG's neuromodulatory role in responding to glutamate levels within the synapse. NAAG was shown to have no effect on other ionotropic glutamate receptors, namely kainate (KA) or AMPA receptors [47, 49].

1.6 Thesis overview

Genetic ablation of Abcc5 transporter expression in an *Abcc5* knockout mouse model (FVB/N-*Abcc5*$^{-/-}$) generated in 2007 caused a 2.7-fold increase in NAAG abundance in FVB/N-*Abcc5*$^{-/-}$ mouse brains [31]. The notable accumulation of NAAG and other glutamate-conjugates in the brains of these *Abcc5*$^{-/-}$ mice was predicted to alter glutamatergic signalling in neurons and affect FVB/N-*Abcc5*$^{-/-}$ mice behaviour. Despite that suggestion, no obvious neurological or behavioural phenotype associated with FVB/N-*Abcc5*$^{-/-}$ mice were reported [31]. In this study, a new *Abcc5* knockout mouse model (C57BL/6N-*Abcc5*$^{-/-}$), generated by CRISPR/Cas9 technology, was used to perform detailed neurobehavioural phenotyping of *Abcc5*$^{-/-}$ mice.

Chapter 3 is dedicated to characterising the extent of behavioural changes mediated by the disruption of *Abcc5* expression using standardised neurobehavioural phenotyping tests, such as pre-pulse inhibition (PPI) and fear conditioning (FC). These tests rely on established behavioural paradigms and are used as a robust measure of altered neuronal circuits. Additionally, the general level of locomotor function and cognitive abilities were examined by standard tests such as open field and Y-maze. *Abcc5*$^{-/-}$ mice were found to display a clear neurobehavioural phenotype marked by increased startle reactivity, loss of PPI and decreased conditioned fear response to an auditory cue. These results are also consistent with disruption of the glutamatergic signalling in *Abcc5*$^{-/-}$ mice, which is further supported by electrophysiological results implicating an ionotropic glutamate-gated ion channel, NMDA receptor, as a potential target receptor affected by *Abcc5* knockout.

The role of the NMDA receptor in the stimulus-secretion coupling of glucagon-like peptide 1 (GLP-1) from gut L cells has not previously been explored. However, it has been reported that C57BL/6N-*Abcc5*$^{-/-}$ mice display a metabolic phenotype marked by increased GLP-1 levels measured *in vivo* in plasma and *in vitro* from primary intestinal cultures [4]. Therefore, in Chapter 4, a model L cell line called GLUTag cells, as well as primary intestinal cultures were

utilised to address the role of signalling through NMDAR in GLP-1 release. Expression of the GluN1 mandatory subunit of the NMDA receptor was found in GLUTag cells, but not in mixed primary intestinal cell cultures. The pharmacological approach to investigate the function of NMDAR showed that blocking these receptors does not affect GLP-1 release in response to glucose in GLUTag cells or primary intestinal cultures. However, the modulatory effect of NMDAR inhibition on GLP-1 release was unmasked in GLUTag cells in the presence of the NMDAR ligands glutamate and glycine. Blocking NMDAR with the non-competitive antagonist MK-801 in the presence of glutamate and glycine increased the secretion of GLP-1. This was also recapitulated by a genetic approach where *Grin1* (encoding GluN1) was knocked down. These results showed that the activity of peripheral NMDAR expressed in L cells might play a direct role in stimulus-secretion coupling of GLP-1 to nutrients and open a new possibility for targeting glutamate receptors to stimulate endogenous secretion of GLP-1, which is a very much sought-after therapeutic strategy to tackle obesity and diabetes.

L cell distribution profile varies throughout the gut with the highest density of L cells and GLP-1 hormone production observed in the distal part of the gastrointestinal (GI) tract. The pH profile of the gut lumen varies along the GI tract [51]. Alterations of the physiological pH profile of the GI tract were reported in multiple pathophysiological conditions. Notably, people with obesity and at risk of type 2 diabetes were shown to have lower luminal pH in the small intestine than non-obese individuals [52]. Therefore, it is plausible that changes in the extracellular pH may affect the secretory function of L cells. Chapter 5 is focused on characterizing the effect of altering the extracellular pH on GLP-1 secretion from L cells using the GLUTag model cell line and primary intestinal cell cultures. The main finding is that lowering the extracellular pH decreases GLP-1 secretion in a proton concentration-dependent manner. The mechanism of pH-regulated GLP-1 secretion was explored further to identify the point of proton entry into the cell and possible proton targets within the cell. By altering buffer

composition during secretion experiments, the potential of different ions being involved in proton transport into GLUTag cells was investigated. The effect of pH on the production and processing of GLP-1 was also measured, including the effect of pH on the expression and processing of the enzyme, prohormone convertase 1/3 (PC1/3), involved in GLP-1 production. Finally, the GLP-1 secretory granules and their content upon stimulated exocytosis at different pH conditions were examined. The mechanism by which extracellular pH regulates GLP-1 secretion does not seem to involve the production or availability of active GLP-1, as secretory granules from cells incubated at acidic pH contained high amounts of active GLP-1. It is therefore possible that low pH inhibits the final stages of GLP-1 exocytosis, causing increased retention of GLP-1-filled granules within the cell.

1.7 Aims of the study

Chapter 3: To investigate possible altered cognitive function of Abcc5 ko mouse.

Chapter 4: To ascertain if the NMDA receptor activity plays a role in stimulus-secretion coupling of GLP-1 secretion from L cells using a model cell line of murine L cells, GLUTag cells, and primary intestinal cultures.

Chapter 5: To investigate the role of extracellular pH in modulating stimulus-secretion coupling of GLP-1 release from L cells in *in vitro* model.

Chapter 2: Methods

2.1 Generation of *Abcc5* knock-out mice (*Abcc5*$^{-/-}$)

Abcc5 knock-out mice (*Abcc5*$^{-/-}$) line was generated by CRISPR/Cas9 technology using a C57BL/6NTac mouse strain at Mary Lyon Centre, MRC Harwell, UK, as a part of the genetic screening programme of the International Mice Phenotyping Consortium (IMPC). The knock-out of an *Abcc5* allele was obtained by the deletion of 372 nucleotides within exon 13, encoding for the cytosolic part of nucleotide-binding domain 1 (NBD1). The heterozygous mice for ABCC5-DEL372-EM1-B6N-IC were subsequently backcrossed to generate the *Abcc5*$^{-/-}$ mice and wild-type littermate controls.

2.2 Mice husbandry

All animal procedures were performed at the Mary Lyon Centre (MLC), MRC, Harwell, UK. All regulated procedures on mice were performed according to the Animals (Scientific Procedures) Act (ASPA), Home Office, UK, under Project Licence No 30/3206. Each experimental procedure on mice was conducted following the appropriate testing protocol as per Standard Operating Procedure (SOP), MLC, Harwell, UK [53].

Animals were housed separated by genotype and sex, in groups of at least 3 mice per cage (unless specified otherwise). Mice were kept in individually ventilated cages (IVC, Techniplast, London, UK) of a size W391 x D199 x H160 mm, filled with sterilised aspen wood bedding and enrichment in the form of paper shavings and cardboard tunnels. Mice were kept under the light/dark cycle (unless specified otherwise) 12:12 hours with lights on at 7.00 am with free access to water (10ppm chlorine) and food (Special Diet Services, Rat and Mouse

No.3 Breeding diet (RM3) containing 3.36g% fat, 22.45g% protein and 71.21g% carbohydrates). Room temperature was 21±2°C, humidity 55%±10%.

Each experimental procedure *in vivo* was performed using the number of mice as indicated within each test. Mice were divided into groups by sex (females/males) and by genotype (wild-type/knock-out) and split between three experimental pipelines. Data from each pipeline were collected independently. The optimal cohort sample size of ~15-20 mice per group has been estimated by MRC, Harwell, UK. GraphPad StatMate module was used to carry out power calculations using similar cohort phenotyping data and to determine sample size in an unpaired t-test using the trait standard deviation and a significance level of p=0.05 and a power of 95%. The effect size was estimated using real data examples corresponding to each particular trait by MRC, Harwell, UK.

2.3 Acoustic startle and pre-pulse inhibition (PPI)

Abcc5$^{-/-}$ mice (n=15 females and n=15 males) and their wild-type littermate controls (n=17 females and n=13 males) were tested for startle and pre-pulse noise inhibition response at 15 weeks of age using the Pre-Pulse Inhibition test (PPI). The system used was Med Associates Inc. (St. Albans City, Vermont, US). Each mouse was placed individually in a plastic-tube holder attached to the startle recording platform (fitted in an industrial sound-proof chamber equipped with a speaker) and connected to the data collection software (Med Associates Inc. (St. Albans City, Vermont, US)). The initial habituation run consisted of 5 recordings without the stimulus, but with the background noise of 53dB, followed by the 5 runs with startle stimulus – noise at a level of 120dB. This was immediately followed by 10 each of the following trials in a pseudorandom order (Table 2.1)

Table 2.1 The trial combination used in measuring maximum startle response and pre-pulse inhibition.

Trial Type	S1 Level (dB)	S2 Level (dB)
Null Stimulus	0	0
Startle Stimulus	0	56
Startle Stimulus	0	58
Startle Stimulus	0	65
Prepulse and Startle Stimulus	0	120
Prepulse and Startle Stimulus	56	120
Prepulse and Startle Stimulus	58	120
Prepulse and Startle Stimulus	65	120

The interstimulus gap was varying between 20-30 seconds, while in the pre-pulse-startling pulse trial, an 80ms gap at the background noise level occurred between pre-pulse and startle pulse. The startle stimulus lasted for 40ms, while the pre-pulse was played for 20ms.

The percentage of pre-pulse inhibition was calculated by the following formula:

$$\% \text{ PPI} = 100 \times (S - PP_S)/S$$

where S is the maximal startle response for the 120dB pulse alone and PP_S is the response for paired Prepulse and Startle stimulus. The initial habituation and startle runs were excluded from the statistical analysis. The PPI testing was carried out by technical scientists at MLC, Harwell, UK.

2.4 Fear conditioning

16-week-old *Abcc5*$^{-/-}$ (n=15 females and n=15 males) as well as wild-type littermate controls (n=17 females and n=13 males) were tested for fear memory and learning using a fear conditioning test. Fear conditioning comprises three linked protocols spread across two days:

Day 1 – conditioning (training)

Day 2 – context test

Day 2– cue test (4hr after context test)

The fear conditioning training and the context tests were performed in special chambers equipped with a camera and included a box with a gridded bottom to deliver a mild foot shock (0.5mA), speakers (Ugo Basile) to play the tone and a source of light (adjusted to 24-26lux). The cue test was done in the same chamber; however, the test box arena was changed to a custom-made different environment (round shaped with stripped paper taped to the outside).

On Day 1 animals were individually placed in the test boxes (Context A) and acclimatised for 150sec, after which a 20sec 10kHz 90dB tone was played, followed by an electric foot shock (0.5mA for 0.5sec). The freezing behaviour before and after the foot shock was measured by Any-Maze tracking software (Version 4.5, Stoelting, USA) in 20sec time-bins.

On Day 2 animals were placed in the same test boxes (Context A) for 300sec with no tone or shock applied. Freezing episodes and total freezing time were again measured by Any-Maze tracking software (Version 4.5, Stoelting, USA).

On Day 3 animals were placed in the same chambers, however, the appearance of the test box was changed (Context B). This was done to measure the association between the cue (the tone) and the foot shock (not applied) in a different environment. Mice were acclimatisation for 120sec, after which a 5sec 90dB tone was played. The freezing behaviour before and after the tone was measured by Any-Maze tracking software (Version 4.5, Stoelting, USA) in 20sec time-bins.

The total amount of freezing time measured in each time bin on each test day was averaged per mouse and plotted as a percentage of the total time of the test. Fear conditioning test was carried out by technical scientists at MLC, Harwell, UK.

2.5 Marble burying assay

Innate digging and burying behaviour were tested by performing the marble burying assay. 12-week-old mice of both, *Abcc5*$^{-/-}$ (n=15 females and n=15 males) and the wild-type littermate controls (n=17 females and n=13 males) were tested in separate batches under standard lighting conditions (around 100 lux) in the quiet testing room. All animals were individually tested in clean standard cages filled with sawdust up to a depth of 5cm and cages were covered with a clear plastic lid. Nine opaque white marbles (diameter 20mm) were equally distributed in rows three by three. Animals were placed in the box and removed from the cage after 20min without disturbing the sawdust or the marbles. The number of fully buried (more than 90% covered by sawdust), partially buried (around 10-90% covered by sawdust) and not buried (less than 10% covered by sawdust) marbles were counted.

2.6 Grip strength

The purpose of grip strength measurements is to assess the muscle strength of the limbs using a grip strength meter. The grip strength test was performed when mice were 14 weeks old of both sexes and genotypes, *Abcc5*$^{-/-}$ knock-out mice and wild-type littermate controls (n=15 females and n=12 males). The measurements were only done for forelimb grip strength and combined forelimb and hindlimb using the grasping grid connected to a sensor (BIO-GT3+MR, Bioseb In Vivo Research Instruments, Florida, US). All measurements were done in triplicates for each mouse, averaged and normalised to body weight. The grip strength testing was carried out by technical scientists at MLC, Harwell, UK.

2.7 Open field

The open field test is used to assess various behavioural parameters such as anxiety level, exploratory drive and also general locomotor activity of the mice. *Abcc5*$^{-/-}$ knock-out mice and their wild-type littermate controls were subject to an Open Field protocol at the age of 10 weeks (n=15 females and n=12 males for both genotypes). During the protocol that lasted 20min, each mouse was singly placed in an Open Field arena of 44x44cm. Animals were placed facing the wall, in the corner of each arena and allowed to explore the chamber freely during the test. Open field setup allowed up to four mice to be tested simultaneously (Fig. 2.1). The arena was located in a quiet, isolated room behind a closed door. The light level of the room was set at 150-200lux in the centre of each arena. Mice activity in the Open field arena was recorded with by camera (Sanyo IR CCD camera, Sanyo/Panasonic, Bracknell, UK) and EthoVision XT video-tracking software (Noldus, Wageningen, Netherlands, EthoVision XT version 8.5) was used to process the data obtained from the recordings. For analysis purposes, each arena was arbitrarily divided into three sections, Periphery, Between Zones and the Centre. The peripheral zone was measured 8cm from the edge of the arena walls, and the Centre was the 12x12cm square in the middle of the Open field chamber (Fig. 2.1). The activity of each mouse was measured in each of the zones per 5min time-bins throughout 20min. EthoVision XT software allowed the analysis and comparison of multiple parameters recorded during the Open field test, such as distance travelled, time spent in each zone, latency to first entry into the central zone, average speed of moving animal, and the number of entries into the zone.

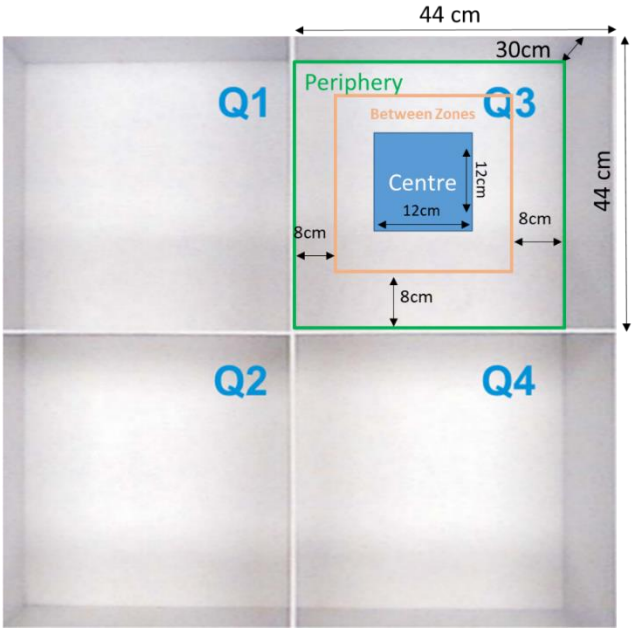


Figure 2.1 Open field arena with the dimensions and marked areas of Centre zone, In Between Zones and Periphery.

2.8 Y-maze

The Y-maze test is used to assess short-term and spatial working memory in mice. 14-week-old females of *Abcc5*$^{-/-}$ knock-out mice, n=6 and their wild-type litter mate controls, n=6, were placed inside a Y-shaped Perspex maze custom-made at MRC Harwell (Fig. 2.2, example image of a Y-Maze for Assessment of Spatial Working and Reference Memory in Mice). Each arm was 39cm x 16cm x 9cm (Length x Width x Height). The inner part of each of the 3 arms of the Y-maze was decorated with different shapes. Mice were allowed to explore freely 2 of 3 arms during the 10min Habituation phase of the test (*Start Arm* and *Familiar Arm*). The arm that was closed during Habituation with the divider is referred to as the *Novel Arm* during the Experimental phase. After initial 10min exploration mice were removed from the Y-maze, and the whole arena was cleaned to avoid bias by odour. Mice were returned to the Y-maze for 5min and placed in the same familiar arm used during the Habituation phase (*Start Arm*), while the Novel Arm was now accessible so that the mice had full access to all 3 arms of the Y-maze: Start Arm, Familiar Arm and Novel Arm. Spontaneous alternation behaviour will lead to an animal exploring a new arm, previously not visited. Also, a mouse with intact short-term and

working spatial memory should remember which of the three arms were explored before and enter more frequently or for longer a novel arm, previously not visited. The Y-maze assay was carried out by technical scientists at MLC, Harwell, UK.

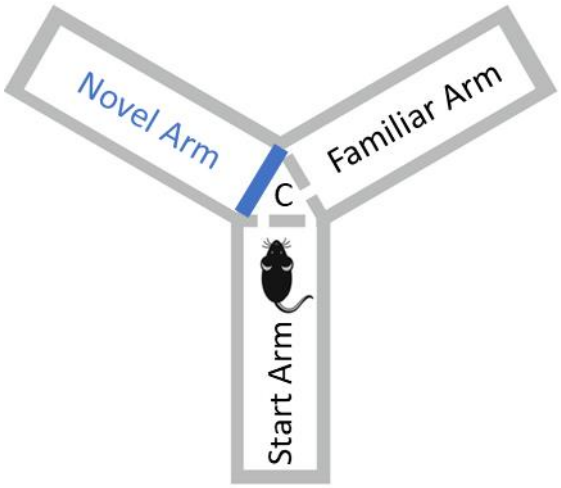


Figure 2.2 Y-maze set up.

Y-maze showing the layout of the arms – the Start and Familiar Arms were accessible to the mice during the Habituation phase while the Novel Arm was closed. During the experiment to test exploratory behaviour, the Novel Arm divider was removed and mice were allowed to freely explore all three arms of the Y-maze.

2.9 Cell culture of GLUTag cells

Immortalised GLUTag cell line was established by Drucker *et al.* from glucagon-producing enteroendocrine tumour cells that arose in glucagon gene-SV40 T antigen transgenic mice [54]. GLUTag cell culture methods were optimised and adjusted throughout the project. Initially, cells were grown in low glucose (1g/L) DMEM with sodium pyruvate, L-Glutamine and phenol red (cat.no.: 11885084, Life Technologies) supplemented with 10% in-house heat-inactivated FBS, foetal bovine serum (F7524-500ML, Sigma) and 1x Penicillin-Streptomycin

(10,000units/mL of penicillin and 10,000µg/mL of streptomycin, cat.no.: 15140122, Life Technologies). Over time, the media was changed to low glucose (1g/L) DMEM with sodium pyruvate, but without L-Glutamine and phenol red (cat.no.: 11880028, Life Technologies). This media was freshly supplemented with 10% heat-inactivated FBS and 1xGlutaMAX (cat.no.: 35050061, Life Technologies) which was more long-term stable than glutamine. The above media will be referred to as 'standard' or growth media.

Cells were routinely grown for experiments in tissue-culture treated, vented flasks T75cm^2 (430641U-SP, Corning) without coating. In these flasks, GLUTag cells grow as small well-defined clumps and clusters of cells firmly attached to the flask. For all experiments, GLUTag cells were re-seeded into cell culture dishes coated with 0.4% Matrigel® Basement Membrane Matrix (cat.no.: 354234, Corning). This was to ensure even cell distribution and uniform monolayer on the day of the experiment. For seeding/maintaining GLUTag cells, they were rinsed once with warm Dulbecco's phosphate-buffered saline (DPBS) without calcium and magnesium (cat.no.: 14190094, Life Technologies) and trypsinised with Trypsin-EDTA (0.05%) solution for 2–3min at 37°C, 5% CO_2. Cell detachment by trypsin was confirmed under the phase-contrast light microscope and cells were resuspended in an appropriate volume of growth media. Cells were thoroughly pipetted up and down until no clumps were visible and single-cell suspension was achieved. For maintenance, cells were split at a 1:4 ratio twice per week or at a 1:8 ratio once per week with the media changed for fresh growth media mid-week. For experiments cells were always counted manually using a Thoma chamber (Marienfeld, Germany) and adjusted to desired density before seeding. Cells were seeded (unless stated otherwise) as follows: 1x10^5 cells per well (cpw) on the 24-well plate, 1x10^6 cpw on 6-well plates, and 5x10^6 cells per T75cm^2 flask, and allowed to grow for either 48hr or 72hr prior the experiments. In all instances, GLUTag cells were grown in the humidified atmosphere with 5% CO_2 and at 37°C.

2.10 Coating tissue culture dishes with Matrigel™

For all experiments using GLUTag cells, dishes were coated with 0.4% Matrigel diluted with plain (no additives) low-glucose DMEM. For primary L cell cultures, dishes for secretion experiments (24-well and 6-well plates) were coated with 1% Matrigel, whereas dishes for imaging (Chamber slides, Lab-Tek™ II Lab-Tek, cat.no.: 154526PK & 154534PK, ThermoFisher Scientific) were coated with 2% Matrigel diluted with plain high glucose DMEM. The volumes of Matrigel solutions used were as follows: 0.5mL/well for 24-well plates, 1mL/well for 6-well plates, 0.25mL/well for 8-well Lab-Tek dishes and 0.5mL/well for 4-well Lab-Tek dishes, 10mL for T75cm^2 flasks. Matrigel was allowed to solidify at 37°C, 5% CO_2 for 20min, then the remaining supernatant was removed and the dishes were used immediately, without washing.

2.11 Heat-inactivation of FBS

FBS was heat-inactivated in-house using the following procedure: room temperature FBS in 0.5L bottle was submerged to its ¾ in the water bath at 56°C for 40min. The bottle was shaken every 10min to ensure uniform temperature distribution. After that, 50mL aliquots were prepared and stored at -20°C.

2.12 Glucagon-like peptide 1 (GLP-1) secretion experiments

For GLP-1 secretion experiments, where the amounts of GLP-1 were measured either in the supernatant and/or in the total cell lysate, GLUTag cells or primary small intestinal mixed cell cultures were seeded in appropriate size dishes coated with Matrigel and grown for up to 72hr (GLUTag cells) or 24hr (primary cell cultures) at 37°C, 5% CO_2. When 80-90% confluent, cells were washed twice with a warm secretion buffer suitable for the experiment and subjected

to treatment with different GLP-1 secretagogues diluted in the secretion buffer of that experiment. GLP-1 secretion under *Basal* (secretion buffer only, no additives) and glucose stimulated conditions (*positive control*) was always included in each experiment to ensure cells were responsive. GLP-1 secretion was measured at the 2hr end-point (unless otherwise stated) in the static cultures incubated at 37°C and 5% CO_2, and the following volumes of secretion buffers were used: for 24-well plate – 0.25mL per well, 6-well plate – 1mL per well, T75cm^2 – 10mL per flask.

After incubation, the supernatant was harvested into Eppendorf tubes pre-loaded with the concentrated mixture of detergents 0.5% Triton-X and 0.4% Tween-20 (w/v) in ultrapure water. This was then diluted 10-fold with the secretion supernatant to the final concentration of 0.05% Triton-X and 0.04% Tween-20. This approach was shown to significantly improve the stability and recovery of GLP-1 for future measurements (Fig. 2.3).

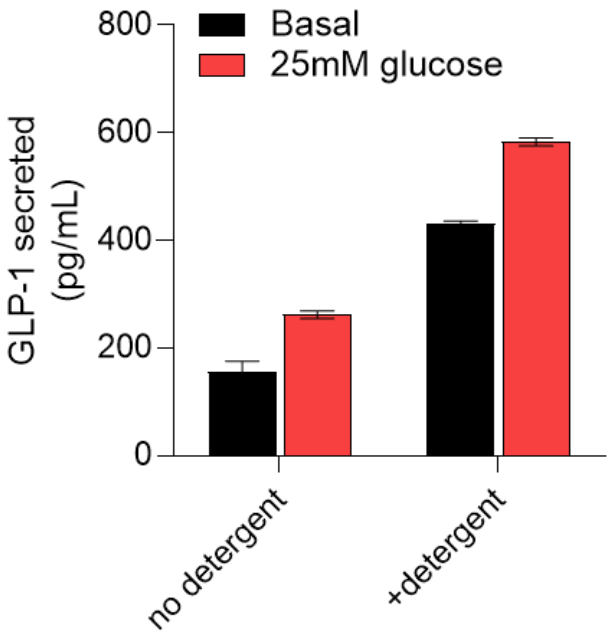


Figure 2.3 Detergent pre-loaded tubes for GLP-1 harvest enhance hormone recovery.

GLP-1 (pg/mL) secreted from GLUTag cells at basal conditions and in stimulation with 25 mM glucose. The supernatant was harvested into empty microcentrifuge tubes (no detergent) or pre-loaded with a

mixture of 0.5% Triton-X and 0.4% Tween-20 (+detergent) that was then diluted 10-fold with supernatant. Enhanced recovery of GLP-1 was observed in the presence of the detergent.

Harvested supernatants were kept on ice and spun at 4°C, 300xg for 5min to remove floating cells. Following the centrifugation, a 120µL sample was kept for assaying GLP-1. Samples were loaded onto 96-well plates made of polypropylene (PP), which further improved the recovery and storage of GLP-1 [55]. Supernatants were stored at -80°C pending GLP-1 measurements.

The remaining cell monolayer was washed twice with ice-cold DPBS and either air-dried and stored at -80°C for future processing or lysed directly in RIPA buffer if required.

Secretion buffer recipes used in the GLP-1 secretion experiments were as in Table 2.2.

The following additives were used when indicated in the experiments:

- glucose at 1mM, 10mM
- dizocilpine (MK-801) at a range of concentrations 0.1-100µM (cat.no.: M107, Sigma)
- D-2-amino-5-phosphonovalerate (D-AP5) at 50µM (cat.no.:0106, Bio-Techne)
- glutamic acid (Glu) at 100µM, glycine (Gly) at 300µM
- bafilomycin A1 at 1µM (cat.no.: 1334, Bio-Techne)
- forskolin at 10µM (cat.no.: F6886, Sigma)
- 30mM potassium chloride, KCl (cat.no.: P5405, Sigma)

Table 2.2 List of secretion buffer recipes used in the experiments of Chapters 4 and 5.

		Chapter 4: RESULTS	Chapter 5: RESULTS				
			Fig 5.12		Fig 5.13		Fig 5.10
Ingredients	**Krebs-HEPES (KRB-H) (mM)**	**Mg^{2+} free buffer (mM)**	**Na^+ free (mM)**	**Na^+ buffer (mM)**	**Cl^- free (mM)**	**Cl^- buffer (mM)**	**Krebs-HEPES Ca^{2+} free (mM)**
NaCl	138	120		144	-	138	138
KCl	4.5	5	4.5	4.5	-	4.5	4.5
$MgCl_2$	1.2	-	1.2	1.2	-	-	1.2
$NaHCO_3$	4.2	24	-	-	4.2	4.2	4.2
NaH_2PO_4	2.1	-	-	-	2.1	2.1	2.1
$CaCl_2$	2.5	2	2.5	2.5	2.5	2.5	-
HEPES	10	15	20	20	20	20	10
Glycine	-	0.01		-	-	-	-
NMDG	-	-	144	-	-	-	-
Na-gluconate	-	-		-	138	-	-
K-gluconate	-	-		-	4.5	-	-
BSA fatty-acid	0.1%	0.1%	0.1%	0.1%	0.1%	0.1%	0.1%
pH adjusted with	NaOH > 7.4 > HCl	NaOH to 7.4	11 > HCl	NaOH > 7.4 > HCl	NaOH > 7.4 > H_3PO_4		NaOH > 7.4 > HCl

2.13 Protein sample preparation and quantification

Cells were lysed in RIPA buffer containing 150mM NaCl, 50mM Tris-HCl at pH 8.0, 1% IGEPAL, 0.2% sodium deoxycholate (DOC), 0.1% sodium dodecyl sulphate (SDS). RIPA lysis buffer was supplemented freshly with Protease Inhibitor Cocktail (PIC) cOmplete (TM), EDTA-free (cat.no.: 11873580001, Roche) as per manufacturer instructions – 1 tablet was dissolved in 1mL of ultrapure water to create 50x stock solution. Cells in 24-well plates were lysed directly in the plate (kept on ice) in 60µL of RIPA + PIC for 10mins, while cells from 6-well plates or flasks were lysed in the smallest practicable volume. After lysis cells were scraped either with a pipette tip (24-well plates) or cell scraper and transferred to pre-chilled Eppendorf tubes. Samples were then centrifuged at 17,200xg, 4°C for 15min to remove the nuclei and cell debris (pellet), and clear cell lysate was collected into the fresh pre-chilled Eppendorf tube and stored at -80°C until analysed. These samples were either used for Western blotting or ELISA. Whole cell lysate samples were quantified for total protein content using a commercial BCA (bicinchoninic acid) assay kit (cat.no.: 23227, Pierce™ BCA Protein Assay

Kit, Thermo Fisher). The kit was used accordingly to the manufacturer's instruction and final protein concentrations were calculated using the bovine serum albumin (BSA) standard curve supplied with the kit. Concentrated samples were always diluted to fit within the linear range of the standard curve and total protein was back-calculated using the dilution factor.

2.14 Glucagon-like peptide 1 (GLP-1) detection

The amounts of active GLP-1 (7-37 and 7-36-NH_2) secreted by either GLUTag cells or native L cells from primary mice intestinal cultures were measured in secretion medium by TR-FRET-based HTRF assay (Active GLP-1, cat.no.: 62GLPPEG, Cisbio, Codolet, France) according to manufacturer's protocols. Final concentrations of secreted GLP-1 were calculated from the standard curve generated by the active GLP-1 peptide standard provided by the manufacturer and presented as pg/mL. GLP-1 stock solution at 2800pg/mL was prepared in ultrapure water and serial dilutions were made in the secretion buffer of the experiment, typically Krebs-HEPES buffer with 0.1% BSA at pH 7.4, unless otherwise indicated. Commercially available synthetic GLP-1 peptide (7-36- NH_2) from Bachem was also used in some experiments as in Figure legends. The stock solution was prepared in ultrapure water at 300µM and the working solution at 2800pg/mL was made freshly on the day of the experiment and then serially diluted as GLP-1 standard from Cisbio. Samples were diluted accordingly to fit within the dynamic range of the standard curve in each assay.

2.15 SDS-PAGE and western blot

Whole-cell lysates were defrosted on ice. Samples were adjusted to the same total protein concentration as per the BCA assay. For SDS polyacrylamide gel electrophoretic separation (SDS-PAGE) samples were prepared as follows: 14µL of cell lysate mixed with 5µL of NuPAGE™ LDS Sample Buffer (4X) (ThermoFisher Scientific) and 0.5mM of reducing agent

- dithiothreitol (DTT) (Sigma). Samples were then heated at 65°C for 10min and cooled down on ice. 12µL of each sample (corresponding to 12µg of total protein) was then loaded onto an appropriate percentage polyacrylamide gel (in-house casting at 5% for stacking gel and 7, 8 or 10% for resolving gel) or commercial Novex WedgeWell 4-12% Tris-Glycine against the PageRuler™ Prestained Protein Ladder, 10 to 180kDa (ThermoFisher Scientific) and stacked for 20min at 70V, then separated at a constant voltage of 150V in SDS-Glycine-Tris buffer for 1hr. Resolved proteins were then transferred onto a PVDF (0.2µm) membrane primed with methanol in the methanol-glycine-Tris buffer at constant amperage of 300mA for 3hr at 4°C. Membranes were then blocked in 5% milk TBS-T buffer and probed with primary antibody (Table 2.3) overnight at 4°C, followed by probing with HRP-conjugated secondary antibody in 5% milk TBS-T for 2hr at room temperature. The Signal was detected using a chemiluminescent reagent system by Amersham ECL Select Western Blotting Detection Reagent (GE Healthcare) and imaged on the X-ray films (Amersham Hyperfilm ECL, GE Healthcare) with the standard developing and fixing agents.

Table 2.3 List of primary and secondary antibodies used for western blotting.

Target protein	Item	Supplier	Host	Band size (kDa)
anti-NMDAR (Grin1, NR1)	AB9864	Merck-Millipore	rabbit, mAb	120
anti-VAMP2	ADI-VAS-SV006-F	Enzo Life Science	rabbit, pAb	18
anti-ABCC5	sc-5781	Santa Cruz Biotechnology	goat, pAb	185
anti-PC1/3	ab220363	Abcam	rabbit, mAb	84 and 66
anti-CgA	20085	ImmunoStar	rabbit, pAb	70
anti-alpha-Tubulin	ab4074	Abcam	rabbit, pAb	50
anti-rabbit IgG (H&L):HRP	A16035	Life Technologies	donkey	NA
anti-goat IgG (H&L):HRP	V8051	Promega	donkey	NA

2.16 Reverse transcription (RT) and quantitative polymerase chain reaction (qPCR)

Total RNA was isolated as per the protocol of the High Pure RNA Isolation kit (Roche) for cell culture (GLUTag cells and primary small intestinal cultures) and tissue (wild-type & *Abcc5*$^{-/-}$ mouse gut sections and wild-type brains). The final concentration and purity of the RNA preparations were confirmed by NanoDrop 1000 UV-Vis Spectrophotometer. 500ng of total RNA from each sample was used for first strand cDNA synthesis with the Revert-Aid First Strand cDNA Synthesis kit (Thermo Scientific) as per manufacturer's protocol for Oligo(d)T18 first strand cDNA synthesis. Samples were diluted 1:20 with RNAse/DNAse free water directly after the reverse transcription and stored at -20°C if needed for qPCR. RT-qPCR was performed with FastStart SYBR Green Master Mix (2x) as per the supplier's instruction with the volume of cDNA template 4µL and custom-designed primers at the final concentration of 10µM (Table 2.4). After an initial 10min at 95°C to activate the hot start polymerase, the qPCR was run for 40 cycles with the following settings: 95°C-10sec, 60°C-30sec.

Table 2.4 List of primers used in RT-qPCR reactions.

Target	Reference sequence	Forward	Reverse	Product size (bp)
β-actin	NM_007393	gcagctccttcgttgccggt	tacagcccggggagcatcgt	119
Grin1	NM_008169.3	ggcctccagcttcaagagac	gctctccctatgacgggaaca	154
Grin2a	NM_008170.4	cattgggagcgggtacatctt	aatgaggtgatgagcagcca	186
Grin2b	NM_008171.4	agtgaacttcccaacccagg	tggtcattcccaaagcgtcc	146

2.17 Murine primary small intestinal cultures – isolation and growth

Wild-type and *Abcc5*$^{-/-}$ mice at the end of the procedures were used at different ages to harvest the small intestine tissue for primary intestinal cell cultures. Mice were sacrificed on the day of the experiment by cervical dislocation, followed by exsanguination to confirm their death. Mice were then dissected and the whole digestive tract from the stomach to the final parts of the large intestine was carefully removed and equilibrated in L-15 medium (cat.no.: L1518, Sigma) on ice. The same section of the gut was always taken for gut crypt isolation: 1cm below the stomach until the caecum (Figure 2.4).

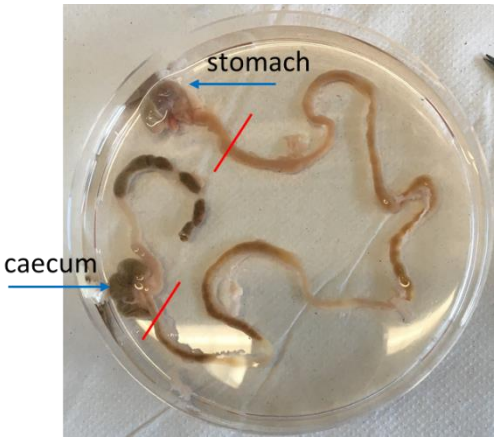


Figure 2.4 Isolation of gastrointestinal (GI) tract from a mouse.

The stomach and caecum were marked with blue arrows, red lines are marking the section of the gut that was always taken for the primary intestinal cultures.

The gut was then placed in 10cm Petri dishes in ice-cold DPBS with calcium and magnesium and cleaned of adipose and pancreatic tissue. The lumen part of the isolated intestinal tube was rinsed multiple times with ice-cold DPBS using a Pasteur pipette. When thoroughly cleaned intestines were cut longitudinally, the villi were gently scraped with the forceps, and the remaining tissue was carefully cut with the scalpel into thin strips, which were then cut horizontally into 1-2mm pieces, and further chopped until fully minced pink tissue pulp was achieved (3-4mL in volume). Minced tissue was transferred with a Pasteur pipette into a 50mL

Falcon tube and was washed 20 times with the ice-cold DPBS allowing the minced tissue to settle under gravity in-between washes.

After washing, the minced tissue fragments were equilibrated using cold high glucose (4.5g/L) DMEM without any additives, followed by at least 5 or more rounds of enzymatic digest with collagenase (C9407, Sigma) at 0.4mg/mL diluted in high glucose (4.5g/L) DMEM without any additives. The collagenase solution was sterile filtered and kept at 37°C throughout the whole isolation. All rounds of tissue digest were performed with 7mL of collagenase solution at 37°C as follows: the collagenase solution was added in a sterile environment to the sedimented tissue fragments in a 50mL sterile Falcon tube, samples were then capped tightly and vigorously shaken, kept in the water bath at 37°C for the following times:

Digest 1° - 5 minutes

Digest 2° - 10 minutes

Digest > 2° - 10 minutes

After each incubation, the cloudy supernatant containing crypts was removed gently to not disturb the pellet of tissue fragments and collected into a 15mL Falcon tube, which was then centrifuged at 300xg for 3min. The pellet resulting from 300xg centrifugation containing gut crypts was dissolved in warm gut crypt growth media up to 2mL per pellet. The growth media for primary intestinal cultures was high glucose DMEM supplemented with 2x GlutaMAX, 2x Pen/Strep, 20% HI-FBS and 10µM ROCK inhibitor (Y-27632, cat.no.: 72302, Stem Cell Technologies). This was repeated for each collagenase digest to obtain 5 or more gut crypt-enriched fractions resuspended in 1–2mL of growth media each. Once all digests were collected, all resuspended pellets (total volume between 5–10mL) were combined, passed through a 100µm cell strainer, and collected in one 50mL Falcon tube. At this stage gut crypts, integrity and numbers were visually assessed using a phase-contrast light microscope and diluted to seed at least 1000 gut crypts/well into a 24-well cell culture dish. Small intestinal

cell cultures resulting from crypts were grown in gut crypt growth media, which was high glucose DMEM with 2x GlutaMAX, 2x Pen/Strep, 20% HI-FBS and 10µM ROCK inhibitor, and used for secretion experiments 24hr after seeding.

2.18 siRNA knock-down of NMDAR (*Grin1)* in GLUTag cells

Overnight culture of GLUTag cells (0.6-1x10^5 cells/well) on a 24-well plate were transfected with siRNA targeting *Grin1* (coding for a mandatory subunit of NMDAR receptor). Probe used ID: 62062 (AM16708, Ambion). The siRNA complex was prepared according to the manufacturer's protocol of Lipofectamine RNAiMAX (Life Technologies). The amount of siRNA used per well was 600nM (15pmol), and 1.5µL of Lipofectamine. The negative control used in the knock-down experiments was non-targeting siRNA sequence Silencer Negative Control No. 1 (AM4611, Life Technologies), prepared alongside the knocking-down complex in the same way. After transfection cells were kept at 37°C, 5% CO_2 for up to 72hr when the secretion experiments were performed.

2.19 Secretory granules (SG) isolation from GLUTag cells

Overnight culture of GLUTag cells (2x10^6 cells/flask) on a T75 cm^2 flask was rinsed with warm PBS without calcium/magnesium ions and cells were detached using Trypsin-EDTA (0.05%) solution for 2-3min at 37°C, 5% CO_2, followed by resuspension in 10mL of full growth media. The cell suspension was then transferred to a 15mL Falcon tube and spun at 300xg for 3min. The cell pellet was washed with warm PBS (no calcium/magnesium) twice and finally resuspended in 10mL of PBS. 0.5mL of that cell suspension was taken as a representative sample of the whole-cell lysate (LYSATE), the remaining 9.5mL was centrifuged at 300xg for 5mins, and the resulting pellet was processed for secretory granules (SG) isolation. The cell pellet was resuspended in 250µL of ice-cold Homogenisation Buffer

(20mM MOPS, 20mM Tris-HCl, 0.5mM EDTA, 300mM sucrose) supplemented with protease inhibitor cocktail (PIC, cOmplete, EDTA-free; cat.no.: 11873580001, Roche) and kept on ice. Dounce homogenizer of 0.5mL capacity was used to homogenise the samples with 10 strokes. The homogenised cell pellets were centrifuged at 2800xg for 10min at 4°C. The resulting pellet was marked as P1 (cell debris), while the supernatant containing secretory granules released from the breakage of the cells was collected into a fresh tube and centrifuged at 8000xg for 15min at 4°C. The small pellet was discarded, while supernatant from 8000xg spin was then collected in pre-cooled ultracentrifuge tubes (343775, Beckman Coulter) and centrifuged at 100,000xg for 60mins at 4°C using TLA-110.3 fixed angle rotor in Optima^{TM} series TL Ultracentrifuge (Beckman Coulter). After high-speed centrifugation, the supernatant (SN100k), pelleted secretory granules, and other vesicular fractions (SG) were collected. Secretory granules pellet was dissolved and lysed in 50µL RIPA buffer, quantified by BCA assay and used for active GLP-1 measurements by western blot analysis. A graphical flowchart of the SG isolation protocol is pictured in Fig. 2.5.

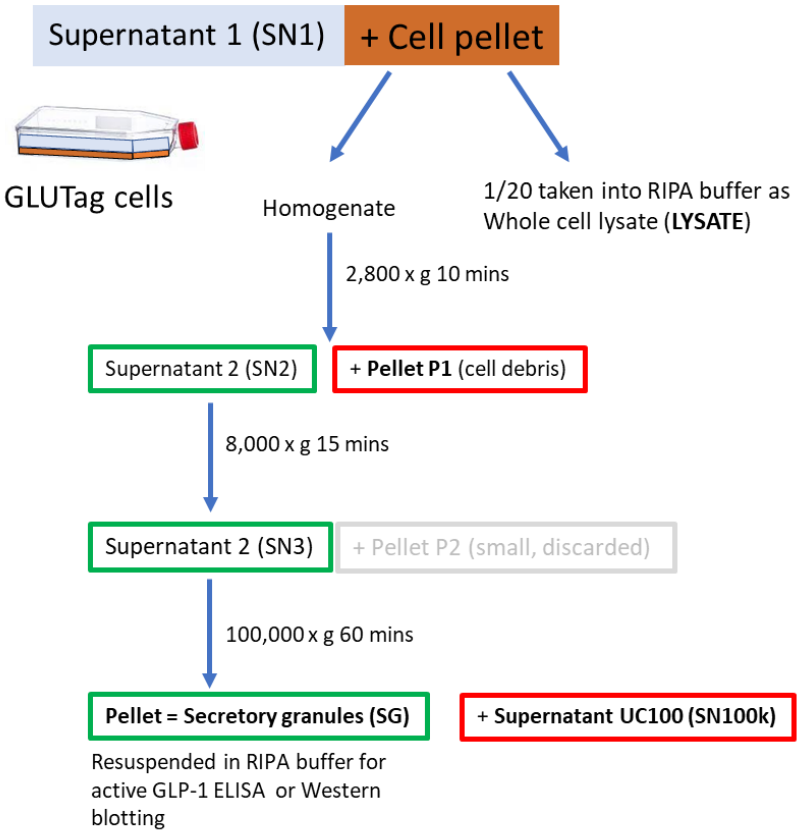


Figure 2.5 Graphical flowchart of secretory granule (SG) isolation protocol.

Fractions used for ELISA or western blot analysis in the Result section are **bolded.**

Common components of SG can be probed using various immune-based techniques as general markers for EECs. Chromogranin A (CgA), which is a soluble glycoprotein and as such, will be contained within the vesicular cargo, is used as a matrix marker for secretory granules, while Synaptobrevin-2 (known also as VAMP-2, Vesicle-Associated Membrane Protein 2) is a marker for LDCV membranes [56]. Thus, collected fractions were validated by immunostaining for CgA and VAMP2. Isolated secretory granules (SG) showed enrichment in soluble granule marker, CgA, as compared to other collected fractions during the granule purification protocol. This was observed at three loading concentrations of total protein amounts for SDS-PAGE (Fig. 2.6). Moreover, the membrane marker for secretory granules

and vesicles, VAMP-2 was also present in all fractions but showed strong enrichments in the SG fraction. This proved that the secretory granule purification protocol provides not only the cytosolic content of the vesicles that can result from lysed or damaged granules but also the membranous part of the secretory vesicles that can be obtained from intact vesicles (Fig. 2.7). No difference in VAMP-2 content was observed between SG isolated from GLUTag cells incubated at acidic pH 6.3 or alkaline pH 7.4. The purity of SG preparations from other membranous fractions such as mitochondria or Golgi complex is not known, but could be tested by blotting for other cellular compartment markers in the SG fraction.

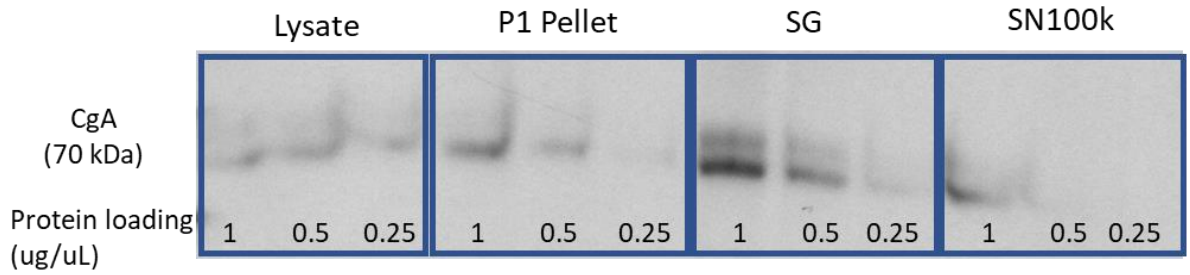


Figure 2.6 Soluble marker of secretory granules (SG) enrichment by western blotting.

Western blotting showing Chromogranin A (CgA) – secretory granules soluble marker expression levels in untreated GLUTag cells. CgA expression was probed in three different loading conditions at 1, 0.5, and 0.25µg/µL of total protein loading per each lane. Samples are whole-cell lysate samples (Lysate) of GLUTag cells as compared to fractions from secretory granules isolation protocol: P1 pellet (cell debris), secretory granules fraction pellet (SG) and supernatant (SN100k). There is an enrichment in CgA in the SG fraction as compared to other fractions.

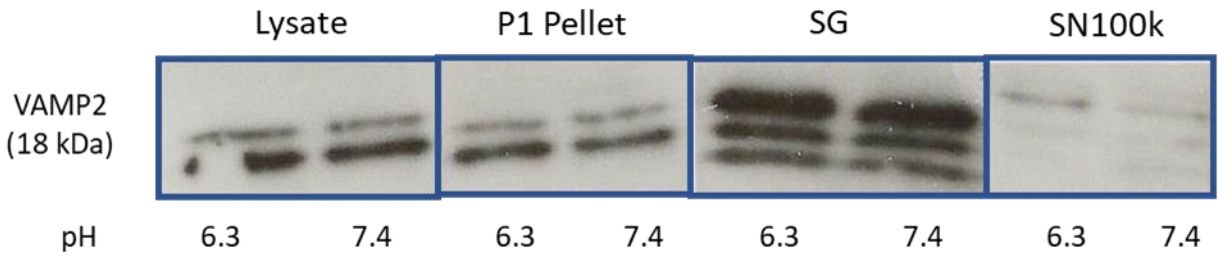


Figure 2.7 Membrane marker expression – VAMP-2 in secretory granules at pH 6.3 and pH 7.4.

Western blotting showing Vesicle-associated membrane protein 2 (VAMP2) – secretory granules membrane marker expression levels in GLUTag cells incubated for 2hr with 10mM glucose at pH 6.3 or 7.4 as indicated above. VAMP2 expression was probed in the whole-cell lysate sample (Lysate) of GLUTag cells as compared to fractions from secretory granules isolation protocol: P1 pellet (cell debris), secretory granules fraction pellet (SG) and supernatant (SN100k). Enrichment of VAMP2 in the SG fraction as compared to whole-cell lysate can be observed.

2.20 RNA sequencing of L cell model cell lines – GLUTag cells

GLUTag cells were cultured in low glucose (1g/L) DMEM (cat.no. 11880028, Life Technologies) supplemented with GlutaMAX (cat.no. 35050061, Life Technologies) and 10% in-house heat-inactivated FBS (cat.no. F7524, Sigma). Cells were seeded at 1×10^6 cells/well in 6-well dishes coated with 0.4% Matrigel (BD, cat. no. 354234) and grown for 48hr until the harvested. Transcriptome (mRNA) library preparation and sequencing have been performed by Novo Nordisk at the NNRCO (Novo Nordisk Research Centre Oxford) as described in [57].

2.21 Immunofluorescence

For immunofluorescence testing of GLP-1 positive cells in primary intestinal cultures, a sample of each gut crypt preparation was seeded into an 8-well Lab-Tek cell culture dish (cat.no.:

154941, Nunc) coated with Matrigel. Gut crypts were then cultured in the same medium as for secretion experiments described above for 24hr. After that, cells were washed twice with 0.5mL of warm PBS and fixed in 10% Neutral Buffered Formalin, 250µL/well (NBF, cat.no.: HT501128-4L, Sigma) for 10min at room temperature with rocking. Cells were then washed with PBS three times and permeabilised with 200µL/well of 0.25% Triton X-100 in PBS for 10mins at room temperature. Following three washes with PBS, cells were blocked with SuperBlock™ solution (cat.no.:37535, ThermoFisher) for 1h at room temperature with rocking. After that cells were probed for GLP-1 with antibody diluted at 1:300 in SuperBlock™ buffer and incubated in a humid chamber overnight at 4°C. The next day, cells were rinsed with PBS three times for 5min and probed with the secondary anti-Rabbit antibody conjugated with green fluorescence probe DyLight 488nm. Following three washes for 5min in PBS, cells were briefly stained with DAPI counterstain diluted at 1:1000 in PBS. After that, the Lab-Tek chamber was removed and samples were mounted with a coverslip under ProLong™ Diamond Antifade mountant (cat.no.: P36970, ThermoFisher Scientific). Slides were imaged soon after or stored in a humid chamber at 4°C. Slides were viewed using EVOS M5000 (ThermoFisher Scientific) imaging system to view cells under transmitted light and also with fluorescence for GFP (green channel) and DAPI (blue channel). GLP-1 positive (green) cells were manually counted under 10x objective across the Lab-Tek chamber ($0.7cm^2$) in duplicates for each primary intestinal culture preparation.

2.22 Statistical analysis

All graphs and statistical analysis were generated using Graph Pad Prism version 9.2.0 software. When two categorical variables were tested (i.e. genotype and treatment) the general effect of the genotype or treatment was compared using a two-way analysis of variance (two-way ANOVA) and results were reported in text in the following format ($F_{x,y}$ = A, P), where x

is Dfn (degrees of freedom in the numerator, k – 1 and k equal to a number of tested groups), y is Dfd (degrees of freedom in the denominator, n -1, and n equal to a number of tested subjects within the groups), A is F ratio calculated as the variance between the groups divided by variance within the groups, with P as p-value, where $P < 0.05$ was considered statistically significant. For comparison of multiple dependent measurements (i.e. pre-pulse levels within or between tested groups, behavioural changes before and after in fear conditioning) multiple comparisons within two-way ANOVA with suitable correction test (Sidak, Bonferroni or Tukey as indicated in the figure legends) were employed. One-way ANOVA was employed when one independent categorical variable (i.e. pH) was assessed to have an effect on the dependent variable (i.e. GLP-1 release). Student's t-test or multiple t-test analyses were used to compare two independent groups with one categorical variable where obtained values were expected to be distributed normally (i.e. grip strength data, audiometry measurements). Mann–Whitney U test was used when normal distribution cannot be assumed (marble burying assay).

Chapter 3: Neurobehavioural phenotype of *Abcc5*$^{-/-}$ knockout (KO) mice

3.1 Introduction

3.1.1 Gene function studies on a mouse model

Mouse models have proved to be invaluable in the study of human disease. Genetically engineered mouse models aid research and therapy developments in oncology [58], diabetes [59], neurodegenerative diseases [60] and metabolic disorders [61]. Mice share close similarities in anatomy, physiology and metabolism with humans. Additionally, they are easy to maintain and breed under laboratory conditions and can be inbred to yield genetically identical strains, and mice have a short generation time and accelerated lifespan, which makes them practical experimental models [62-64]. With technological advances in genetic engineering and gene editing, mouse models are easily and cost-effectively employed in genome screening studies to identify the yet unknown function of protein-coding genes [65]. Such a strategy would include the knockout of the gene of interest and in-depth phenotyping of the created mouse strain. On the large scale, this concept represents the work of the International Mouse Phenotyping Consortium (IMPC) which generated almost 9000 gene knockout mouse lines and phenotyped over 6000 of them [66, 67]. The knockout of the *Abcc5* gene (*Abcc5*$^{-/-}$) in the mouse model presented in this study was made available in 2017 via IMPC, and its novel metabolic phenotype has previously been reported [4].

3.1.2 Behavioural phenotyping of mouse model

The usefulness of the mouse model extends to studies of complex behavioural conditions and traits. Different behavioural paradigms of humans, such as fear conditioning (FC) or sensory-motor gating, can be also observed, and more importantly, quantified in mice [68]. Multiple behavioural assays can be employed to measure specific behavioural traits, called endophenotypes, that are known to be affected in psychiatric disorders. Most endophenotypes are not specific and would occur in different neurological conditions. For example, deficits of pre-pulse inhibition of startle response (PPI) are present not only in schizophrenia, but also in Huntington's disease, Tourette's syndrome, obsessive-compulsive disorder (OCD), and autism [69]. Nonetheless, behavioural paradigms are useful and scalable tools to investigate the phenotypes caused by changes in the expression of particular genes with predicted function or known association in the pathophysiology of these diseases. For example, knocking out the murine *Grm5* gene encoding metabotropic glutamate receptor 5 (mGluR5), which is widely expressed in neural tissue, caused a dramatic decrease in PPI, implicating a role for mGluR5 in the pathophysiology of schizophrenia and providing a potential new drug target [70-72]. Behavioural phenotypes of genetic mutants can also serve to identify novel genes that have a role in the development or function of the nervous system. As an example, this bottom-up approach identified a role for the atypical cadherin gene (*Cdh23*) in PPI regulation [73].

3.1.3 PPI as a neurological biomarker

Acoustic Startle Response (ASR) and PPI are considered relatively stable neurobiological markers that are conserved across the species and are among the most reliable and robust quantitative behavioural tests [74]. PPI in particular serves as a biomarker to assess the condition of neuronal circuits, but it can also be used to examine the integrity of hearing mechanisms since it is also affected by the changes in the pre-pulse frequency or intensity, the

detection of which depends on the condition of the peripheral and central auditory components [75]. During PPI, tested animals are exposed to a series of paired acoustic stimuli that are loud enough to elicit a startle response. When the lower-intensity 'prepulse' is played immediately before the louder 'pulse' sound, the measured output of the startle response (i.e. whole-body flinch) is reduced.

Schizophrenic patients display large PPI deficits, but PPI deficits are also observed in these patients' first-degree relatives who are not affected by the disease [76]. This suggests that there is a genetic component in the pathway regulating PPI expression. Therefore, PPI is also considered a valid and useful tool to investigate the genetic basis of schizophrenia and identify risk genes involved in the pathophysiology of the disease [77, 78]. Especially with the current advances in molecular genetics, manipulating genes regulating PPI phenotypes provides various mouse models of schizophrenia. This is to further findings from pharmacological studies, i.e. mouse models genetically lacking NMDA receptor subunits, confirm the role of the identified susceptibility genes of schizophrenia or identify new genes, i.e. NRG1 knockout mouse linked neuregulin (NRG1) expression to schizophrenia (models reviewed [69]).

3.1.4 Acoustic Startle Response (ASR)

The acoustic startle reflex (ASR) is an automatic reaction to a sudden startling stimulus of loud noise facilitated by rapid, involuntary muscle contraction. The ASR is a part of the survival mechanism that prepares an animal to defend itself or escape. In mammals, the most effective ASR is triggered by sounds louder than 80-90dB (the sound level of an alarm clock or power tools, respectively), and in small mammals such as mice, ASR induces the whole body to flinch which can be measured using stabilimeter chambers [79].

Measurements of PPI depend on ASR response. There are mouse models of schizophrenia showing reduced PPI response and no baseline startle changes, i.e. mGluR5 knockout mice

[70]. In other animal models differentially inbred to exhibit low or high PPI, it was shown that rats exhibiting low PPI also have an increased startle response as compared to high PPI animals [80]. No difference, however, was found in the magnitude of the startle response between schizophrenic human patients and controls in the absence of a pre-pulse [76].

3.1.5 Neuronal circuits driving ASR

Neuronal circuits driving ASR are well-described and mainly located in the brain stem [81]. In rodents, the ASR neuronal pathway involves the cochlear root neurons (CRNs) receiving information directly from the spiral ganglion cells in the cochlea and registering the sensory input (sound). The CRNs then innervate giant neurons in the caudal pontine reticular nucleus (PnC) of both hemispheres in the brain, and PnC giant neurons project to the facial, cranial, and spinal motoneurons to rapidly activate muscle contractions [81] (Fig 3.1). The activity of PnC giant neurons is the primary modulator of ASR. Selective loss of giant neurons within the PnC is correlated with a reduction of the startle amplitude, whereas general loss of the total number of neurons did not correlate with ASR amplitude [46]. The synaptic transmission of startle within PnC is predominantly fast and glutamatergic, mediated by glutamate-gated ion channels, NMDA and AMPA receptors [82]. The innervation pattern of the CRNs indicates that high-frequency cochlear regions dominate the auditory input, thus mice with high-frequency hearing loss due to ageing display reduced ASR and loss in PPI [83]. The ASR amplitude can be modulated in multiple ways by the preceding sounds, background noise level,

other sensory modalities or the behavioural state of a subject [79]. The most common modification of ASR is PPI.

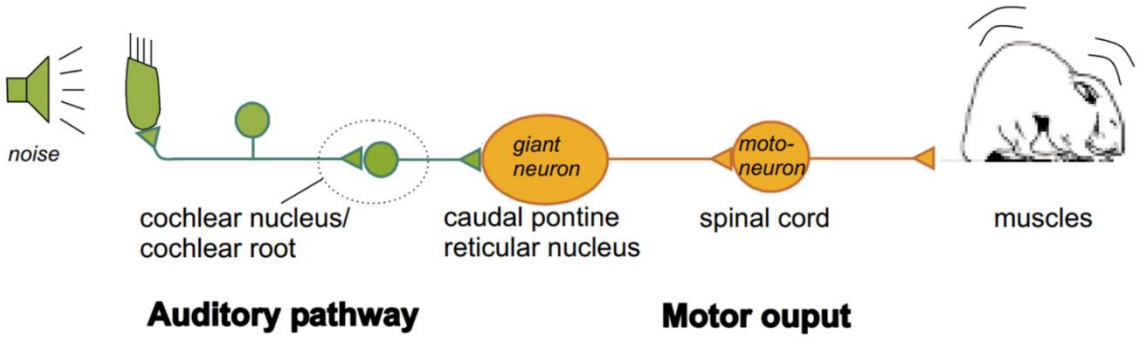


Figure 3.1 Schematic drawing of the primary acoustic startle circuit in rodents.

Sudden loud noise activates sensory hair cells in the cochlea and the acoustic information is conveyed by the sensory auditory neurons to the giant neurons in the pontine reticular nucleus (PnC). Axons of PnC giant neurons directly innervate motoneurons in the facial nucleus and spinal cord. Their activation causes a startle reflex – a whole-body flinch. Adapted from [84].

3.1.6 ASR – methodological considerations

In mice, most strains display robust ASR for sounds stimuli 80-90dB and above, but the maximal amplitude of the ASR response can vary between the mouse strains. In most strains, sound levels of 70dB and lower do not trigger ASR. The analysis of 40 different mouse strains showed that a 100dB stimulus elicited average ASR levels among C57BL sub-strains whereas FVB strains displayed the highest ASR levels. The mean change in amplitude between the most- and least-reactive strain was ten-fold [85]. The magnitude of ASR also depends on the age of mice as age will affect hearing sensitivity. Some strains, such as C57BL mice, are more prone to hearing loss, resulting in decreased ASR amplitude. Mice up to the age of 6 weeks despite different genetic backgrounds and hearing sensitivity, were shown to display similar magnitudes of ASR responses [86]. The startle reflex to acoustic stimulation represents the

non-associative learning response; therefore, with repeated exposure to the startling stimulus, the ASR amplitude will gradually decrease, an effect known as habituation [87].

3.1.7 Pre-pulse inhibition (PPI) – modification of the ASR

Pre-pulse inhibition (PPI) is the most common modification of acoustic startle response. PPI measures the ability of a weaker pre-pulse stimulus to activate the innate inhibitory system to allow the efficient processing of ongoing sensory information (pre-pulse) and suppress the information from a new stimulus (startle pulse) to avoid sensory overload [88] (Fig. 3.2). The exact mechanism producing the inhibitory effect on ASR is not fully elucidated and the neuronal circuits involved in PPI are not completely mapped and understood [89]. PPI has two components – automatic (involuntary and pre-attentive) and attentional (mediated by higher-order cognitive processes) [81].

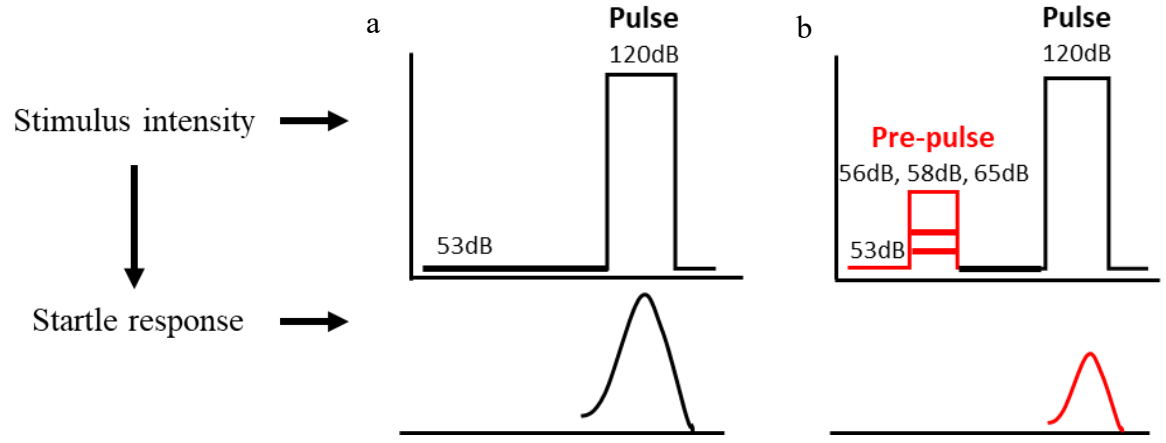


Figure 3.2 Graphical overview of the acoustic startle response and pre-pulse inhibition (PPI) principle.

a) application of sudden, loud acoustic stimulation 120dB pulse over 53dB background causes a maximal startle response (lower panel, in black). b) application of weaker pre-pulse stimulus 56, 58 or 65dB (red line) preceding the startle pulse (black line) inhibits startle response (lower panel, in red).

3.1.8 PPI neuronal circuit

PPI is a multimodal phenomenon and can occur when prepulse and the startling stimulus are of either the same or of different sensory modalities, e.g. visual pre-pulse and acoustic startle (cross-modal) or acoustic pre-pulse and acoustic startle stimuli (intra-modal). Multiple neuronal pathways have been shown to take part in PPI expression and modulation., but the basic neuronal circuit for PPI is located in the brainstem [90]. Confirmed brain structures involved in PPI include mid-brain nuclei, namely, the inferior colliculus (IC), superior colliculus (SC) and the pedunculopontine tegmental nucleus (PPTg) that converge at the level of PnC [81, 91, 92], where acoustic pre-pulses can inhibit the activity of PnC neurons and reduce the startle response [93]. The SC can receive input from other sensory modalities (auditory, visual and tactile), and it has a direct anatomical connection to PPTg. Therefore, activation of SC directly activates inhibitory cholinergic neurons in PPTg that project to giant neurons within the PnC, where the startle pathway inhibition ultimately occurs [90] (Fig 3.3).

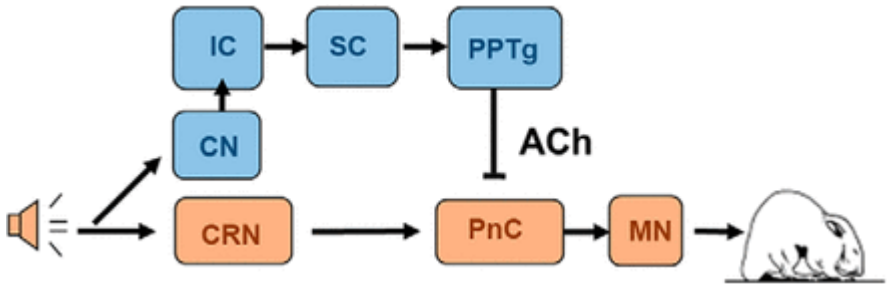


Figure 3.3 The basic neuronal pathway involved in the expression of pre-pulse inhibition.

The primary startle pathway is shown in orange. The startle pathway includes the cochlear root neurons (CRNs), and giant neurons in the PnC that directly innervate cervical and spinal motor neurons (MNs). Inhibition of this pathway (shown in blue) by the prepulse is assumed to happen at the level of PnC. Weaker prepulse is processed through the ascending auditory pathway including the cochlear nucleus (CN) and the inferior colliculus (IC). From there, auditory information is signalled to the multisensory

superior colliculus (SC) and the PPTg, which inhibits PnC via acetylcholine (ACh) sensitive pathways. Adapted from [94].

New evidence, however, using optogenetics in rats reveals that activation or inhibition of cholinergic neurons within PPTg does not affect PPI expression [94]. It has been postulated instead that PPI may be a function of GABAergic and/or glutamatergic cells in the PPTg, which may either directly project to the PnC or indirectly inhibit the startle pathway, e.g. through GABAergic projections from the substantia nigra [94]. This same study demonstrates that PPTg cholinergic neurons mediate both, the startle and pre-pulse facilitation (PPF), while non-cholinergic neurons mainly regulate PPI [94].

Moreover, multiple behavioural, pharmacological and psychophysiological studies suggest that regulation of PPI involves a complex neural network extending beyond the brainstem nuclei and includes different cortical and subcortical areas within the limbic corticostriatal-pallido-pontine (CSPP) circuitry [77]. Manipulating the activity of the prefrontal cortex, thalamus, hippocampus, basolateral amygdala, nucleus accumbens (NAC), and dorsal striatum was also shown to affect PPI [89]. Recent studies also pointed at structures directly projecting to the PnC like excitatory neurons of the central nucleus of the amygdala (CeA) that send direct inputs to the PnC, where they activate a subpopulation of glycine transporter-positive neurons to contribute to PPI as well [95].

3.1.9 Receptors involved in PPI

Various receptors and associated neurotransmitters are functionally important in the expression and/or modulation of PPI response. $GABA_B$ receptor antagonist (phaclofen), but not $GABA_A$ antagonist (picrotoxin), was shown to decrease PPI response at the level of PnC, while $GABA_A$ agonist injected at PPTg attenuated the PPI but caused an increase to the baseline startle

amplitude [91]. PPI is also reduced by the systemic delivery of dopamine (DA) or serotonin (5-HT) agonists or glutamatergic N-methyl-D-aspartate (NMDA) receptor antagonists [96]. Non-competitive antagonists of NMDA receptors, such as phencyclidine (PCP) and dizocilpine (MK-801), were proven to disrupt PPI robustly in rats. Both drugs reduced PPI in both intra-modal (acoustic-acoustic) and cross-modal (acoustic-tactile) paradigms, mimicking the PPI deficits seen in schizophrenia [97]. Multiple genetic studies further supported the role of specific receptors in the expression and modulation of PPI, e.g. dopamine active transporter (DAT) knock-out mice are missing the dopamine transporter and thus have higher circulating levels of dopamine. These mice display large PPI deficits that can be reversed by dopamine receptor D_1 or D_2 antagonists [98].

3.1.10 Methodological caveats of measuring PPI in mice

Various factors play a role in modulating PPI. PPI increases with an increasing pre-pulse sound intensity above the background up to the level that triggers ASR (>80dB). Pre-pulse intensity, and increased pre-pulse duration (beyond 0-25ms) also significantly increase PPI response, especially at lower pre-pulse intensity/sound [99].

PPI is usually depicted as a percentage of maximal ASR response. Typical PPI results of wild-type C57BL/6N mice are normally 50-60% for the highest prepulse level (70dB) and gradually less for weaker pre-pulses [100]. There is evidence that the sound frequency of the prepulse also has an impact on the PPI level. Detailed studies using C57 mice on the relationship between age, prepulse frequency and prepulse intensity revealed that, in general, high frequency pre-pulses (24kHz) caused lower PPI responses than low-frequency pre-pulses (4kHz). Gradual loss of PPI with age until complete loss of PPI at age of 12 months was observed for high-frequency pre-pulses. On the contrary, low-frequency pre-pulses (4kHz) enhanced PPI response in older mice. This happens due to C57 mice exhibiting high-frequency

hearing loss with age as higher frequencies are less noticeable in older age. The optimal condition for measuring PPI in C57 mice appears to be mid-range frequency prepulse sounds (8-16kHz) applied for the age range of 4-20 weeks [75].

Also, the time interval between pre-pulse and startle stimulation plays a role in modulating PPI responses. It was shown that, depending on the mouse strain and genetic background, the optimal lead time (pause) between pre-pulse and startle stimuli to observe 'pure' PPI is approximately 100ms [101]. Too short (0-12.5ms) of a leading time, especially for the low-intensity pre-pulse levels similar to the background noise, causes a phenomenon called pre-pulse facilitation (PPF), which is discussed below [99].

PPF occurs when a weaker pre-pulse is capable of enhancing the magnitude of the ASR response instead of inhibiting it and/or reducing the latency of the startle response [102, 103]. Unlike PPI, the effect of PPF is non-linear and does not increase gradually in line with the pre-pulse intensity. It increases at first, but further increases in pre-pulse intensity cause a sharp decrease in PPF. PPF occurs also at the sensory threshold for the stimuli, as increments of just 1.5dB over the background noise were shown to trigger the PPF [74]. A shorter pre-pulse duration was also shown to trigger PPF rather than PPI for the same pre-pulse sound intensity [99]. PPF, just like PPI, shows no signs of habituation over repeated trials [74]. The mechanism underlaying PPF remains unclear and neuronal pathways of PPF are unknown as it is a less studied phenomenon, though it is reported to be present in mice, rats and humans. It has been suggested that PPI and PPF involve independent processes but can occur simultaneously in a competitive manner [101, 104].

Generally, males display larger ASR and PPI levels than females [98], however, there are also studies showing no sex-specific difference [105]. A large study of 40 different mouse strains showed that significant sex differences are observed in some strains. For example, females of sub-strain C57BL/10J displayed larger ASR than males, while no sex-related difference was

observed for other sub-strains of C57BL mice [85]. Artificial manipulation of the oestrus cycle has shown the dependence of ASR and PPI responses on oestrogen levels in mice. Removal of ovaries caused a significant decrease in PPI, whereas exogenous supplementation of oestrogen restores the PPI response [106]. The weight of the animals does not correlate with any of the measures of ASR and PPI response [85].

3.1.11 Definition of fear

Fear is considered a defensive mechanism. Fear as a response to certain stimuli is an innate and hard-wired mechanism that evolved to protect us from danger – loud noises evoke fear in newborn infants, and naive laboratory rats show a fear response to cats. Fear can be also acquired in a rapid and long-lasting manner as a form of adaption to a new or changing environment [107].

3.1.12 Fear conditioning – method

Fear conditioning (FC) is a behavioural paradigm that utilises the principles of Pavlov's reflex to measure associative learning and memory. Fear conditioning task in mice relies on providing the neutral, conditioned stimulus (CS, here acoustic tone, loud noise) that is paired with the aversive, unconditioned stimulus (US, here mild electric foot shock). Upon successful conditioning (fear learning), a mouse is expected to associate the CS (tone) with the aversive US and produce conditioned (cued) responses that are similar to innate fear responses [107]. In mice, fear is expressed as freezing behaviour – not voluntary movements. Successfully conditioned mice are expected to exhibit robust fear response, freezing, when presented with neutral stimulus only, without the aversive stimulus to follow (fear expression). FC can be learnt in one session when neutral-aversive stimulus is played as it is rapidly learnt and has long-lasting effects.

3.1.13 Anatomy of fear

The central brain structure involved in FC is the amygdala as shown by tissue lesions, and pharmacological and neurophysiological studies [107]. The amygdala receives sensory input from various brain regions such as the thalamus, neocortex and hippocampus. In turn, it sends projections to multiple brain structures that are responsible for mediating specific fear responses, e.g. stress hormone release (hypothalamus) or freezing (via periaqueductal gray matter) [107]. The acquisition of fear (memory of CS-US pairing) occurs in the basolateral complex of the amygdala (BLA) and involves its basal (BA) and lateral nuclei (LA). In auditory fear conditioning, the CS (tone) and US (foot shock) inputs converge onto a single neuron in the LA (Fig. 3.4). Auditory CS inputs to the LA come from both the auditory thalamus and cortex, while US input to the LA comes from somatosensory areas of thalamus and cortex. It was shown that lesions of the specific regions of the amygdala receiving input from the medial geniculate nucleus (MGN) of the thalamus, which is responsible for relaying auditory information to the amygdala, block formation of noise-foot shock association, but not conditioning from other sensory modalities, such as light [108]. The LA nucleus is directly interconnected with the central nucleus of amygdala (CeA), which serves as an output pathway to various brain structures such as the hypothalamus and brainstem, to generate freezing and other specific fear responses [109]. Expression of previously conditioned fear is also led by CeA but the network of CS-driven neurons within the BA is required to activate CeA and initiate a conditioned fear response [110].

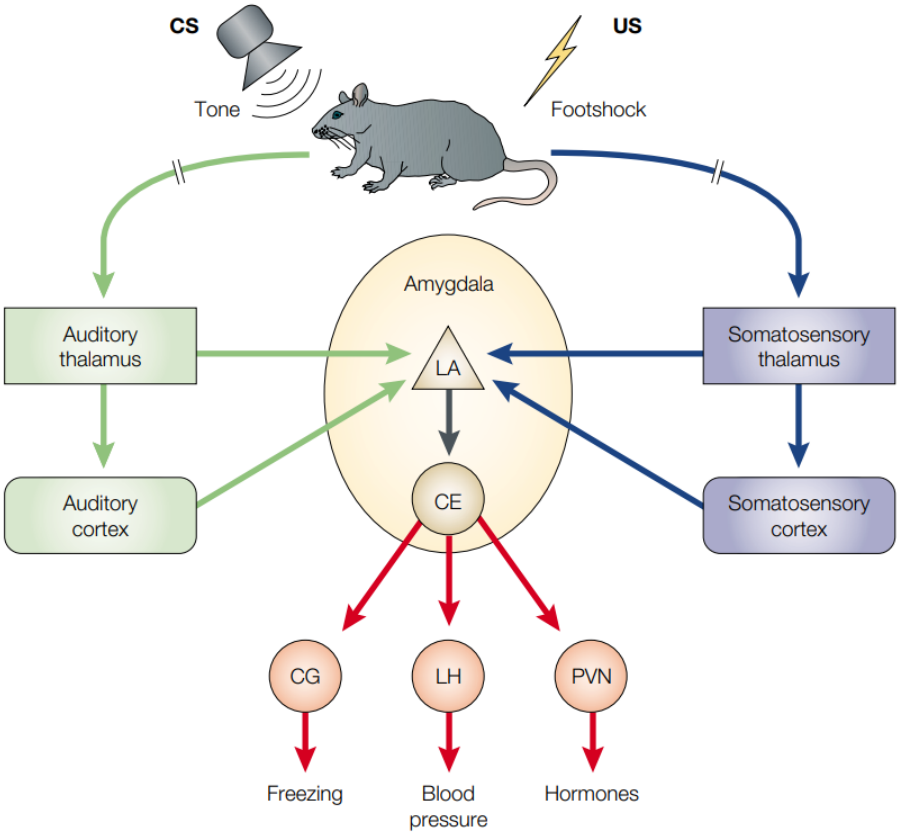


Figure 3.4 Neuronal circuits involved in fear conditioning.

During fear conditioning, the conditioned stimulus (CS, tone) and unconditioned stimulus (US, foot shock) from thalamocortical regions of the auditory and somatosensory systems, respectively converge in the lateral nucleus of the amygdala (LA). The LA also communicates with the CeA which sends an output projection to mediate fear responses. CG, central grey; LH, lateral hypothalamus; PVN, paraventricular hypothalamus. Adapted from [109].

3.1.14 Receptors involved in fear

FC is a form of associative learning. The cellular mechanisms underlying learning and memory involve synaptic plasticity processes [107], the most well-characterised of which is synaptic plasticity is long-term potentiation (LTP). LTP is the process of strengthening synaptic efficacy depending on the synapse activity. At the synapse level, LTP is mediated by signalling by

glutamatergic NMDA and AMPA receptors [111]. Studies have shown that blocking NMDA receptors with the competitive antagonist D-AP5 by direct injection into the amygdala prior to the conditioning abolished fear acquisition in rats [112]. Moreover, previously conditioned rats displayed decreased fear responses to the context and tone cues when NDMA antagonist infusions were made post-conditioning. Thus, blocking NMDA receptors influence fear acquisition as well as the expression of conditioned fear responses after successful fear learning. This applies irrespective of different CS modalities, such as light or tone, and different output responses, such as startle or freezing, used in the conditioning training [113]. These findings strongly support the role of NMDA receptors in synaptic plasticity during learning (fear acquisition, conditioning training) but also the importance of glutamatergic signalling in normal synaptic transmission within the amygdala (fear expression) [107].

3.1.15 *Abcc5* knockout mouse model

In this thesis, a new whole-body knock-out of the *Abcc5* gene in mice was generated using CRISPR-Cas9 technology on the C57BL/6NTac background (Fig. 3.5). Multiple cohorts of viable male and female mice groups were created with homozygous deletion for the *Abcc5* gene (*Abcc5*$^{-/-}$) [4].

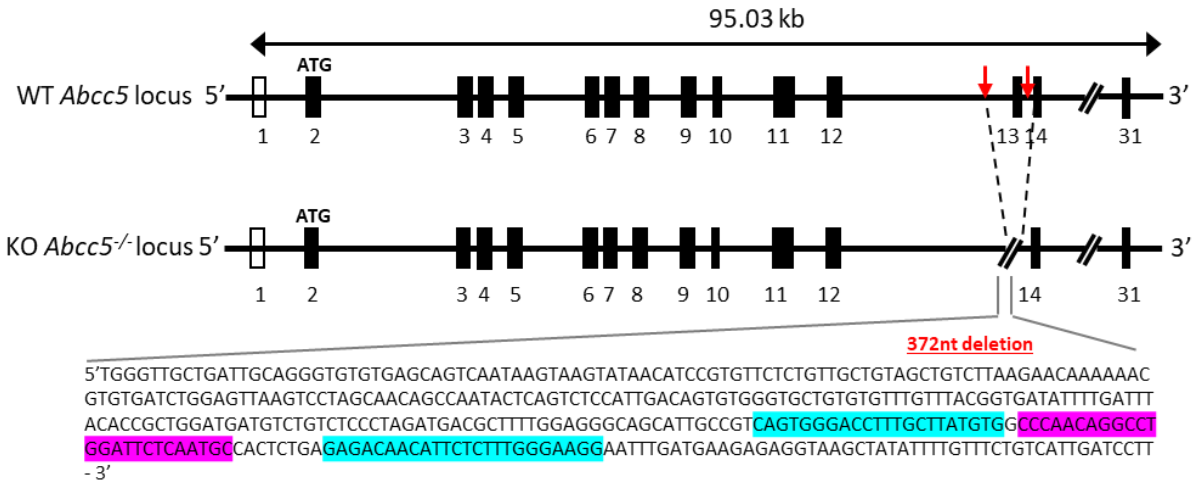


Figure 3.5 Genomic overview of *Abcc5*$^{-/-}$ CRISPR/Cas9 knock-out design.

The 372-nucleotide deletion resulting in full ablation of exon 13 and frameshift of the remaining coding sequence is shown. Marked in blue are genotyping primers, and marked in pink is the internal probe control. Exon 13 is coding amino acids 612-646aa corresponding to the nucleotide-binding domain 1 (NBD1) region on the protein (see also Figure 1.1).

In humans, it has been reported that exons 1-7 of *ABCC5* gene can be expressed as three short transcripts within the retina. One of these splice variants (*ABCC5_SV2*) is translated into a truncated 208aa protein abundantly present in endothelial cells of inner retinal blood vessels and along retinal pigment epithelial membranes [114]. Based on these results similar prediction has been made for *Abcc5* expression in mice. Currently, however, there is no experimental evidence to support this finding in mice.

Importantly, all previous publications of *Abcc5*$^{-/-}$ mice referenced in this thesis from other research groups were generated by a process of creating chimeric mice via embryonic stem (ES) cell injection and then backcrossing the homozygous mice to 100% Friend virus B-type (FVB mice) genetic background. The *Abcc5*$^{-/-}$ mouse model generated on an FVB background was reported to have 1.5kb deletion in the *Abcc5* sequence containing exon 17, which encodes amino acids 678–745 of the first ATP-binding domain [18]. Interestingly, as described by Jansen *et al.* no phenotypic abnormalities were found from behavioural tests carried out on these mice. These tests included spontaneous activity in the dark phase only, using an automatic home-cage monitoring system and locomotor activity assessment over 5min after the phencyclidine (PCP) administration [31]. PCP is an NMDA antagonist and has a variety of behavioural effects in humans. Most importantly, it produces symptoms of schizophrenia and PCP-induced psychosis serves as a pharmacological model of schizophrenic disease. Thus, PCP is also used to study mouse models of schizophrenia. The most prominent effect of PCP injection in mice is increased general locomotor activity [115]. *Abcc5*$^{-/-}$ mouse brains showed a marked accumulation of multiple glutamate conjugate compounds, including NAAG, a

neuroprotective neuropeptide. The authors hypothesised that due to high NAAG levels in the brain, the *Abcc5*$^{-/-}$ mice will be protected from PCP-induced locomotor effects. Surprisingly, no change in mice activity was observed when compared to PCP-injected control mice [31].

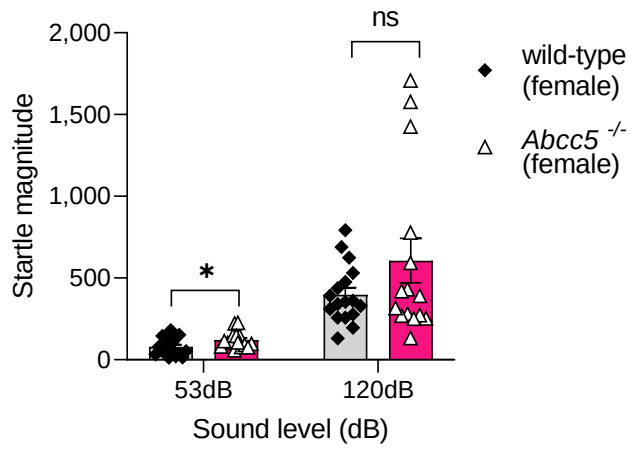
The Chapter 3 hypothesis is that accumulation of glutamate-conjugates, including NAAG, in *Abcc5*$^{-/-}$ mouse brains will cause the disruption of glutamatergic signalling and present a schizophrenic-like phenotype. The neurobehavioural screening tests were performed to quantify these behavioural changes caused by the absence of *Abcc5* expression using *Abcc5*$^{-/-}$ mice.

3.2 Results

3.2.1 *Abcc5*$^{-/-}$ mice have higher acoustic startle reactivity

Abcc5$^{-/-}$ (n_{ko}=15 females, n_{ko}=15 males) and wild-type control mice (n_{wt}=17 females, n_{wt}=13 males) were exposed to a startle pulse to determine baseline ASR. The background tone elicited a small increase in *Abcc5*$^{-/-}$ females 120±12 vs 79±12, p=0.03 (Fig. 3.6a, pink bar, open triangle symbols) and males 148±16 vs 81±15, *p*=0.006 (Fig. 3.6b, yellow bar/open circle) relative to wild-type controls. A significant statistical difference was also observed, as *Abcc5*$^{-/-}$ males demonstrated higher reactivity to the 120dB startle noise relative to wild-type controls (725±91 vs 386±29.7, *p*=0.0026, unpaired t-test), while *Abcc5*$^{-/-}$ females showed a similar, increasing trend in startle reactivity, but their response to 120dB pulse was not statistically different compared with wild-types (606±135 vs 397±42, *p*=0.131).

a



b

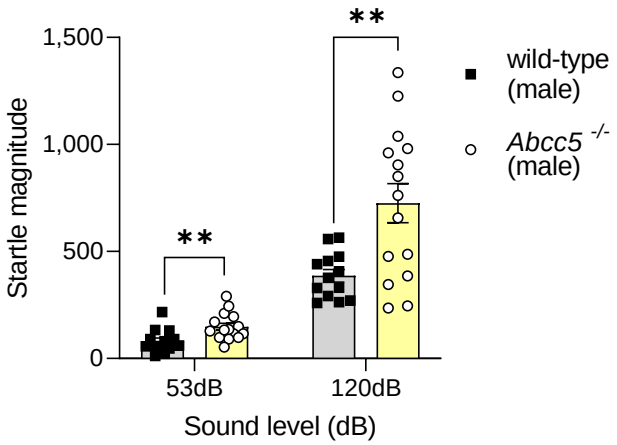


Figure 3.6. Startle response in *Abcc5*$^{-/-}$ and wild-type mice.

The magnitude of the response to the background noise (53dB) and maximal startle response to pulse (120dB) alone in *Abcc5*$^{-/-}$ and wild-type mice, (a) in females and (b) males. Data presented as mean±SEM, each data point representing an average of 10 measurements from a single mouse, results were compared by unpaired two-tailed Student's t-test; $p<0.05$*, $p<0.01$**, $p<0.001$***, $p<0.0001$****

Baseline response to the background noise and the magnitude of startle reactivity was also presented per individual mouse (Fig. 3.7a-d) to illustrate that the startle response in *Abcc5*$^{-/-}$ was not as uniform as in wild-type mice, and there are some high responders to the startle stimulus within the *Abcc5*$^{-/-}$ group. Males of *Abcc5*$^{-/-}$ mice have more high responders than females, which may underlie the non-significant trend in *Abcc5*$^{-/-}$ females for higher startle response relative to wildtype.

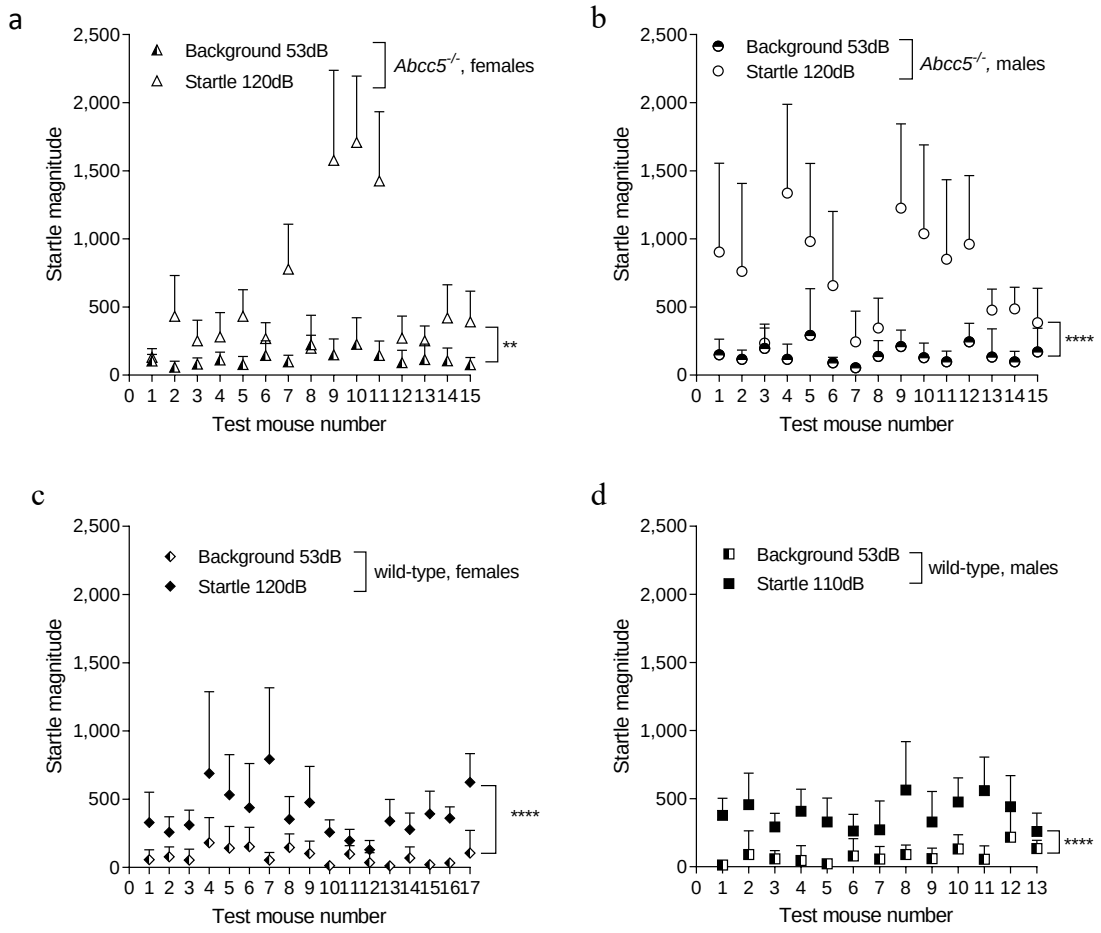


Figure 3.7 Comparison of background and startle responses obtain from individual mice.

Background and startle response from a) *Abcc5*$^{-/-}$ females, b) *Abcc5*$^{-/-}$ males, c) wild-type females d) wild-type males. Data presented as a single point per mouse, averaged from 10 measurements, mean±SD, area under the curve (AUC) for background response vs startle response was compared with a two-tailed, paired t-Test; p<0.05*, p<0.01**, p<0.001***, p<0.0001****

3.2.2 *Abcc5* knockout mice display loss of pre-pulse inhibition

Since *Abcc5*$^{-/-}$ mice of both sexes showed robust reactivity to startle stimulus confirming the presence of intact acoustic startle reflex, next the PPI paradigm was tested. *Abcc5*$^{-/-}$ mice (n_{ko}=15 females, n_{ko}=15 males) and their wild-type littermate controls (n_{wt}=17 females, n_{wt}=13 males), were subjected to three pre-pulse levels of 56dB, 58dB, or 65dB preceding the startle pulse of 120dB. The startle reflex inhibition elicited by each pre-pulse level was calculated and

plotted as the percentage of startle response alone. Two-way ANOVA revealed a dramatic loss of PPI in *Abcc5*$^{-/-}$ females ($F_{1,28} = 15.88$, $p<0.001$) and males ($F_{1,26} = 23.87$, $p<0.0001$) relative to wild-type controls (Fig. 3.8).

Abcc5$^{-/-}$ females demonstrated significant decreases in PPI relative to wild-type controls at 56dB (-8.9%±4.9 vs 2.99%±5.2), 58dB (11.3%±9.9 vs 47.6%±4.2), and 65dB (10.1%±6.9 vs 47.7%±4.0) (Fig. 3.8a). These differences proved highly significant at pre-pulse levels 58dB (p=0.01) and 65 (p=0.0004) but not at 56 (p=0.3). Loss of PPI was even larger in *Abcc5*$^{-/-}$ males relative to wild-type males at 56dB (14.7%±5.8 vs 18.9%±5.4, p=0.0007), 58dB (9.6%±8 vs 41.4%±5.2, p=0.009) and 65dB (8.9%±6.1 vs 47.9%±6.1, p=0.004) (Fig. 3.8b).

The consensus of the PPI paradigm is that increasing the pre-pulse sound level would gradually increase the percentage of PPI. Indeed, a statistically significant increase in PPI was observed between pre-pulses of 56dB vs 58dB and 56dB vs 65dB in *Abcc5*$^{-/-}$ females (p=0.002, and p=0.005, respectively) and wild-type controls ($p<0.001$) (Fig. 3.8a). Similarly, *Abcc5*$^{-/-}$ and wild-type males showed a significant increase in PPI expression between pre-pulses 56dB vs 58dB (p=0.01 and p=0.005, respectively), and 56dB vs 65dB (p=0.0013 and p=0.0012, respectively) (Fig. 3.8b).

No significant difference in PPI expression was recorded between pre-pulses 58dB vs 65dB in females or males of both genotypes, likely due to minimal changes in the pre-pulse sound intensity to elicit a larger response.

All tested pre-pulse sound levels caused prepulse facilitation (PPF) effect in multiple *Abcc5*$^{-/-}$ mice of both sexes (Fig. 3.8a and Fig. 3.8b). PPF resulted in a negative percentage value of PPI. In wild-type controls of both sexes, PPF was measured with a pre-pulse of 56dB and disappeared with pre-pulse levels of 58 and 65dB.

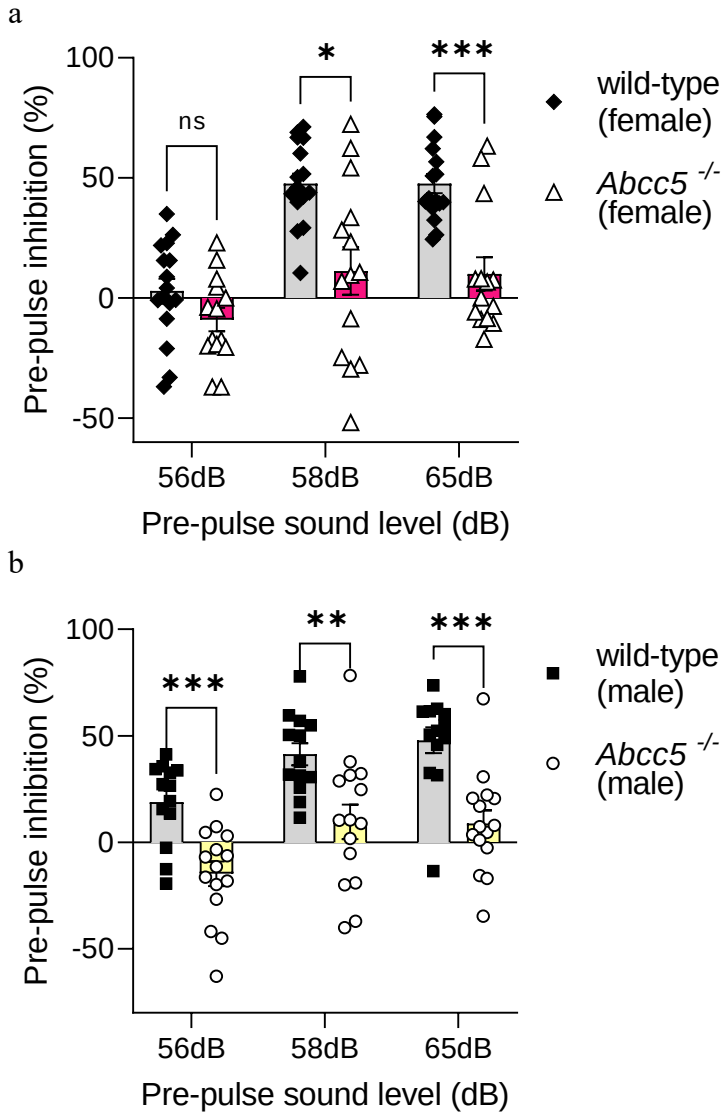


Figure 3.8. Loss of pre-pulse inhibition in *Abcc5*$^{-/-}$ mice compared to wild-type

Percentage of pre-pulse inhibition tested for 3 pre-pulse levels 56dB, 58dB, 65dB measured in *Abcc5*$^{-/-}$ and wild-type mice, a) in females (n_{ko}=15, n_{wt}=17) and b) in males (n_{ko}=15, n_{wt}=12). Each data point represents an average of 10 measurements from a single mouse. Data presented as mean±SEM, results were compared by two-way ANOVA with Sidak multiple comparison tests; p<0.05*, p<0.01**, p<0.001***, p<0.0001****

3.2.3 No gradient reactivity in *Abcc5*$^{-/-}$ mice to pre-pulse sound levels alone

In the same experiment, the response magnitude to the different levels of the pre-pulse sounds alone preceded by the background (53dB) was measured in *Abcc5*$^{-/-}$ and wild-type mice, for both females (Fig. 3.9a) and males (Fig. 3.9b).

Two-way ANOVA showed no significant genotype-dependent effect in females between *Abcc5*$^{-/-}$ and wild-type mice ($F_{1,30}$ =0.018, p=0.9) in responding to different pre-pulse sound levels tested alone (Fig. 3.9a). However, the responses to all pre-pulse levels in *Abcc5*$^{-/-}$ males were significantly higher than that in wild-type controls by a two-way ANOVA comparison ($F_{1,26}$ =8.69, p=0.0067) (Fig. 3.9b). Multiple comparison tests within each genotype group showed that reactivity of *Abcc5*$^{-/-}$ females to any tested pre-pulse sound level (56dB, 58dB or 65dB) were not significantly different than their response to background noise (53db) and on average equalled to 116±12, while wild-type females displayed increasing gradient in their responses to increasing sound levels over 56dB (Fig. 3.9a). Background response in wild-type females was 79.4±12.7, followed by 64.3±12.6, 153.7±12.9, and 161±11.9 for 56dB, 58dB and 65dB, respectively, with the significant difference between 53-56dB and 58-65dB responses (p<0.0001). Similarly, wild-type males show significantly higher responses to the 58dB and 65dB sounds level of 129.6±22 and 149.8±15.6, respectively, as compared to background 81±15.1 (p=0.022 and p<0.001, respectively), but not to the lowest pre-pulse level of 56dB (67.9±20). *Abcc5*$^{-/-}$ males instead follow the trend of the knockout females, showing no significant gradient response to 58dB or 65dB (175.9±20.8 and 162.2±12, respectively) when compared to the background (148.5±16.4), but unlike females and their wild-type controls – display significant reactivity to the lowest pre-pulse level of 56dB (198.4±22.9) vs background (p=0.009). In summary, it would appear that wild-type animals can distinguish sounds louder than 56dB and display a clear increase in response to 58dB and 65dB when compared to a

53dB background. Knockout mice, on the other hand, showed an equal degree of reactivity throughout in response to 53-65dB pulses.

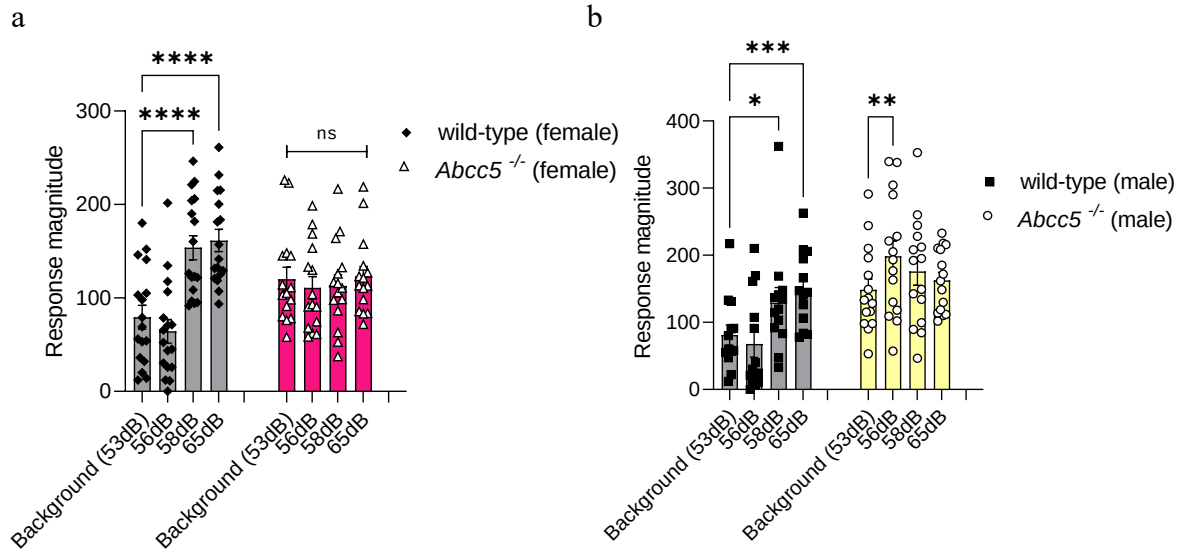


Figure 3.9. Reactivity of *Abcc5*$^{-/-}$ and wild-type controls to pre-pulse sounds alone vs background.

The magnitude of the response (arbitrary units) to the background noise (53dB) and three different pre-pulse levels alone (56, 58, 65dB) in *Abcc5*$^{-/-}$ and wild-type mice, in females (a) and males (b). Data presented as mean ± SEM, each data point representing an average of 10 measurements from a single mouse (females, n_{ko}=17, n_{wt}=15; males, n_{ko}=15, n_{wt}=12), results were compared by two-way ANOVA with Bonferroni's multiple comparison tests; p<0.05*, p<0.01**, p<0.001***, p<0.0001****

3.2.4 *Abcc5*$^{-/-}$ mice display abnormal marble burying distribution patterns

The marble burying assay utilises the natural drive of mice for digging behaviour that can be used to measure anxiety level or repetitive behaviour. The marble burying test was performed in females (n_{ko}=15, n_{wt}=18) and males (n_{ko}=14, n_{wt}=13) of *Abcc5*$^{-/-}$ (ko) mice and wild-type litter mate controls (wt). No difference was observed in the average number of buried marbles between the genotypes within a female or male group (Fig. 3.10a and 3.10c) as analysed by a

non-parametric two-tailed Mann-Whitney test. However, plotting the percentage of the frequency distribution of the buried marbles revealed an abnormal pattern of marble burying distribution in *Abcc5*$^{-/-}$ mice, in both the female and male groups (Fig. 3.10b and 3.10d). While wild-type distribution of buried marbles, for both females and males, appears to follow a normal distribution pattern [116] with the most frequently buried 7-8 marbles out of 9 (46 and 44% of mice, respectively for male and female), *Abcc5*$^{-/-}$ male mice tend to bury most frequently 8-9 marbles (50% mice), and females exhibit a steady distribution of 26% of the cohort burying between 6 and 9 marbles.

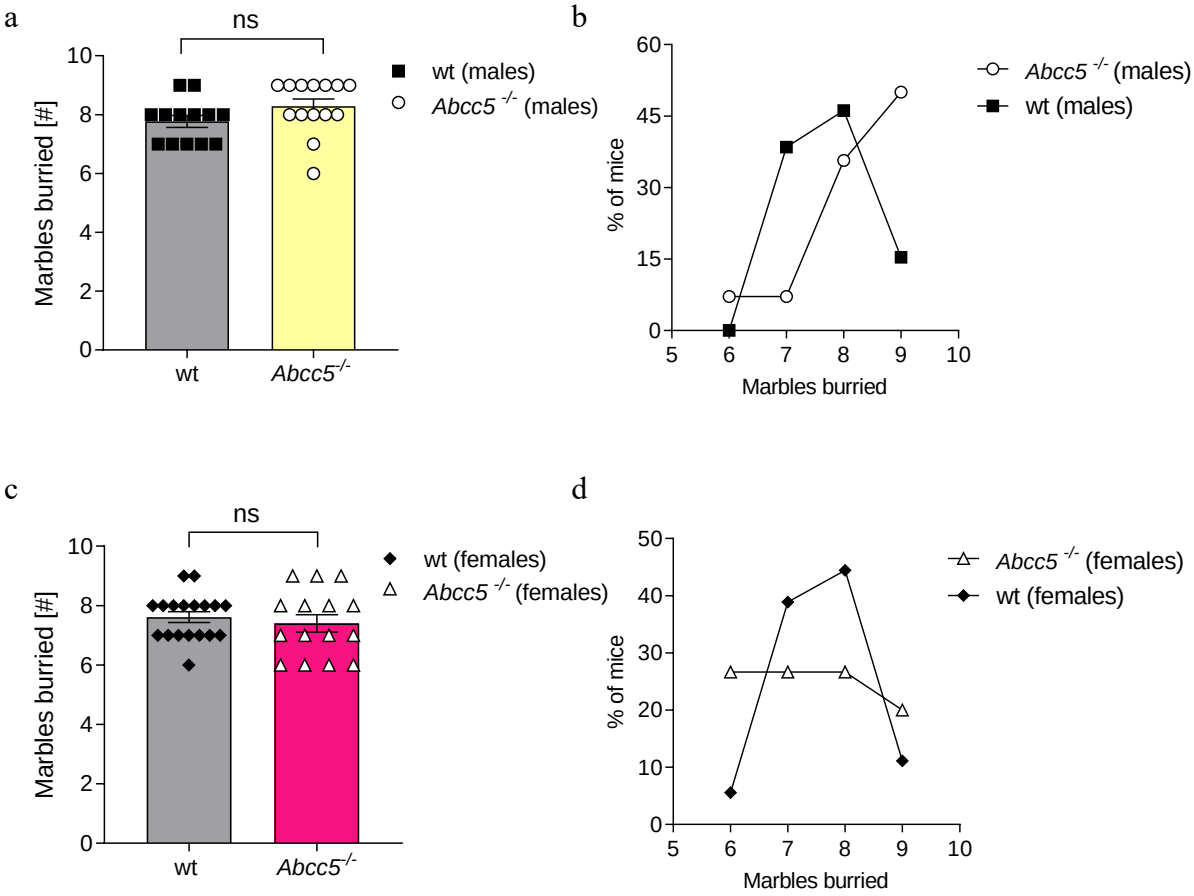


Figure 3.10. Marble burying assay in *Abcc5*$^{-/-}$ mice and wild-type littermate controls.

Total number of buried marbles between *Abcc5*$^{-/-}$ mice and wild-type controls in a) females (n_{ko}=15, n_{wt}=18) and c) males (n_{ko}=14, n_{wt}=13). Visual comparison of the frequency distribution pattern of the number of marbles buried by the percentage of mice in the tested cohort in *Abcc5*$^{-/-}$ mice and wild-type

controls for b) females and d) males. Bar graph results are shown as mean±SEM, each data point represents a marble score from an individual mouse (a&b) or percentage of mice (c&d). Data were analysed using non-parametric two-tailed Mann-Whitney, ns (no significance).

3.2.5 *Abcc5*$^{-/-}$ mice retain learning ability in fear conditioning trial

A fear conditioning (FC) test was conducted on 16 weeks old *Abcc5*$^{-/-}$ mice (female, n_{ko}=15; male, n_{ko}=15) and corresponding wild-type litter mate controls (female, n_{wt}=17; male, n_{wt}=13) (Fig. 3.11, 3.12, 3.13). The graphical flowchart and an overview of the fear conditioning protocol applied are shown in Fig. 3.11a, 3.12a, and 3.13a (left side panel). In principle, during the conditioning trial (Fig. 3.11a) mice exhibit an increased percentage of freezing, defined as the amount of time when they are completely immobile, in response to aversive, unconditioned stimulus (US; mild electric shock) that is applied directly on or after the conditioned stimulus (CS; loud acoustic tone). The percentage of freezing time before and after foot-shock was calculated and plotted for each mouse.

The level of baseline, pre-US freezing for *Abcc5*$^{-/-}$ and wild-type mice was 4.9±1.4% vs 5.7±1.0%, respectively, in females (Fig. 3.11b), and 4.1±1.1% vs 9.3±2.1% in males (Fig. 3.11c). Freezing after foot-shock (post-US) increased to 11.6±3.2% vs 16±2.9% and 11.4±2.1% vs 17.6±2.9% in *Abcc5*$^{-/-}$ vs wild-type females and males, respectively. The difference in freezing before (pre-US) and after (post-US) electric shock was significant in females ($F_{1, 30}$ = 24.75, p<0.0001) (Fig. 3.11b) and males ($F_{1, 26}$ = 27.03, p<0.0001) (Fig. 3.11c). There was no significant effect of genotype observed between *Abcc5*$^{-/-}$ mice and wild-type in the level of freezing pre- and post-US. This suggests that mice of both genotypes responded the same to the fear conditioning training.

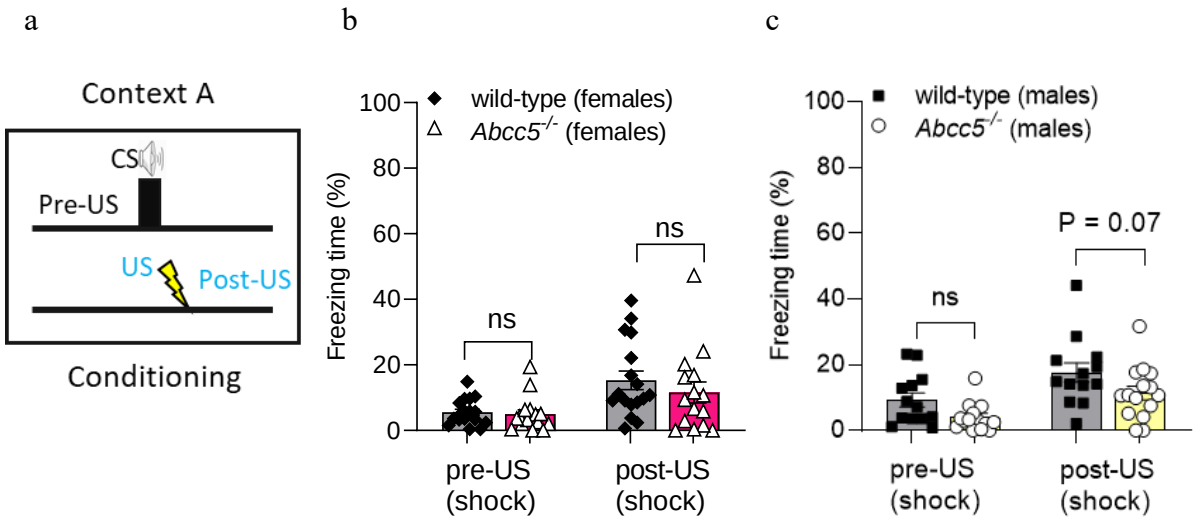


Figure 3.11. Fear conditioning trial in *Abcc5*$^{-/-}$ mice and wild-type controls.

a) Overview of conditioning by fear using auditory cue on Day 1. Percentage of freezing (%) during the conditioning trial session before (pre-US) and after (post-US) electric shock was applied to *Abcc5*$^{-/-}$ and wild-type mice for b) females (n_{wt}=15, n_{ko}=17) and (c) males, (n_{wt}=15, n_{ko}=13). Each data point represents a measurement from an individual mouse, bar graphs are mean±SEM. Data were analysed using two-way ANOVA followed by multiple comparison Sidak tests; ns (no significance), p<0.05*, p<0.01**, p<0.001***, p<0.0001****

3.2.6 Knock-out of *Abcc5* gene does not affect contextual fear

Contextual fear (Fig. 3.12a) was measured the following day (Day 2) by placing mice in the same cages as for the conditioning trial and left to explore freely without any disturbance. This test assesses the contextual fear triggered by the memory of an unpleasant experience from 24hr before in the same settings (Fig. 3.12a). The multiple two-way ANOVA showed no significant differences between *Abcc5*$^{-/-}$ mice and wild-type controls in the percentage of freezing during the test, for both females (Fig. 3.12b) and males (Fig. 3.12c). This suggests that the lack of *Abcc5* does not change contextual fear intensity. The average contextual freezing of *Abcc5*$^{-/-}$ vs wild-type mice was 24.1%±3.6 vs 21.4%±2.4 for females, and 18.1%±2.4 vs

12.3%±2.3 for males. This was significantly different for both genotypes and sexes when compared to the baseline freezing level from the previous day (pre-US freezing levels during conditioning on Day 1). Two-way ANOVA showed high significance for females ($F_{1,30}$=72.79, p<0.0001) and males ($F_{1,26}$=28.38, p<0.0001). There was no genotype-related effect on the specificity of contextual fear in females ($F_{1,30}$=0.178, P=0.67) or males ($F_{1,26}$=0.014, p=0.91), meaning that the increase in freezing between Day 1 and Day 2 is independent of the genotype.

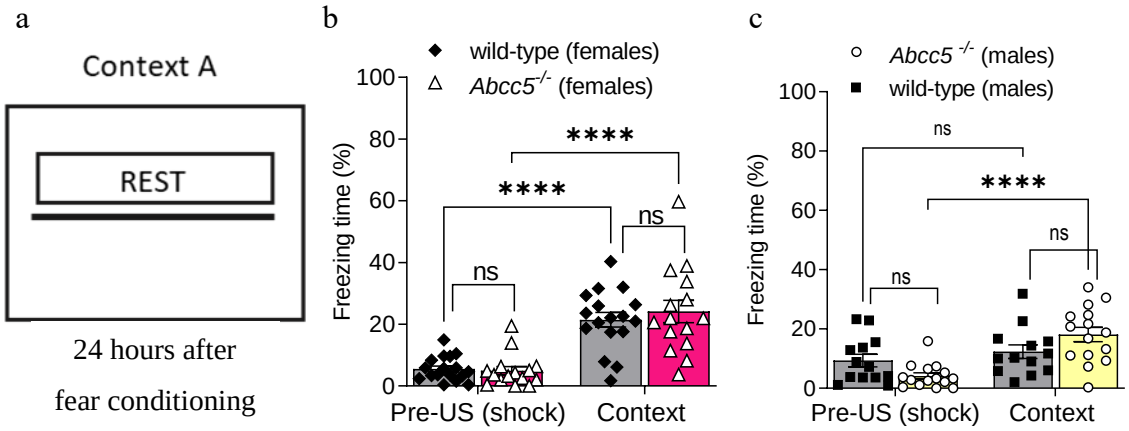


Figure 3.12 Percentage of freezing during contextual test.

24hr after conditioning in the same testing chambers tested on the same cohort of mice as in Fig. 3.11. a) Overview of the test. Contextual fear in *Abcc5*$^{-/-}$ and wild-type (b) females and (c) males was expressed as a percentage of total test time. Baseline freezing preceding the US (foot shock) from the day before as shown in (Fig. 3.11b & 3.11c). Each data point represents a measurement from an individual mouse, bar graphs are mean±SEM. Data were analysed using two-way ANOVA followed by multiple comparison Sidak tests; ns (no significance), p<0.05*, p<0.01**, p<0.001***, p<0.0001****

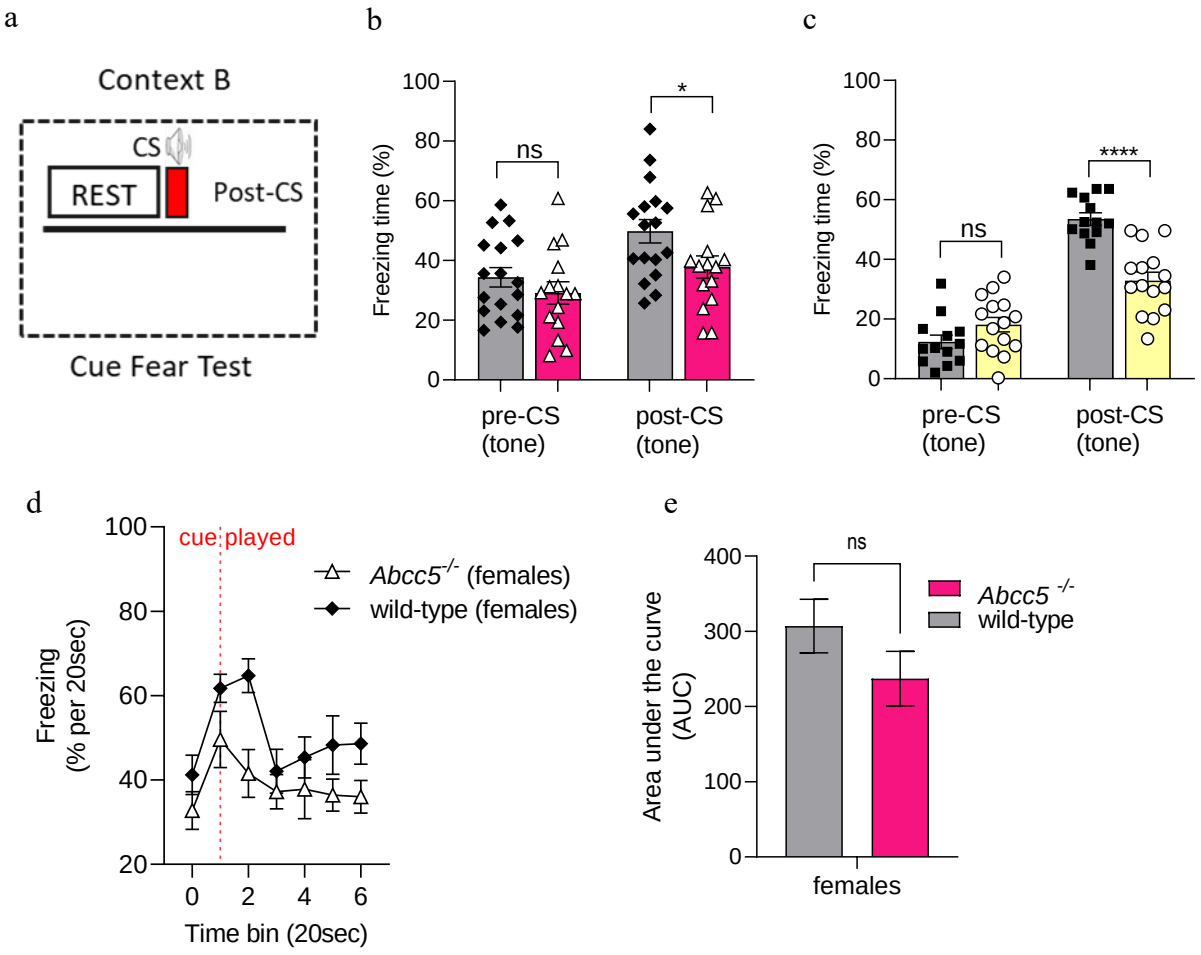
3.2.7 *Abcc5* gene plays a role in the expression of acquired fear in auditory-cued test

Fear memory recall was assessed during an auditory cued fear test, 4hr after the contextual fear test. Here, mice were exposed to a new cage (Context B), which was visually different from previous tests. After a period of acclimatisation (pre-CS), a cue, which was the same as the conditioning stimulus (CS, loud tone) was played (post-CS) (Fig. 3.13a). The average percentage of freezing pre-CS for *Abcc5*$^{-/-}$ vs wild-type mice was 29.1±3.7% vs 35.6±3.3%, in females, respectively (Fig. 3.13b), and 31.8±3.3% vs 41.9±3.2% in males (Fig. 3.13c), while it increased for each group to the following levels post-CS 37.8±3.7% vs 50.8±3.9% for *Abcc5*$^{-/-}$ vs wild-type in females, and 32.9±2.8% vs 53.5±2.1% for *Abcc5*$^{-/-}$ vs wild-type in males (Fig. 3.13b and 3.13c). Two-way ANOVA revealed a significant general effect of the cue (tone) presentation in females ($F_{1,30}$ =29.54, p<0.0001) and males ($F_{1,26}$ =115.9, p=0.0001) in both genotypes. This result indicates that both sexes of both genotypes formed an auditory-cued fear memory and were able to re-call it.

Abcc5$^{-/-}$ mice, females and males, however, freeze less as a reaction to the auditory cue (post-CS) than wild-type controls. *Abcc5*$^{-/-}$ males built significantly weaker tone-shock association than their wild-type controls ($F_{1,26}$ =10, p=0.004) (Fig. 3.13c), while a similar trend was also observed in *Abcc5*$^{-/-}$ females ($F_{1,30}$ =3.34, p=0.07) (Fig. 3.13b). The main difference between *Abcc5*$^{-/-}$ mice and wild-type controls, for both females and males as shown by multiple comparison tests, is driven by the changes in the level of freezing post-cue. *Abcc5*$^{-/-}$ mice freeze significantly less than their wild-type counterparts. *Abcc5*$^{-/-}$ mice response to the auditory cue was on average 12.0±5.5% lower than wild-types for females, and 20.6±3.6% for males (Fig. 3.13b and 3.13c, post-CS).

The tone cue (CS) is played in the middle of the test. Before that mice are allowed to explore the new cage (Context B). To separate the auditory fear from the general fear and fear of the

new cage (Context B), the auditory cued fear was calculated as per [117]. Data were plotted as the percentage of freezing in 20sec time-bins, 20sec time-bin freezing directly preceding the cue (loud tone) marked with a red line was used as a baseline (Fig. 3.13d and 3.13f) The baseline percentage of freezing was taken at 20 seconds intervals directly preceding the loud tone, but after the period of acclimatisation to avoid general or contextual fear contamination. The area under the curve (AUC) showed a significant difference in response to auditory cues in males between *Abcc5*$^{-/-}$ mice and their wild-type controls (t-test, p=0.01) (Fig. 3.13g), but the difference in females didn't show statistical significance, yet followed the same trend (p=0.16) (Fig. 3.13e).



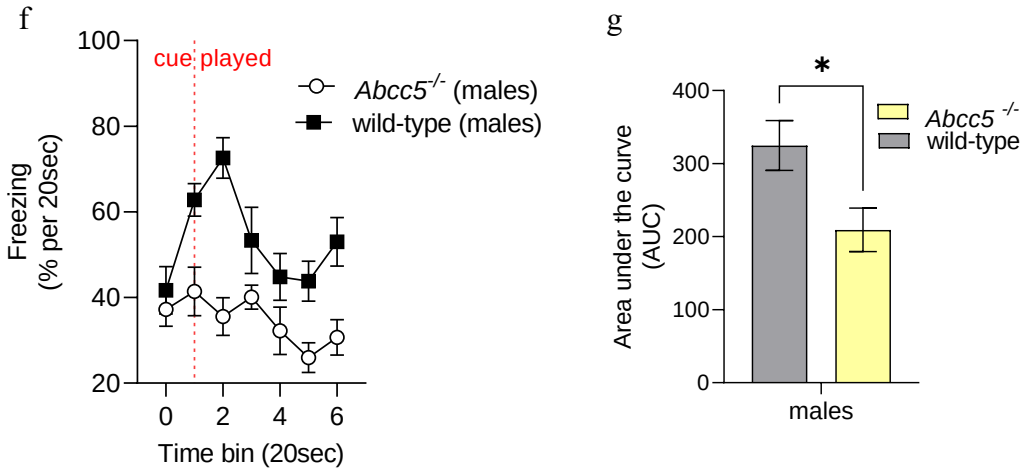


Figure 3.13 *Abcc5*$^{-/-}$ mice show less freezing in cued fear conditioning.

a) Overview of the cued fear test performed 4hr after the contextual fear test. Mice are presented with a loud tone in the new context B and their % of freezing was measured before the tone was played (pre-CS) and after (post-CS) in (b) females and (c) males. Percentage of freezing normalised to freezing level in 20sec directly preceding the acoustic cue (red line – cue played) plotted in (d) for females and (f) males. Corresponding analysis of area under the curve (AUC) is shown in (e) for females and (g) males. The time of freezing in bar graphs in (b & c) is expressed as a percentage mean±SEM of total time. Each data point represents a measurement from an individual mouse (b-c) or an average of n mice numbers per genotype ± SEM (d & f). For bar graphs (b & c) Data were analysed using two-way ANOVA followed by multiple comparison Sidak test; (e & g) AUC bar graph was analysed by Student's t-test; ns (no significance), $p<0.05$*, $p<0.01$**, $p<0.001$***, $p<0.0001$****

3.2.8 No change in grip strength

PPI and FC output, both rely on muscle contraction. The *in vivo* function of the muscle was assessed by testing the grip strength in *Abcc5*$^{-/-}$ mice and wild-type littermate controls. Forelimb strength and combined forelimb and hindlimb strength was measured and normalised to the weight of an animal. No change was found in the grip strength of forelimbs between *Abcc5*$^{-/-}$ mice and wild-type controls in females (3.2±0.6 vs 2.9±0.1) or males (2.6±0.2 vs 2.6±0.2) (Fig. 3.14a and 3.14b, respectively). Combined grip strength of forelimb and hindlimbs also revealed no significant changes in females (2.6±0.2 vs 2.2±0.1) or males (2.5±0.2 vs 2.5±0.3) regardless of the genotype (Fig. 3.14c and 3.14d).

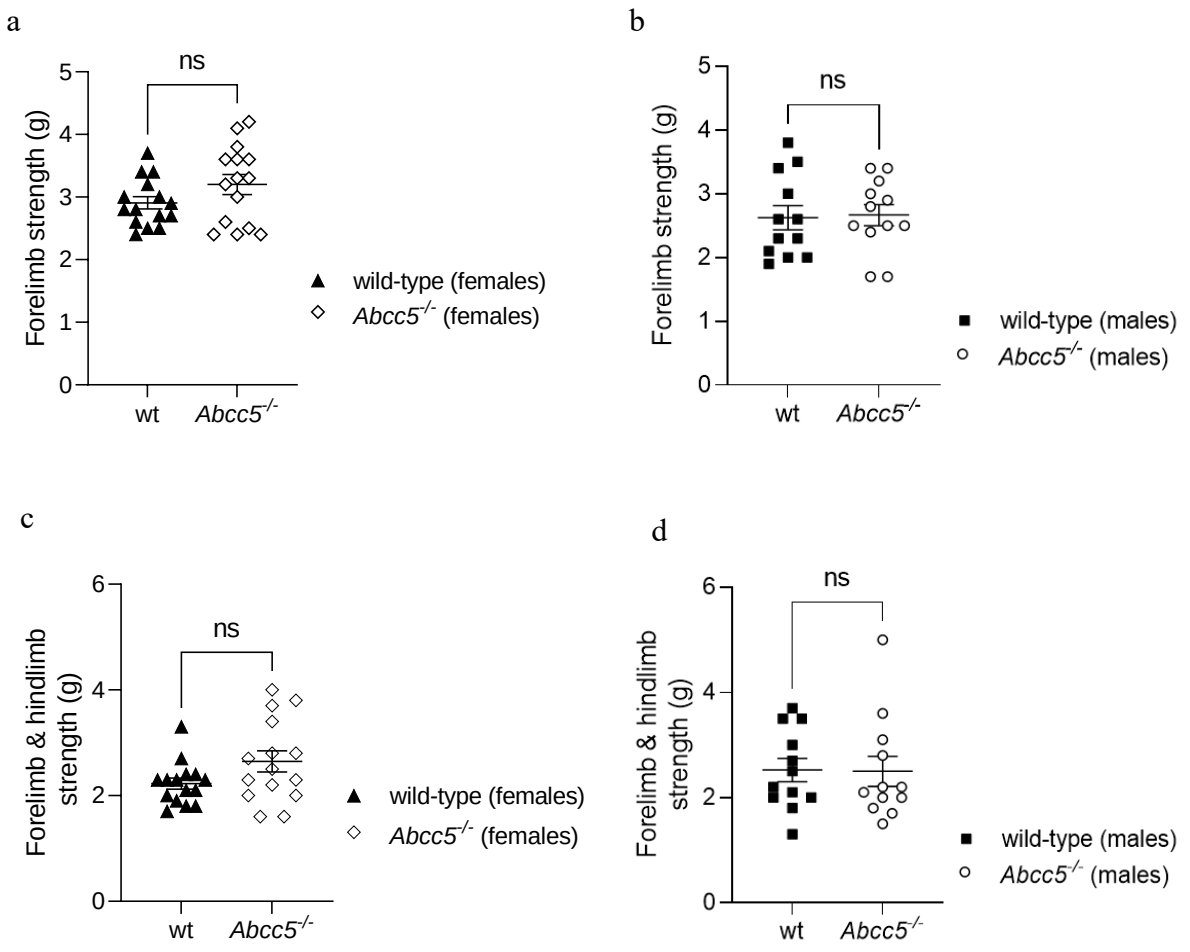


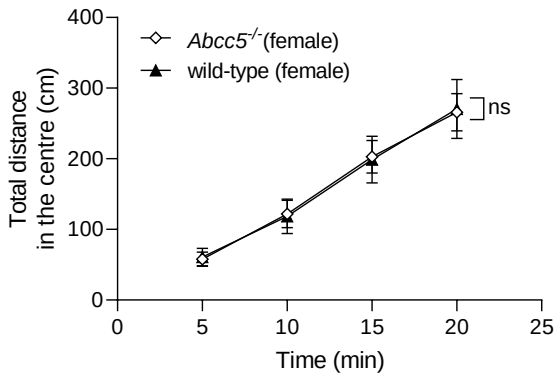
Figure 3.14. No change in grip strength of Abcc5$^{-/-}$ mice as compared to wild-types

Forelimb (a & b) and combined forelimb and hindlimb grip strength (c & d) for knock-out and wild-type mice, (a & c) females (n_{wt}=15, n_{ko}=15) and (b & d) males (n_{wt} =12, n_{ko} =12) expressed in grams (g). Each data point represents an average of 3 measurements from a single mouse, mean±SEM. Data were analysed using Student's t-test; ns (no significance), p<0.05*, p<0.01**, p<0.001***, p<0.0001****

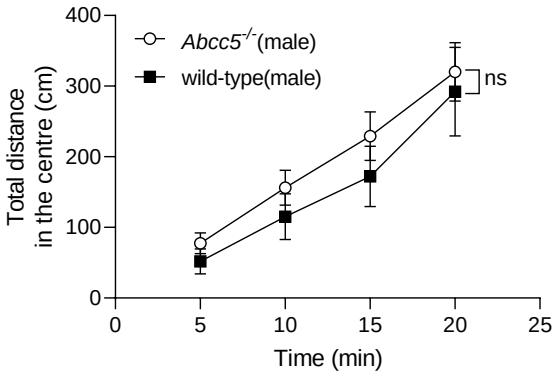
3.2.9 Absence of *Abcc5* has no effect in open field locomotor activity

An open field test was performed on 10-week-old *Abcc5*$^{-/-}$ mice and wild-type controls, both females (n_{ko}=15, n_{wt}=15) and males (n_{ko}=12, n_{wt} =12). The test lasted 20min and was performed only once per mouse. The analysis of the parameters of anxiety-like or exploratory behaviour found no significant differences between the genotypes of both sexes. The distance travelled within 20mins in the centre of the arena measured for *Abcc5*$^{-/-}$ and wild-type was 265±26cm vs 270±41cm, respectively in females (Fig. 3.15a), and 320±41cm vs 292±62cm in males (Fig. 3.15b). The number of entries into the centre of the arena was not significantly different for *Abcc5*$^{-/-}$ and wild-type and averaged at 21.7±2.2 vs 18.6±2.6 in females (Fig. 3.15c), and 22.6±2.5 vs 24.8±4.6 in males (Fig. 3.15d). Similarly, total time spent by mice in the centre of the arena showed no difference between the genotypes in females (*Abcc5*$^{-/-}$ vs wild-type) 28.7±4.1s vs 25.7±4.9s (Fig. 3.15e), or males, 27.8±4.3s vs 27.8±6.6s (Fig. 3.15f), respectively. To assess the general locomotor activity of *Abcc5*$^{-/-}$ mice, total distance travelled in the whole arena throughout the 20mins of the test was compared to the wild types. There was no change between *Abcc5*$^{-/-}$ mice and their controls, for both females (5447±229cm vs 4710±238cm) and males (5472±231cm vs 5372±210cm) (Fig. 3.15g and 3.15h, respectively). Only a small change was observed in the average speed of *Abcc5*$^{-/-}$ females being higher than that of wild-types, 18.2±0.7cm/s vs 15.7±0.8cm/s, (p=0.03, t-test) (Fig. 3.15i), however, no change was observed in males, 18.3±0.8cm/s vs 17.9±0.7cm/s (Fig. 3.15j).

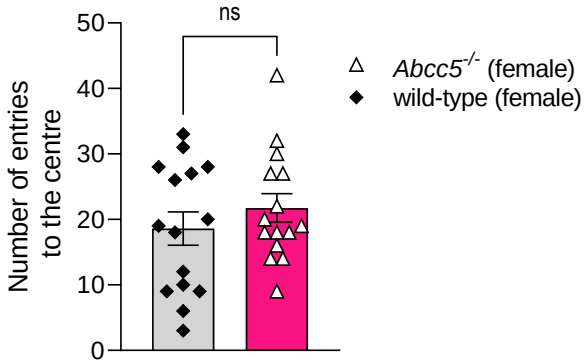
a


Abcc5-/-(female)
wild-type (female)
Total distance in the centre (cm)
Time (min)
ns

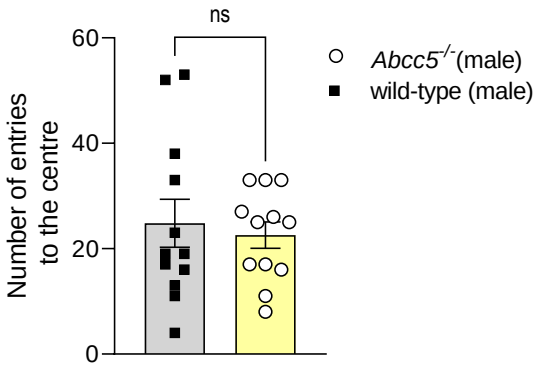
b


Abcc5-/-(male)
wild-type(male)
Total distance in the centre (cm)
Time (min)
ns

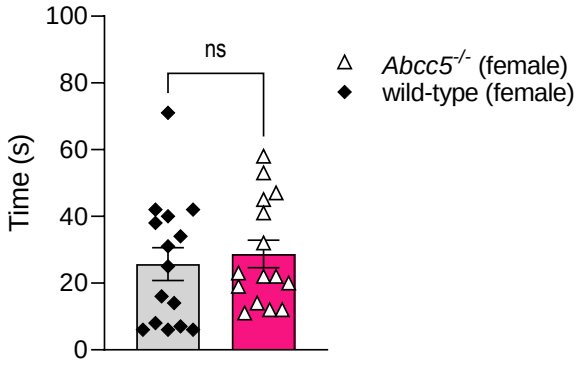
c


Abcc5-/- (female)
wild-type (female)
Number of entries to the centre
ns

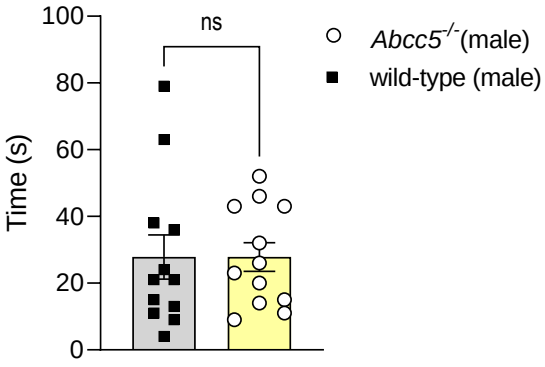
d


Abcc5-/-(male)
wild-type (male)
Number of entries to the centre
ns

e


Abcc5-/- (female)
wild-type (female)
Time (s)
ns

f


Abcc5-/-(male)
wild-type (male)
Time (s)
ns

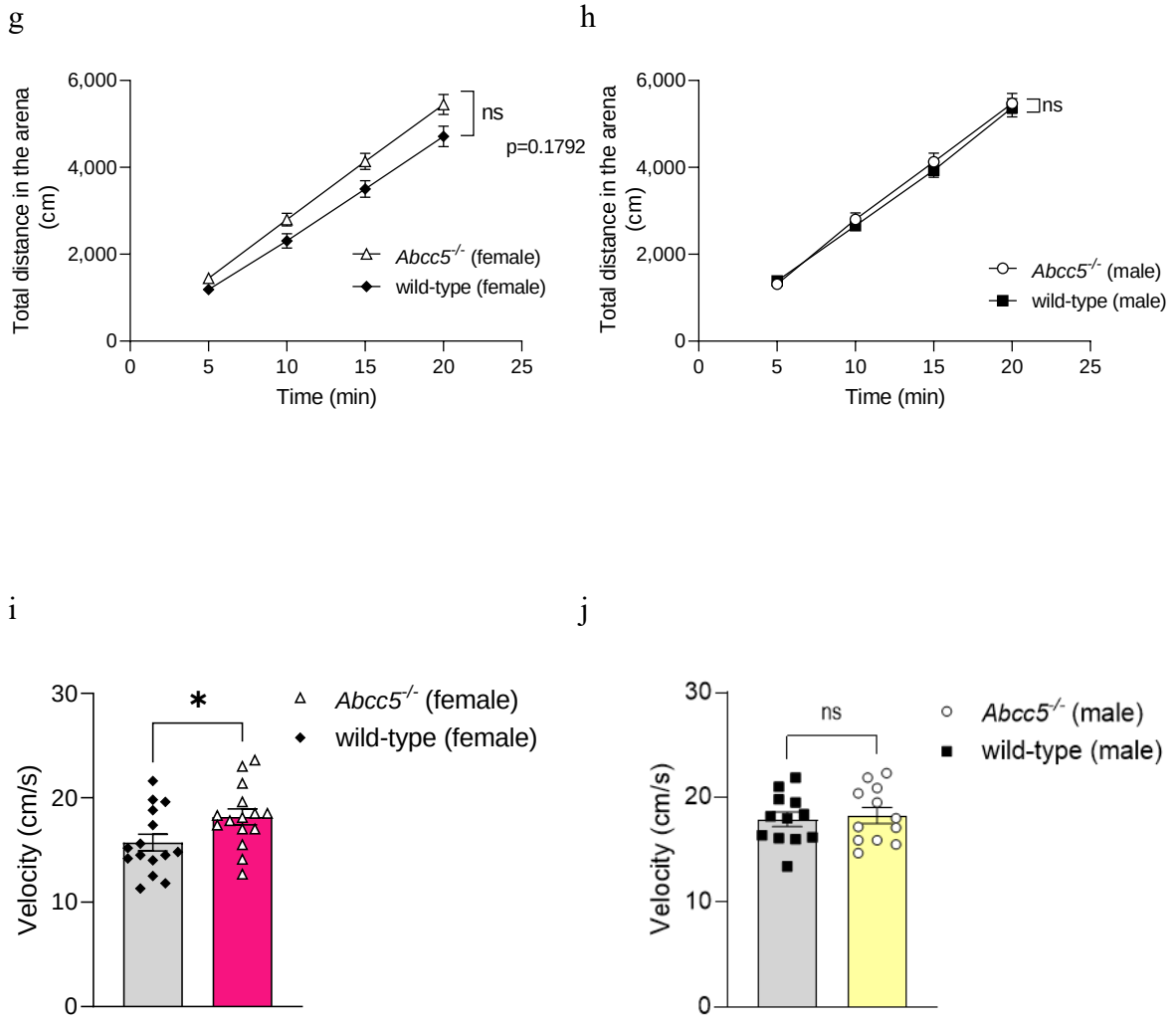


Figure 3.15. Open field test of Abcc5$^{-/-}$ mice show no change in anxiety-like behaviour or general locomotor activity.

Distance (cm) travelled in the centre of the open field arena plotted as a cumulative function of the time in 5min time-bins for Abcc5$^{-/-}$ mice and wild-type controls, a) females (n_{wt} =15, n_{ko} =15) and b) males (n_{wt} =12, n_{ko} =12). The total number of entries into the centre of the arena is shown in c) females and d) males. Total time spent in the centre of the arena within 20 minutes duration of the test for e) females and f) males. Total distance (cm) travelled in the whole arena plotted as a cumulative function of the time in 5min time-bins in g) females and h) males of both genotypes. The velocity of movement (cm/s) in the whole arena of i) females and j) males. Each data point represents a single mouse ± SEM (c-f & i-j). Each point is a mean from n number of mice ± SEM (a-b & g-h). The area under the curve was

analysed by Student's t-test. Data were analysed using Student's t-test; ns (no significance), $p<0.05$*, $p<0.01$**, $p<0.001$***, $p<0.0001$****

3.2.10 *Abcc5*$^{-/-}$ females display enhanced exploratory behaviour in Y-maze assay

Due to technical constraints, the Y-maze test was performed only on females in this study ($n_{ko}=6$, $n_{wt}=6$). *Abcc5*$^{-/-}$ females and wild-type litter mate controls were first subjected to a habituation phase of the Y-maze test. There, mice were placed in Y-maze with only two arms available (Start Arm and Familiar Arm), with the third arm (Novel Arm) closed off for the duration of the test. No significant difference was found between the knock-out mice and wild-type in the preference for any arm with two-way ANOVA ($F_{1,10}=0.29$, $p=0.6$) (Fig. 3.16a). Both genotypes, *Abcc5*$^{-/-}$ vs wild-type, respectively, split their time equally between Start Arm (44.5±2.1% vs 44.1±4.1%) and Familiar Arm (41.5±2.2% vs 43.2±3.8%).

During the experimental phase, mice were placed again in the Y-maze, this time with all 3 arms available for exploration (Fig. 3.16b). Two-way ANOVA showed no significant difference ($F_{1,10}=0.17$, $p=0.68$) between *Abcc5*$^{-/-}$ and wild-type females in the percentage of time spent preferably in any arms. The multiple comparisons, however, revealed that in the wild-type group percentage of time spent in the Novel Arm (32.4±4.1%) was not significantly higher than in Start Arm (31±7.2%) or Familiar Arm (22±2.6%), while *Abcc5*$^{-/-}$ females spent significantly more time in the Novel Arm (40.9±2.4%) compared to the Start Arm (23.5±2.8%, $p=0.015$) or the Familiar Arm (19.5±2.8%, $p=0.0025$).

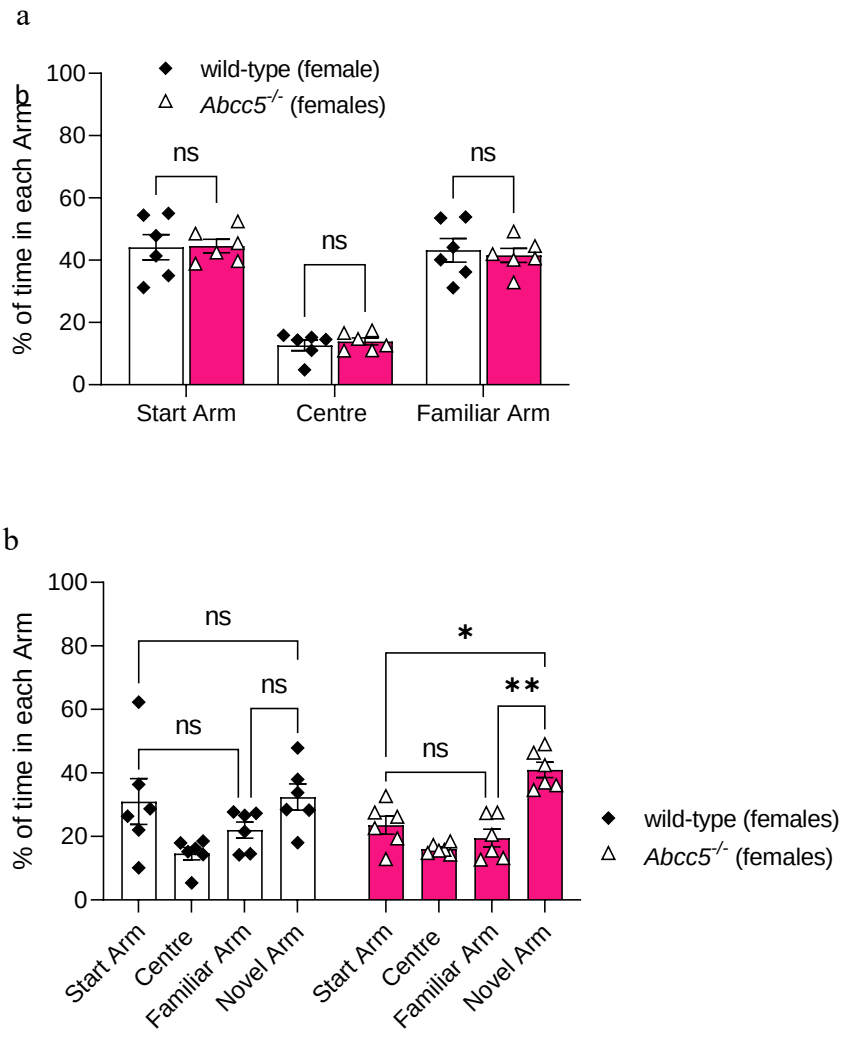


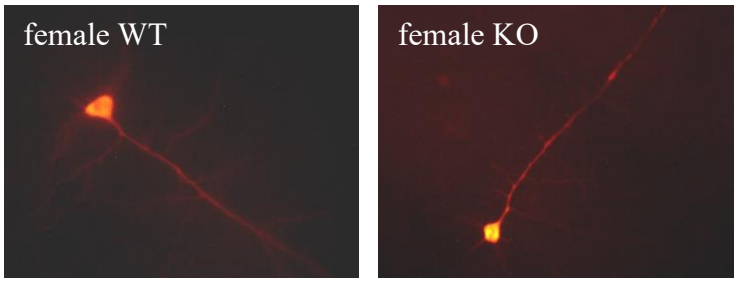
Figure 3.16 Exploratory behaviours of *Abcc5*$^{-/-}$ females and controls assessed by Y-maze.

Percentage of time spent by *Abcc5*$^{-/-}$ females or wild-type controls (n_{wt}=6, n_{ko}=6) a) during the habituation phase of the test in each of the two arms and the centre of Y-maze. b) Percentage of time spent by the same female mice during the Y-maze exploration experiment in each of the three arms of the Y-maze where the newly open arm is novel to the mice. Bar graphs show mean±SEM, while each data point represents a single mouse. Data were analysed using two-way ANOVA followed by multiple comparison Tukey's test; ns (no significance), p<0.05*, p<0.01**, p<0.001***, p<0.0001****

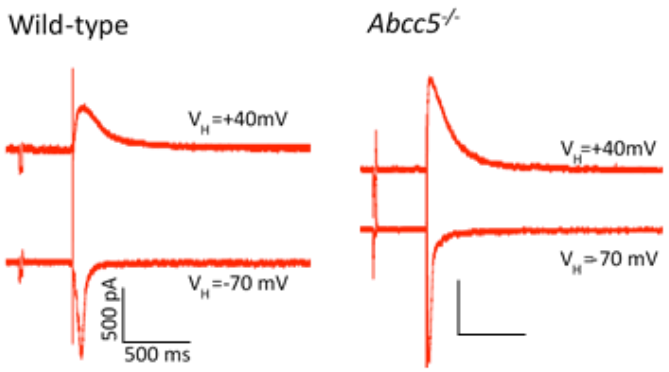
3.2.11 *Abcc5*$^{-/-}$ mice behavioural phenotype is driven by NMDA receptor transmission

Previous studies have identified that lack of Abcc5 transporter causes accumulation of various glutamate analogues *in vivo* in the brains of *Abcc5*$^{-/-}$ mice. Most notably the neuropeptide NAAG was found to be increased 2.4-fold in the absence of Abcc5 [31]. Main role of NAAG in the brain is to protect neurons from excitotoxicity caused by excessive glutamate transmission, which is mediated mainly by ionotropic glutamate-gated ion channels, AMPA and NMDA receptors [38]. Additionally, loss of pre-pulse inhibition which was the strongest behavioural trait observed in *Abcc5*$^{-/-}$ mice, is also mediated by reduced function of NMDA receptor [96, 97]. In order to investigate the function of AMPA and NMDA receptors in *Abcc5*$^{-/-}$ mice, the electrophysiological recordings were made from pyramidal neurons located in the frontal cortex of fresh brain slices isolated from *Abcc5*$^{-/-}$ mice and wild-type controls. These data were generated by Dr Natascia Vedovato and presented with permission. The electrophysiological recordings were made from 10-15 neurons per each group (sex and genotype). The calculated ratios of AMPAR/NMDAR (A/N) peak amplitude currents show that the electrical activity of the *Abcc5*$^{-/-}$ mice brains is substantially affected by the lack of the *Abcc5* gene in both, females and males of *Abcc5*$^{-/-}$ mice relative to their wild-type controls (Fig. 3.17c).

a



b



c

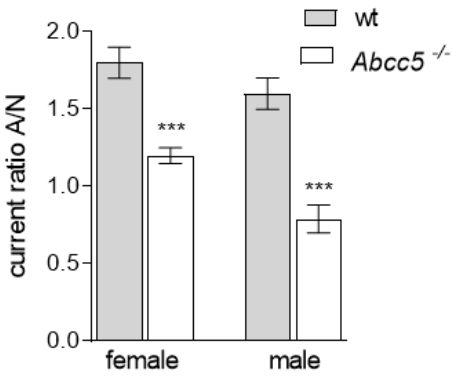


Figure 3.17. Lack of *Abcc5* affects the glutamatergic signalling in neurons via AMPAR/NMDAR.

a) Representative picture of biotin-labelled pyramidal neurons from the frontal cortex of brain slices isolated from wild-type (left) and *Abcc5*$^{-/-}$ female that was used for the whole-cell voltage-clamp recordings b) Representative traces of AMPAR (V_h=-70mV) and NMDAR (V_h=+40mV) current responses to a fixed stimulus recorded from pyramidal neurons from wild-type (wt) and *Abcc5*$^{-/-}$ mice c) Summary of AMPAR/NMDAR peak current ratios for *Abcc5*$^{-/-}$ and wild-type controls, females and males, respectively. Data presented as bar graph mean±SEM, calculated from 4-10 cells per mouse, from at least 3 mice per each genotype/sex. Data were analysed by Student's t-test; ns (no significance), p<0.05*, p<0.01**, p<0.001***, p<0.0001****

3.3 Discussion

3.3.1 Locomotor activity is not affected by *Abcc5 k*nockout in Open field test

We previously reported that the *Abcc5*$^{-/-}$ mice on a C57BL/6N background were more physically active relative to wild-type controls [4]. Surprisingly, no significant differences were observed in an open field test from this study. The distance travelled by *Abcc5*$^{-/-}$ mice in the whole arena was the same as the wild-type, but *Abcc5*$^{-/-}$ females demonstrated a marginally higher velocity relative to their wild-type counterparts whereas no difference in velocity was observed in males *Abcc5*$^{-/-}$. In our previous work, differences in activity of *Abcc5*$^{-/-}$ mice relative to wild-type controls emerged from monitoring over 24hrs [4]. It could be that the 20min duration of the test was not sufficiently long to fully assess the locomotor activity in *Abcc5*$^{-/-}$ mice. We also reported previously that *Abcc5*$^{-/-}$ mice of both sexes display metabolically lean phenotype and have lower adipose tissue depots than wild-type mice, as measured by Echo-MRI and at post-mortem [4]. To ascertain that the weight differences in *Abcc5*$^{-/-}$ mice did not affect muscle function, we confirmed that the grip strength between *Abcc5*$^{-/-}$ and wild-type mice was unchanged. *Abcc5*$^{-/-}$ mice have a normal grip of the hind and forelimbs, hence their performance in tests requiring muscle contraction (ASR/PPI/FC) was not due to their weight change.

3.3.2 *Abcc5 k*nockout phenotype is not anxiety-related

The open field test and marble burying assay are indicative of anxiety levels, among other outputs [118, 119]. No differences were observed between *Abcc5*$^{-/-}$ and wild-type mice in the open field test or marble burying assay, suggesting that differences in anxiety levels should not affect other behavioural tests, such as fear conditioning. The distribution frequency of buried marbles displays an increasing trend in *Abcc5*$^{-/-}$ male mice when compared with the wild-type group, but the significance of this finding is unclear. The conclusion on this assay is difficult

to make as the number of marbles presented to the mice appeared to be a limiting factor [116]. Increasing the pool of marbles or shortening the time of the test will provide a greater resolution of the test to discern any subtle trait differences between *Abcc5*$^{-/-}$ compared to the control groups.

3.3.3 Increased amplitude of ASR

Interestingly, male *Abcc5*$^{-/-}$ mice exhibited a significantly exaggerated ASR to the startling sound of 120dB as measured by the ASR amplitude, which was also the trend observed in the female *Abcc5*$^{-/-}$ cohorts (Fig. 3.6a-b). The amplitude of ASR response is sex-dependent for some mice strains, and in female mice of C57BL/6J background, it was found to be generally lower than that observed in male mice [105]. It may be that subtle differences in ASR between the *Abcc5*$^{-/-}$ females and their wild-type controls were confounded by the lower sensitivity of ASR measurements in the female cohorts.

While *Abcc5*$^{-/-}$ males as a group exhibit a significantly higher acoustic startle, there was a level of heterogenicity observed within the *Abcc5*$^{-/-}$ mice group of both sexes relative to wild-type cohorts, which showed more homogenous ASR responses (Fig. 3.7a-d). Some of *Abcc5*$^{-/-}$ males and females were 'high-responders', mice that exhibited an ultra-high amplitude of ASR response, which was above the highest responses recorded from wild-types. Experimentally, the ASR measurements are prone to two opposite effects caused by the repetition of a stimulus. One is sensitization, when the amplitude of ASR gradually increases with stimulus repetition during the experiment, and the second effect is known as habituation when a gradual decrease of ASR amplitude is observed [79].

In this study, the ASR response from each mouse was measured in 10 separate repeats, which were intertwined with the combination of other paired pulses of sounds that were played in pseudorandom order, different for each batch of mice tested. This approach was employed to minimise the habituation effect, which has been shown to be more common in mice than

sensitization [79]. The extent of short-term habituation also depends on the strain of mice. C57BL/6J mice are closely related to C57BL/6NTac used in this study and are quite resistant to the habituation effect [84]. The limited data on C57BL/6NTac sub-strains showed that only wild-type females are more prone to habituation [120]. It is then highly unlikely that the increased amplitude of ASR response in *Abcc5*$^{-/-}$ mice compared to the wild-type was due to a higher habituation rate in the control wild-type mice. It is possible that *Abcc5*$^{-/-}$ mice experience sensitization and therefore show enhancement of the ASR with each repeat of the stimulus. The method employed here, however, should minimise the ASR sensitization effect to the same extent as the habituation effect. Further measurements of ASR response in consecutive order might be advantageous to address this question.

Overall, the results suggest that loss of the *Abcc5* gene causes increased ASR response in mice and implicates *Abcc5* gene to have a role in the neuronal pathways involved in the ASR. Importantly, this effect extends further to the modulation of these pathways involved in pre-pulse inhibition (PPI) expression.

3.3.4 Loss of PPI

Male and female *Abcc5*$^{-/-}$ mice exhibit a significant loss of PPI (Fig. 3.7a-b). The loss of PPI response was observed at all three tested pre-pulse levels, namely, 56, 58 and 65dB. The level of PPI depends on the intensity of the pre-pulse, and the consensus of the PPI paradigm is that PPI increases with pre-pulse intensity and duration [99]. Consistent with this paradigm, both male and female wild-type mice display a marked increase in PPI percentage between the pre-pulse levels of 56dB vs 58dB and 56dB vs 65dB. Interestingly, while *Abcc5*$^{-/-}$ male mice showed a similar PPI pattern to wild-types, *Abcc5*$^{-/-}$ females displayed significant pre-pulse inhibition only at 65dB pre-pulse level and for lower pre-pulses, 56dB and 58dB, pre-pulse facilitation (PPF, negative PPI percentage) was more pronounced. For all tested groups, there was no change observed between pre-pulses 58dB and 65dB as it seems both of these pre-pulse

sounds were equally efficient and elicited maximal inhibition in mice of both sexes and genotypes.

Despite the expected trend of increasing PPI with increasing pre-pulse intensity, the overall percentage of PPI in *Abcc5*$^{-/-}$ mice was markedly lower than in the wild-type controls at pre-pulses 58dB and 65dB, and additionally 56dB in males. While the dramatic loss of PPI could result from severe hearing impairments, it is unlikely in the case of *Abcc5*$^{-/-}$ mice as this is usually accompanied by measurably lower ASR amplitudes in mice [85].

In contrast, *Abcc5*$^{-/-}$ mice showed higher ASR amplitudes than wild-type mice. Standard IMPC screening done at MRC Harwell also revealed that *Abcc5*$^{-/-}$ mice have normal hearing sensitivity as measured using the auditory-evoked brainstem response (ABR) threshold [53].

The relationship between ASR, PPI and ABR is, however, very complex. Studies performed on the adult mice of the C57BL/6J strain have shown that the central auditory system exhibits certain plasticity in response to partial damage of peripheral auditory input. Mice exposed to noise-induced damage of the peripheral auditory system paradoxically display increased ASR amplitudes, and are hyperactive to loud sounds, but show nearly normal behavioural sound detection thresholds (conditioned response to sound was normal) [121]. There is no evidence that *Abcc5* gene underlies peripheral hearing damage to trigger these compensatory mechanisms. Sensorineural cochlear degeneration can also occur with age. The age-related hearing impairment when high-frequency (>20kHz) sounds become less noticeable in older age contributes to complete loss of PPI even at the highest pre-pulse intensity of 80dB [75]. In C57 mice, this effect was the most pronounced in mice older than >5 months [122]. The assessment of PPI in *Abcc5*$^{-/-}$ mice was performed at the age of 14 weeks. At the same age, *Abcc5*$^{-/-}$ mice hearing was confirmed as normal by the ABR threshold method for frequencies ranging from 6-30kHz and the click-evoked ABR threshold was 40dB – the same as for wild-type mice [53]. Taken together, it is unlikely that abnormalities in ASR/PPI observed in *Abcc5*$^{-}$

$^{-/-}$ mice are due to progressive hearing impairment. Interestingly, evoked ABR measurements are done in mice under anaesthesia, and therefore might not fully reflect perceptual changes in hearing loss or behavioural response thresholds that can be obtained from awake animals during the PPI test. The PPI test used in audiometry studies in mice has been shown to complement the ABR measurements and be more sensitive in detecting some hearing deficits than ABR thresholds. Since PPI modulation is regulated by the auditory structures of a higher order than that of ABR (which occur at the level of inferior collicus, IC), it was suggested that changes in PPI audiometric thresholds can reveal the elements of higher-level plasticity in the auditory pathway during hearing damage [123]. Therefore, it would be advantageous to assess if knock-out of the *Abcc5* gene produces any auditory phenotype. To confirm general PPI deficits in *Abcc5*$^{-/-}$ mice and exclude auditory processing involvement, experiments with PPI driven by visual or tactile modality would be beneficial to be performed.

However, since ABR measurements were normal, it is also possible that the *Abcc5* gene might mediate the loss of PPI through the behavioural-perceptual components of higher-order in the descending pathway. Evidence from human studies shows that the filtering of sensory information is under executive (top-down) control from the prefrontal cortex. Prefrontal cortex damage impairs the ability to attend to relevant stimuli over irrelevant stimuli [124] and disturbed glutamatergic transmission via NMDA receptors within the prefrontal cortex has been implicated in several mental disorders, including schizophrenia [125]. Electrophysiological results from the de Wet laboratory suggest that glutamatergic signalling in the prefrontal cortex of *Abcc5*$^{-/-}$ mice is largely affected as AMPAR/NMDAR peak current ratios are lower in *Abcc5*$^{-/-}$ mice.

Since reduced PPI is considered an endophenotype of schizophrenia and a valid tool to identify genes involved in the pathophysiology of the disease, this flags up the *Abcc5* gene, as a novel gene of relevance to regulate PPI, and thus implicates *Abcc5* role in the development or

manifestation of this neuropsychiatric disorder. Additionally, NAAG a putative Abcc5 substrate is highly implicated in schizophrenia with reports showing an increase of NAAG levels *in vivo* in the white matter in schizophrenic patients [126]. Overall, it would appear that the majority of females can compensate for the loss of *Abcc5* from birth, while males are less able to do so. This agrees with the increased susceptibility to schizophrenia in men compared to women [127].

3.3.5 Pre-pulse facilitation (PPF)

At the pre-pulse level of 56dB some animals of both groups, *Abcc5*$^{-/-}$ and wild-type, display PPF rather than PPI (Fig. 3.8a and Fig. 3.8b, negative values on the y-axis). PPF is an effect observed when the weaker pre-pulse enhances ASR instead of inhibiting it. PPF usually occurs in rodents when the time gap between pre-pulse and pulse is very short – 0-10ms [128] and it is also triggered by the pre-pulse intensities at low levels above the background [74]. PPF in *Abcc5*$^{-/-}$ mice seems to persist to some extent at all tested pre-pulse levels, even at 65dB. Ison *et al.* showed that small sound increments of the otherwise near-maximal background of 70dB (as 80dB would elicit ASR in mice) produced large and long-lasting increases in ASR amplitude, thus triggering PPF. The facilitation of the ASR was shown to be dependent on the increase in sound increment over the background rather than the absolute background level, and PPF was a more sensitive measure to detect small sound changes over the background (3dB), while PPI would be triggered at higher detection thresholds [74]. This seems to be the case for the wild-type mice showing enhanced PPF over PPI at 56dB, but flipping towards PPI at 58dB (5dB over background). Increased facilitation in *Abcc5*$^{-/-}$ mice persists even at 65dB (12dB over background) and suggests that lack of *Abcc5* expression increases the sound detection threshold for PPF or PPF-PPI transition in knockout mice. This cannot be simply explained by hearing thresholds as there is no significant difference in hearing sensitivity between *Abcc5*$^{-/-}$ and controls at 65dB pulse alone (Fig. 3.9a and Fig. 3.9b). Though, it is also

evident that the response to 56dB pulse alone in *Abcc5*$^{-/-}$ female must be the maximal response as it is the same as their response to 65dB noise (Fig. 3.9a). This suggests that *Abcc5*$^{-/-}$ female mice are not able to gradually adjust their response to discriminate different sounds above background noise. At the same time, *Abcc5*$^{-/-}$ male mice significantly discriminated only between the background and 56dB sound, and displayed higher reactivity to lower sounds level of 53-56dB than wild-type controls, which would rather suggest that lack of the *Abcc5* gene increases sensitivity to sound changes over background noise. Different ranges of sound intensity will have to be used to unmask and investigate this phenomenon further.

3.3.6 Fear Conditioning

Abcc5$^{-/-}$ mice show that they can be successfully conditioned within a single training session to the same extent as wild-type mice, with both females and males showing similar conditional responses (fear) as measured by freezing (Fig. 3.11b-c) [129]. This suggests that fear acquisition pathways are not affected by the absence of the *Abcc5* gene, despite *Abcc5*$^{-/-}$ mice having higher ASR responses.

3.3.7 Contextual fear

The contextual fear test measures the short-term memory association between the cage (context) and unpleasant experiences from the previous day. The short-term memory and its retrieval, as evident from the contextual test, are normal in *Abcc5*$^{-/-}$ mice and comparable to that of wild-type mice (Fig. 3.12b-c). This result would exclude the involvement of the hippocampus in mediating the behavioural phenotype of the *Abcc5*$^{-/-}$ mice. Hippocampus and hippocampal long-term potentiation (LTP) are crucial in the formation and storing of contextual fear memory [130], but do not affect tone fear memory [131, 132].

3.3.8 Auditory-cued fear expression

As revealed by the cue (tone)-fear test, *Abcc5*$^{-/-}$ mice of both sexes, although more significantly in males, showed decreased freezing in response to the cue – loud tone (Fig.3.13b-c). A

possible reason for these results includes effects specific to freezing behaviours. To execute fear at a physiological level, in response to the cue the amygdala promotes increased blood pressure and freezing responses via projections to the lateral hypothalamus and periaqueductal gray matter (PAG), respectively [107]. Single lesions of these structures would abolish the physiological reaction in response to CS-elicited fear, i.e. lesions of PAG would cease the freezing response, but not the increased blood pressure response. It is then possible that a lack of *Abcc5* gene affects downstream post-amygdalar signalling, thus only having an effect on freezing as it's the only conditioned response measured in *Abcc5*$^{-/-}$ mice. The way to address these caveats would be to try different sensory modalities (i.e. light as opposed to tone) and measure different physiological outputs as conditioned fear responses (i.e. fear-potentiated startle response or blood pressure).

A decrease in conditioned fear expression observed in *Abcc5*$^{-/-}$ mice during an auditory cue test can suggest that *Abcc5* gene expression is important during the process of establishing memory association between the auditory cue and foot-shock and/or memory consolidation. Glutamatergic signalling via NMDA and AMPA receptors is crucial for the formation of memory during the synaptic plasticity process via long-term potentiation (LTP). Blocking NMDA receptors before a fear conditioning trial was shown to block the acquisition of conditioned fear as measured by a decrease in freezing [112]. As discussed above, this does not apply to our *Abcc5*$^{-/-}$ mice as their fear learning was the same as wild-type mice. However, given the importance of glutamatergic signalling in fear conditioning, the accumulation of glutamate-conjugates in the brains of *Abcc5*$^{-/-}$ mice could be a cause or consequence of the disruption of NMDAR signalling that in turn will affect the expression and re-call of the fear memory as measured by lower freezing in *Abcc5*$^{-/-}$ mice in response to the auditory cue. Additionally, cellular mechanisms of NMDAR activation include accelerated Ca^{2+} entry and activation of its downstream targets, including nitric oxide (NO) signalling cascade [133]. NO

production is increased during fear conditioning and triggers high levels of cGMP that act on cGMP-dependent protein kinase (cGK) – a major transducer of cGMP signalling in neuronal cells [134]. Both of these pathways might cross over with the postulated function of Abcc5 transporter, either as glutamate conjugates exporter (NAAG would directly target NMDAR or mGluR3) or cGMP transporter [27, 31]. Interestingly, homozygous brain-specific *cGKI* (cGMP-dependent protein kinase type I) knockout mice display a significant reduction in the freezing fear response to an auditory cue while their contextual fear memory remains unaffected [134]. This decrease in freezing observed after 24hrs of the fear-recall test in *cGKI*$^{-/-}$ mice is similar to the level observed in *Abcc5*$^{-/-}$ mice. Thus, putative changes in cGMP levels due to absence of *Abcc5* may account for the fear conditioning phenotype observed in *Abcc5*$^{-/-}$ mice.

3.3.9 Mouse strain differences

The contrasting neurobehavioural phenotypes from *Abcc5*$^{-/-}$ mice observed in our study compared with Jansen *et al.* may be due to the differences in the genetic background of the mice used in these studies. Jansen *et al.* used the FVB mouse strain, which carries the mutation in Pdeb^{rd1} that causes the degeneration of the retina that leads to blindness by the age of 8 weeks. This severe visual impairment poses a challenge and adds additional complexity to the behavioural phenotyping of this strain [135]. FVB mice are also more active and mobile compared to C57BL/6N mice and exhibited more repetitive behaviours such as rearing and climbing [136]. Additionally, the FVB mice scored significantly lower in cognitive tasks involving learning and memory while C57BL/6N mice showed the best ability compared to other strains for context and cued memories [135, 136]. This study shows that significant differences in behavioural phenotypes from C57BL/6N-*Abcc5*$^{-/-}$ mice were only revealed in specific tests (ASR, PPI, FC, Y-maze), but were absent from other assessments (Marble burying and Open field test). Possibly, the innate strain characteristics of the FVB mice may

have concealed notable behavioural differences between the *Abcc5*$^{-/-}$ mice and their control groups, which were revealed by this study. The genetic models of *Abcc5* knock-out mice, C57BL/6N-*Abcc5*$^{-/-}$ (de Wet's group) [4, 18] and FVB- *Abcc5*$^{-/-}$ [4, 18] relied on the deletion of exon 13 and 17, respectively. Both exons encode for the different fragments of the same functional domain of Abcc5 transporter, first nucleotide binding domain (NBD1). Both of these strategies were designed to disrupt the predicted function of the Abcc5 transporter as an exporter, which would require ATP binding and hydrolysis [31]. In this study, similarly to previous studies using FVB- *Abcc5*$^{-/-}$ mice, the expression of *Abcc5* isoforms and possible compensation has not been tested. The isoform 2 of *ABCC5*, which includes exons 1-7, has been reported to be expressed on protein level in human retina as short 208aa product and predicted to be similarly expressed in mice [114]. The possibility of this isoform expression in *Abcc5*$^{-/-}$ mice has not been explored in this study.

3.4 Summary

In summary, this chapter reports the detailed phenotyping of a newly generated *Abcc5* knockout mouse and the impact of the loss of Abcc5 transporter activity on the cognitive function in mice. *Abcc5* gene expression and the function of Abcc5 transporter is associated with disruption of neuronal circuits underlying the regulation of ASR, PPI and auditory-cued fear expression. Additional work from our laboratory suggests that the potential target receptor affected by *Abcc5* knockout is AMPA or NMDA receptor. Thus, disruption of glutamatergic signalling, possibly via NMDA receptor transmission is implicated to drive the neurobehavioural phenotype observed in *Abcc5*$^{-/-}$mice.

Chapter 4: Role of NMDA receptor in GLP-1 secretion

4.1 Introduction

4.1.1 Gut as an endocrine organ

Gut hormones are bioactive peptides produced and released from enteroendocrine cells (EECs). EECs are scattered throughout the gastrointestinal (GI) tract and represent less than 1% of total gut epithelial cells [137] and in some gut sections such as colon, GLP-1 positive L cells comprise as few as only 0.46% of total epithelial cells [138]. There are over 20 identified gut peptides secreted from 15 different enteroendocrine cell types, making the gut the largest endocrine organ of the human body [139]. EECs occur in two different forms, 'open' cells and 'closed' cells. Open cells contain microvilli protruding to the lumen and they respond directly to the luminal content via chemoreceptors sensing the nutrients. Closed cells are regulated indirectly by luminal content through neural and humoral mechanisms [137]. EECs produce gastrointestinal peptides from multiple different genes and in multiple forms due to alternative splicing or differential post-translation processing [140]. These gut peptides are released from the basolateral side of the EECs into the interstitial space to exert their paracrine effect, and into the bloodstream for endocrine effect on target organs [137]. EECs respond to different stimuli and their secreted products play various functions as summarised in Table 4.1. Each of the gut hormones has a characteristic profile of secretion into the bloodstream dependent on food intake, nutrient absorption and its location within the GI tract [139]. Here the main focus is given to L cells as they are GLP-1 producing and secreting cells.

Table 4.1 Enteroendocrine cell types – location, hormonal products and their role. Adapted from [141] and [139].

Gut region	Intestinal processes	Luminal stimuli of EECs	Principal gut hormones	Cell	Hormone role
Stomach	Acid secretion Mechanical disruption	Acid Digested protein	somatostatin (SST)	D cell	high levels at fasting, suppress gastric acid secretion
			ghrelin	A (X-like)	high levels at fasting , promotes food intake
			gastrin, histamine	G cells, ECL cell	rise posprandailly and promomte satiety and release of digestive juices by the stomach
			serotonin (5-HT)	enterochromaffin	regulation of GI motility
Duodenum Jejunum Proximal ileum	Release of bile acids, pancreatic and intestinal enzymes, bicarbonate Digestion Absorption	Monosaccharides Free fatty acids Monoacylglycerols Amino acids Di/tripeptides Bile acids	Duodenum: somatostatin, serotonin, gherlin	as above	as above
			glucose-dependent insulinotropic polypeptide (GIP)	K cells	potentiate glucose-dependent insulin secretion, elevates glucagon and promote SST release
			cholecystokinin (CCK)	I cells	rise postprandailly, supress hunger and promotes release of digestive enzymes from pancreas and bile from gallbladder
			Jejunum and ileum:		
			glucagon-like peptide 1 (GLP-1)	L cells	rise postprandailly, regulate metabolism and appetite by signalling satiety, amplify glucose-dependent insulin secretion, promote SST release, lowers glucagons secretion, inhibits gastric emptying
			glucagon-like peptide 2 (GLP-2)	L cells	promotes proliferation and regenration of the intestinal epitehlium,
			peptide YY (PYY)	L cells	rise postprandailly, inhibits gastric emptying, regulate food intake and signals satiety
			neurotensin (Nts)	N cells	inhibits postprandail gastric acid secretion and pancreatic exocrine secretion, stimulates colonic motility, and inhibits small intestine motility
Terminal ileum	Bile acid reabsorption	Bile acids Unabsorbed	GLP-1, GLP-2, PYY, Nts, 5-HT	as above	as above
Colon Rectum	Bacterial metabolism	Short-chain fatty acids Indole Secondary bile acids	GLP-1, GLP-2, PYY, Nts, 5-HT	as above	colonic L cells regulate tonic basal levels of GLP-1 at fasting state
			insulin-like peptide 5 (Insl5)	L cells	high levels at fasting, contribute to the regulation of metabolism and appetite by promoting food intake; biosynthesis and regulation of release are yet unknown

4.1.2 L cell – definition and distribution *in vivo*

Historically, different subtypes of enteroendocrine cells were defined by their hormone production, and a general one-cell one-hormone classification was proposed that would characterise different enteroendocrine cells such as GLP-1 and PYY producing cells as L cells, glucose-dependent insulinotropic polypeptide (GIP) – K cells, cholecystokinin (CCK) – I cells, neurotensin (NTs) – N cells, secretin (SCT) – S cells, somatostatin (SST) – D cells, serotonin (5-HT) – enterochromaffin cells (EC) and ghrelin (GHRL) – X cells [142]. There is, however, ample evidence that the hormone repertoire of EECs is more flexible [143] and also capable of switching from one cell type to another during the cell migration process up the crypt-villus axis [144]. The density of different EECs types within the GI tract also shows differential distribution along the proximal-distal axis of the GI tract, which was confirmed by early immunohistochemical studies for cell-type specific hormonal markers [145-147] and later refined by the transcriptome and peptidome studies [138, 148].

4.1.3 Transcriptome profile of L cells

Gene expression analysis performed on FACS-purified EECs from mouse intestines provided further details for better identification of K and L cells. Transcriptome analysis of mouse gut segments revealed that proximal L cells differ from the L cells found in the distal small intestine and colon. L cells from the upper small intestine in addition to proglucagon encoding *Gcg* expression were found to express also mRNA encoding CCK, GIP, SCT, NTs and PYY (*Cck*, *Gip*, *Sct*, *Nts* and *Pyy*, respectively). Colonic L cells, which mainly produced mRNA for *Gcg* and *Pyy*, had much lower levels of *Cck* and *Sct*, and no *Gip* expression. The production of the protein from these transcripts was also variable and while all L cells from the upper small intestine produced CCK, only a small percentage immunostained positive for GIP (15%), and very few for PYY (0.02%). In contrast, 40% of GLP-1 positive cells located in the distal small

intestine of jejunum and ileum showed positive expression for PPY by immunostaining, and 10% also expressed GIP. Interestingly, the majority of colonic L cells are positive for PYY, no GIP expression was observed, and despite *Cck* mRNA expression, the production of CCK peptide was not detected [138]. Similarly, transcriptome analysis of GLP-1 positive L cells from human ileum and jejunum tissue samples showed expression of mRNA encoding for GCG, GIP, CCK, NTS, PYY, SCT and, unlike murine L cells, also the *MLN* gene that encodes for motilin. Consistent also with the mRNA expression pattern of *Gcg* in murine samples – human ileum showed higher expression of *GCG* when compared to human jejunum [148].

In addition, peptidome analysis confirmed previous immunohistochemical results that L cell number and/or their production of GLP-1 is increasing gradually from the jejunum to ileum and stays relatively high in the colon to peak in the rectum [148]. Some L cells were also found in the human duodenum, which has been also previously reported for humans, where immunostaining showed co-localisation with GIP [146]. The overlapping production of other peptides such as GLP-2 and oxyntomodulin expressed from the *GCG* gene in human L cells was also evaluated. Interestingly, secretory granules of L cells isolated from the ileum were all positively labelled for GLP-1, while only half of them were also positive for PYY. GLP-1 and PYY were found to be co-stored in the secretory granules, but not at equal ratios [145]. The co-release of GLP-1 and PYY was confirmed using human primary colonic cultures, where the majority of the cells were shown to produce both hormones [149]. Distribution of GLP-1 secreting cells throughout the GI along with secretion profile of other endocrine cells was schematically depicted in Figure 4.1.

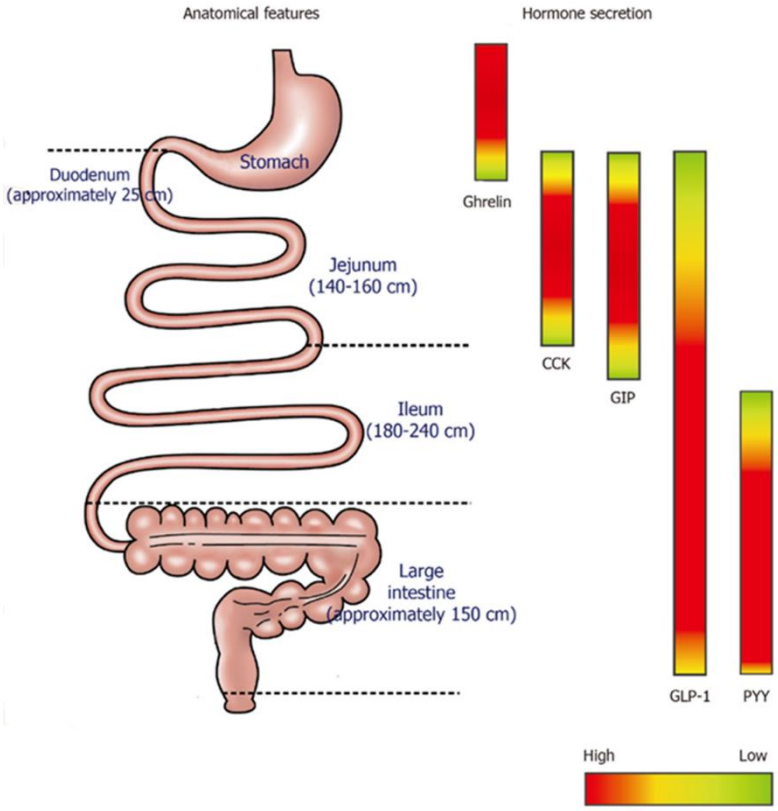


Figure 4.1 Schematic overview of secretion profile of different gut hormones along the human GI tract.

Highest density of GLP-1 secreting L cells was found in the more distal intestine, the ileum and colon, whereas the lowest levels of GLP-1 are reported in the duodenum as marked by gradient bar. Typical length of different sections of gastrointestinal tract was marked and labelled; regionally specific secretion profile of different gut hormones, including ghrelin, cholecystokinin (CCK), glucose-dependent insulinotropic polypeptide (GIP), glucagon-like peptide 1 (GLP-1) and peptide YY (PYY) is also depicted as a gradient bar. Adapted from [150]

4.1.4 Experimental models for GLP-1 secretion studies

Since L cells comprise only a small percentage of total epithelial cells of the gut, studying the function of native L cells *in vivo* has been challenging. GLP-1 secretion can be measured in blood samples following oral glucose or meal challenge. The main complications with measuring GLP-1 *in vivo* are that it is rapidly degraded by dipeptidyl peptidase IV (DDP-IV), and there are no established protocols on the timeline for the sample collection to produce the most reliable measurements, which further complicates the comparison between different studies. Multiple different models and tools were developed to aid research of stimulus-secretion coupling of GLP-1 from L cells, reviewed in [151]. *Ex vivo* models using isolated intestinal perfusions of mice, rats and pigs are commonly employed to research the function of L cells in different regions of the GI tract, but also to investigate whether nutrients or drug target the apical or basolateral surface of the L cells. Similarly, Ussing chambers allow for the research of L cells within intact gut tissue where the cells retain their polarised nature and epithelial gut barrier integrity. Multiple models of L cells can be used as 2D cell cultures. Intestinal primary cell cultures of mixed gut epithelial cells can be grown from gut crypts isolated from the small intestine or colon of rodents, but also humans. The advantage of these primary cultures is that L cells can be investigated in the context of interaction with their neighbour cells. However, some limitations including the lack of apico-basal polarity reinforced 2D architecture of the cultures, short life span, and also measuring GLP-1 release from a limited number of L cells, which reflects the L cell density *in situ* within the cell population, may be challenging [152]. Recently, 3D intestinal organoids grown from murine, but also human stem cells, have been shown as a promising research model for L cells [153, 154]. Several model cell lines for L cells are also available for investigating GLP-1 production, including GLUTag or NCI-H716 cells. GLUTag is a murine cell line derived from a colonic neuroendocrine tumour that was generated in a transgenic mouse expressing the simian virus

40 (SV40) T-antigen under the control of the proglucagon promoter [54], while NCI-H716 is a suspension cell line derived from a human colorectal adenocarcinoma [155]. Both are commonly used in GLP-1 secretion studies, and GLUTag cells, in particular, show multiple nutrient sensing mechanisms and signalling pathways for GLP-1 stimulus-secretion coupling that are more consistent with native L cells, i.e. glucose-stimulated GLP-1 release [156].

4.1.5 GLP-1 as an incretin – clinical relevance

Intestinal L cells, regardless of the location within the GI tract and gene expression profile, are the main source for production and secretion of GLP-1 hormone. The most prominent function of GLP-1 is to regulate post-prandial glucose levels by potently stimulating insulin secretion from pancreatic β-cells via specific G-protein-coupled receptor GLP-1R [157], and suppressing glucagon secretion from pancreatic α-cells through a mechanism that remains unclear as GLP-1R expression in α-cells is debatable [158]. Together with GIP, GLP-1 takes part in the 'incretin effect', wherein oral glucose challenge produces a larger insulin response from pancreatic β-cells than the equivalent intravenous infusion of glucose. It has been estimated that in humans 60-72% of the insulin secretion after 100g glucose administration is due to incretin factors (when insulin is measured as the readout), and 57% for the same glucose load when insulin by-product, C-peptide is monitored [159]. The incretin effect, however, was found to be defective or even absent in patients with impaired glucose tolerance, hyperglycaemia and diabetes [160-162]. Further infusion studies revealed that only GLP-1, but not GIP, is able to stimulate insulin secretion when infused during oral glucose challenge in both, type 2 diabetic patients and healthy controls [163, 164]. At the same time, i.v. infusions of GLP-1 (110pmol/L) were found to inhibit postprandial acid secretion, decrease gastric emptying rate by 50% [165], and suppress pre-prandial glucagon release in a dose-dependent manner up to 70% for a maximum of 47pmol/L steady-state GLP-1 infusion [166]. These

effects persisted as long as the GLP-1 plasma levels were elevated by infusions, in healthy subjects, but also type 2 diabetic patients [166]. The upregulated glucagon levels in T2D patients in oral glucose challenge, but not during isoglycaemic i.v. injection, were also attributed to incretin effect defects in T2D patients [167].

4.1.6 Active GLP-1 in therapy of diabetes

Beneficial effects of GLP-1 are widely recognised and GLP-1-based therapies have become a part of standard care in the treatment of type 2 diabetes (T2D). This includes stable, long-acting GLP-1 analogues (incretin mimetics) such as liraglutide and semaglutide [168, 169], which not only help to control glucose levels in diabetic patients but also were shown to lower appetite, induce and maintain weight loss and as of recently are used as the most efficacious, non-surgical treatment of obesity [170]. Another therapeutic strategy utilising the incretin effect is to prevent the degradation of endogenous GLP-1 and prolong its half-life. Active GLP-1 circulates as two equally potent forms, GLP-1(7-37) and GLP-1(7-36-NH_2). Amidated GLP-1 (7-36-NH_2) constitutes 80% of released active GLP-1 [171]. The half-life of circulating native bioactive GLP-1 is 1-2min mostly because it is cleared by the kidney or cleaved at the N-terminal by dipeptidyl peptidase IV (DPP)-4 (known also as CD26) to inactive GLP-1(9-36-NH_2) or GLP-1 (9-37) [172]. DPP-4 is widely expressed in different organs with the highest levels found in the kidney, but also the luminal surface of endothelial cells of the gut mucosal capillaries. Thus DPP-4 rapidly degrades the GLP-1 released from L cells into the blood stream [173]. The new class of anti-diabetic medications targets the DPP-4 to inhibit its enzymatic activity. DPP-4 inhibitors used in the therapy of diabetes are called gliptins and act as anti-hyperglycaemic, they are weight neutral and do not cause hypoglycaemia [174].

There is no consensus on general deficiency in GIP/GLP-1 secretion stimulated by nutrient digestion in patients with type 2 diabetes and other forms of diabetes (type 1 diabetes, MODY,

diabetes associated with chronic pancreatitis) [146, 167, 175], and also the rate of degradation by DPP-4 and clearance of GLP-1 is reported to be the same between a healthy individual and type 2 diabetics [176]. Despite that increasing GLP-1 levels in the plasma of T2D patients exerts its beneficial effects on insulin secretion in a dose-dependent manner [177, 178]. Insulinotropic properties of GLP-1, together with the ability to suppress glucagon release, gastric emptying and food intake, are the focus of new therapeutic strategies to tackle diabetes and obesity. It is then of great interest to investigate the factors that can affect and modulate GLP-1 release upon stimulation with nutrients, but also at the basal, low to no nutrient conditions, where the release of GLP-1 is 'tonic' and low, mediated at fasting mainly by L cells in the colon [139].

4.1.7 Stimulus-secretion coupling of GLP-1 secretion

L cells within the gut epithelium are mainly open-type, heavily polarised cells which sense nutrients via micro-villi protruding into the gut lumen (Fig 4.1) [179]. GLP-1 secretion occurs in response to nutrients arriving at the proximal small intestine following food digestion. This occurs through nutrient uptake/interaction at the luminal/apical side of the L cell, which stimulates the release of GLP-1 from the basolateral membrane, which faces the bloodstream. Previous studies have demonstrated that sugars, lipids, oligopeptides, amino acids and bile acids are all capable of stimulating GLP-1 secretion, with variable potency, via different cellular mechanisms, reviewed extensively in [139, 180, 181].

In healthy human subjects, GLP-1 secretion occurs within the first 10min following an oral glucose challenge, peaking at ~15min [146]. For hormones that are expressed at high levels in the colon, such as GLP-1, the observed timeframe of 15–30 min after meal initiation is surprising. This suggests that additional factors besides nutrients may stimulate GLP-1 secretion through hormonal or neural loops relaying the presence of duodenal nutrients to ileal

and colonic EECs [139]. It has been postulated that L cells are capable of receiving input from the basolateral membrane that would act to regulate the release of the GLP-1 in response to nutrients [182]. GLP-1 positive endocrine cells were shown to express both pre-and postsynaptic proteins [183], and thus they might receive signals from the nervous system and act on intrinsic sensory neurons or vagal afferent nerves. The schematic overview of that connection and characteristic *in vivo* morphology of the L cells within the gut epithelial layer forming neuron-like projections called neuropod is shown in Fig. 4.2 [179]. Additionally, studies of endocrine cells of the pancreas have reported that neurotransmitters can influence the stimulus-secretion coupling of insulin, glucagon and somatostatin. Thus, neurotransmitter target receptors are emerging as new potential therapeutic targets to treat diabetes as reviewed in [184].

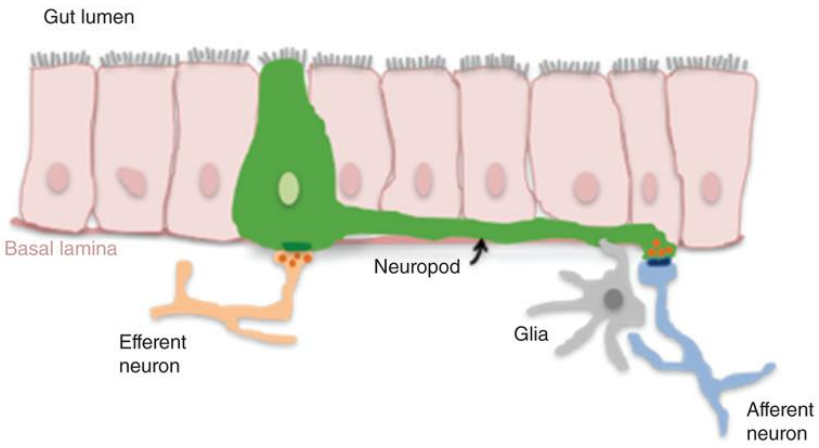


Figure 4.2 Enteroendocrine cell (EEC) and EEC-neural connection.

Schematic diagram illustrating the recently described connection between EECs and enteric nerves. It is believed that both enteric and vagal nerves innervate EECs via a synapse-like structure termed neuropod. Adapted from [179].

4.1.8 Glucose stimulated GLP-1 release

There are some similarities in the mechanism of stimulus-secretion coupling between the L cell and the insulin-secreting pancreatic β-cell. However, unlike the pancreatic β-cell, circulating blood glucose does not regulate GLP-1 release. In human studies, healthy subjects and those with T2D show no increase in GLP-1 secretion in response to i.v. glucose infusion, at varying concentrations [185]. It is well-documented that during a rise in ambient glucose concentration, glucose is metabolised by the pancreatic β-cell to increase the intracellular ATP:ADP ratio. Increased cytosolic ATP binds to and inhibits the ATP-sensitive potassium (K_{ATP}) channel at the plasma membrane, triggering membrane depolarisation and activation of voltage-gated Ca^{2+} channels. This results in increased $[Ca^{2+}]_i$ which facilitates exocytosis of insulin granules [186]. Similarly, glucose-stimulated GLP-1 secretion is also partially K_{ATP} channel dependent, however, the predominant mechanism involves sodium-glucose co-transporter 1 (SGLT1) (Fig. 4.3) [187-190]. The SGLT-1 involvement in glucose-stimulated GLP-1 release will be discussed in greater detail in Chapter 5.1.9.

Primary L cells as well as immortalised GLUTag cells have been shown to express functional K_{ATP} channels, which play a role in the triggering of glucose-stimulated GLP-1 secretion [188, 189]. Previous studies have demonstrated that closure of the K_{ATP} channel by tolbutamide stimulates the secretion of GLP-1, but that this effect was not potentiated by increasing extracellular glucose availability [188, 191]. Additionally, basolateral application of the tolbutamide was shown to trigger GLP-1 secretion from the perfused small intestine of rats [192]. Conversely, in human studies, treatment with different K_{ATP}-closing sulfonylureas (e.g. glibenclamide) did not influence GLP-1 secretion during oral glucose challenge in T2D patients [193]. Thus, K_{ATP} channels are not considered the molecular link between luminal glucose and GLP-1 release and their role in the secretion of GLP-1 remains from gut enteroendocrine cells remains ambiguous.

The glucose-sensitivity of L cells differs from that of β-cells in that GLUTag cells secrete GLP-1 in response to very low glucose concentrations (0–5mM) and, unlike β-cells, this response is not potentiated by additional glucose increments (5–25mM) [188]. Primary murine L cells express higher levels of the *Glut2* gene than the non-endocrine cells. GLUT2–facilitated glucose transport was found to mediate electroneutral glucose uptake in L cells in addition to the electrogenic SGLT1 glucose transporter [189]. Glucose uptake in β-cells via GLUT2 plays important role in triggering insulin release [194]. Mice lacking both GLUT2 and GLUT1 displayed reduced GLP-1 concentrations following an oral glucose challenge and had lower intestinal GLP-1 content [195]. Additionally, luminal glucose has also been found to be less effective in stimulating GLP-1 secretion in the presence of a GLUT2 inhibitor [192]. However, in primary L cells, although inhibition of GLUT2 abolished the uptake of glucose, it did not significantly impair GLP-1 secretion [196]. Taken together, these findings suggest that some uptake of luminal glucose via GLUT2 is required for normal glucose-stimulated GLP-1 secretion. This was supported by the finding that the first phase of glucose-stimulated GLP-1 secretion is greatly diminished by SGLT1 inhibitor as expected, but prolonged inhibition of SGLT1 does not affect the second phase of GLP-1 release, especially to high luminal glucose levels [197]. Therefore, glucose metabolism and K_{ATP} channels were suggested to perhaps play the modulatory role in response to a high luminal glucose load, which would then cause high blood glucose levels. This, however, remains to be confirmed.

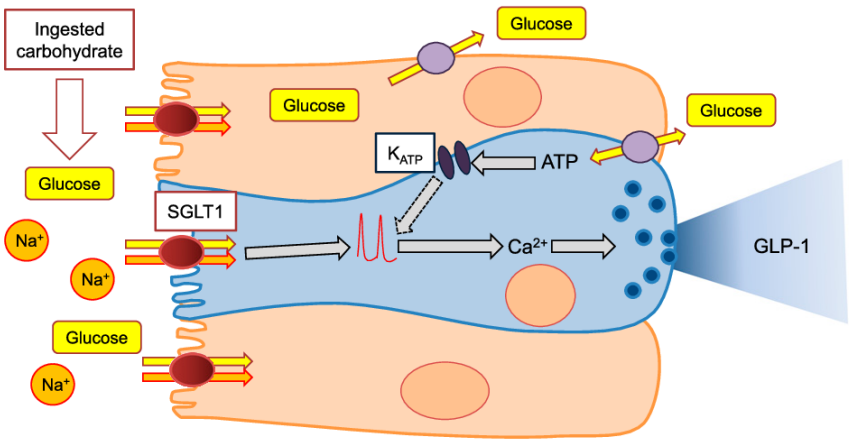


Figure 4.3 Mechanism of glucose-triggered GLP-1 secretion.

SGLT1 is responsible for glucose absorption across the small intestinal brush border, and on the apical membrane of L-cells. Glucose entry via SGLT1 into L cell coupled with sodium flux triggers electrical activity and GLP-1 secretion. K_{ATP} channels modulate some control over GLP-1 release but are not responsible for peak postprandial GLP-1 levels and their role is not fully elucidated. Image adapted from [198].

4.1.9 Role of neurotransmitters in stimulus-secretion coupling of GLP-1 secretion

The enteric nervous system (ENS) comprises of a network of local nerve fibres and ganglia that communicates with efferent and afferent branches of parasympathetic and sympathetic nerves. Neurons of the ENS communicate through neurotransmitters such as acetylcholine, noradrenaline, dopamine or serotonin [199]. The main role of ENS is to orchestrate gastrointestinal behaviour independently from CNS [200]. L cells were shown to express various neurotransmitter receptors as the L cell function is continuously fine-tuned by neuronal signals from ENS. Perfusion studies using porcine ileum have shown that acetylcholine increases GLP-1 secretion [201]. The expression of the acetylcholine target muscarinic (G-protein coupled) receptors M1, M2 and M3 was ascertained in the human L cell model cell line, NCI-H716 cells and showed that their activation by specific agonists induces GLP-1 secretion [202]. *In vivo* studies in rats showed that inhibiting muscarinic receptors with atropine completely abolished nutrient-stimulated GLP-1 release proving that muscarinic receptors are involved in the postprandial regulation of GLP-1 release. Expression of muscarinic receptors M1, M2 and M3 in native L cells of rat ileum was confirmed by co-localisation immunostaining with GLP-1 [203]. Recently, the α7 nicotinic acetylcholine receptor (α7nAChR) was shown to be expressed in primary murine L cells as well as in various model cell lines of L cells, murine

GLUTag and STC-1 cells and human NCI-H716 cell line. Acute activation of α7nAChR by selective agonist GTS-21 caused a dose-dependent increase in GLP-1 secretion from every model of L cell tested [204].

4.1.10 Role of glutamate in GLP-1 secretion

Glutamate is a non-essential amino acid widely distributed and used in the central nervous system as an excitatory neurotransmitter [205], but also one of the most abundant amino acids in foods [206]. Different amino acids resulting from the digestion of proteins were shown to trigger GLP-1 secretion with different potency and by employing various mechanisms. Some amino acids, like glutamine, are known to be transported in a sodium-coupled manner, which might depolarize cell membranes, followed by voltage-dependent calcium entry that stimulates GLP-1 release [207]. Studies on perfused rat intestines considering the polarised nature of L cells revealed that the stimulatory effect of amino acids is differential and depends if the amino acid is applied on the apical or basolateral side of the L cell. Glutamine predominantly stimulated GLP-1 secretion when applied intraluminally, while arginine or tryptophan stimulated GLP-1 secretion mainly by basolateral activation suggesting that it happens through post-absorptive mechanisms. Glutamate was shown to modestly stimulate GLP-1 release irrespective of the side of application [208]. Surprisingly, no effect of glutamate on GLP-1 secretion was observed in primary intestinal cultures from the murine colon *in vitro* [209]. But in GLUTag cells, glutamate was shown to increase intracellular calcium levels and stimulate GLP-1 release, however, less potently than glutamine or glucose. Glutamate also triggered action potentials, however, they were much weaker than that of glutamine. It was found that glutamate had a potentiating effect on GLP-1 release downstream of calcium signalling, suggesting that intracellular glutamate levels and its metabolism also play a role in regulating GLP-1 secretion [207, 210]. G protein-coupled receptors such as metabotropic glutamate

receptors (mGluRs) and umami taste receptors (Tas1R1/Tas1R3) were suggested to be responsible for glutamate sensing in L cells. Receptors genes of *tas1R1* and *tas1R3* were found to be expressed in murine L cells and GLUTag cells, however, the expression level was similar to non-endocrine cells [189]. The allosteric positive modulator of Tas1R1/Tas1R3 also did not increase the GLP-1 release in response to glutamate, suggesting that further studies are needed to clarify the mechanism underlying glutamate sensing by L cells [208].

While the role of dietary glutamate as a GLP-1 stimulant was addressed in the literature, very little is known of the role of glutamate as a neurotransmitter in the regulation of GLP-1 secretion. L cells, similarly to neurons, are electrically excitable [211]. It was shown that vesicular storage of glutamate within GLUTag cells is mediated by VGLUT1 and VGLUT2 (Vesicular glutamate transporters). Glutamate was also found to be released from GLUTag cells in response to stimulation, i.e. glucose, which also triggers GLP-1 release. Therefore, it was suggested that GLP-1 is co-stored with glutamate in the secretory granules and when released upon stimulation it might play a role in regulating GLP-1 secretion by a feedback mechanism. The proposed target receptors such as metabotropic glutamate receptors, mGluR5/6 and the ionotropic glutamate receptor, kainate receptor KA1, were found to be expressed in GLUTag cells and L cells from mouse ileum, but their role in GLP-1 release was not explored [212]. The expression profile of other glutamate receptors in L cells and their role in GLP-1 secretion remains unknown.

4.1.11 Glutamate receptors

There are two major types of glutamate receptors: inotropic receptors and metabotropic receptors. While metabotropic receptors are G protein-coupled receptors (GPCRs) which rely on second messengers inside the cell, ionotropic receptors are ligand-gated ion channels which alter the membrane potential to excite or inhibit cell activity [184].

4.1.12 NMDA receptors

N-methyl-D-aspartate (NMDA) receptor (NMDAR) is a ligand-gated ion channel that opens selectively for cations upon activation with high permeability to Ca^{2+}, but also Na^{+} and K^{+}. NMDAR channels are activated by depolarization, to release the Mg^{2+} block out of the pore, and by simultaneous binding of their ligand (e.g. glutamate) and co-activator (e.g. glycine) [213]. NMDARs are expressed at the synapse, but also exist on the extrasynaptic membrane of neurons, and other cell types as it has been reported for pancreatic β-cells. Each NMDAR consist of two GluN1 (Grin1) mandatory subunits and usually, two GluN2 subunits of which there are four subtypes GluN2A-D, encoded by *Grin2A*, *Grin2B*, *Grin2C*, *Grin2D* genes. There are also two subtypes of GluN3 subunit (encoded *Grin3A* and *Grin3B*). Classic NMDAR occur as a di-heterotetrameric receptor consisting of two GluN1 and two of the same type GluN2 subunits or tri-heteromeric when two GluN1 subunits assemble with two different types of GluN2 subunits or combination of GluN2 and GluN3. GluN2 subunits bind glutamate as the activating endogenous agonist, while GluN1 and GluN3A-B have a binding site for the co-agonist of NMDAR (e.g. glycine) [214]. The existence of glycine-activated NMDARs composed of GluN1/GluN3 subunits has been reported in heterologous recombinant expression systems previously [215], but only recently functional excitatory glycine GluN1/GluN3A receptors were found in native neurons of CA1 hippocampal region of young mouse brain slices [216].

The subunit makeup of NMDAR largely determines many properties and functions of NMDARs such as receptor pharmacokinetic, signalling interactions, ion permeability and expression patterns in the central nervous system or subcellular localisation. For example, it has been shown that the composition of NMDARs expressed at the synaptic cleft within the CNS switches from predominantly GluN2B to GluN2A during postnatal development, which is crucial for the synapse maturation and hence occurs at a specific time window [217, 218].

NMDARs containing GluN2C and GluN2D subunits were shown to be expressed mainly in the interneurons within the hippocampus and cortex [219, 220], while Grin3A is present in many brain regions at different levels during development and localise to excitatory neurons, but also GABAergic and cholinergic interneurons at perisynaptic and extrasynaptic location [221]. Competitive antagonists for glutamate-binding site such as D-AP5 blocks only NMDAR containing GluN2 subunits and have little effect on GluN1/GluN3 NMDARs since these receptors are not activated by glutamate [222]. There are also channel blockers that require the NMDAR channel to be open for binding and prevent ion flux, these are voltage and use-dependent as they require channel to be open and activated first. Dizocilpine (MK-801) is a high affinity NMDAR blocker, so called trapping blocker – as it's retained within the pore of the channel after closure and agonist unbinding, and remains there until channel re-opening after subsequent agonist exposure. GluN1/GluN3 NMDARs exhibited reduced sensitivity to open channel blockers like MK-801 when compared with GluN1/GluN2 receptors [222]. Glutamatergic transmission through NMDARs plays a pivotal role in CNS regulating brain plasticity and synapse maturation [223], they are involved in long-term potentiation [224], cell death and survival [225]. NMDAR dysfunctions are involved in various neurological and psychiatric disorders such as stroke, and schizophrenia, but also pathological pain, therefore they serve as a useful therapeutic drug target for various diseases [226, 227]. Recently, NMDARs have also become a potential therapeutic target to tackle diabetes [228].

4.1.13 Peripheral tissues – role of NMDAR

The role and expression patterns of NMDA receptors have been also investigated outside of CNS. It has been demonstrated that functional NMDARs are expressed widely in various peripheral tissues and specialised cells within such as keratinocytes, lymphocytes, osteoclasts or cardiomyocytes and have multiple roles in physiological and pathological processes in the

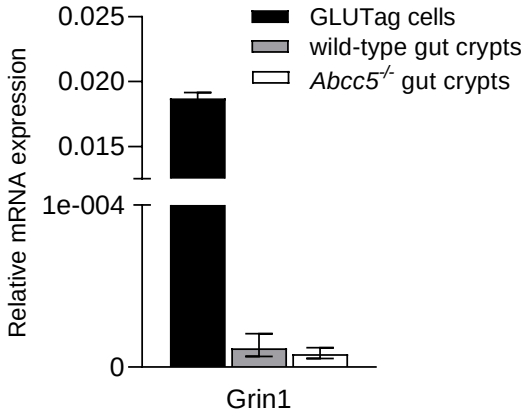
kidney, heart, and bone [229, 230]. There is also some evidence of a non-neuronal NMDAR role in the endocrine system. GluN1 expression was visualised by immunofluorescence in all of the mucosa cells of the stomach wall in rat tissues. Functionally, NMDAR activation by NMDA was shown to inhibit histamine-induced gastric acid secretion, but potentiate acetylcholine-induced acid secretion in stomach perfusion experiments [231]. NMDAR expressed in rat parathyroid gland was found to regulate parathyroid hormone (PTH) secretion. Activation of NMDAR caused a decrease in low-calcium stimulated secretion of PTH, and when NMDAR was subsequently blocked with MK-801 the PTH secretion was restored [232]. Functional NMDA receptors were shown to be required to control glucose-stimulated insulin secretion (GSIS) in pancreatic islets as they act upstream from K_{ATP} channels and possibly form a part of the negative feedback loop in β-cells that prevents excessive release of insulin at high blood glucose concentrations. Blocking NMDAR in β-cells was shown to potentiate glucose-stimulated insulin release from islets *in vitro* and *in vivo* [233]. The NMDA receptor antagonist dextromethorphan (DXM) and its metabolite dextrorphan (DXO) have been recommended for the treatment of T2D as they were shown to enhance glucose tolerance in mice by increasing glucose-stimulated insulin release without affecting basal insulin secretion [234, 235]. The effect of this over-the-counter NMDA receptor antagonist on the secretion of hormones from the L cells remains unknown. Recent transcriptome analysis of various human and mouse L cell models, as well as human native gut tissue, reports the mRNA expression of NMDAR subunits in L cells [57].

4.2 Results

4.2.1 Expression of *Grin1* encoding GluN1 in primary small intestinal cell cultures of *Abcc5*$^{-/-}$ and wild-type mice

The relative mRNA levels of the *Grin1* target gene encoding for the GluN1 mandatory subunit of NMDA receptor were measured by RT-qPCR in primary intestinal cultures isolated from *Abcc5*$^{-/-}$ and wild-type mice alongside with GLUTag cells (Fig. 4.4a). GLUTag cells, a clonal line of L cells, showed a marked expression of *Grin1*, while *Grin1* gene expression levels were below the detection thresholds of the qPCR protocols used in these experiments in primary intestinal cultures grown for 24hr. Western blot analysis confirmed these results and no GluN1 protein expression was detected in primary intestinal cultures, while GluN1 showed robust expression in GLUTag cells (Fig. 4.4b, lower panel). As a protein expression control, *Abcc5*$^{-/-}$ or wild-type mice primary intestinal cultures, showed the expected absence or presence of Abcc5, respectively (Fig. 4.4b, upper panel). *Grin1* mRNA expression in GLUTag cells was confirmed at the protein level in the same Western blot (Fig. 4.4b).

a



b

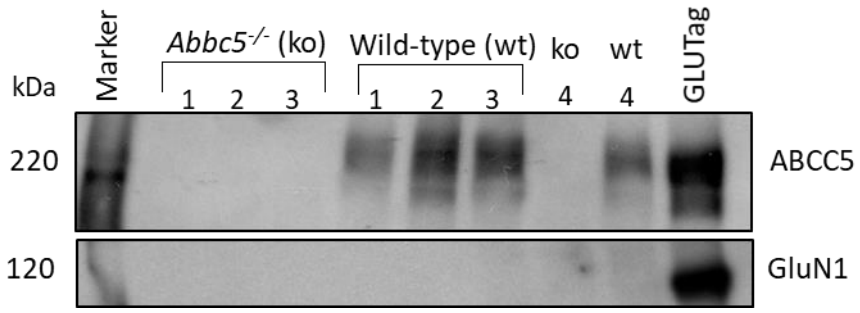


Figure 4.4 Primary intestinal cultures of *Abcc5*$^{-/-}$ or wild-type mice show no detectable *Grin1*/GluN1 expression.

a) Relative mRNA expression of *Grin1* NMDAR subunit tested by RT-qPCR in GLUTag cells, wild-type and *Abcc5*$^{-/-}$ mixed primary intestinal cultures. b) Western blot analysis of whole-cell protein isolated from 24hr gut cultures of *Abcc5*$^{-/-}$ and wild-type mice showing lack of *Abcc5* expression in knock-out samples as expected and Abcc5 transporter expression in wild-type samples and GLUTag cells (upper panel).

4.2.2 The NMDA receptor blocker MK-801 does not affect glucose-stimulated GLP-1 release from primary L cells

Low detectable levels of *Grin1* mRNA and no detectable levels of GluN1 protein expression in primary cell cultures could have resulted from the fact that these cultures are a mixture of different populations of cells, where L cells contribute only to 1% of the total cell number or less. Therefore, a functional approach was undertaken to assay the release of GLP-1, exclusively secreted by L cells. GLP-1 secretion in basal buffer conditions and upon glucose-stimulation with 6mM glucose was measured from primary intestinal cultures isolated from *Abcc5*$^{-/-}$ (Fig. 4.5a, white bars) and wild-type (Fig. 4.5b, grey bars) mice. The secretion buffer was modified as per [233] (see *Methods*), briefly Mg^{2+} ions were omitted to increase the NMDAR channel open probability and 10µM of NMDAR co-agonist, glycine was added. GLP-1 secretion was measured from cell cultures incubated for 25min, to minimise the risk of cell detachment in the absence of Mg^{2+} ions. NMDA receptor channel pore blocker, MK-801 was added at 10µM to the glucose-stimulation buffer to assess its effect on GLP1 release as compared to glucose-evoked GLP-1 release alone (Fig. 4.5a-b). Primary cultures of both genotypes, *Abcc5*$^{-/-}$ and wild-type, showed a significant increase in response to 6mM glucose when compared to basal (0mM glucose) secretion (9.5±4.6pg/mL vs 123±23pg/mL and 20.9±2.3pg/mL vs 114±17pg/mL, respectively) proving the presence of responsive L cells within the cultures of both genotypes. The addition of the MK-801, however, did not significantly change the release of GLP-1 in comparison with 6mM glucose alone irrespective of the genotype. The specific inhibitory action of 10µM MK-801 on NMDAR in L cells within primary small intestinal cultures has not been established. To avoid the risk of false negative result, the method to measure the antagonistic effect of MK-801 on L cells may include testing electrical activity of the L cells with and without the NMDAR inhibitor.

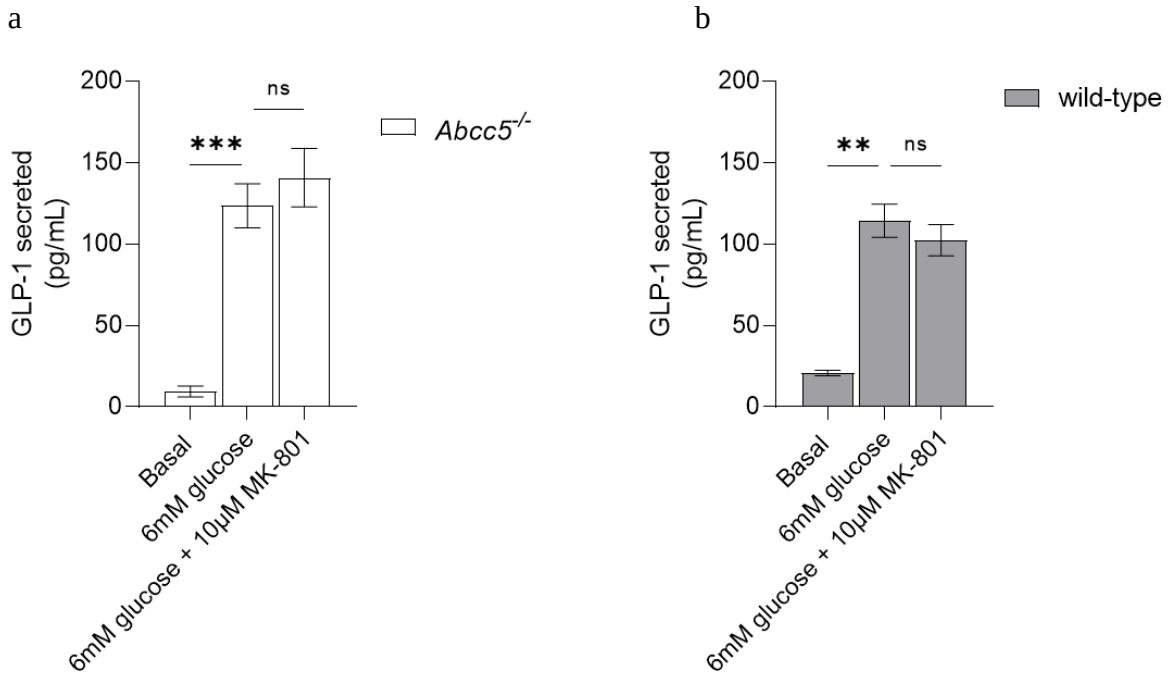


Figure 4.5 No effect of NMDAR inhibition on glucose-stimulated GLP-1 secretion from primary intestinal cultures.

GLP-1 secretion was measured in a) *Abcc5*$^{-/-}$ (white bars) and b) wild-type (grey bars) gut crypt cultures at basal condition (Mg^{2+} free, 0mM glucose buffer) and upon stimulation with 6mM glucose for 25min with and without NMDAR inhibitor MK-801. Significant values depicted as (*) as indicated; *p<0.05, **p<0.01, (Student's t-test), ns – not significant.

4.2.3 Expression of NMDA receptor subunits in GLUTag cells.

The GLUTag cell line is a clonal cell line of L cells commonly used to investigate mechanisms of GLP-1 secretion. Since the expression level of Grin1 and its product, GluN1 were proved to be enriched in GLUTag cells as compared to mixed primary intestinal cultures (Fig 4.4), GLUTag cells were used in further experiments. The expression of the Grin1 gene was shown to be present at the mRNA and protein (GluN1) levels in GLUTag cells (Fig 4.4a and 4.4b, respectively). The NMDA receptor, however, requires other subunits to form a functional channel as it is a heterotetramer composed usually of two GluN1 and two GluN2 or GluN3 subunits [214]. Using the RT-qPCR *Grin1* levels in GLUTag as compared to whole-brain expression of wild-type mice was ascertained (Fig 4.6a), but no *Grin2a* and *Grin2b* were present in GLUTag cells at mRNA level. Grin2a and Grin2b are coding for the main predominant GluN2 NMDA subunits forming NMDA receptor, however, there are also two other GluN2 coding genes (*Grin2c* and *Grin2d*) and two genes coding for GluN3 subunit (*Grin3a* and *Grin3b*). The RNA sequencing of GLUTag cells was used to investigate the expression levels of all genes coding for NMDA receptor subunits (Fig 4.6b). 3' mRNA sequencing confirmed the abundant expression of Grin1 coding for mandatory subunit GluN1 and revealed expression of *Grin2a* and *Grin2d* (GluN2), as well as *Grin3a* and lower levels of *Grin3b* (GluN3). No expression of *Grin2b* and *Grin2c* was detected in GLUTag cells at the mRNA level.

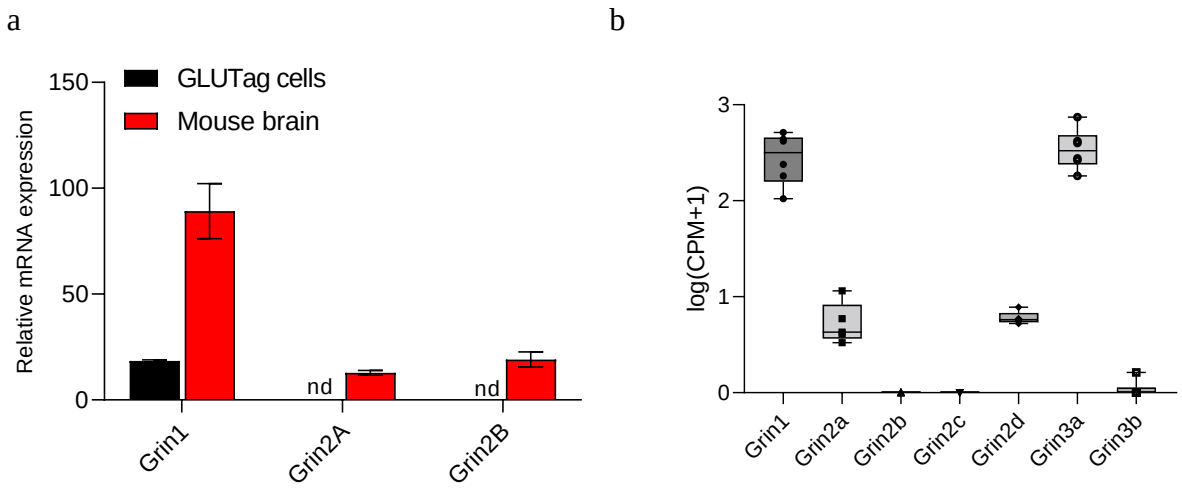


Figure 4.6 Glutamate receptors expression profile of GLUTag cells.

a) NMDAR subunits relative expression in GLUTag cells as compared to wild-type mouse brain tissue expression by RT-qPCR method. b) NMDAR subunits transcript abundance as measured via RNA sequencing method. Absolute count per million (CPM), equivalent to transcript per million (TPM) by other methods, values were expressed as log(CPM+1).

4.2.4 The NMDA receptor blocker MK-801 does not affect glucose-stimulated GLP-1 release from GLUTag cells

The dose-response curves of glucose-stimulated GLP-1 secretion from GLUTag cells were measured in 5.6mM (Fig. 4.7a) or 10mM glucose (Fig 4.7b) in acute 2hr stimulation in the presence of NMDAR antagonist, MK-801 (concentration range 0.01-100µM). No effect of any of the MK-801 concentrations tested was observed on the GLP-1 release in the presence of 5.6mM or 10mM glucose. The increase of GLP-1 secretion upon glucose stimulation alone at both tested glucose concentrations over the basal was confirmed to be highly significant (p<0.001, two-tailed, unpaired, Student's t-test) with the values reaching 1289±119pg/mL and 1364±11pg/mL for 5.6mM glucose and 10mM stimulation, respectively (Fig. 4.7c).

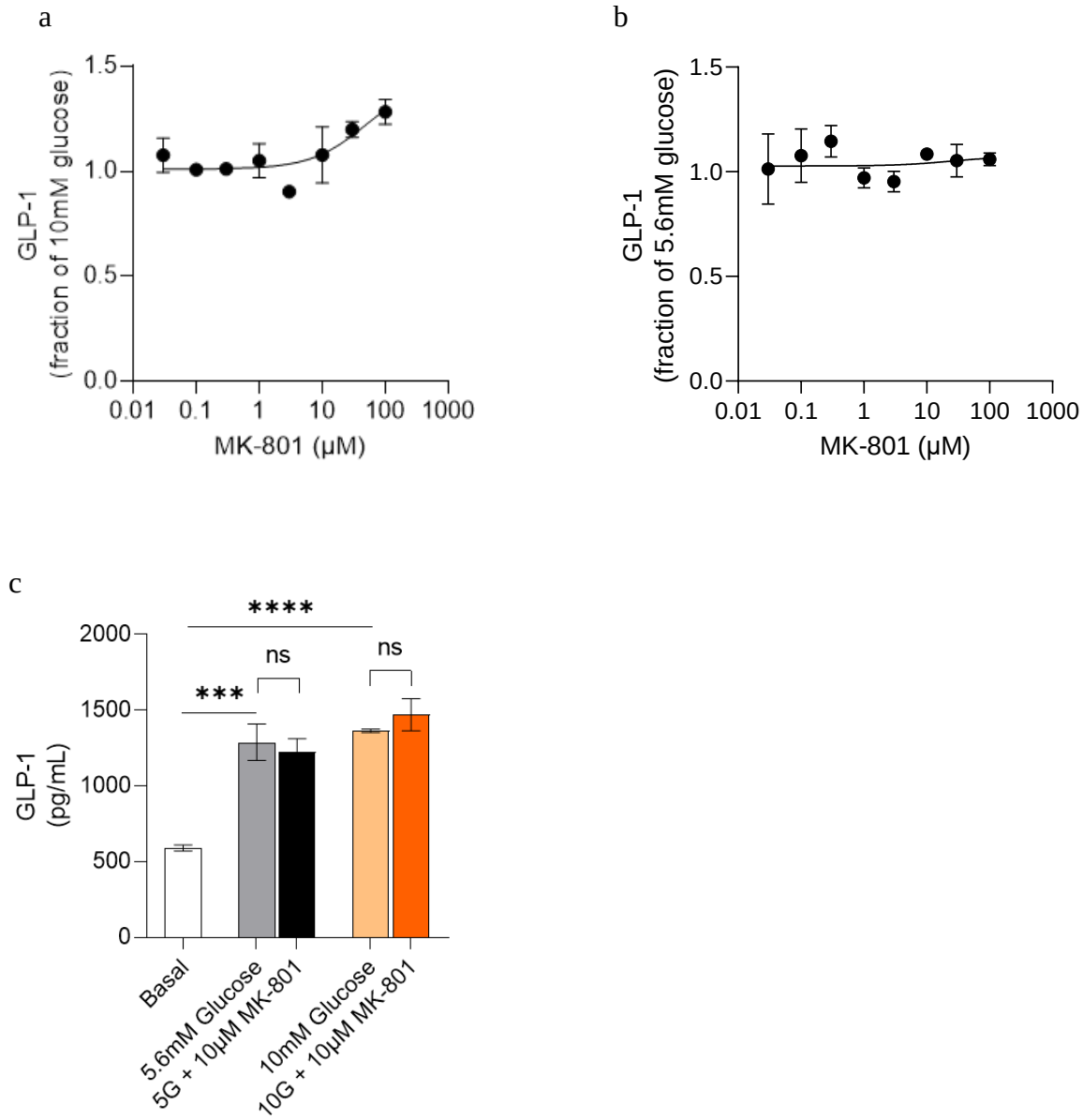


Figure 4.7 NMDAR inhibition by MK-801 does not affect glucose-stimulated GLP-1 secretion in GLUTag cells.

a) Dose response of increasing concentration of NMDAR blocker MK-801 on acute GLP-1 secretion from GLUTag cells stimulated with a) 10mM glucose (10G) or b) 5.6mM glucose (5G). Results were expressed as a fraction of glucose-stimulated GLP-1 release alone. The range of MK-801 concentration was from 0.01μM to 100μM. c) Effect of NMDAR blocker MK-801 at 10μM used acutely for 2hr on glucose-stimulated GLP-1 secretion from GLUTag cells at two tested doses of glucose 5.6mM (5G) and 10mM (10G). Significant values depicted as (*); *p<0.05, **p<0.01, ***p<0.001, ****p<0.0001 (multiple unpaired t-tests), ns – not significant.

4.2.5 siRNA knock-down of *Grin1* in GLUTag cells

Genetic ablation of *Grin1* coding for the GluN1 NMDAR subunit was performed in GLUTag cells via the siRNA-lipofectamine complex method. The downregulation of the *Grin1* expression at mRNA level reached almost 50% compared to control cells transfected with non-targeting scrambled siRNA complexes (Fig. 4.8a), and similar efficiency was observed at protein level quantified by image densitometry from Western blot probed for the GluN1 subunit (Fig. 4.8b). The representative *Grin1* knock-down protein levels are shown in Fig 4.8c.

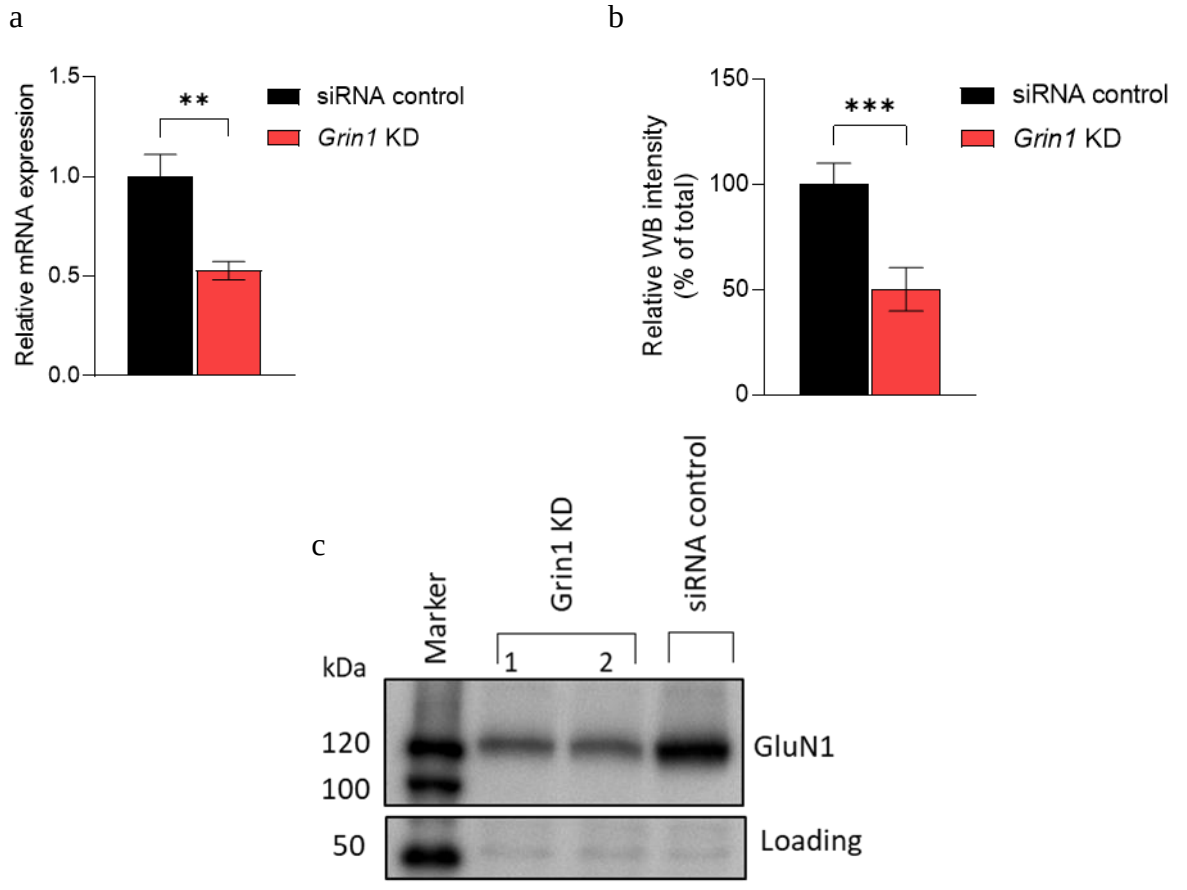


Figure 4.8 *Grin1* knock-down in GLUTag cells validation.

a) *Grin1* expression upon siRNA-mediated knock-down in GLUTag cells 72hrs after the Lipofectamine transfection showing a significant decrease in *Grin1* mRNA levels b) The *Grin1* knock-down (KD) via siRNA-mediated method confirmed on protein level by Western blot densitometry showing 50% decrease in GluN1 subunit expression c) representative western blot with *Grin1* KD (1,2) and control

sample (siRNA control). Data plotted as mean±SEM of n=3. Significant values depicted as (*); *p<0.05, **p<0.01, ***p<0.001, ****p<0.0001 (multiple unpaired t-tests), ns – not significant.

4.2.6 Downregulation of NMDAR *Grin1* subunit expression in GLUTag cells increased glucose-stimulated GLP-1 secretion

Transient siRNA knock-down of the *Grin1* (and corresponding GluN1 protein expression levels) caused a significant 1.6-fold increase in GLP-1 secretion at the basal secretion (717±29 pg/mL vs 432±35pg/mL vs, p<0.01) and more prominent 3.5-fold vs 1.8-fold increase over basal when cells were stimulated with 10mM glucose (1555±166pg/mL vs 814±27pg/mL, p<0.05). There was no effect of *Grin1* knockdown on the GLP-1 secretion stimulated by an intermediate glucose level of 1mM (Fig 4.9).

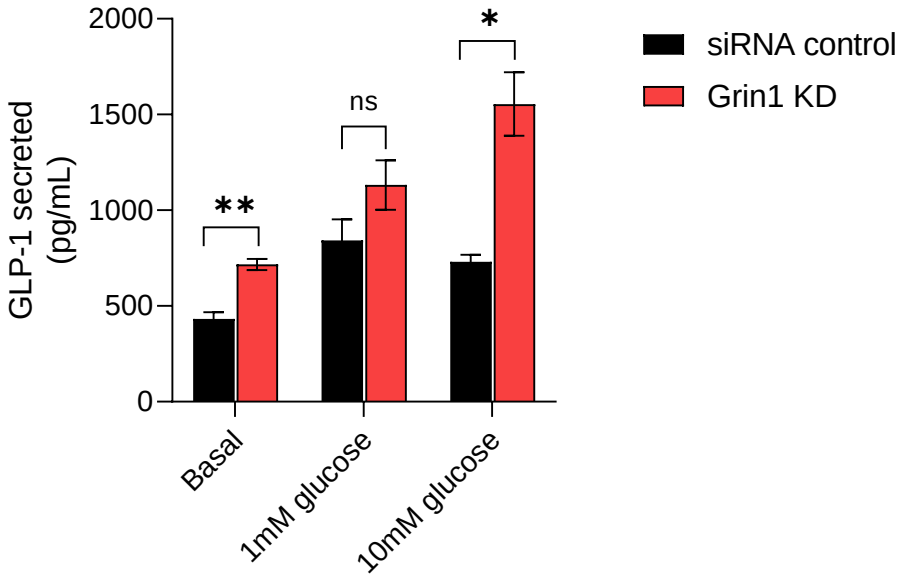


Figure 4.9 *Grin1* knock-down increases GLP-1 secretion from GLUTag cells upon acute glucose stimulation.

GLP-1 secretion from GLUTag cells at the basal condition and upon stimulation with 1mM and 10mM glucose as per labelling. Data plotted as mean±SEM of n=3. Significant values depicted as (*); *p<0.05,

**p<0.01, ***p<0.001, ****p<0.0001, ns – not significant (multiple unpaired t-tests with Holm-Šídák's correction).

4.2.7 NMDA receptor blocker MK-801 increases GLP-1 secretion in GLUTag cells stimulated with glycine and glutamate

Since NMDA receptor antagonist, MK-801 did not affect glucose-stimulated GLP-1 release (Fig. 4.8), but siRNA-mediated downregulation of *Grin1* caused a significant increase in GLP-1 secretion in the presence of 10mM glucose (Fig. 4.9), further optimisation of secretion protocol was done in an attempt to unmask the effect the NMDA receptor inhibition on GLP-1 secretion without using genetic modification. Therefore, NMDAR receptor agonist glutamate was added to the secretion buffer at the final concentration of 0.1mM to avoid glutamate cytotoxicity but to provide saturating levels of NMDAR agonist (EC_{50} for glutamate = 2.3µM, but typically used *in vitro* at 30µM in patching experiments) [236, 237]. Glutamate alone increased GLP-1 secretion from GLUTag cells modestly as reported before (651±74pg/mL vs 420±38pg/mL at basal) [207]. Additionally, GLUTag cells were reported to display sensitivity to different amino acids and employ various sensing mechanisms to respond to amino acids as nutrients. The NMDAR co-agonist, glycine was shown to elevate intracellular [Ca^{2+}] levels and trigger depolarising current in GLUTag cells with an EC_{50} of 0.2mM as GLUTag cells were shown to express glycine-gated chloride channels [238]. Therefore 0.3mM glycine was used in the secretion buffer for two reasons (1) as a co-agonist to NMDAR and (2) as a membrane depolarisation agent to release the Mg^{2+} block of the NMDAR channel. Under these optimised conditions which would maximise the activation of NMDAR, GLP-1 secretion from GLUTag cells was increased from 420±38pg/mL at basal to 1049±87pg/mL in the presence of 0.1mM glutamate and 0.3mM glycine (GlyGlu) (p<0.0001, unpaired t-test) (Fig 4.10). Assuming these conditions would cause most of the NMDAR channels present in GLUTag

cells to open, subsequent blocking of the NMDAR with MK-801 increased the GLP-1 secretion even further to 1694±90pg/mL (p<0.0001, unpaired t-test).

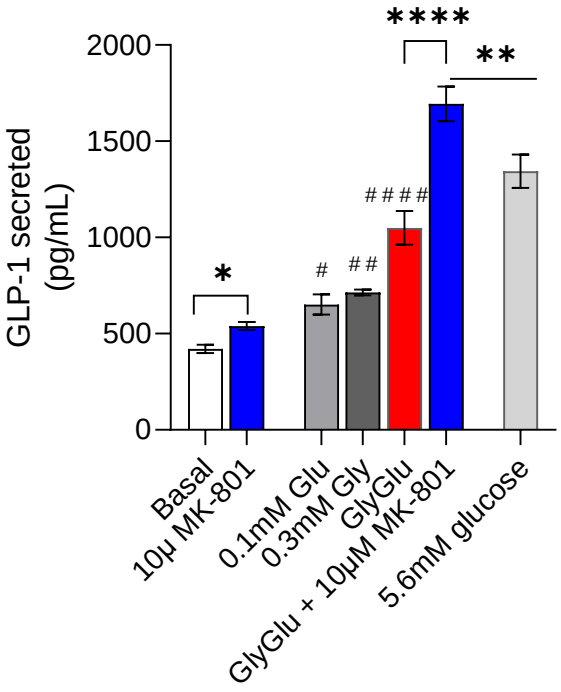


Figure 4.10 The NMDAR blocker MK-801 increases GLP-1 secretion in the presence of glutamate and glycine.

GLP-1 secretion from GLUTag cells at Basal (white bar) and upon stimulation with 0.1mM glutamate (light grey), 0.3mM glycine (dark grey) alone or glutamate and glycine together (GlyGlu) without the MK-801 (red) or with 10µM MK-801 (blue). Glucose-stimulated GLP-1 release (light grey) was added for comparison. Data plotted as GLP-1 secreted (pg/mL) mean±SEM from n=4. Significant values depicted as (*) in pairwise comparison or as (#) when compared to Basal control; Significant values depicted as (*); *p<0.05, **p<0.01, ***p<0.001, ****p<0.0001 (multiple unpaired t-test), ns – not significant.

4.2.8 Competitive NMDAR antagonist – D-AP5 showed no effect on GLP-1 secretion

To ascertain the NMDAR inhibition specificity in regulating GLP-1 secretion the effect of different NMDAR inhibitors, a competitive NMDAR antagonist, D-AP5 was also tested. Using an optimised secretion buffer condition where 0.1mM glutamate and 0.3mM glycine were added to activate the NMDA receptor, blocking NMDAR with D-AP5 at 50µM concentration was assessed. At this concentration, D-AP5 failed to significantly increase the GLP-1 secretion in the presence of glutamate and glycine and did not affect GLP-1 secretion as opposed to non-competitive channel blocker MK-801 (Fig 4.11).

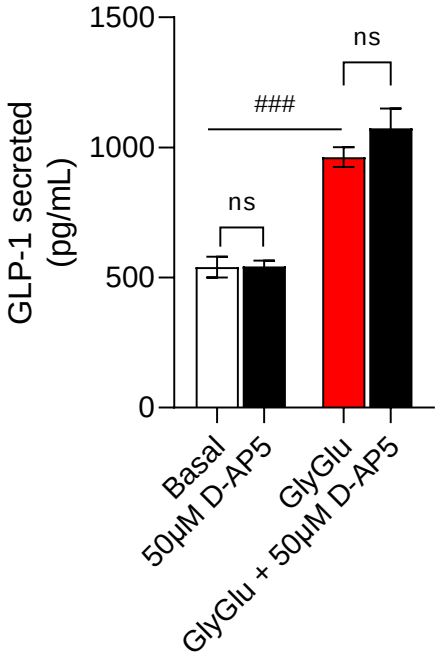


Figure 4.11 Competitive NMDAR inhibitor shows no effect on GLP-1 secretion at the optimised condition.

GLP-1 secretion from GLUTag cells at basal (white bar) and upon stimulation with 0.1mM glutamate, 0.3mM glycine (GlyGlu) without the D-AP5 (red) or with 50µM D-AP5 (black). Data plotted as GLP-1 secreted (pg/mL) mean±SEM from n=4. Significant values depicted as (*) in pairwise comparison or

as (#) when compared to Basal control; *p<0.05, **p<0.01, ***p<0.001, ****p<0.0001 (multiple unpaired t-test), ns – not significant.

4.3 Discussion

4.3.1 NMDAR expression in L cells

The level of *Grin1* detected in primary intestinal cultures of both genotypes, *Abcc5*$^{-/-}$ and wild-type was very low and below the detection limit of the RT-qPCR used (Fig. 4.4). Also, no protein coded by the *Grin1* gene (GluN1 subunit) was detected by western blot in primary intestinal cultures of both genotypes, while GLUTag cells, a clonal model of L cells showed abundant expression of *Grin1* and corresponding GluN1 protein (Fig. 4.4b). This could be explained by the fact that the primary cultures are established from gut crypts, which are gut pluripotent stem cells that within 24hrs form mixed cell cultures consisting of multiple different cell types [152]. In these cultures, GLP-1 positive endocrine cells comprise only a small percentage of total cells, similar to the 1% observed *in vivo* [152]. GLUTag cells on the other hand are established cell lines formed of 100% endocrine and GLP-1 positive cells [239]. Transcriptomic evidence, however, from mouse duodenum, human ileum and jejunum, as well as human ileal organoids shows that enteroendocrine cells (EECs) of these models, mainly GLP-1 positive cells express *Grin1* and also other NMDAR subunits [57]. Despite that little is known about the role of glutamatergic signalling in primary L cells.

4.3.2 NMDAR inhibition

Despite very low expression of NMDAR in primary intestinal cultures, the attempt to investigate the role of NMDA receptor activity in L cells was done with the approach to measuring glucose-stimulated GLP-1 secretion. GLP-1 is only released from L cells in mixed-cell intestinal cultures. Glucose-stimulated GLP-1 release was measured in the presence or absence of an NMDA receptor channel blocker, MK-801. No significant effect of MK-801-blocked NMDAR in primary intestinal cell cultures was observed on glucose-stimulated GLP-

1 release regardless if the primary intestinal cultures were established from wild-type or *Abcc5*$^{-/-}$ mice gut (Fig.4.5a-b). This suggests that the role of NMDAR if any would be not affected by the presence or absence of the Abcc5 transporter. Since GLUTag cells showed abundant expression of the *Grin1* gene and the GluN1 mandatory NMDAR subunit, in addition to other genes coding for other subunits required to form a functional NMDAR channel (GluN2 and GluN3), further experiments were performed using GLUTag cell line (Fig. 4.6).

Pharmacological inhibition of NMDAR with the range of MK-801 concentrations in GLUTag cells confirmed results from primary L cells that glucose-stimulated GLP-1 release operates independently from NMDAR signalling. There was no effect of the MK-801 block at either 6mM or 10mM glucose-stimulated GLP-1 release from GLUTag cells in unoptimized buffer conditions (Fig. 4.7).

However, the siRNA-mediated knock-down of NMDAR mandatory subunit *Grin1* (GluN1) provides evidence of the NMDAR role in regulating GLP-1 secretion from GLUTag cells. A decrease in GluN1 expression increased GLP-1 secretion from GLUTag cells stimulated with 10mM glucose, but also at basal conditions suggesting further that the role of NMDAR in GLP-1 secretion is independent of glucose-dependent membrane depolarization (Fig. 4.9). This result, pointed to NMDAR playing an inhibitory role in regulating the exocytosis of GLP-1 from GLUTag cells as it is the absence of the NMDAR subunit that caused a marked increase in GLP-1 release. This is consistent with emerging evidence for the role of NMDA receptors in stimulus-secretion coupling from endocrine cells, i.e. β-cell specific knock-out of GluN1 was shown to enhance glucose-stimulated insulin release *in vitro* in mouse and human pancreatic islets and improve glucose tolerance in mice [233]. Dextro-methorphan (DXM), one of the most clinically used NMDAR antagonists and its metabolite dextrorphan (DXO) were shown in proof-of-concept human clinical studies to significantly maximise plasma insulin concentration after oral glucose uptake and thus improving glucose tolerance in T2D patients

as compared to placebo treatment [233]. Also, a combination of DXM with sitagliptin (DDPIV inhibitor) in a different clinical trial was shown to restore the early phase of insulin secretion in T2D patients [234]. Mechanistically, the effect of NMDA receptor antagonists on GSIS depends on functional K_{ATP} channels expression and NMDARs likely act upstream of K_{ATP} channels [233, 235]. Role of K_{ATP} channels in glucose-stimulated GLP-1 release from L cells was shown to be less prominent as opposed to the main mechanism involving SGLT1 sodium-glucose co-transporter. Nonetheless, L cells of various models were shown to express functional K_{ATP} channels, however, their role in glucose-stimulated secretion remains a mystery, reviewed in [240]. Since native L cells are polarised, it is unclear if K_{ATP} channels are expressed on the apical or basolateral side of these cells. It has been reported that the application of K_{ATP} channel blocker tolbutamide on the vascular side triggers GLP-1 secretion in rat intestinal perfusion [192], but *in vivo* use of sulphonylureas in T2D patients does not enhance GLP-1 release upon oral glucose challenge. There is also evidence that the application of tolbutamide on the apical side during intestinal perfusions in rats triggered GLP-1 release in response to glucose, but that required inhibition of SGLT1 [197]. It is then possible, that in order to unravel the full effect of NMDAR inhibition on glucose-stimulated GLP-1 secretion via K_{ATP} channels mechanism, the predominant SGLT1 glucose-sensing mechanism would have to be switched off.

4.3.3 Different NMDAR antagonists

To ascertain the specificity of NMDAR-inhibition on increasing GLP-1 secretion, the secretion conditions were optimised to maximise the activation of the NMDAR channel by using saturating concentrations of NMDAR agonist – glutamate, 0.1mM and co-agonist – glycine, 0.3mM. These conditions additionally depolarised the membrane to relieve the Mg^{2+} block. The pharmacological block of NMDAR with MK-801 under these conditions reproduced the

significant increase in GLP-1 secretion from GLUTag cells with *Grin1* knocked down and also confirmed a small effect on increasing basal GLP-1 release (Fig. 4.10). However, using different NMDAR antagonists competitive for the glutamate binding site D-AP5, even the optimised secretory conditions to keep the NMDAR channel open did not produce the GLP-1 increase (Fig. 4.11). MK-801 is widely reported as a potent, selective and non-competitive NMDAR antagonist acting as a channel pore blocker, but it is also a non-specific inhibitor to α7 nicotinic acetylcholine receptor channel (nAChRα7) [241, 242]. The effect of MK-801 on GLP-1 secretion mediated through nAChRα7 seems to be unlikely as the gene (*Chrna7*) coding for the subunit of this monomeric receptor showed almost no expression in GLUTag cells in RNA sequencing (GEO accession number GSE193866). A recent study that reports nAChRα7 expression in GLUTag cells also points out that activation of this receptor stimulated GLP-1 secretion *in vitro*, and this effect was attenuated by specific α7nAChR antagonist [204]. Also, to minimise the off-target effects of MK-801 on other receptors and cellular functions such as the reported effect of maleate and maleic acid (MK-801 conjugate) on calcium levels [243], a low 10μM extracellular concentration of MK-801 was used. The difference in results with different NMDAR antagonists, MK-801 and D-AP5, can stem from the intrinsic differences in pharmacological properties of inhibitory mechanisms between these antagonists. MK-801 blocks the channel by binding within the open (glutamate-bound) activated state [244, 245], but does not directly affect the receptor's binding ability of glutamate [246]. Similarly, to other non-competitive NMDAR antagonists, like PCP or ketamine, MK-801 is both use- and voltage-dependent and not easily removed even when agonists are no longer present [247, 248]. MK-801 produces a progressive, long-lasting blockade of the current through the ion channel of the NMDA receptor as the open channel that was blocked by MK-801 can lose its transmitter function and close with the drug still bound to it [244]. Also, the addition of glutamate and glycine was reported to co-operatively enhance the maximally effective concentrations of MK-

801 by increasing the binding affinity of MK-801 to the NMDA receptor complex, which could help unmask the effect of MK-801 under optimised conditions of secretion protocol, while it did not when D-AP5 was used [249].

Also, because the channel pore is relatively conserved among NMDARs, channel blockers like MK-801 show little subunit selectivity and will block any NMDAR complex assembly [214]. D-AP5, however, is a competitive NMDAR antagonist that binds to GluN2 subunits on the glutamate binding site and shows a tendency to selectivity for GluN2A and GluN2B containing NMDA receptor complexes [250, 251]. Although GLUTag cells express the *Grin2A* gene (GluN2A subunit) and *Grin2D* (GluN2D subunit), no *Grin2b* (GluN2B) expression was found. GLUTag cells also show the most abundant expression of *Grin3a* (coding for the GluN3A subunit). The effect of D-AP5 has been mainly characterised by the most common combination of GluN1/GluN2 of NMDA receptor complexes, co-assemblies of GluN3 subunits with GluN1/GluN2 were shown to produce functionally distinct tri-heteromeric NMDAR, which are not yet fully characterised [251]. No GluN3-specific drug has been identified yet as well [220].

Additional complexity of NMDAR function is related to the tissue-, cell- and synapse-specific coupling of different NMDAR subunits to signalling molecules (protein kinases, phosphatases, and cytoskeletal regulators) of postsynaptic density. These non-ionotropic functions of NMDA receptors depend on the scaffolding and signalling proteins that interact with the intracellular C-terminal domain of NMDAR subunits [252, 253]. The interaction of NMDAR with intracellular signalling pathways can occur differentially depending if the signalling happens via the binding of both co-agonists, glutamate and glycine, or each agonist separately. For example, high concentrations of co-agonist, glycine or D-serine, prime NMDA receptor internalisation and this signalling depends solely on specific splice variants of GluN1 subunit

[254, 255]. This feature of NMDA receptor adds additional difficulty in interpreting the role of NMDAR in GLP-1 secretion.

4.4 Summary

In summary, it is shown that blocking NMDAR increased the amino acid-stimulated GLP-1 release, suggesting that glutamatergic signalling via NMDAR indeed plays a regulatory role in inhibiting GLP-1 secretion in response to nutrients, but it might not be necessary for glucose-mediated stimulation. NMDAR inhibitor MK-801 showed no effect on glucose-stimulated GLP-1 release from GLUTag cells, which was in line with the results from the primary intestinal cultures suggesting that the NMDA receptor might not have a direct role in modulating GLP-1 release in the presence of glucose. siRNA-mediated downregulation of NMDAR expression, however, proved to increase glucose-stimulated GLP-1 release relative to control. This effect could be mediated by the signalling cascades of intracellular domains of NMDAR. Further characteristics and confirmation of the NMDA-gated ion-channel function in gut endocrine cells will need to be addressed with more sophisticated methods, i.e. electrophysiological methods. The unclear role of K_{ATP} channels in the stimulus-secretion coupling of GLP-1 release adds additional complexity to the role of NMDAR in GLP-1 secretion, which in pancreatic β-cells was shown to exert its inhibitory function via K_{ATP} channels. It is possible, though, that NMDAR may play a more important role in the endocrine response to the arrival of digested protein in the gut and the mechanistic basis of that is not related to K_{ATP} channels.

Chapter 5: Regulation of GLP-1 secretion by pH

5.1 Introduction

5.1.1 Secretion of gut hormones known to be affected by pH

The known effects of extracellular pH alterations on the secretory response of the endocrine cells within the GI tract will be mainly restricted to the stomach and duodenum, where acid/base balance is important for nutrient digestion [256]. Secretin, which is released from S cells in the duodenum, signals the arrival of chyme and is responsive to pH below 4.5 [257]. Similarly, the release of another gut hormone, motilin from M cells in the proximal intestine is also stimulated by an acidic extracellular pH. However, the mechanism of low-pH-triggered motilin secretion has been attributed to the acid-sensing ion channels (ASIC1-4) [258]. The effect of acidic extracellular pH on the secretion of GLP-1 from L cells is currently unknown.

5.1.2 pH profile of the gut

Intraluminal pH of the gastrointestinal (GI) tract varies between the different parts of the gut (Fig. 5.1). In healthy human subjects, the pH of the stomach is very acidic (pH 1.0 - 2.5) at fasting, and it increases in the proximal intestine to pH 6.6 and further to pH 7.5 in the terminal ileum. There is a sharp drop in pH to pH 5.5 at the caecum, which is marking the entry into the colon [51, 259, 260]. The pH within the colon fluctuates between 5.0 and 8.0 [259], averaging at pH 6.63 [51]. The colon was found to have the highest variability of pH within the parts of the GI tract [51] and it also shows the highest level of intra-individual differences in pH profile between human subjects [259, 261]. Interestingly, 82% of the GI transit time happens in the

colon and it differs significantly between subjects, while small intestine pH profile and transit times were found to be more robustly predictable [259, 262]. The GI transit times and pH profile have been assessed by the ingestion of the radiotelemetry capsules or wireless motility capsules such as IntelliCap or SmartPill [259-261]. Intraluminal pH, although easy to measure, might not reflect the pH that the epithelial layer of the gut is exposed to. The peri-mucosal pH on the surface of colonic cells, measured *in vivo* in humans and rats, was higher and in the range of 7.1-7.5 as opposed to the intraluminal pH values of 6.6 [263]. The main reason for the difference between intraluminal and peri-mucosal pH is that the GI tract has a single layer of very active epithelial cells, which are protected on the luminal side by mucus and glycocalyx that is 100-800µm thick [264, 265]. The measurement of the peri-mucosal pH at the surface of the cells is difficult, but it is possible to measure pH *in vivo* at a single endoscopic site. That, however, might not be representative of other segments of the gut [264]. Interestingly, the *in vitro* studies suggest that the luminal pH changes will translate into peri-mucosal pH changes and lowering in steps luminal pH resulted in small changes to the pH at the surface of the cells, i.e. pH 7.06 resulted in surface pH 6.64, and luminal pH 6.09 caused surface pH 6.39 [266].

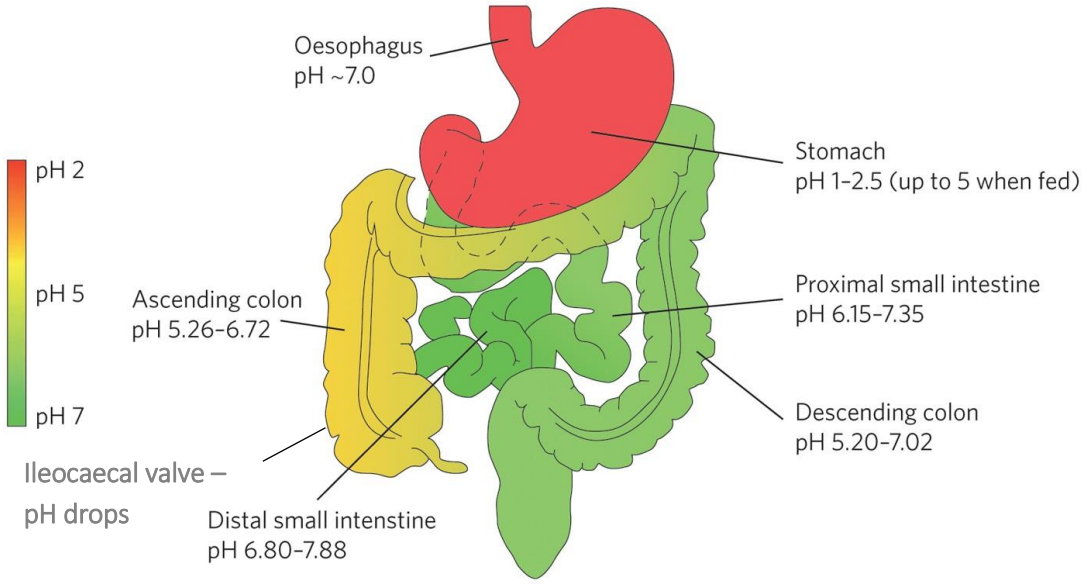


Figure 5.1 Physiological pH profile of the human gastrointestinal (GI) tract. Adapted from [267].

The pH of the gut is dynamic and influenced by factors such as digestive juice production and secretion, motility and metabolism. Delivery of food into the stomach increases the pH from 1-3 to pH >5-6, depending on the meal content and volume [259]. Regulation of the intraluminal pH in the colon, for example, depends on the mucosal production of bicarbonate and lactate, bacterial fermentation of carbohydrates and mucosal absorption of short-chain fatty acids (SCFA), and possibly intestinal transit [264]. Despite these findings, there has been limited research into whether changes in intraluminal pH affect the function of gut endocrine L cells. As L cells are scattered alongside the GI tract and enriched in the colon, where the pH is the most variable, investigating the effect of pH on the function of L cells should enable a better understanding of the conditions regulating stimulus-secretion coupling of GLP-1.

5.1.3 pH in the gut is disrupted in the pathology of obesity, diabetes and after bariatric surgery

The clinical relevance of the pH within the GI tract is not clear. Evidence suggests that the intraluminal pH of the gut influences inflammatory bowel disease (IBD), chronic bowel disorder, ulcerative colitis, Crohn's disease [264], cancer formation [268] and cystic fibrosis [269]. Active ulcerative colitis was shown to shift the pH in the colon to the more acidic range, while Crohn's disease data were not conclusive of pH changes in patients. In general, patients suffering from inflammation of the colonic mucosa also exhibit lower pH in the colon [264]. Obese subjects were found to have lower intraluminal pH within the small intestine when compared to controls, in both the fasted and fed states. The median pH in the small intestine of the normal-weight patients was 7.15 at fasted and 7.33 fed, while in obese individuals it was 6.68 and 6.71, respectively. Interestingly, following food intake, pH was found to increase

significantly in both groups by comparable amounts [52]. Patients with cystic fibrosis (CF) and CF-related diabetes were found to have decreased post-prandial levels of active GLP-1, in comparison to healthy subjects [270]. Gastrointestinal symptoms and indigestion in CF are partially attributed to impaired bicarbonate secretion in the gastrointestinal lumen that changes the pH profile of the proximal small intestine which causes inadequate acid neutralization. It has been proposed that CF patients might benefit from pH-optimising therapies [271]. The mechanism of lowered GLP-1 secretion in CF patients is, however, unknown.

Changes in the GI pH profile were also reported in patients after bariatric surgery. Bariatric surgery is performed by a variety of different procedures, including Roux-en-Y gastric bypass (RYGB) and sleeve gastrectomy, to re-direct food from the stomach to more distal parts of the GI tract. Each of these bariatric procedures is used as an effective therapy for obesity and T2D. The beneficial effects of bariatric surgery in resolving hyperglycaemia in T2D patients have been in part attributed to increased levels of gut hormones such as GLP-1 and PYY secreted in abundance from the distal intestine. Reproducing these hormonal changes using pharmacological compounds (i.e. GLP-1 mimetics) or dietary modifications has been the focus for new therapeutic targets in treating diabetes and obesity [272, 273]. The pH of the stomach, but also of the proximal part of the gut, following bariatric surgery has been reported to increase. While the normal pH of the stomach at fasted state is 1-3, following RYGB this can increase to as high as pH 5 [274]. The median pH in patients after RYGB in the oro-caecal segment of the gut (from ingestion to ileocecal valve) was higher than in healthy controls (pH 6.45 vs 3.45). Transit time through the colon was found longer in patients after RYGB, while oro-caecal transit times were shorter [275]. The clinical relevance of these findings is mainly explored in the context that changes in the intraluminal pH may affect the bioavailability of the medications used to treat the diseases of the GI tract itself or other associated conditions, i.e. diabetes. For example, the pharmacokinetics of semaglutide, the first GLP-1 mimetic to be

taken orally, considers the patient's pH profile of the gut [276]. The effect of the pH profile within the GI tract on the secretion of endogenous GLP-1 remains unknown.

5.1.4 pH-dependence of stimulus-secretion coupling in pancreatic β-cells

Gut endocrine L cells share certain similarities in stimulus-secretion coupling with pancreatic β-cells [188, 189]. Alterations of the extracellular pH (pH_o) were reported to affect glucose-stimulated insulin secretion from pancreatic β-cells of rat islets in *ex vivo* live-time perfusion experiments [277, 278]. Changes in the extracellular pH_o from 7.4 to 7.0 decreased the glucose-stimulated insulin secretion by almost 50%. Insulin release was found to decrease in the presence of extracellular protons in a dose-dependent manner, as pH_o of 6.8 caused an 80% decrease in insulin with a further decrease in insulin secretion at pH 6.0 [277, 279, 280]. The inhibition of insulin secretion by acidic pH_o was shown to be relatively fast and occurred within 30 minutes from the decrease in pH_o, and equally affected both phases of insulin release [278]. The pH-dependence of insulin release occurred also with different secretagogues than glucose, such as α-ketoisocaproic acid [278]. Increasing pH_o from 7.4 to 7.8 was shown to either not affect glucose-stimulated insulin release [277] or decrease it similarly to acidic pH [278].

K_{ATP} channel serves as a sensor of the β-cell metabolic state and is closed by rising internal levels of ATP in response to glucose, closure of the K_{ATP} channel triggers membrane depolarization and subsequent insulin release [186]. However, despite a correlation between changes in pH_o and the ATP/ADP ratio of pancreatic islets, the mechanism and interplay of how these factors influence insulin secretion remains unclear [278]. Patch-clamping studies using mouse pancreatic β-cells have reported that lowering pH_o from 7.2 to 6.2 did not affect the function of the K_{ATP} channel [281].

To further elucidate the role of pH in the stimulus-secretion coupling of insulin from pancreatic β-cells, research interests were shifted to focus on investigating the intracellular pH (pH_i)

changes within β-cells upon glucose stimulation. It was postulated that glucose-induced changes in pH_i may participate in glucose-induced insulin secretion from pancreatic β-cells [282]. Multiple studies have tried to address the pH_i changes in pancreatic β-cells and their effects on glucose-stimulated insulin release with conflicting results and the role of pH_i changes in insulin secretion remain unclear [283-286].

5.1.5 Exocytosis of GLP-1

Little is known about the details of the GLP-1 exocytosis events and the variants and assembly of the core SNARE (N-ethylmaleimide-sensitive factor (NSF) attachment protein receptor) proteins in endocrine L cells. In addition, the exocytotic machinery and events leading to the release of GLP-1-filled secretory granules are only partially established (hence often compared with β-cells). In β-cells, the release of insulin occurs in several steps and involves docking of the insulin secretory granule to the plasma membrane, followed by priming and Ca^{2+}-dependent release and refilling (Fig. 5.2). Before the release, the insulin secretory granules undergo maturation and ATP-dependent proton pump (V-ATPase) acidify the granule lumen and increases the proteolytic activity of the pro-hormone convertase enzymes (PC1/3 and PC2) to cleave off the C-peptide to generate insulin from the proinsulin precursor [287]. The granules are only released when they undergo the priming process, which in itself remains to be fully elucidated, and in β-cells have been shown to depend on intracellular chloride fluxes via CLC3 [288].

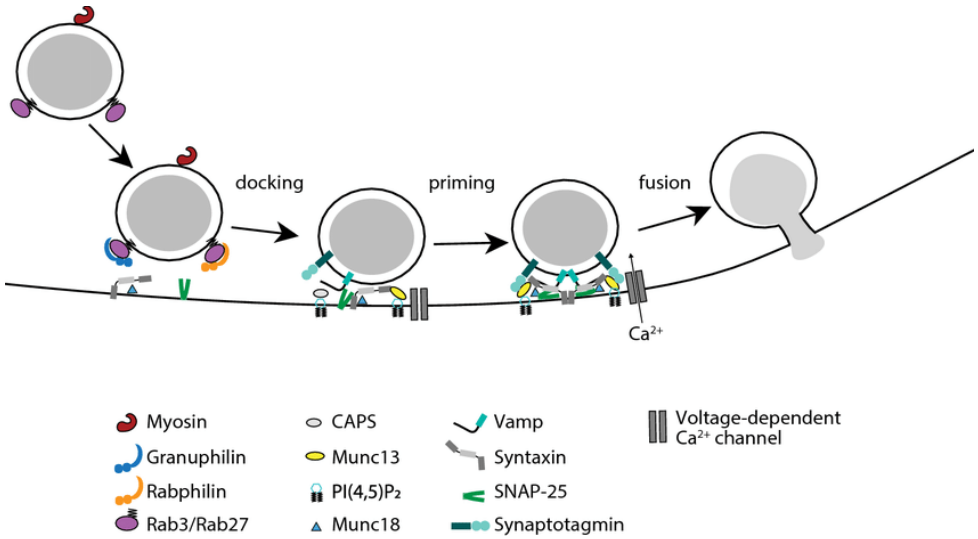


Figure 5.2 The sequence of events of regulated exocytosis of insulin from pancreatic beta cells. Adapted from [287].

Similar to insulin, GLP-1 release occurs in response to increased intracellular calcium levels. The entry of Ca^{2+} into the L cells is mediated by L- and Q-type voltage-gated calcium channels [211]. As a rise in intracellular calcium can also be mediated via increased cAMP levels, compounds such as forskolin, an adenylate cyclase activator, are generally used to increase intracellular cAMP for stimulation of GLP-1 secretion [180, 289]. Electron microscopy evidence showed that GLP-1-secreting L cells have large dense core secretory granules (LDCV), which are homogenous and situated on the basolateral side of the L cells facing the capillaries [290]. Exocytosis of GLP-1 hormone was found to be bi-phasic under stimulating conditions with forskolin, the first phase of forskolin-induced GLP-1 granules release peaks at 1-6min after stimulation, and the second phase at 7-12mins thereafter [291]. Murine L cells express SNARE protein syntaxin-1a and the knock-out mouse model of syntaxin-1a (Syn1a KO) showed a reduced first phase of GLP-1 exocytosis (low number of events) with the second phase of the exocytosis being completely abolished. Syn1a KO male mice display also higher glucose levels in OGTT and reduced plasma levels of GLP-1 were found in both females and

males [291]. Exocytotic events of the L cells are characterised as short single-granule fusions and multi-granular secretory granules fusion that differed in the magnitude and the duration of the event. The majority of the exocytosis of GLP-1-filled secretory granules in native L cells occurs as multi-granular or compound (sequential) fusion (75% of total events)[291], whereas in pancreatic β-cells less than 10% exocytotic events were reported to occur as sequential or multigranular exocytosis [292] GLUTag cells were found to have basal 'leaky' exocytosis of 1.9/100μm^2 granule fusions that would increase almost 9-fold upon depolarization in the presence of KCl [293]. VAMP2 has been confirmed to be pivotal for the exocytosis of GLP-1, while VAMP8, although detected at the mRNA level in GLUTag cells, showed low expression on the protein level [293]. It appears that GLUTag cells may have a higher percentage of primed, pre-docked granules as compared to β-cell model cell lines. However, the exact roles of Munc18-1/2 and Munc13-1 that mediate pre-fusion docking and priming are not known in GLP-1 secretion [293]. Synaptotagmin7 (encoded by *Syn7*), the vesicle-associated calcium sensor, was also detected in murine intestinal L cells as well as in GLUTag cells. The *Syn7* knockout mouse model was shown to have impaired GLP-1 secretion in response to oral glucose gavage. Similarly, the knock-down of *Syn7* in GLUTag cells resulted in a 60% reduction in GLP-1 release in response to glucose and smaller capacitance changes after the depolarization pulse. Altering the expression of Syn7 did not affect the GLP-1 production and peptide processing, and impaired GLP-1 exocytosis was solely attributed to the downstream effector of calcium signalling [294].

5.1.6 Regulation of intracellular pH

Living cells utilise multiple different systems to control the intracellular pH in the cytosol and the luminal pH of their secretory pathway. Changes in pH to the extracellular environment of the cells can induce parallel changes to the intracellular pH of the cell. Studies on cell cultures

have shown that acidification of culture media to pH 6.3 causes the intracellular pH (pH_i) of the cytosol to decrease to pH 6.8, while it can be maintained at pHi 6.9-7.0 if the extracellular pH (pH_o) is controlled at 7.2-7.4 [295]. Cellular pH homeostasis is maintained due to the activation of membrane transport processes such as acid-loaders and acid-extruders (Fig. 5.3). These involve primary active acid-extruders (V-ATPase proton pumps and P-type H^+/K^+ ATPases) and sodium-driven secondary active acid-extruders (members of SLC4 family), such as electrogenic Na^+/HCO_3^- co-transporters (NBCn) and electroneutral Na^+/HCO_3^- co-transporters (NBCe) together with Na^+/H^+ exchangers (NHE, SLC9 family) [296]. In addition to acid extruders, cells also express acid loaders and various Cl^--coupled transporters belonging to the SLC4 or SLC26 families of genes [297-299].

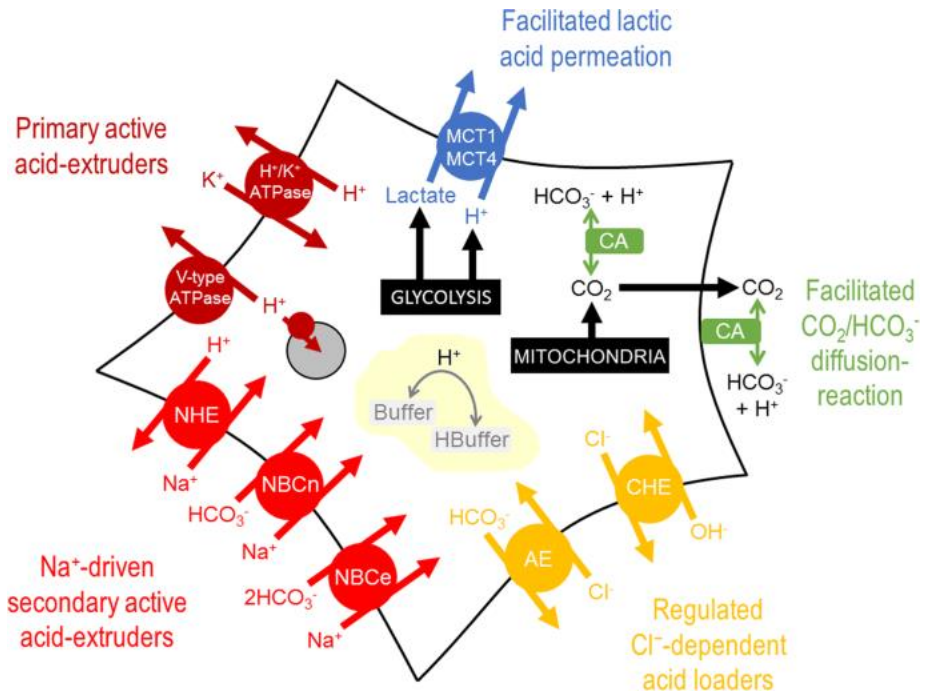


Figure 5.3 Acid loaders and extruders.

Various acid loaders and acid extruders that are expressed in the plasma cell membrane and intracellular compartments play a key role in regulating intracellular pH. Adapted from [300].

Membrane conductance to H^+ ions was found to be small, however, proton currents have been reported in snail neurons [301]. More recently, the voltage-gated proton channel Hv1 (gene *Hvcn1*) located in pancreatic β-cells was shown to play a role in regulating insulin secretion [302]. Within the cell, pH is also tightly controlled within the different intracellular compartments, including the lumen of the ER and secretory pathway. This is mainly achieved by various chloride channels and V-ATPases, ATP-dependent proton pumps expressed on the vesicular membrane of intracellular organelles [303]. The transmembrane subunit of the V-ATPase proton pump, $V_{0,}$ was found to serve as a sensor of intragranular pH that controls exocytosis and synaptic transmission via the reversible dissociation of soluble subunit V_1 at acidic pH. It has been shown that the V-ATPase V_0 domain allows the exocytotic machinery to discriminate between fully loaded and acidified vesicles from vesicles undergoing the reloading of neurotransmitters in neuronal cells [304]. Intragranular pH of secretory pathway vesicles was also shown to modulate exocytosis of insulin from β-cells. The acidification of insulin secretory granules in β-cells is also driven by V-ATPase proton pumps, while the granular Cl^- fluxes are important in modulating granule acidification. In the case of β-cells, the correct pH of the secretory granule was reported to be required for replenishing the readily releasable pool of insulin-filled secretory granules [288]. Additionally, Na^+-coupled mechanisms of moving protons outside of cells via Na^+/H^+ exchangers (NHE) were also implicated in regulating the cytosolic pH of β-cells and insulin release [284, 286]. Currently, the role of acid-loaders and acid-extruders in the stimulus-secretion coupling of GLP-1 from L cells remains unknown.

5.1.7 Production of GLP-1 is pH-sensitive

GLP-1 is expressed from the preproglucagon gene (Gcg). Preproglucagon peptide is differentially processed after translation in a tissue-specific manner by prohormone convertases

(PC). In pancreatic α-cells, high levels of PC2 (protein, PC2; gene, *PCSK2*) expression produces glucagon, while in the intestinal endocrine cells, predominant PC1/3 (protein, PC1/3; gene, *PCSK1*) cleaves preproglucagon peptide exclusively into GLP-1, GLP-2, oxyntomodulin, IP2 and glicentin-related pancreatic polypeptide (GRPP) [305]. PC1/3 is also responsible for cleaving proinsulin into insulin and C-peptide in pancreatic β-cells, as such is responsible for the first step of the biosynthesis of insulin [306]. PC1/3 is a calcium-dependent protease that is synthesized as an inactive proPC1/3 94kDa zymogen and undergoes autocatalytic processing within the ER to generate 87kDa protein [307], which is further cleaved within Trans Golgi Network (TGN) to 74kDa form and targeted to the dense core secretory granules of the endocrine regulated secretory pathway [308]. Within the TGN and secretory granules, the mature 74kDa form is further processed to the much more active 66kDa form [307]. PC1/3 is co-stored with its prohormone substrates within the dense core secretory granules (Fig. 5.4). The pH of the secretory granules alongside regulated secretory pathways (as opposed to constitutive) has been reported to be acidic with average pH of 5.2, which would ensure optimal conditions for PC1/3 processing into the fully active form [303, 309]. It has been reported that while the activity of the 66kDa form of PC1/3 is higher compared to the 74kDa and 87kDa forms, the 66kDa form is less stable and has a very narrow condition for optimal activity at acidic pH of 5.5-5.0 and requires high calcium (mM) levels [310-312]. The optimum pH of PC1/3 activity is between pH 5.5 and 6.5, and increasing pH to neutral values dramatically decreases PC1/3 enzymatic activity. The requirement of high calcium levels for optimal PC1/3 activity increases linearly up to the concentration of 5mM calcium, and only a minimal increase in activity is observed with calcium levels of 10mM and higher. The proteolytic activity of PC1/3 is both, time- and substrate concentration-dependent. There is an initial 9-10 minutes pre-steady state lag phase of activation by substrates followed by the linear phase in increased activity with the constant velocity of substrate hydrolysis [313].

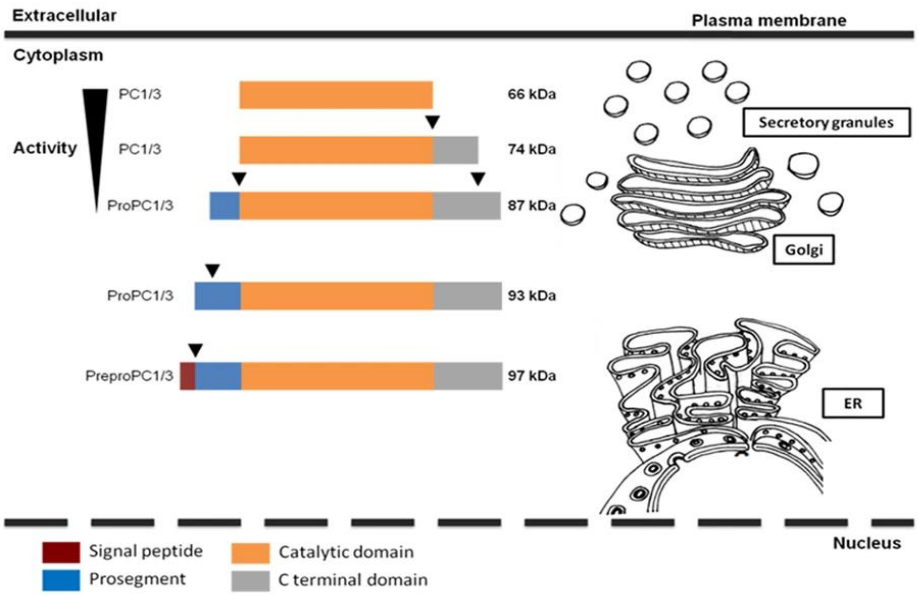


Figure 5.4 Prohormone convertase 1/3 (PC1/3) processing and trafficking. Adapted from [307].

5.1.8 Role of chloride in GLP-1 secretion from L cells

The role of chloride-current in the electrical activity of GLUTag cells has been reported as a mechanism for GLP-1 release in response to GABA and glycine stimulation. Glycine and ionotropic GABA receptors (which are ligand-gated Cl^- channels) were found to be expressed in GLUTag cells and are functionally responsible for membrane depolarisation and GLP-1 release in response to glycine and GABA [238]. While the role of chloride channels (CLC, CLICs) and Cl^-/H^+ exchangers in the secretion of GLP-1 from L cells remains unexplored, there is substantial evidence of the importance of chloride ions in regulating insulin secretion. Removal of extracellular chloride was shown to abolish insulin release from pancreatic β-cells upon glucose stimulation [314]. Similarly, a reduction in intracellular chloride was reported to have an effect and decrease the exocytosis events by 93% in pancreatic β-cells [288]. The inhibition of insulin release by extracellular chloride depletion was found to be rapid and easily reversible by re-introducing chloride into the buffer and lack of chloride ions did not affect the

net calcium uptake of glucose-stimulated islets [314, 315]. Furthermore, it was shown that the influx of chloride through granular CLC-3 stimulates insulin exocytosis by facilitating ATP-dependent priming of the newly emerging insulin granules through the acidification of the secretory granules [288]. While there is a consensus that loss of CLC3 expression can result in reduced insulin exocytosis and lowers the release of secretory granules [316, 317], the exact mechanism remains debatable [318]. Some reports have argued against the localisation of CLC3 expression on the membrane of secretory granules, and thus the ability of CLC3 to directly affect granule acidification, suggesting instead that CLC3 localizes to synaptic-like microvesicles (SLMV) and endosomes, and thus is regulating the exocytosis indirectly [319]. It was also shown that β-cells express volume-sensitive anionic conductance that is activated by cell swelling in hypotonic conditions and allows chloride efflux through outwardly rectifying Cl^- channel [320, 321]. The function of this channel has been linked with the electrical activity of β-cells and insulin secretion [321]. More recently it has been shown that the possible candidate might be SWELL1, a subunit of volume-regulated anion channel (VRAC) that is responsible for chloride efflux during osmotic swelling [322]. Murine and human model cell lines of β-cells, including pancreatic islets, showed a reduction in glucose-stimulated insulin release when the Swell1 gene was knocked out [322].

Due to a certain degree of similarities between gut endocrine L cells and pancreatic β-cells, it is plausible that chloride also has a regulatory role in the secretion of GLP-1.

5.1.9 Glucose-sensing in L cells – the role of sodium ions

The main mechanism of glucose-triggered GLP-1 secretion involves Na^+-coupled electrogenic glucose co-transporter, SGLT1 (SLC5A1). SGLT1 activation has been shown to account for a large proportion of GLP-1 secretion *in vitro* from GLUTag cells [187], primary L cells [196], and also *in vivo* from rat perfused intestine and from human ileal and colonic tissue preparations

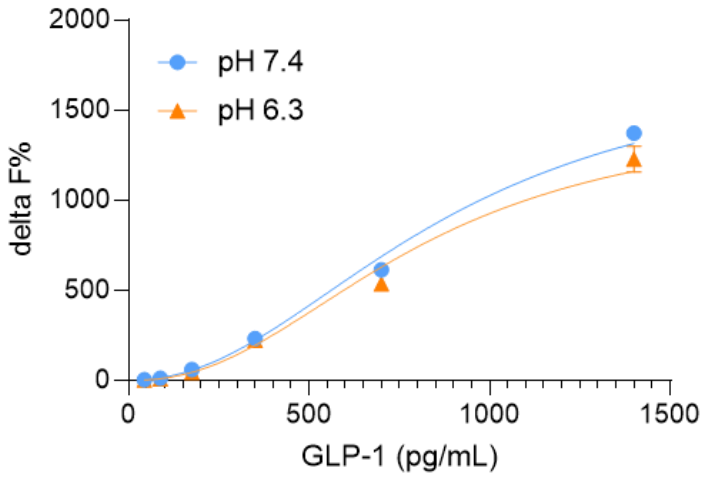
[190, 192]. SGLT1 is expressed on the apical surface of the epithelial cells across the intestinal brush border and is responsible for glucose absorption into gut epithelial cells. It regulates glucose transport against a concentration gradient by coupling the uptake of two Na^+ ions with one molecule of glucose [323]. The glucose flux via SGLT1 into L cells in response to sugar in the gut lumen is associated with inward Na^+ current, sufficient to drive membrane depolarisation and subsequent opening of voltage-gated Ca^{2+} channels (VGCC). This results in an increase in intracellular Ca^{2+} which triggers GLP-1 exocytosis [187, 323, 324]. It was shown that the transport capacity of SGLT1 and its affinity for glucose depends on the extracellular pH and sodium levels. Previous studies have shown that, in the absence of sodium and in an acidified environment, the SGLT1 sodium-glucose co-transporter can utilise protons to drive glucose transport into cells. SGLT1 affinity to protons was found to be over 1000-fold greater than that of sodium, and the maximal rate of H^+/sugar transport was greater than Na^+/sugar transport. However, SGLT1 affinity for glucose at these conditions is very low and requires a high glucose concentration (K_m=7-35mM, voltage-dependent) as compared to glucose affinity in the presence of sodium at pH 7.4 (Km=0.2-0.3mM) [325]. Thus, in the presence of sodium at an acidic pH, the SGLT1 transporter exhibit a high capacity for transport albeit with low glucose affinity, however at an alkalic pH, SGLT1 acts as a low-capacity, but high-affinity glucose transporter [326]. It has been suggested that this intrinsic property of the SGLT1 transporter might be physiologically relevant and regulate glucose uptake into gut epithelial cells according to the intestinal pH profile.

5.3 Results

5.3.1 Low pH does not affect the readout of the HTRF ELISA signal

In this study, only active forms of GLP-1 hormone (GLP-1(7-36)-NH_2 and GLP-1(7-37)), as opposed to the inactive forms (GLP-1(9-37) and its amide GLP-1(9-36)-NH_2), were quantified by Homogeneous Time-Resolved Fluorescence (HTRF) immunoassay. To confirm that the HTRF ELISA signal was not affected by the pH of the secretion buffer and could reliably detect GLP-1 at different buffer conditions, a standard curve for active GLP-1 gold standard peptide was tested at extreme pH conditions. Samples were prepared at a two-fold dilution range from 1400pg/mL to 43.8pg/mL in secretion buffer at pH 6.3 and pH 7.4 (Fig. 5.5a). Additionally, commercially available active GLP-1 (7-36-NH_2) from a different source was also tested (Bachem) (Fig. 5.5b). As shown in Figure 5.5, the pH of the secretion buffer/supernatant had no effect on the HTRF ELISA signal.

a



b

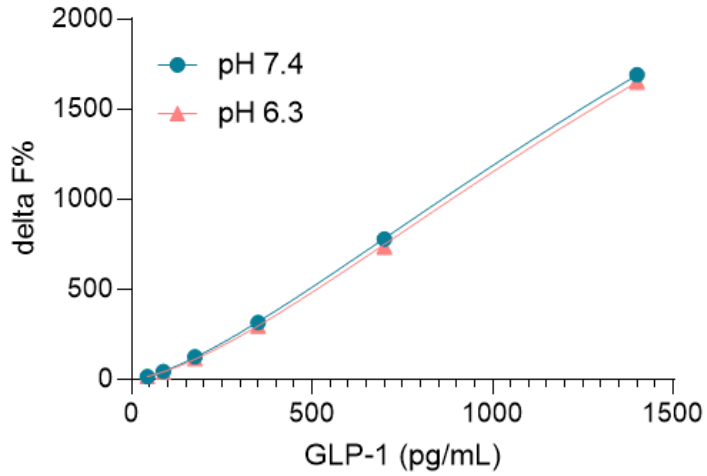


Figure 5.5 Active GLP-1 standard curves generated by GLP-1 dilution in secretion buffer at pH 6.3 and 7.4.

a) GLP-1 standard curve generated from peptide gold standard provided by the manufacturer (Cisbio) at the stock concentration of 56ng/mL. GLP-1 standard was diluted as per instruction to 1400pg/mL and further two-fold until 43.8pg/mL in KRB-H buffer adjusted to pH 6.3 and 7.4. Signal plotted as delta F%. b) Commercial GLP-1 (7-36)-NH_2 (Bachem) at the stock concentration of 300µM diluted to match the concentrations of GLP-1 peptide from a) in KRB-H buffer at pH 6.3 and 7.4. The signal measured is plotted as delta F%. Each data point is mean±SD.

5.3.2 Extracellular pH affects GLP-1 secretion

The pH_o dependence of GLP-1 secretion in the presence of 1mM or 10mM glucose was determined in GLUTag cells. GLUTag cells were incubated in basal buffer (KRB-H buffer, 0mM glucose) or the presence of 1mM or 10mM glucose. Each glucose condition was tested at pH 6.5, 6.7, 6.9, 7.0, 7.2, 7.3, 7.4, and 7.6 (Fig 5.6). The overall glucose stimulatory effect over the basal condition was highly significant for both glucose concentrations tested, 1mM and 10mM (p<0.0001, one-way ANOVA), and there was no significant difference in the pH effect between the two glucose concentrations. At the assessed pH_o range of 6.4 to 7.6, both

1mM and 10mM concentrations of glucose-induced comparable changes in GLP-1 secretion. As the secretion of GLP-1 stimulated with 10mM glucose was more robustly measured compared to the 1mM glucose, the 10mM glucose concentration was used in all subsequent experiments.

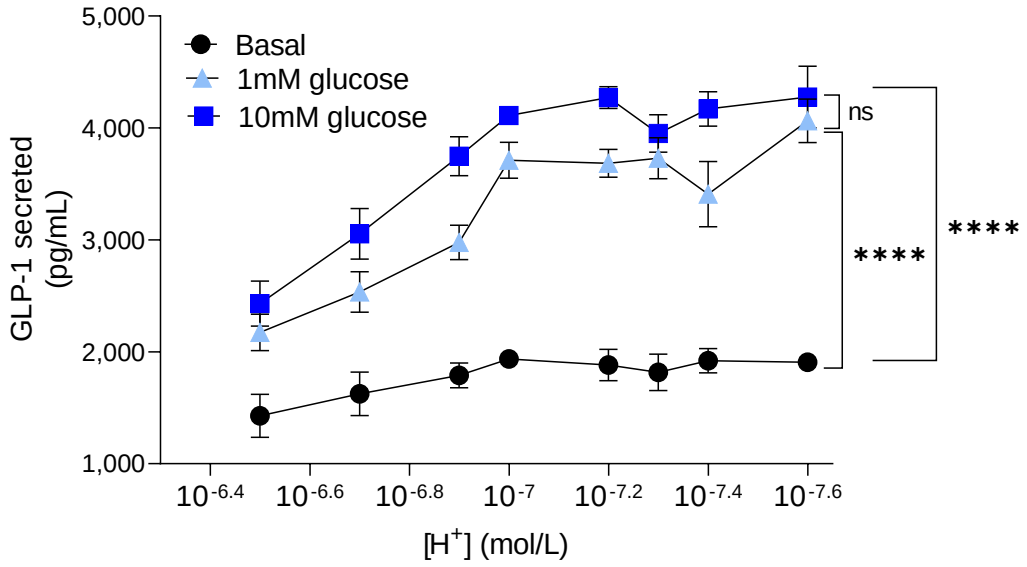


Figure 5.6 Glucose-triggered release of GLP-1 from GLUTag cells stimulated with 1mM and 10mM glucose at extracellular pH gradient.

Overall stimulatory effect of glucose at 1mM and 10mM in triggering GLP-1 (pg/mL) release from GLUTag cells as compared to basal condition upon manipulation of extracellular $[H^+]$ concentration ranging from $1x10^{-6.5}$ (pH=6.5) to $1x10^{-7.6}$ (pH=7.6) (mol/L). Each data point represents mean±SEM from n=6. Significant values depicted as *p<0.05, **p<0.01, ***p<0.001, ****p<0.0001, ns – not significant (one-way ANOVA with Tukey's post hoc test).

The stimulatory effect of 10mM glucose in response to the range of proton concentrations from pH_o 6.5 to 7.6 was assessed further (Fig. 5.7). While glucose-triggered GLP-1 secretion was comparable within the pH_o of 6.9 to 7.6, decreasing the pH_o to 6.7 and 6.5 resulted in a significant decrease in GLP-1 secretion from 4171±262pg/mL at pH 7.4 to 3054±183pg/mL and 2432±236pg/mL, respectively (p<0.0001, one-way ANOVA). Notably, there was no difference between basal GLP-1 secretion at pH 7.4 and glucose-stimulated GLP-1 release at pH 6.5 (p=0.50), suggesting that the stimulatory effect of 10mM glucose is absent at acidic pH.

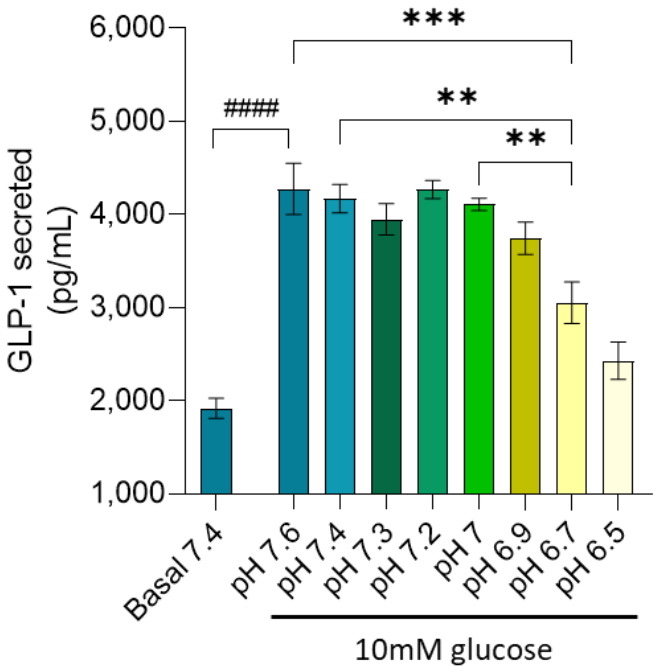


Figure 5.7 Acidic extracellular pH decreases GLP-1 secretion in a gradient manner.

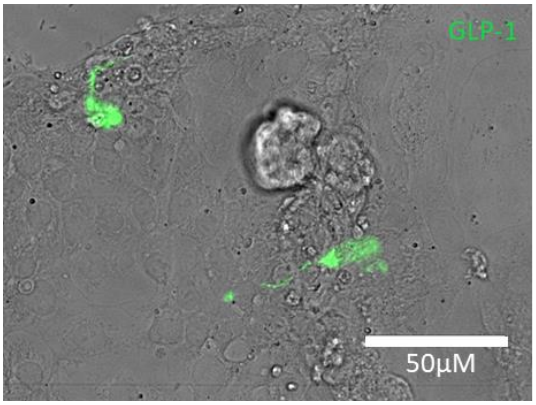
Detailed pH-dependence of GLP-1 secretion (pg/mL) triggered by 10mM glucose measured from GLUTag cells at the extracellular pH ranging from 6.5 to 7.6 as compared to basal (0mM glucose) secretion at pH 7.4. The statistical comparison was made to either the basal secretion at pH 7.4 (#) or glucose-stimulated secretion at pH 6.7 (*). HCl was used to adjust pH below 7.0 and NaOH to adjust it over 7.0. Each bar graph represents mean±SEM from n=6. Significant values depicted as *p<0.05,

**p<0.01, ***p<0.001, ****p<0.0001, ns – not significant (one-way ANOVA with Tukey's post hoc test).

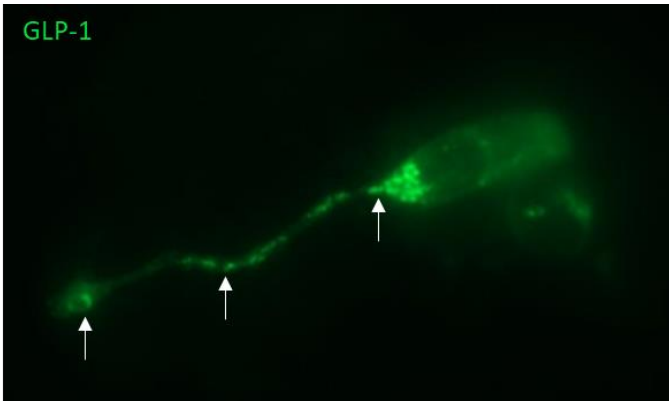
5.3.3 Acidic extracellular pH inhibits GLP-1 secretion primary L cell cultures

The pH-dependent release of GLP-1 observed in GLUTag cells was also recapitulated in *ex vivo* primary small intestinal cultures grown for 24hr from gut crypts (Fig. 5.8a-b). Glucose-stimulated GLP-1 secretion from primary L cells was significantly decreased when the pH_o was lowered from pH 7.2 to 6.8 (127±4pg/mL vs. 100±7pg/mL, p<0.01) (Fig 5.8c). Further decrease in secretion was observed at pH 6.3 (73±5pg/mL, p<0.0001) (Fig. 5.8c). At basal condition (pH 7.6), GLP-1 levels were determined at an average of 78±3pg/mL, which increased significantly to 111±5pg/mL (p<0.001) upon 10mM glucose stimulation (Fig. 5.8c). Importantly, this result also confirmed the presence of glucose-responsive L cells within the primary small intestinal cultures.

a



b



c

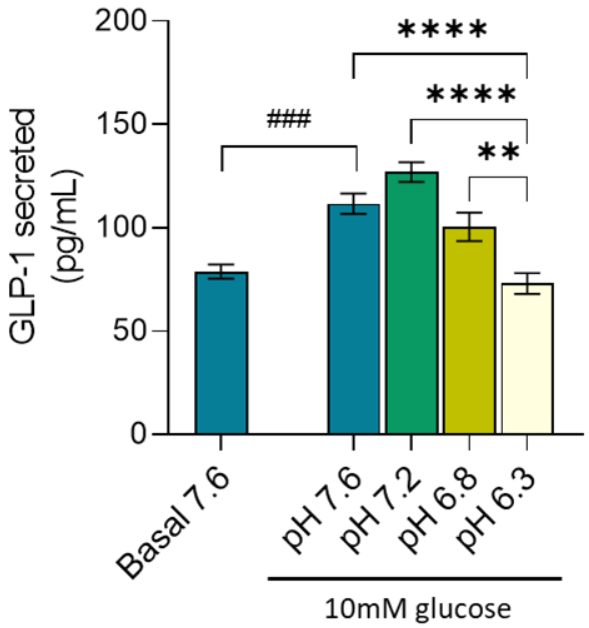


Figure 5.8 Glucose-stimulated GLP-1 secretion is pH-dependent in primary murine L cells.

GLP-1 secretion (pg/mL) was measured from mixed primary small intestinal cultures isolated from C57BL/6NTac wild-type mice (n=3). Cells were allowed to grow for 24 hours until the secretion experiment. a) Representative picture showing a phase-contrast view of the 2D primary small intestinal cultures. It has been overlaid with an immunofluorescence picture showing the GLP-1 positive L –cells (green). b) digitally zoomed L cell from a). White arrows mark GLP-1-filled secretory granules (green). c) Cultures were incubated at pH 7.6 in basal condition or stimulated with 10mM glucose at pH 7.6,

7.2, 6.8 and 6.3. Each bar graph represents mean±SEM from n=3 per condition. Significant values depicted as *p<0.05, **p<0.01, ***p<0.001, ****p<0.0001, ns – not significant (one-way ANOVA with Tukey's post-hoc test).

5.3.4 Decreased GLP-1 secretion in acidic pH is not caused by accelerated degradation of GLP-1 at low pH_o

Next, to determine whether the reduced levels of glucose-stimulated GLP-1 observed in an acidic pH were due to the degradation of the GLP-1 peptide, the extracellular buffer used in secretion experiments was supplemented with various protease inhibitors (Fig 5.9). Aprotinin is a broad-spectrum serine protease inhibitor generally used in *in vitro* studies to prevent the degradation of small peptides and to increase the recovery of an active GLP-1 from plasma samples [327]. The addition of 3µM aprotinin to the basal buffer at pH 6.3 (yellow bars) or 7.4 (blue bars) did not prevent attenuation of glucose-stimulated GLP-1 secretion in acidic conditions (Fig 5.9a). These results were confirmed with a general protease inhibitor cocktail (PIC) (Fig. 5.9b). No difference in glucose-stimulated GLP-1 secretion, with or without the addition of PIC, was observed at pH 6.3 or pH 7.4 (Fig. 5.9b). To further determine whether GLP-1 is degraded at low pH, GLUTag cells were incubated in basal buffer at pH 6.3 or 7.4 and synthetic active GLP-1(7-36-NH_2,) was added at various concentrations (1,000–4,000pg/mL) (Fig. 5.9c). Following 2hr incubation period at pH 6.3 or 7.4, the recovery ratio of GLP-1 was calculated by normalising the amount of active GLP-1 measured to the basal secretion in the absence of synthetic GLP-1, at the corresponding pH. No difference in synthetic GLP-1 degradation was detected between pH 6.3 and 7.4 (Fig. 5.9c).

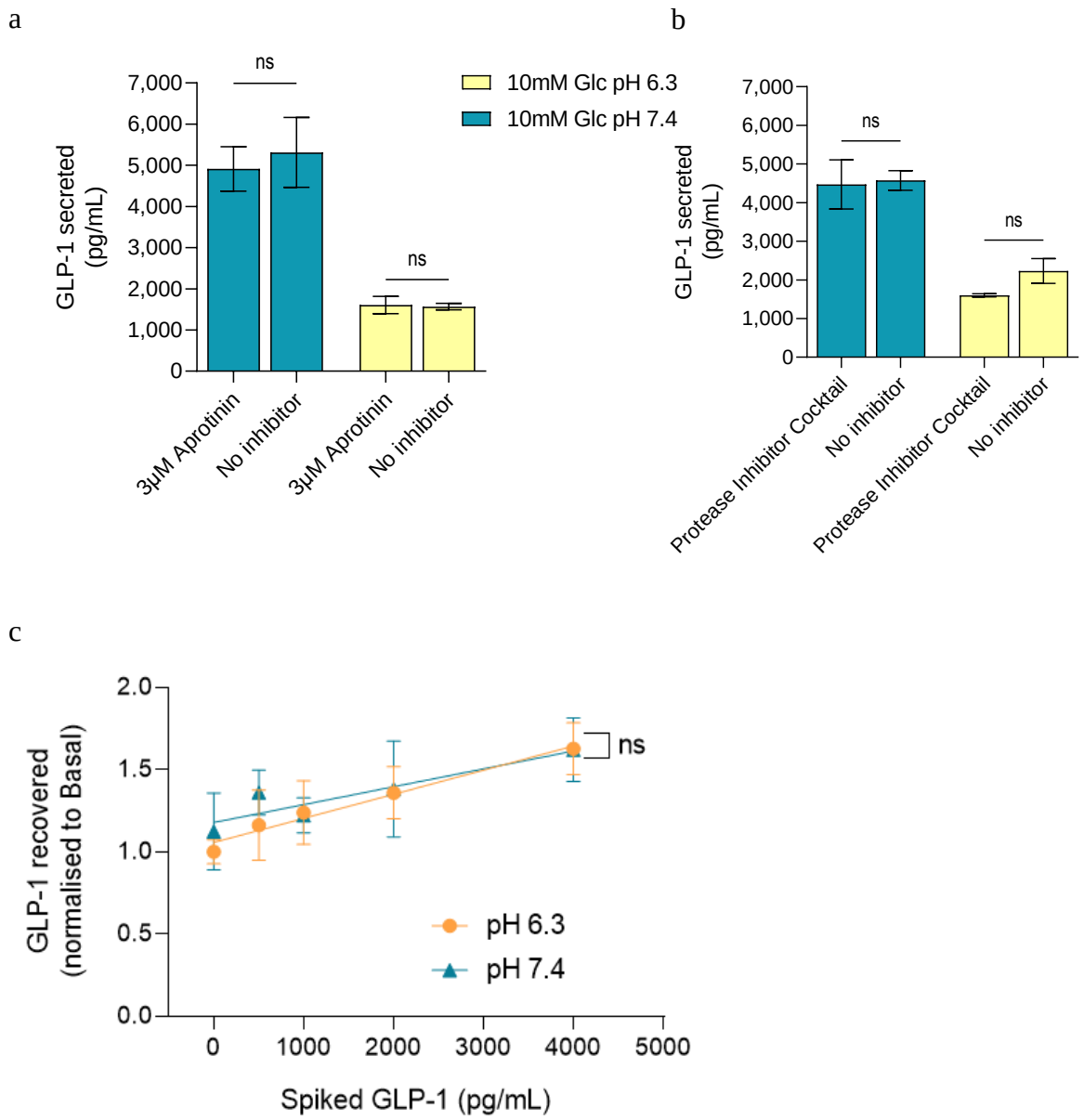


Figure 5.9 Degradation of secreted GLP-1 and GLP-1 peptide stability is not affected by pH_o.

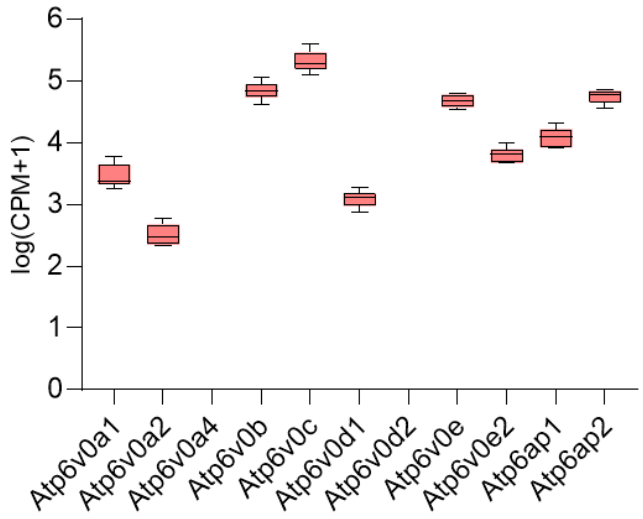
GLP-1 secretion (pg/mL) from GLUTag cells after 2hr incubation in the presence of 10mM glucose at pH 6.3 (yellow bars) or 7.4 (blue bars) a) without protease inhibitor supplementation (No inhibitor) or with 3μM aprotinin added to secretion buffer and in b) without protease inhibitor supplementation (No inhibitor) or with commercial protease inhibitor cocktail against most common proteases added to secretion buffer. c) Ratio of recovered GLP-1 after 2hr incubation of GLUTag cells with the basal buffer at pH 6.3 (orange) or 7.4 (blue) when the secretion buffer was supplemented with synthetic active GLP-

1 (7-36)-NH_2 at the two-fold concentrations from 500 to 4000pg/mL. Data normalised for basal secretion without peptide supplementation at the corresponding pH. Bar graph/point represents mean±SD from n=3 per condition. Significant values depicted as *p<0.05, **p<0.01, ***p<0.001, ****p<0.0001, ns – not significant. (two-way ANOVA with Bonferroni's comparison in a) and b) and AUC Student's t-test in c)).

5.3.5 Inhibition of V-ATPase proton pump mimics the effect of low pH_o on GLP-1 release

The vacuolar-type H^+-ATPase (V-ATPase) is a proton pump which transports protons across either the plasma membrane or the intracellular membranes of organelles, such as the lysosomes, endosomes and secretory vesicles against its gradient in an ATP-dependent manner. V-ATPases contain a membrane-spanning domain of subunit V_0 that forms a proton pore to allow proton flux into the vesicular compartment and subunit V_1, which is the cytosolic domain of V-ATPase responsible for ATP hydrolysis [328]. GLUTag cells express mRNA encoding all the necessary subunits components to form a functional V-ATPase pump, as demonstrated in RNA sequencing data (Fig 5.10). The expression of genes encoding different subunits of the V_0 domain is shown in Fig. 5.10a, while the expression of mRNA encoding subunits for domain V_1 is in Fig. 5.10b.

a



b

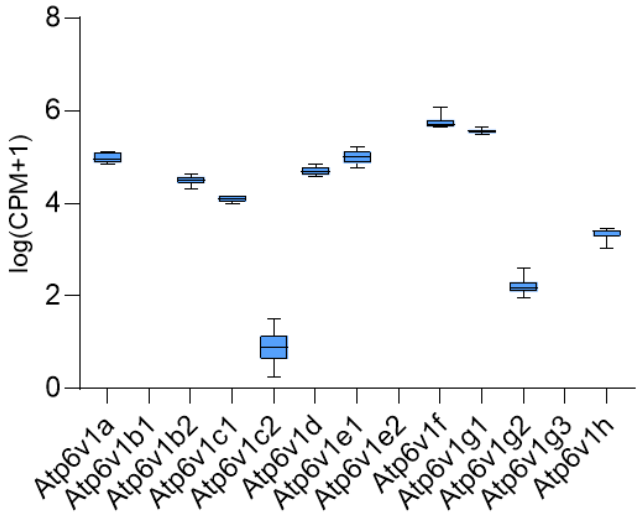


Figure 5.10 mRNA expression profile of genes encoding different subunits of V_0 and V_1 domain that are required to form functional V-ATPase proton pump.

a) mRNA expression level of subunits required to form V_0 transmembrane domain and b) mRNA expression level of subunits required to form V_1 cytosolic domain. Relative transcript abundance was quantified by 3' RNA-Seq of GLUTag cells maintained under standard conditions (n=6). Absolute transcript values as counts per million (CPM) were expressed as log(CPM+1).

Inhibition of the V-ATPase proton pump increases the accumulation of protons and subsequently acidifies the cytoplasm, whilst increasing the pH within the lysosomes and secretory vesicles [329]. Bafilomycin A1 is a specific inhibitor of the V-ATPase [330, 331] and was used to test if the acidification of cytoplasm affects GLP-1 secretion. GLUTag cells were treated with 1µM bafilomycin A1 at basal and upon stimulation with either 1mM or 10mM glucose at pH 7.4 (the blue bar with white stripes) (Fig. 5.11). The addition of bafilomycin A1, at pH 7.4, attenuated GLP-1 secretion at all glucose conditions, in comparison to cells examined in the absence of bafilomycin A1 (Fig. 5.11). These results resembled those obtained at pH 6.8, in the absence of bafilomycin A1 (dark yellow bar) (Fig. 5.11). GLP-1 secretion at pH 7.4 in response to glucose was 5110±340pg/mL and 6762±752pg/mL, at 1mM and 10mM respectively. The addition of bafilomycin A1 to the secretion buffer at pH 7.4 lowered the amount of GLP-1 secreted in response to glucose to 3425±210pg/mL and 4175±121pg/mL at 1mM and 10mM, respectively (Fig. 5.11). The overall effect of the bafilomycin A1 treatment in decreasing GLP-1 secretion in the presence of glucose is highly significant at pH 7.4 ($F_{1,20}$=24.62, p<0.0001, two-way ANOVA). This result demonstrates that acidification of the cytoplasm, with bafilomycin A1, is equally as effective at reducing GLP-1 secretion as lowering the extracellular pH to 6.8. Hence, it is reasonable to assume that acidification of the extracellular environment acidifies the intracellular environment in this model.

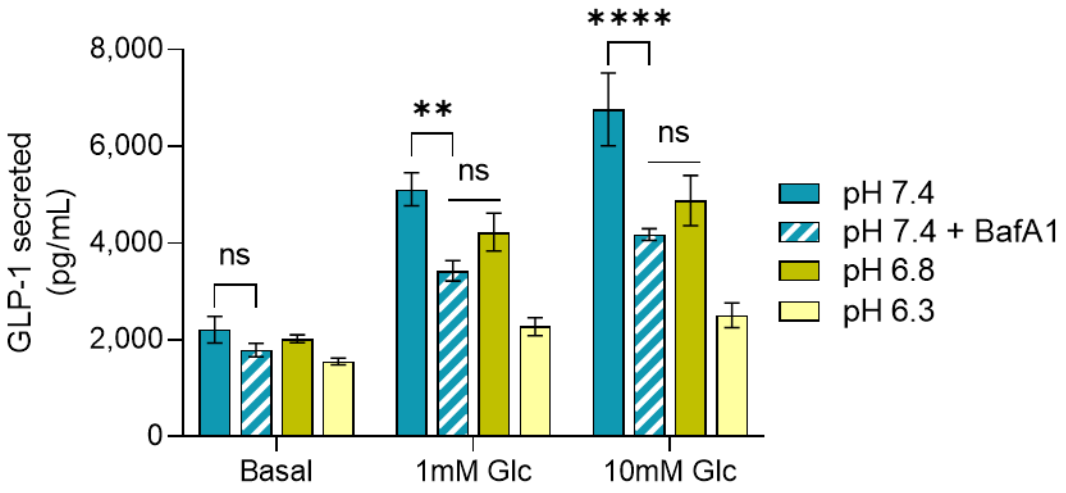


Figure 5.11 V-ATPase proton pump inhibitor bafilomycin A1 mimics the effect of extracellular pH 6.8 on GLP-1 secretion from GLUTag cells.

GLP-1 secretion (pg/mL) from GLUTag cells after 2hr incubation with basal (0mM glucose) or upon glucose stimulation with 1mM or 10mM glucose at pH 6.3 (yellow), 6.8 (dark yellow) and pH 7.4 without inhibitor (blue) or with 1µM Bafilomycin A1 (BafA1, blue with white stripes). Bar graphs represent mean±SEM from n=6 per condition. Significant values depicted as *p<0.05, **p<0.01, ***p<0.001, ****p<0.0001 (two-way ANOVA with Bonferroni's post hoc test), ns – not significant.

5.3.6 Acidity-induced inhibition of GLP-1 secretion occurs rapidly and is reversible

GLUTag cells were incubated with 10mM glucose for 1hr at pH 6.3 or pH 7.4. After the first hour of incubation, the incubation buffer was either swapped to a different pH or replaced with the same, i.e. 1hr at pH 6.3 followed by 1hr at pH 6.3 or pH 7.4 and vice versa. Paired GLP-1 secretions of each condition after each hour are plotted in Fig 5.12 (yellow-filled circles represent 10mM glucose at pH 6.3, blue-filled circles 10mM glucose at pH 7.4). Replacing 10mM glucose at pH 7.4 after the first hour of incubation with 10mM glucose at pH 6.3 (7.4 -> 6.3) shows a significant decrease in GLP-1 secretion brought about by acidification of the

secretion buffer (4,170±451pg/mL vs 2,714±451pg/mL, *p*=0.007, one-way ANOVA, Tukey's test). This effect was found to be also reversible when cells were incubated at pH 6.3 followed by incubation at pH 7.4 (1,529±331pg/mL vs 5,382±948pg/mL, *p*=0.04, one-way ANOVA, Tukey's test). Control treatments with the buffer at the same pH (6.3 -> 6.3 and 7.4 -> 7.4) were not significantly different.

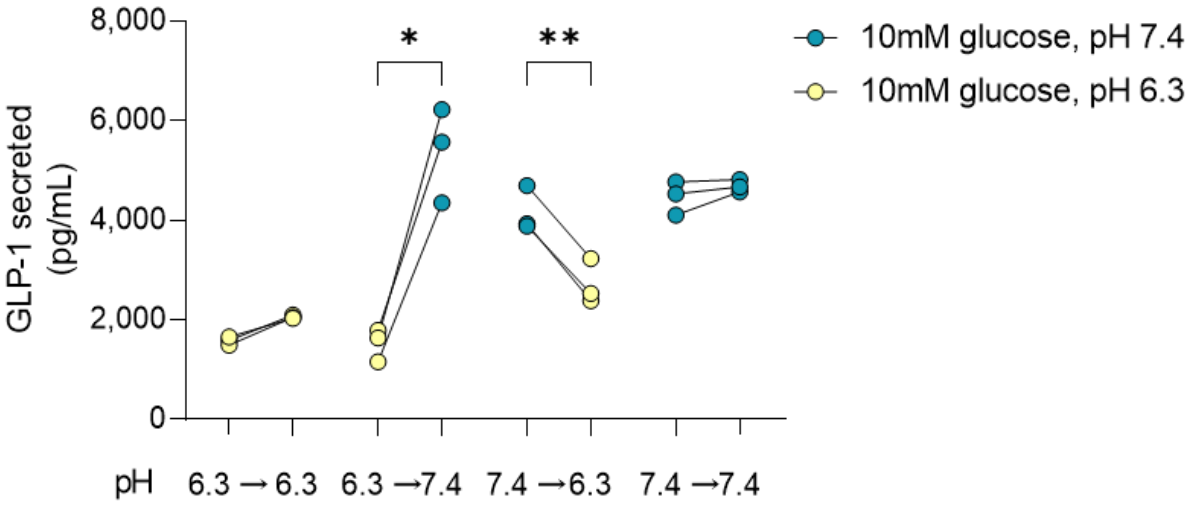


Figure 5.12 pH effect on GLP-1 secretion from GLUTag cells is rapid and reversible.

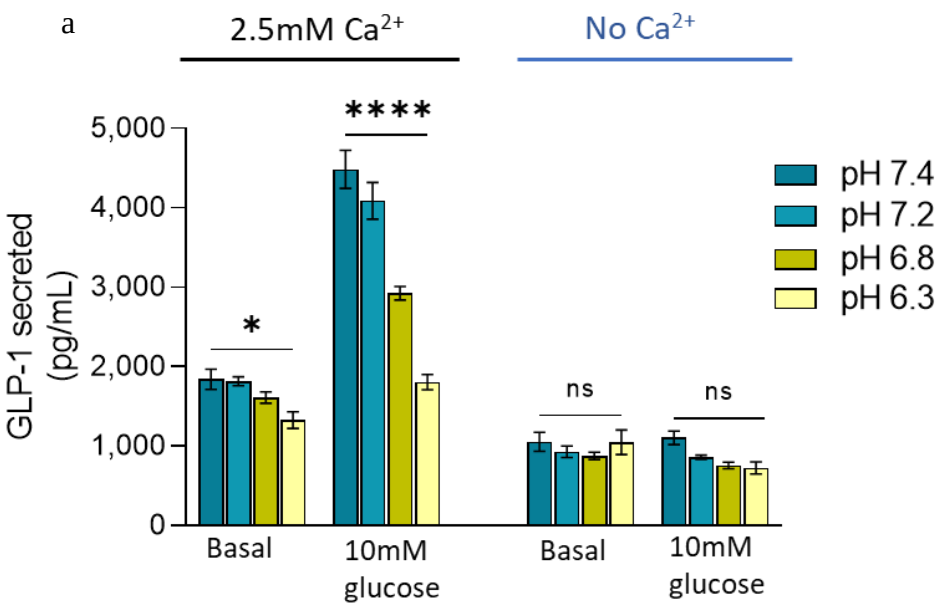
GLP-1 secretion (pg/mL) from GLUTag cells stimulated for 1hr with 10mM glucose at pH 6.3 (yellow dots) or pH 7.4 (blue dots). Each condition after 1hr of incubation was replaced with the 10mM glucose solution at the pH indicated by an arrow, i.e. pH 6.3 buffer was replaced with buffer either at pH 6.3 or 7.4 for another 1hr of incubation. Each dot represents a cell culture dish (n=3) per condition. Connecting lines are drawn between the same dishes (paired) and measured after each hour of incubation. Significant values depicted as *p<0.05, **p<0.01, ***p<0.001, ****p<0.0001, (one-way ANOVA with Tukey's post hoc test). Non-significant comparison is not shown on the graph.

5.3.7 The role of calcium in the pH dependence of GLP-1 secretion

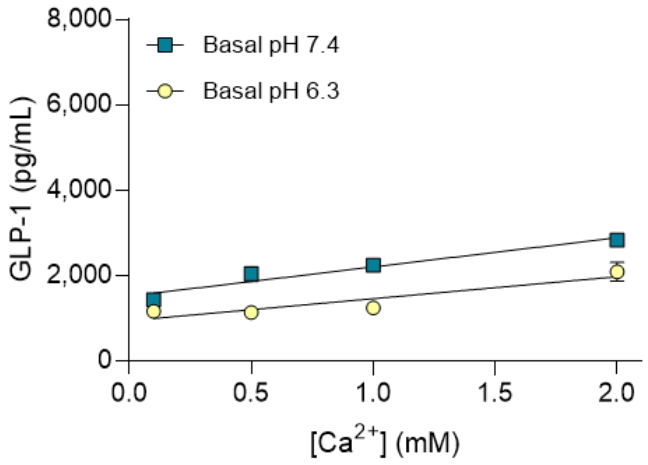
Glucose-stimulated GLP-1 release is mediated through the glucose/Na^+ symporter SGLT1 (Slc5A1) and it is well established that glucose-triggered GLP-1 exocytosis relies on the subsequent membrane depolarisation and calcium entry through voltage-gated calcium channels (VGCC) [324]. To investigate if extracellular calcium levels play a role in pH-dependence of GLP-1 secretion, GLUTag cells were incubated in either 0mM (basal) or 10mM glucose in the presence or absence of extracellular calcium at pH 6.3, 6.8, 7.2 and 7.4 (Fig. 5.13a). The left-hand side panel of Fig. 5.13a depicts glucose-stimulated GLP-1 secretion in the presence of physiological extracellular calcium plasma concentration (2.5 mM). These results show a strong pH-dependence of stimulated GLP-1 release (1806±168pg/mL at pH 6.3 vs 4,484±416pg/mL at pH 7.4, $p<0.0001$, one-way ANOVA, Tukey's test). However, removing extracellular calcium from the secretion buffer completely abolished GLP-1 secretion. This is expected as Ca^{2+} signalling plays a pivotal role in the exocytosis of GLP-1 [289]. Due to the relationship between extracellular calcium and GLP-1 exocytosis, the pH-dependence of GLP-1 release cannot be observed (Fig. 5.13a, right panel). To investigate this further, GLP-1 secretion was measured at 0mM glucose (basal) (Fig. 5.13b) or 10mM glucose (Fig. 5.13c) at acidic pH 6.3 (yellow circles) and neutral pH 7.4 (blue squares) at a range of increasing extracellular Ca^{2+} concentrations (0.1-2 mM). The correlation between extracellular Ca^{2+} and secreted GLP-1 in response to 10mM glucose by Pearson correlation coefficients was significant, with almost identical R^2 values for both, pH 6.3 and 7.4 (R^2=0.946, p=0.03 and R^2=0.945, p=0.03, respectively). This positive correlation suggests that the GLP-1 secretion is expected to increase/decrease in line with increasing/decreasing Ca^{2+} concentration significantly at both tested pH. Linear regression analysis showed that there was no difference in the slope (steepness) of the dose-response curves for GLP-1 secretion at pH 6.3 and 7.4, in the absence of glucose (basal). This result suggests that, in the absence of glucose, GLP-1

secretion is stimulated by increasing extracellular Ca^{2+} via mechanisms that are not sensitive to changes in extracellular pH. However, when the experiment was repeated in the presence of 10mM glucose, there was a trend for a significant difference in the steepness of the dose-response curve between pH 6.3 and pH 7.4 (p=0.053). This may be due to the activity of enzymes involved in glucose metabolism being altered at pH 6.3, as reported in β-cells [332]. Therefore, it cannot be excluded that the calcium entry or intracellular calcium levels might be affected by the pH treatment, and subsequently alter the GLP-1 exocytosis. Additionally, the highest calcium concentration tested in this experiment was 2.5mM, however, luminal calcium concentration in the intestinal fluid varies greatly and it can range between 0.6-10mM depending on the gut segment, fed state and diet [333, 334]. It is unclear if L-type voltage-gated calcium channels that are in L cells can be exposed to such ranges of calcium concentrations as it is presumed that VGCCs reside on the basolateral membrane of enteroendocrine cells [335], but apical location of these channels was also reported in various models of enterocytes [336].

a


2.5mM Ca2+
No Ca2+
****
*
ns
ns
GLP-1 secreted (pg/mL)
5,000
4,000
3,000
2,000
1,000
0
Basal
10mM glucose
Basal
10mM glucose
pH 7.4
pH 7.2
pH 6.8
pH 6.3

b


Basal pH 7.4
Basal pH 6.3
GLP-1 (pg/mL)
8,000
6,000
4,000
2,000
0
0.0
0.5
1.0
1.5
2.0
[Ca2+] (mM)

c

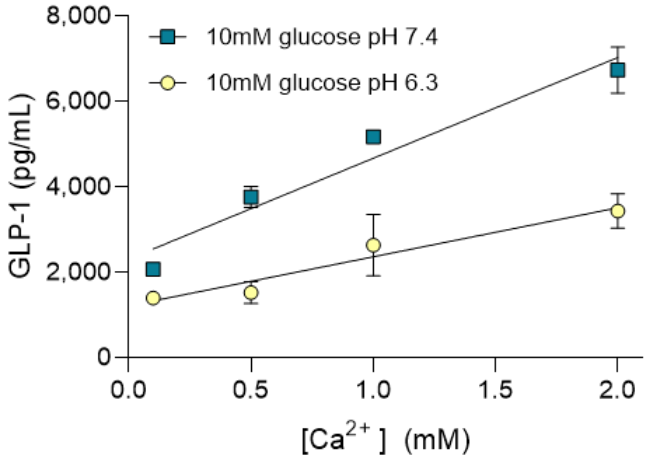

10mM glucose pH 7.4
10mM glucose pH 6.3
GLP-1 (pg/mL)
8,000
6,000
4,000
2,000
0
0.0
0.5
1.0
1.5
2.0
[Ca2+] (mM)

Figure 5.13. pH effect on GLP-1 secretion at different extracellular calcium levels.

a) GLP-1 secretion (pg/mL) from GLUTag cells in response to basal (0mM glucose) or 10mM glucose as indicated below the data sets in the presence of 2.5mM Ca^{2+} (left panel) or absence of calcium (right panel) measured at pH 6.3, 6.8, 7.2 and 7.4 as per figure legend. b) GLP-1 secretion measured at the basal at pH 6.3 (yellow circles) or 7.4 (blue squares) across increasing extracellular calcium $[Ca^{2+}]_o$ levels ranging from 0.1mM to 2mM. c) GLP-1 secretion stimulated with 10mM glucose tested at pH 6.3 (yellow circles) or 7.4 (blue squares) at increasing levels of extracellular calcium starting at 0.1mM to 2mM. Each dot/bar graph represents mean±SEM (n=3) per condition. Significant values depicted as *p<0.05, **p<0.01, ***p<0.001, ****p<0.0001 (one-way ANOVA with Tukey's post hoc test). Data in b) and c) were analysed by linear regression curve and slope comparison between pH 6.3 and pH 7.4, which is non-significant for both tested conditions, basal and 10mM.

5.3.8 pH-sensitive GLP-1 secretion is independent of extracellular sodium levels

GLUTag cells express various levels of plasma membrane transporters and exchangers which regulate intracellular pH by extruding H^+ via Na^+-coupled mechanisms (Fig. 5.14a). These include Na^+/H^+ antiporters (NHE1-9, SLC9A family) which expel H^+ in exchange for Na^+; Na^+/HCO_3^- co-transporters (NBC, SLC4A family) which mediate the coupled movement of Na^+ and HCO_3^- across plasma membranes in an electrogenic (NBCe1 and NBCe2) or electroneutral (NBCn1 and NBCn2) manner; and finally the Na^+-dependent Cl^--HCO_3^- exchanger (NDCBE) which is an electroneutral transporter that exchanges Na^+ and CO_3^{2-} for Cl^- (Fig. 5.14b).

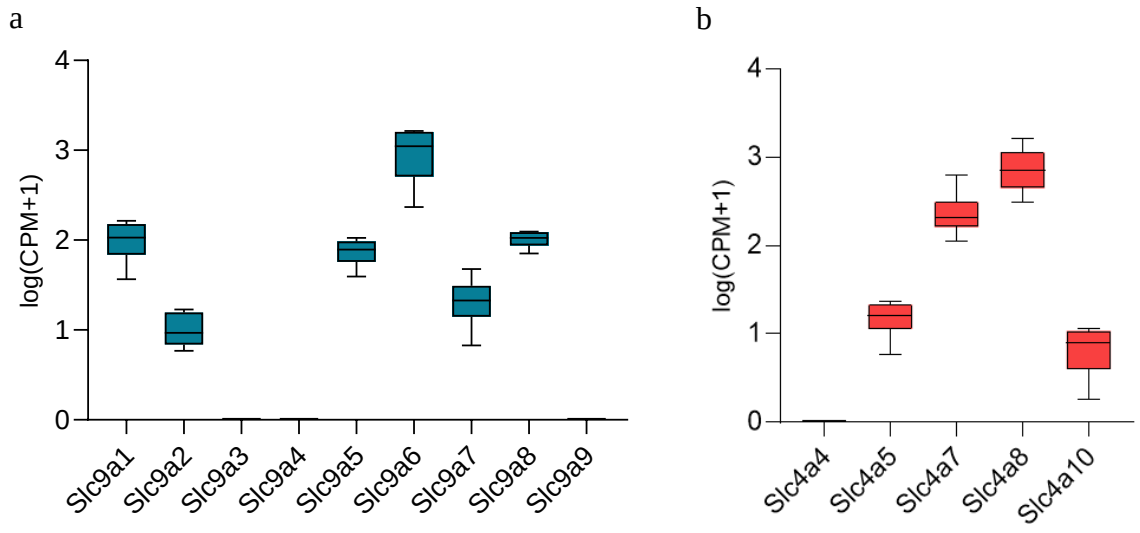


Figure 5.14 mRNA expression profile of genes encoding various Na^+-coupled acid extruders in GLUTag cells.

a) mRNA expression level of Na^+/H^+ antiporter (NHE1-9, SLC9A family) and b) NBC family Na^+/HCO_3^- co-transporters (SLC4A) which includes NBCe1 (SLC4A4), NBCe2 (SLC4A5), NBCn1 (SLC4A7) and NBCn2 (SLC4A10) and NDCBE (SLC4A8). Relative transcript abundance was quantified by 3' RNA-Seq of GLUTag cells maintained at standard conditions (n=6). Absolute transcript values as counts per million (CPM) were expressed as log(CPM+1).

The glucose sensing mechanism which stimulates GLP-1 secretion from GLUTag cells is known to be dependent on sodium entry via sodium-glucose co-transporter (SGLT1). As discussed earlier, the inward sodium current is sufficient to trigger membrane depolarisation and an increase in intracellular calcium levels that initiate exocytosis of GLP-1. To investigate if Na^+-coupled H^+ transport mechanisms are important for GLP-1 secretion, cells were exposed to 0mM glucose (basal), 10mM glucose or 30mM KCl at pH 6.3-7.4 in the presence of sodium (130mM) or when sodium was removed and replaced with its cationic, non-permeable equivalent $NMDG^+$ (Fig. 5.15, left-hand panel). At 10mM glucose in the presence of Na^+, pH_o 6.3 significantly lowers GLP-1 secretion in comparison with pH_o 6.8, 7.2 and 7.4

(1,405±126pg/mL vs 3,238±208pg/mL p=0.0005; vs 5,604±705pg/mL p<0.0001; vs 7,032±745pg/mL p<0.0001, respectively). Surprisingly, 30mM KCl, which triggers GLP-1 release by directly depolarising the membrane also exhibited pH-sensitivity. GLP-1 release in the presence of KCl was significantly decreased at pH_o 6.3 in comparison with pH_o 6.8 (2,661±571pg/mL vs 4,245±351pg/mL, p=0.003), and pH 7.2 (6,076±1,855pg/mL, p<0.0001) and 7.4 (6,894±569pg/mL, p<0.0001) (Fig. 5.15, left panel). Removal of extracellular Na^+ from the secretion buffer abolished GLP-1 secretion in response to 10mM glucose, as expected because SGLT1 will be inhibited (Fig. 5.15, right panel). 30mM KCl stimulated GLP-1 release to similar levels in the presence or absence of Na^+, as depolarisation-triggered GLP-1 secretion induced by KCl is independent from Na^+-dependent processes. In both, the presence and absence of Na^+, GLP-1 secretion in response to 30mM KCl showed highly significant pH-dependence between pH_o 6.3 – 6.8 and 7.2 – 7.4. This result demonstrates that acidification of the extracellular environment attenuates GLP-1 secretion regardless of extracellular Na^+, thus suggesting that the H^+ entry and accumulation are not coupled or dependent on extracellular Na^+ levels. Furthermore, the pH sensitivity of GLP-1 secretion is independent from the stimulus-secretion coupling mechanism related to glucose sensing as pH also affects KCl-induced GLP-1 release. It is then possible that changes in pH_o might represent a general factor modulating the GLP-1 release from L cells, i.e. exocytosis.

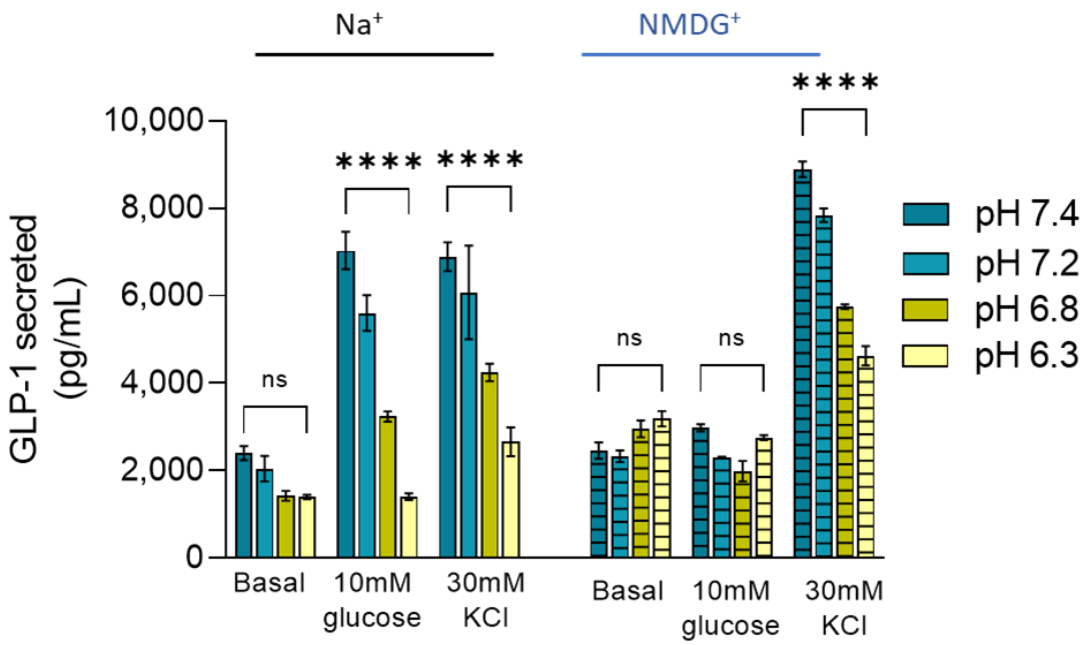


Figure 5.15 Proton influx into GLUTag cells does not depend on extracellular sodium levels.

GLP-1 secretion (pg/mL) from GLUTag cells incubated for 2hr at the basal condition or with 10mM glucose or 30mM KCl as indicated below the data sets in the secretion buffer containing sodium ($+Na^+$, left-panel) or with sodium removed and replaced by non-membrane permeable cation ($NMDG^+$, right panel). GLP-1 secretion in each condition was tested at pH 6.3, 6.8, 7.2, and 7.4 adjusted with HCl below 7.0 and NaOH above 7.0. Each bar graph represents mean±SEM from n=3 per condition. Data were analysed by two-way ANOVA and statistical significance shows the multiple comparisons Tukey's test where *p<0.05, **p<0.01, ***p<0.001, ****p<0.0001, ns – not significant.

5.3.9 The role of chloride in the pH_o effect on GLP-1 secretion

Since H^+ entry in GLUTag cells appears to be independent of extracellular Na^+, the possible role of the most abundant anion, chloride (Cl^-), was investigated next. RNAseq confirmed that GLUTag cells express the genes encoding for anion exchangers AE2 and AE3, but not AE1 (Fig. 5.16a). AEs belong to the SLC4A family group of sodium-independent electroneutral Cl^-/HCO_3^- exchangers that act as acid extruders (export of Na^+ and HCO_3^-) and are regulated by chloride (import of Cl^-). The direction of chloride movement depends on the chloride gradient. Additionally, GLUTag cells express acid loaders belonging to the SLC26A family that are also chloride-dependent (Fig. 5.16b) and various chloride channels with CLC-3 (*Clnc3*) implicated for priming of insulin granules (Fig. 5.16c), and also multiple intracellular chloride channels of CLIC family (*Clic*) (Fig. 5.16d). No *Abcc7* (encoding CFTR -Abcc9 is SUR2) expression was detected in GLUTag cells.

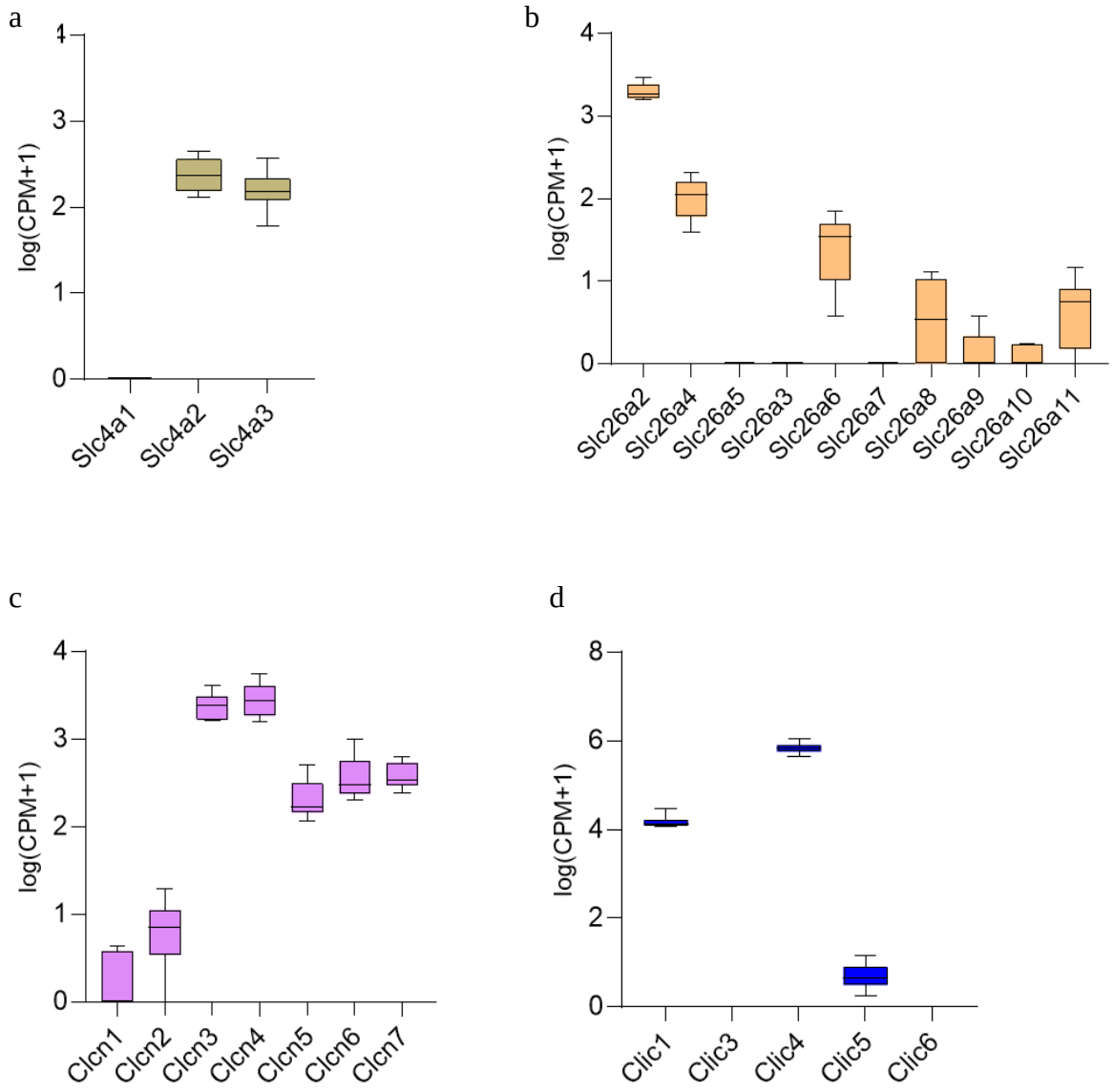


Figure 5.16 mRNA expression profile of genes encoding various Cl^- dependent acid loaders and channels in GLUTag cells.

a) mRNA expression level of anion exchangers (SLC4A family, AE) importing chloride into the cell in exchange for sodium and bicarbonate b) SLC26A family of anion exchangers and anion channels that uses chloride as substrate. Chloride channel expression from c) CLCN and d) CLIC family. Relative transcript abundance was quantified by 3' RNA-Seq of GLUTag cells maintained in standard conditions (n=6). Absolute transcript values as counts per million (CPM) were expressed as log(CPM+1).

To investigate if Cl^- is required for extracellular proton entry, GLUTag cells were incubated at pH 6.3 and 7.4 and exposed to 0mM glucose, 10mM glucose or 10μM forskolin in the presence of Cl^- (Fig. 5.17, left panel) or when the Cl^- was replaced by gluconic acid, large organic anion, that does not penetrate into the cells (Fig. 5.17, right panel). Forskolin is an activator of adenylate cyclase, an enzyme which potently increases cAMP levels. cAMP enhances GLP-1 by secretion by increasing intracellular Ca^{2+} mobilisation, in both the presence and absence of glucose [289]. GLP-1 release in response to 10mM glucose at pH 6.3 was significantly decreased as opposed to secretion at pH 7.4, which confirmed previous results ($p<0.0001$, two-way ANOVA Sidak's multiple comparisons). Forskolin-stimulated GLP-1 secretion did not show significant pH dependence, which suggests that the pH effect on GLP-1 secretion is not mediated via the cAMP signalling pathway. Interestingly, the removal of chloride from the secretion buffer and replacing it with gluconate completely abolished glucose-stimulated GLP-1 secretion and significantly attenuated the GLP-1 release in response to forskolin (Fig. 5.17, right panel). These changes are unlikely to be the result of stretch-activated channels as the osmolarity of the secretion buffer without chloride was measured at 291mOsm/kg, while with chloride 311mOsm/kg. Furthermore, cell morphology by phase-contrast light microscopy showed no visible difference between cells treated with gluconate and controls (data not shown). It would therefore appear that chloride ions play an essential, and previously unknown, role in the regulation of GLP-1 release.

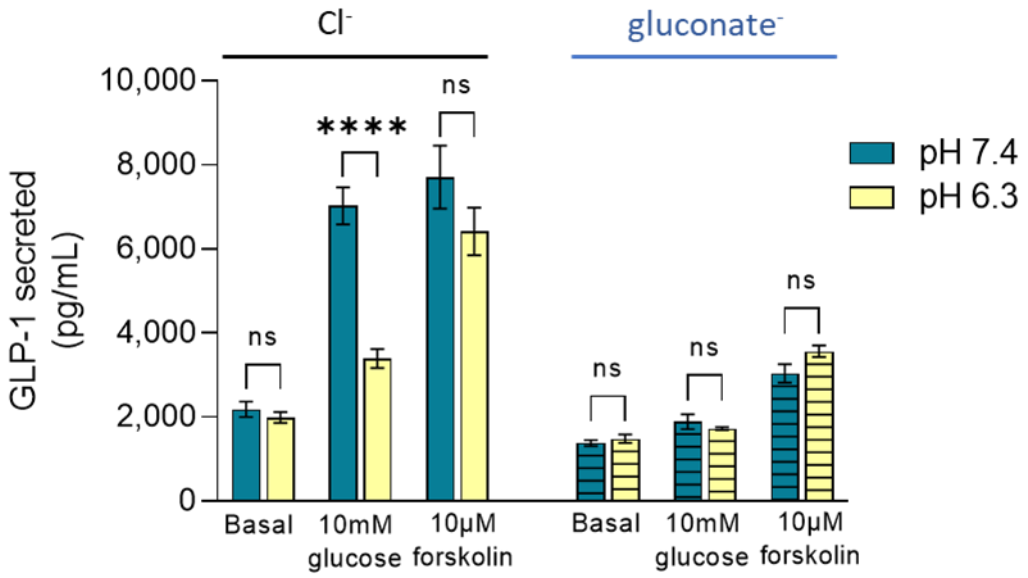


Figure 5.17. Removing chloride from the secretion buffer blocks exocytosis of GLP-1.

GLP-1 secretion (pg/mL) from GLUTag cells incubated for 2hr at the basal, 10mM glucose or 10µM forskolin as indicated below the data sets in the secretion buffer containing chloride (Cl^-, left-panel) or when chloride was removed and replaced by non-membrane permeable anion (Na/K-gluconate, right panel). GLP-1 secretion in each condition was tested at pH 6.3 and 7.4 adjusted with H_3PO_4 below 7.0 and NaOH above 7.0. Each bar graph represents mean±SEM from n=6 per condition. Data were analysed by two-way ANOVA and statistical significance shows the multiple comparisons Sidak's test where *p<0.05, **p<0.01, ***p<0.001, ****p<0.0001, ns – not significant.

5.3.10 Production of GLP-1 is not affected by pH_o

To investigate if acidification of the extracellular environment altered the synthesis or post-translational activation (cleavage) of GLP-1, stored in the secretory granules (SG), cells were exposed to 10mM glucose at pH 6.3 or 7.4 for 2hr and collected thereafter. The decrease in GLP-1 release at acidic pH was confirmed as described previously, by measuring the secreted active GLP-1 in the supernatant (Fig. 5.18a). Additionally, secretory granules (SG) were harvested alongside whole-cell lysates in order to measure active GLP-1 content in SGs. The amount of active GLP-1 produced by GLUTag cells in the whole-cell lysate did not significantly differ between cells exposed to pH 6.3 or 7.4, suggesting that the extracellular pH does not affect the overall production of active GLP-1 (Fig. 5.18b).

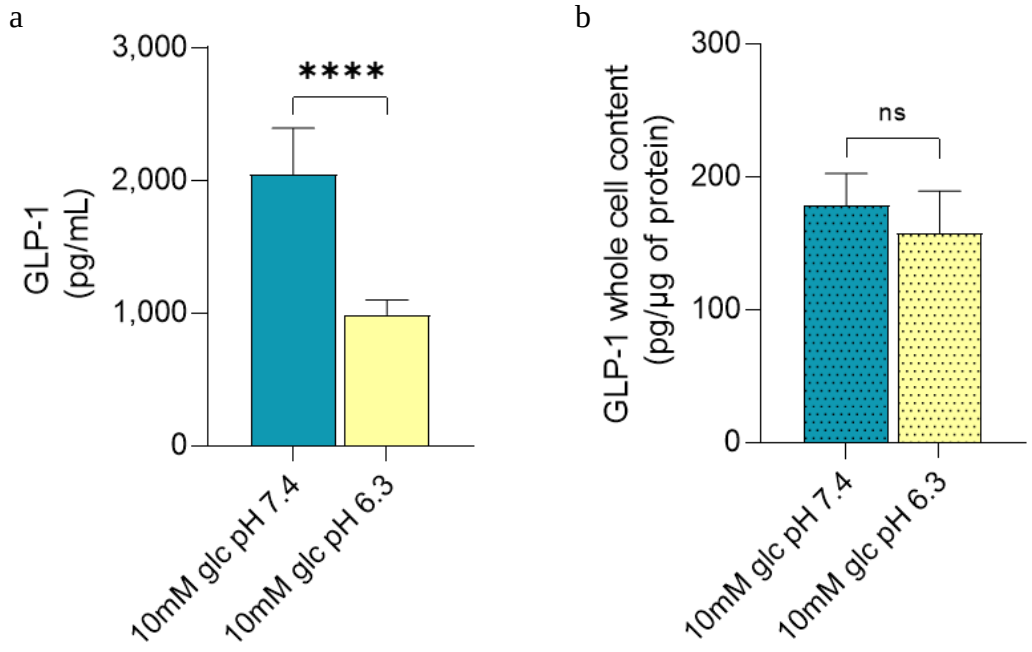


Figure 5.18 Acidic pH does not affect whole-cell production of active GLP-1.

GLUTag cells were stimulated for 2hr with 10mM glucose at pH 6.3 or pH 7.4 as indicated below the bars. Active GLP-1 was measured in a) supernatant and b) whole cell lysate. Each bar graph represents mean±SEM per condition from n=3. Data were analysed by t-test and statistical significance was *p<0.05, **p<0.01, ***p<0.001, ****p<0.0001, ns – not significant.

5.3.11 Acidic pH_o causes higher GLP-1 retention within the secretory granules

Expression of genes encoding SNARE family proteins, the core of vesicle fusion machinery, was confirmed by RNAseq in GLUTag cells. The main components of SNARE include vesicle-associated SNAREs (v-SNAREs), synaptobrevins, which are also known as VAMPs, Vesicle-associated membrane proteins (encoded by *Vamp* genes) (Fig. 5.19a), and target cell-associated SNAREs (t-SNAREs) that include syntaxins (encoded by *Stx*) (Fig. 5.19b) and Soluble N-ethylmaleimide-sensitive factor (NSF) Attachment Proteins (SNAP, encoded by *Snap* genes). SNAP-25 and SNAP-23 display the most abundant expression in GLUTag cells (Fig. 5.19c). Other components include synaptotagmins (encoded by *Syt* genes) (Fig. 5.19d), which act as calcium sensors and regulate zippering, and syntaxin binding protein (encoded by *Stxbp* genes) (Fig. 5.19e), also known as Munc-18 which plays a key role in the vesicle docking process [337].

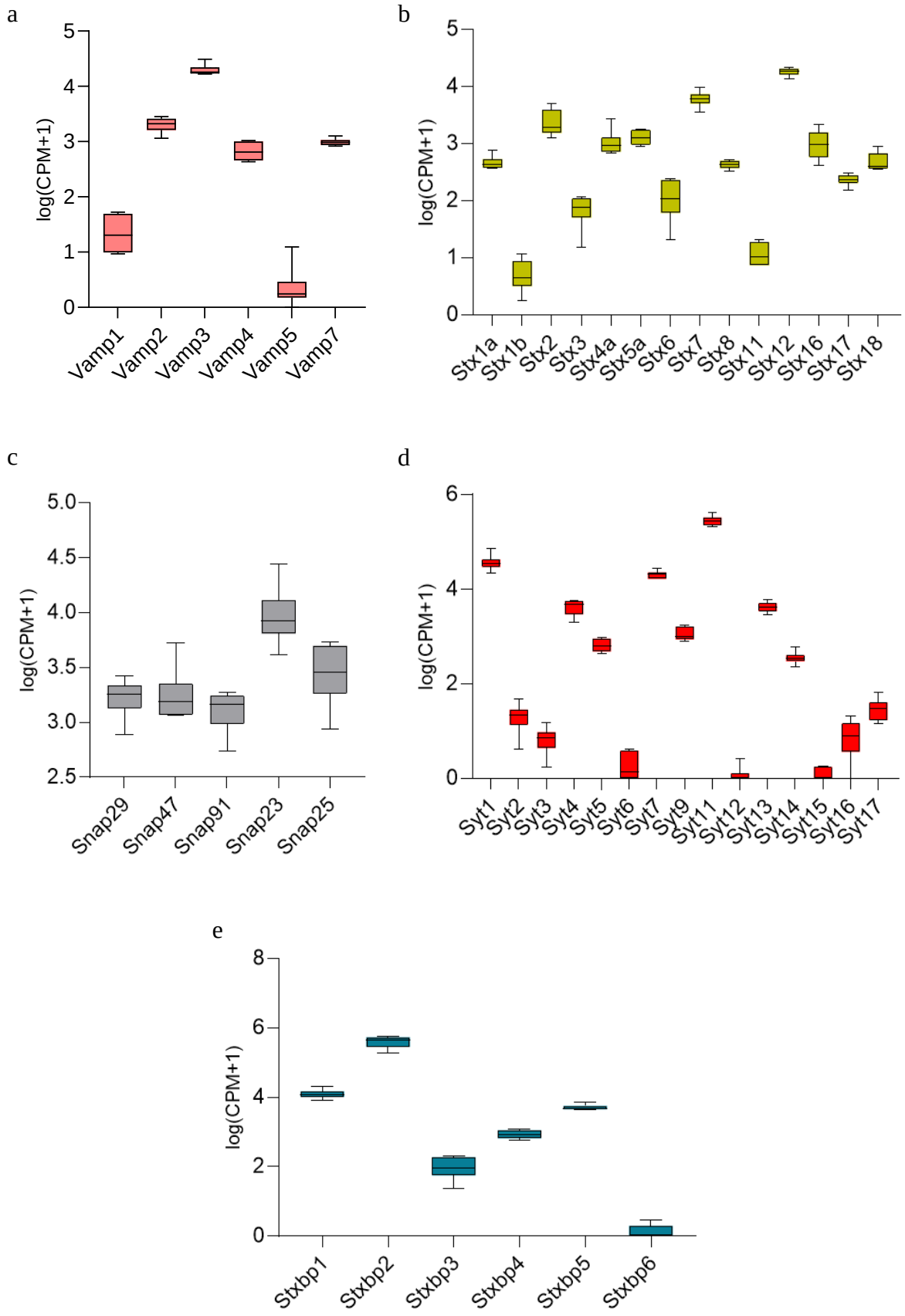


Figure 5.19 mRNA expression profile of genes encoding core SNARE and regulatory.

the mRNA expression level of a) Vesicle-associated membrane proteins (*Vamp*), b) syntaxins, c) Soluble N-ethylmaleimide-sensitive factor (NSF) Attachment Proteins (*Snap*), d) synaptotagmins (*Syt*) and e) syntaxin binding protein known as Munc-18 (*Stxbp*). Relative transcript abundance was quantified by 3' RNA-Seq of GLUTag cells maintained in standard conditions (n=6). Absolute transcript values as counts per million (CPM) were expressed as log(CPM+1).

The secretory granules isolated from the 10mM glucose-stimulated cells show significantly higher amounts of active GLP-1 per µg of total protein at acidic pH 6.3 as compared to the secretory granules isolated from the cells stimulated at pH 7.4 (169±10pg/µg protein vs 227±22pg/µg protein, p=0.02, t-test). While GLUTag cells were shown to secrete less GLP-1 at acidic extracellular pH, it appears that at the same time, more of the GLP-1 is retained in the secretory granules of cells incubated at pH 6.3, suggesting that acidic pH affected the exocytosis of GLP-1 filled SGs (Fig. 5.20).

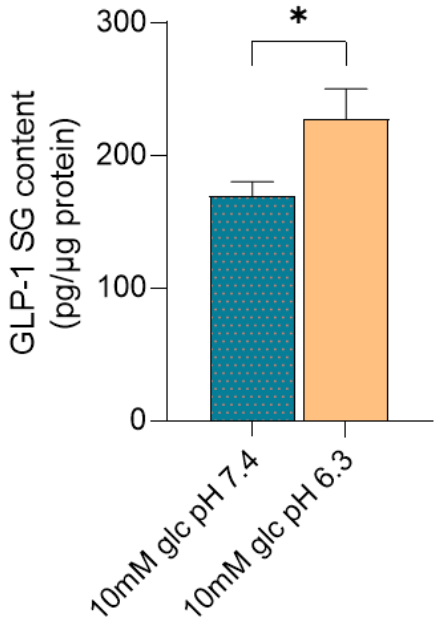


Figure 5.20. More GLP-1 is retained in the secretory granules (SG) from cells stimulated at acidic pH.

The GLP-1 content (pg/µg protein) was measured in secretory granules isolated from GLUTag cells stimulated with 10mM glucose at pH 6.3 (orange bar) or pH 7.4 (blue bar) as indicated below the graph. Each bar graph represents mean±SD per condition from n=3. Data were analysed by paired Student's t-test and statistical significance was *p<0.05.

5.3.12 PC1/3 expression is not changed at acidic pH_o

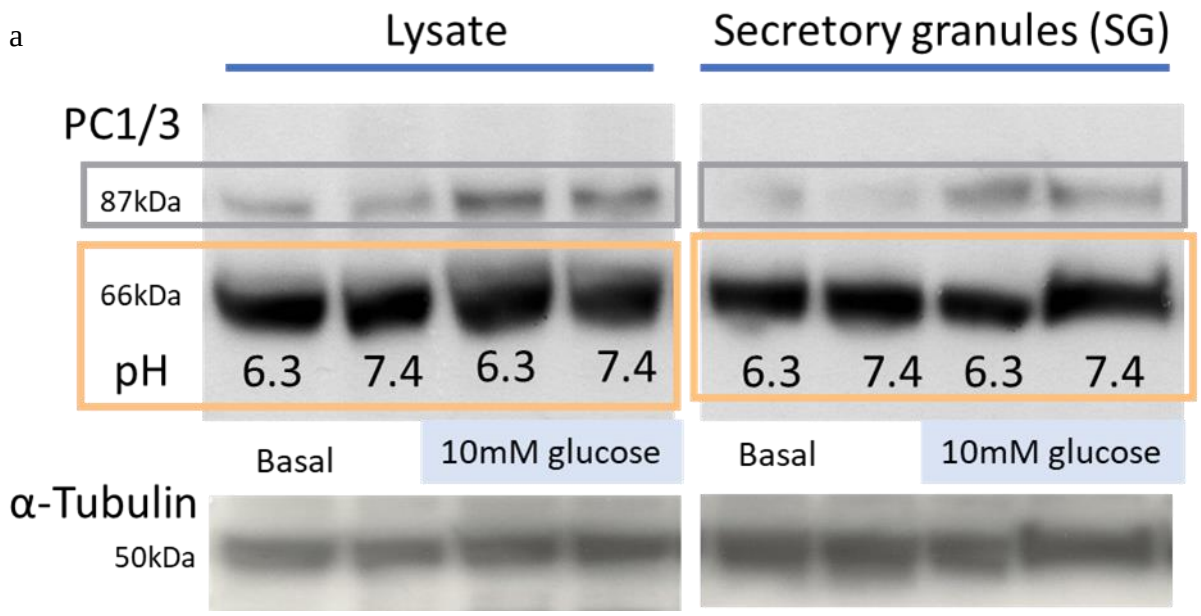
Since the intragranular pool of active GLP-1 from GLUTag cells stimulated at pH 6.3 was larger than at pH 7.4, the possibility of acidic pH_o altering the processing of GLP-1 from an inactive to active peptide was investigated. Preproglucagon peptide is cleaved by proteolytic enzyme prohormone convertase 1/3 (PC1/3) to form active GLP-1. It has been reported that PC1/3 has a low activity form (87kDa) that undergoes proteolytic autocleavage, within secretory granules, to form fully active PC1/3 (66kDa). It has been reported previously that this process is pH-dependent [309]. Using western blot analysis, the expression of PC1/3 was examined with an antibody which recognises both forms of PC1/3 (Fig. 5.21a). The expression level of each form of PC1/3 was checked in whole-cell lysate samples (Fig. 5.21a, left panel) and secretory granules (Fig. 5.21a, right panel) isolated from the GLUTag cells treated with 0mM (basal) or 10mM glucose at pH 6.3 and 7.4.

The densitometric analysis of the western blot between the inactive PC1/3 fraction (upper band, 87kDa) and fully active PC1/3 enzyme (lower band, 66kDa) was expressed as a percentage of total PC1/3 expression for each tested condition in whole-cell lysate samples (Fig. 5.21b) and secretory granules (Fig. 5.21c). No difference was identified in the amount of inactive fraction in the whole-cell lysates between the pH 6.3 or pH 7.4 treated cells under basal conditions (17% vs 16.8%, respectively) or in the 10mM glucose-stimulated samples (29.5% vs 27.8%). The active form also showed no difference between pH 6.3 and 7.4 at basal (82.8% vs 83.2%) or upon glucose stimulation (70% vs 72%) (Fig 5.21b).

The percentage of inactive PC1/3 fraction in secretory granules at pH 6.3 and 7.4 basal condition was 16.5% vs 12.6%, respectively, and increased upon 10mM glucose stimulation to 41.5% and 31.7% for the pH 6.3 and 7.4, respectively. The corresponding percentage of the active fraction of PC1/3 was similar at the basal condition between pH 6.3 and 7.4 – 83.5% vs 87.4%, respectively. There was also no major change in active fraction at 10mM glucose between pH 6.3 and pH 7.4 – 58.5% vs 68.3% (Fig. 5.21c).

Due to Covid-19 restrictions, I was unable to pursue this line of research further.

a



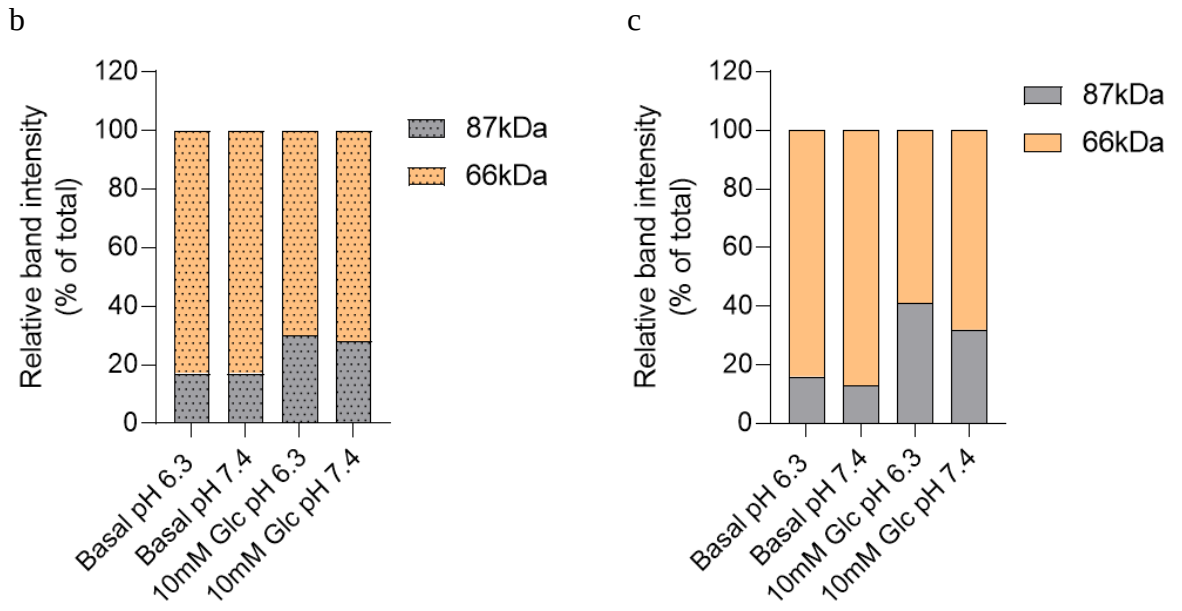


Figure 5.21 Prohormone convertase 1/3 (PC1/3) expression in GLUTag cell whole-cell lysate and secretory granules is not affected by pH.

a) Western blotting showing expression of GLP-1 processing enzyme PC1/3 in GLUTag cells whole-cell lysate (left) and secretory granules (right) at the basal and upon 10mM glucose stimulation at pH 6.3 or 7.4 as indicated. The upper band of 87kDa represents an inactive form of PC1/3, while the lower band at 66kDa is fully active PC1/3 that cleaves GLP-1 into 7-37 or 7-36-NH_2 active peptides. α-tubulin was probed as a loading control (shown below) at 50kDa. Densitometry analysis of the expression of 87kDa and 66kDa PC1/3 forms show the expression of each fraction as a percentage of total PC1/3 expression in b) whole-cell GLUTag cells lysate and c) in corresponding secretory granules isolated from the cells untreated (basal) and treated with 10mM glucose at pH 6.3 or 7.4.

5.4 Discussion

5.4.1 The effect of pH on GLP-1 secretion is not caused by the degradation of the hormone after release

This thesis reports for the first time that GLP-1 secretion from L cells is regulated by the pH of the extracellular environment. It has been demonstrated that acidification of the extracellular environment significantly lowers GLP-1 secretion from both GLUTag cells and primary rodent L cells. Reducing the extracellular pH from 7.0 to 6.3 decreased GLP-1 secretion by 40% in GLUTag cells. Maximal GLP-1 secretion was observed at pH 7.0 and no additive effect was observed by increasing the pH to 7.6 (Fig. 5.7 & 5.8). The modulatory effect of extracellular pH on GLP-1 secretion is most likely caused by proton accumulation intracellularly rather than extracellular degradation of secreted GLP-1, as synthetic GLP-1 was not degraded under acidic conditions (Fig. 5.9c). Supplementing the incubation buffer with protease inhibitors did not amplify the amount of GLP-1 that was recovered following stimulation with glucose at acidic pH (Fig. 5.9a-b). This excludes the possibility that greater extracellular degradation of secreted active GLP-1 occurs under acidic conditions. Dipeptidyl peptidase IV (DPP4), which is known to cleave the active N-terminal of GLP-1 (7-36-NH_2 or 7-37) into an inactive form, was not specifically targeted in these studies. However, using aprotinin - a known competitive substrate of DPP4 [338] did not rescue the GLP-1 secretion in acidic pH. Additionally, RNAseq demonstrated that GLUTag cells express very low levels of genes encoding *DPP4*, further supporting the notion that acidic pH does not affect the proteolytic modification of secreted GLP-1.

The role of pH in the amidation of the GLP-1 was also considered. Studies have shown that 80% of secreted GLP-1 *in vivo* and *in vitro* is amidated at the C-terminal by the peptidyl-α-hydroxyglycine α-amidating lyase (PAM) [339, 340]. The activity of PAM is regulated by pH, as it is optimally active in the acidic range with an optimum pH of 5.0 [341]. However, the

FRET-based ELISA used in this study detects both amidated and non-amidated GLP-1 with very high cross-reactivity (>98%,). Hence, if acidic pH were to alter the amidation state of GLP-1, it would not be reflected in the readout of the immunoassay.

5.4.2 The role of intracellular acidification in the regulation of GLP-1 exocytosis

Since the possibility of extracellular GLP-1 degradation or protonation effect was excluded and it has been reported previously that extracellular pH changes cause parallel intracellular pH changes in cells *in vitro* [295, 342], the pH sensitivity of GLP-1 secretion occurs most likely in response to proton influx when cells are exposed to low extracellular pH. While cytoplasmic pH within the cell is controlled by multiple transporters such as i.e. Na^+/H^+ exchangers, the luminal pH of intracellular compartments is regulated mainly by a family of ATP-dependent proton pumps known as the vacuolar (H^+)-ATPases [328]. V-ATPases can be also inhibited pharmacologically by bafilomycin A1, which was utilised in this study. Bafilomycin A1 impairs the translocation of protons into intracellular vesicles [330] and leads to cytosol acidification [343, 344]. In this study addition of bafilomycin A1 at pH 7.4 in GLUTag cells decreased the glucose-stimulated GLP-1 release to the same level as changing the extracellular pH to 6.8. This suggests that, during glucose stimulation at acidic pH_o, there is an intracellular proton flux into GLUTag cells that is responsible for the reduction of GLP-1 secretion. It is clear from the presented results (Fig. 5.11) that a reduction in pH_o from 7.4 to 6.8 yields similar proton influx and intracellular pH changes as blocking the V-ATPase-dependent proton transport with bafilomycin A1.

Alternatively, bafilomycin A1 inhibition of GLP-1 secretion may also involve a change in the acidification of the secretory granules. In the pancreatic β-cell, V-ATPase-driven acidification of the secretory granules has been shown to be pivotal for the priming and release of insulin

granules [288], and the proteolytic processing of proinsulin into mature insulin [345]. While bafilomycin A1 has been reported to efficiently inhibit V-ATPases at nanomolar concentrations [331], a much higher concentration of 1μM was also used in this study to exaggerate the inhibitory effect and also because this concentration was reported to previously for GLUTag cells [212]. Studies have shown that while bafilomycin A1 will cause the acidification of the cytosol, at the same time the effect of bafilomycin A1 at 1μM on cell culture *in vitro* was found to gradually increase the intravesicular pH by 1 unit from pH 5.5 to 6.3 within 50 minutes of incubation [346].

While both of these effects, acidification of cytoplasm and alkalinisation of vesicles, can contribute to the decrease of GLP-1 secretion, interestingly, acidification of the extracellular media to pH 6.3 showed a stronger effect in attenuating GLP-1 secretion than high-dose of V-ATPase inhibitor at pH 7.4. At present, it is also unclear how much proton flux due to the extracellular pH changes affects V-ATPase function and if this effect is more potent than bafilomycin A1 inhibition alone, and thus contributes to the larger impairment of the GLP-1 secretion at the acidic pH of 6.3. V-ATPase activity is tightly regulated by reversible assembly/disassembly of V_1 and V_o domains, i.e. glucose starvation is known to trigger local disassembly of V-ATPases in the vacuoles in yeast to conserve the ATP [347]. These events were found to co-occur with the cytosolic pH reduction under glucose-starvation conditions [348]. However, the extracellular pH changes ranging from pH 5 to 7.0 did not show that the parallel changes in cytosolic pH play a direct role in controlling V-ATPase stability or activity in yeast [349]. In neurons, it has been shown that the V_o subunit of V-ATPase serves as an intragranular pH sensor that regulates the exocytotic machinery and V-ATPase assembly strongly depends on intravesicular pH, with fully acidified synaptic vesicles showing a low abundance of cytosolic subunit V_1 domain [350]. Also, incompletely acidified synaptic vesicles were shown to fuse with lower probability [304]. While this might be the case when GLUTag

cells were treated with bafilomycin A1, the fact that acidic pH 6.3 lowered GLP-1 secretion even further suggests that there may be an additional effect of pH on exocytosis, which requires further investigation. Furthermore, intracellular changes in pH due to proton influx at low extracellular pH and their dynamics within the cellular compartments will need to be confirmed with pH-sensitive fluorescent probes and parallel measurements of extracellular pH. This can be done by live monitoring of pH-sensitive probe distribution, i.e. SNARF-5 AM and organelle-targeted pHluorin-based sensor.

5.4.3 The effect of pH on GLP-1 secretion is independent of glucose sensing

The removal of extracellular Na^+ and replacing it with non-permeable cation $NMDG^+$ abolished the glucose-stimulated secretory GLP-1 response from GLUTag cells (Fig 5.15). This was expected as the major glucose-sensing mechanism in L cells relies on the co-transport of glucose with Na^+ through the SGLT1 (Slc5a) transporter [187]. SGLT1 has been shown to utilise H^+ at low pH and in the absence of Na^+, which increases the rate of glucose uptake compared with when Na^+ is present at pH 7.4 [326]. The pH dependence of GLP-1 secretion may reflect the changes in the transport kinetics of sodium-driven glucose transport via SGLT1 into the cells under acidic conditions. To bypass the need for glucose-triggered inward sodium current and to observe the GLP-1 secretory response in the absence of sodium, 30mM KCl was used. KCl directly depolarised the membrane and caused global depolarisation and the voltage-gated L-type calcium channels to open to allow calcium entry [351]. Increased intracellular calcium levels trigger the exocytosis of GLP-1 [324, 352]. The KCl-induced depolarization evoked an equally strong GLP-1 secretory response in the presence or absence of extracellular Na^+. The pH-dependence of GLP-1 secretion upon KCl treatment was also conserved and irrespective of extracellular Na^+ presence. This result points to two interesting aspects of the pH sensitivity of GLP-1 secretion. First, that extracellular pH changes and the effect they exert

on GLP-1 secretion are independent of the glucose sensing (SGLT1) mechanism and it can be also speculated that mechanistically the pH effect acts downstream from membrane depolarisation and is not coupled to metabolising the nutrients.

Second, if the proton influx occurs during acidic treatment it does not require extracellular sodium to drive the proton entry into the cell. The data suggest that pH-dependence of GLP-1 secretion does not rely on the movement of sodium across the membrane as in the absence of sodium increased extracellular proton concentration was still able to inhibit GLP-1 secretion. Sodium is used by multiple Na^+-driven secondary active acid extruders that take part in regulating intracellular pH by removing or neutralising the excess of protons. These would include Na^+/H^+ exchangers of the SLC9 gene family and transporters that carry Na^+ into the cells altogether with HCO_3^- ions to counter flux the H^+ ions (SLC4 family) [300]. GLUTag cells as shown by the RNAseq results can express various members of both of these transporters families. The role of active proton extrusion coupled with sodium in the stimulus-secretion coupling of GLP-1 in L cells remains, however, unexplored.

5.4.4 The role of calcium in pH-dependence of GLP-1 release remains unexplored

Release of GLP-1 granules is calcium-dependent and the increased intracellular calcium entry through calcium channels activates the calcium sensor synaptotagmin-7, which relieves the block on the SNARE fusion machinery and thus permits the hormone release [294]. Reduction in intracellular calcium entry upon low pH would cause a decrease in GLP-1 secretion. In GLUTag cells, it has been shown that calcium entry is mediated by the voltage-gated L-type calcium channels (VGCCs) and it has been reported previously that L-type VGCCs are pH-sensitive. Increased extracellular protons are known to inhibit ion permeation through open VGCCs as well as modify their gating properties [353]. It is then possible that in the presented

experiments acidic pH may affect VGCC activation and subsequent calcium entry leading to reduction in GLP-1 exocytosis. Studies in myocytes, however, have shown that extracellular protons can inhibit, while intracellular protons stimulate, calcium currents through L-type calcium channels. The effects of low intracellular and extracellular pH on the calcium currents conducted through VGCCs were additive, and tend to cancel when appropriately combined [354]. Complete removal of the extracellular calcium halted exocytosis and incremental re-introduction of calcium into the incubation buffer increased GLP-1 release in a dose-dependent manner (Fig. 5.13a-c). The pH dependence of glucose-stimulated GLP-1 secretion was present at the lowest tested calcium level of 0.1mM extracellular calcium. Though the slopes of the linear correlation between calcium concentration and GLP-1 release were not significantly different between the acidic and alkalic treatment of GLUTag cells, the *p*-value was close to reaching significance (0.053). Hence, extracellular proton concentration may affect plasma membrane Ca^{2+} transport. Studies on rat pancreatic β-cells showed that net calcium uptake by β-cells was decreased at low extracellular pH, in the absence of glucose. Though, upon glucose treatment depending on glucose concentration calcium uptake was down only by 10-22% at acidic pH of 6.8, whereas glucose-stimulated insulin release was decreased by 70% [279]. This might suggest that the metabolic pathways downstream of calcium entry might play a role in the pH dependence of insulin secretion [355], and similarly GLP-1 secretion. The effect of pH_o on intracellular calcium levels in L cells requires further investigation with more sophisticated methods (i.e. fluorescent Ca^{2+} imaging) which were not possible during the timeframe of this study.

5.4.5 Extracellular chloride is essential for GLP-1 exocytosis

Removal of extracellular chloride completely abolished glucose-stimulated GLP-1 secretion, and significantly reduced forskolin-induced GLP-1 release (Fig. 5.17). Since the effect of

extracellular chloride on the exocytosis from GLUTag cells was so detrimental, we observed no pH dependence of GLP-1 secretion in the absence of chloride. Thus, extracellular chloride levels are essential for GLP-1 release and upstream from the pH-exerted effect on GLP-1 secretion. Similarly, it has been previously reported that the removal of extracellular chloride abolishes insulin secretion from mouse pancreatic β-cells, while the net uptake of calcium upon glucose stimulation was found unaffected. This effect was fast and fully reversed by supplementation of secretion buffer with chloride [315], however, the exact mechanism remains unknown. Some studies attributed the chloride-driven role in insulin exocytosis to be mediated by the alkalinisation of the β-cell cytosol when chloride is removed at extracellular pH 7.4 [284]. This agrees with early reports that pulse alkalinisation of the cytoplasm significantly decreases insulin secretion [356]. In GLUTag cells, however, the lack of chloride abolished the GLP-1 secretion at pH_o 7.4, but also at pH_o 6.3, which would cause cytosolic acidification. From other reports, the mechanism behind chloride-dependence of insulin exocytosis was suggested to be mediated via Cl^- channel, CLC3, which is expressed on insulin-containing secretory granules [316]. As reported here, GLUTag cells express mRNA encoding CLC3 and other members of the chloride channels superfamily, however, their expression patterns are unclear. In β-cells CLC-3 was found essential for providing Cl^- conductance to counterbalance protons pumped by V-ATPases. CLC-3 inhibition similar to lowering intracellular chloride was found to affect the vesicle acidification and thus reduce the exocytosis measured as membrane capacitance. Interestingly, the same authors did not observe the effect of varying the extracellular chloride concentrations on exocytosis [288]. Other reports also point out the importance of other chloride channels and Cl^-/H^+ exchangers in maintaining the correct intraluminal pH within the cells, which is crucial for protein trafficking and correct post-translational modification [318]. This presumably will take a considerable amount of time to affect hormone secretion. The GLP-1 secretion assays were performed over

2hr for the best fold-change in stimulated GLP-1 release [57]. However, we observed that the pH dependence of GLP-1 secretion upon glucose stimulation was transient and reversible within 1 hour after swapping the secretions buffers of different pH values. GLUTag cells kept initially at acidic pH that would suppress GLP-1 secretion regained the normal secretion rate when at pH 7.4, and vice versa (Fig. 5.12). This result would suggest that the pH effect on GLP-1 secretion is rapid and most likely acts through the fast-acting and reversible mechanisms involved in the enzymatic reaction cascades or final stages of exocytosis rather than gene or protein expression changes.

5.4.6 Expression and autocleavage of PC1/3

Low extracellular pH did not affect the expression levels of enzyme PC1/3 which cleaves GLP-1 into its active form (Fig. 5.21a-c). Thus, the mechanism of pH-dependence of GLP-1 secretion cannot be attributed to the amount of active GLP-1 made within secretory granules and ready to be released. If this was the case, then cells incubated at pH 6.3 would be expected to have lower amounts of active GLP-1 within secretory granules available for release. Our data show the opposite result, secretory granules of cells stimulated at acidic pH contained more active GLP-1 than those at pH 7.4.

PC1/3 undergoes proteolytic maturation itself within the regulated secretory pathway. The acidic environment of secretory granules (pH 5.5) prompts PC1/3 to self-activate and form two truncated forms, 74- and 66kDa. These are the most enzymatically active forms of PC1/3, they require a millimolar concentration of calcium and very low pH for optimum activity (5-5.5) [313]. Here, the western blot analysis did not allow distinguishing between the 74kDa and 66kDa forms of PC1/3, but it confirmed the abundant expression of the fully activated 66kDa form in GLUTag cells. The expression levels of the inactive 87kDa or active 66kDa form of PC1/3 in the whole cell lysate of GLUTag cells did not differ between pH_o 6.3 and 7.4.

Similarly, within the secretory granules, there was no significant difference in the levels of 87kDa vs 66kDa forms of PC1/3 between glucose-stimulated cells in acidic or alkalic pH. This suggests that acidic pH_o did not affect the rate of PC1/3 processing and autocleavage from 87kDa into 66kDa within the timeframe of the experiment. This was further confirmed by the result showing that whole-cell production of active GLP-1 requiring fully active PC1/3 remained unchanged between the pH treatments (Fig. 5.18b). It is possible that while the processing of PC1/3 was unchanged, the catalytic activity rate of the convertase enzyme differs when cells are exposed to different pH_o conditions. This aspect, however, will have to be addressed with the dedicated assay to measure the catalytic activity of PC1/3 such as an *ex vivo* enzymatic activity assay. This might be crucial to establish since a similar effect of low pH was observed in insulin secretion [277], while decreasing extracellular pH had no effect on glucagon secretion from rat pancreatic α-cells [280]. Interestingly, in pancreatic α-cells, preproglucagon processing into active glucagon is mainly mediated by PC2. Similarly, to PC1/3, PC2 activity is calcium-dependent with a low pH optimum. However, these properties differ considerably from that of PC1/3; the calcium requirement is much lower (micromolar range) [357] and unlike PC1/3, PC2 is known to transit the secretory pathway as a zymogen and is converted to mature PC2 only within secretory granules [358]. Thus, this differential catalytic and trafficking profile of PC1/3 and PC2 might contribute to the pH-dependence of stimulated secretion of their respective hormonal substrates.

5.4.7 Acidic pH affects exocytotic machinery as more GLP-1 is retained in secretory granules at low pH

Secretory granules were isolated from GLUTag cells stimulated with glucose at pH 6.3 or 7.4. to investigate the levels of active GLP-1 within. This approach allowed us to give a preliminary indication that pH dependence of GLP-1 secretion might be mediated at the final steps of the

exocytosis and downstream from calcium entry. Secretory granules isolated from GLUTag cells stimulated at low pH were found to contain more active GLP-1 as compared to cells stimulated at pH 7.4 (Fig. 5.20). This result shows that acidic pH caused the retention of the GLP-1-filled secretory granules and prevented successful exocytosis. The complex of SNARE proteins is responsible for the exocytosis of GLP-1 via docking, priming and fusion of the secretory granules with the plasma membrane. However, apart from core players such as SNAP25, VAMP2, synaptotagmin 7 and syntaxin-1a, little is known about the exact exocytotic machinery and events leading to the release of GLP-1 from L cells [291]. GLUTag cells were found to express all isoforms of VAMPs and syntaxin [293], which has been also confirmed by our RNAseq results. Among pH-sensitive targets within SNARE is NSF, the N-ethylmaleimide-sensitive fusion protein (NSF) that together with SNAP plays a key role in regulated exocytosis. The role of NSF is to hydrolyse ATP and cause the disassembly of used SNARE complex and facilitate their reuse for further fusion events. NSF displays ATPase activity that is pH sensitive and optimal fusion kinetics requires pH 6-7 [359, 360]. Additional more sophisticated methods will have to be employed to confirm that acidic pH is inhibiting secretory granules fusion. The exocytosis events at the membrane level can be assessed by the measurements of capacitance changes. Capacitance is a parameter linearly related to membrane surface area and its increases upon the fusion of secretory granules with the plasma membrane [361]. This approach would directly address whether acidic pH affects secretory granule fusion.

5.4 Summary

In summary, extracellular pH at the acidic range inhibits GLP-1 secretion from endocrine L cells by a mechanism that is independent from glucose-sensing. This effect is mediated by the proton accumulation within the cell, however, it remains unclear which transport system of acid loaders/extruders is utilised. The data shown here exclude sodium-driven proton transport,

however different experimental approach is required to investigate the relationship between pH and calcium levels. Exocytosis of GLP-1 is shown to be dependent on extracellular Cl^- levels, which suggests that Cl^--permeable channels are pivotal for GLP-1 secretion. Production and availability of active GLP-1, as well as the abundance and processing of PC1/3 involved in GLP-1 synthesis is not affected by extracellular pH changes. Finally, acidic pH causes higher levels of GLP-1 retention within the secretory granules suggesting that pH-dependence of GLP-1 release occurs at the stage of exocytosis.

Chapter 6: Conclusions and future perspectives

Overexpression of the gene encoding *ABCC5* in adipose tissue has been implicated to confer a higher risk of T2D in humans [3], while previous work from our laboratory reported that the knockout of the *Abcc5* gene in a mouse model promotes a lean metabolic phenotype marked by lower adipose tissue depots, increased insulin sensitivity and higher plasma levels of GLP-1 [4]. Additionally, our unpublished work shows that the absence of the *Abcc5* gene most likely affects glutamatergic transmission via AMPA/NMDA receptors in *Abcc5*$^{-/-}$ mice brains. The disruption of glutamatergic signalling, possibly via NMDA receptors, most likely underpins the loss of PPI in *Abcc5*$^{-/-}$ mice reported here. Reduced PPI in humans serves as a biomarker of schizophrenia. Schizophrenic symptoms and cognitive impairment, according to the glutamate hypothesis of schizophrenia, are caused by the hypoactivity of NMDA receptors and excessive glutamate release, especially in brain areas including the prefrontal cortex [362]. Since expression of *ABCC5* in human and mouse brains is reported to be ubiquitous [16, 363], and the behavioural tests we employed to confirm a cognitive phenotype of *Abcc5*$^{-/-}$ mice do not isolate a specific brain circuit *per se*, it was not possible to identify the specific neuronal pathways underlying the neurobehavioural changes of *Abcc5*$^{-/-}$ mice. In order to isolate the specific neurons and cells affected by the loss of *Abcc5*$^{-/-}$ it would require using cell-specific knockouts, where *Abcc5* deficiency would occur in specific neuronal cells (neurons, glia, astrocytes) or specific populations of inhibitory (GABAergic) or excitatory neurons (glutamatergic). The latter can be also investigated *ex vivo* using neuronal organoids from *Abcc5*$^{-/-}$ mice to ascertain if lack of *Abcc5* affects the development of these neuronal populations, as a recent study reported that excitatory and inhibitory neurons originate from

common progenitors in cerebellar organoids [364]. There is also the salient question which remains: what is the real physiological substrate(s) of the ABCC5 transporter? Previously reported ABCC5 substrates include cyclic nucleotide second messengers (cAMP and cGMP), but also various glutamate-conjugated analogues, such as NAAG [27, 31]. NAAG has been implicated to play the neuroprotective role from glutamate excitotoxicity at the synapse level [365]. The pharmacological inhibition of NAAG peptidase, which would elevate NAAG levels at the synaptic cleft, was reported to reduce PCP-induced symptoms of schizophrenia and proposed as a therapeutic target for schizophrenia [366]. *Abcc5*$^{-/-}$ mice display elevated levels of NAAG in their brains, but paradoxically, are more prone to PPI deficits, a hallmark of schizophrenic symptoms. Since cellular localisation of ABCC5 remains uncertain, higher levels of NAAG in *Abcc5*$^{-/-}$ mice brains, but lack of NAAG protective effect, may suggest that the accumulated NAAG remains trapped within the neuronal cells and is not accessible in the synapse to exert its beneficial effects. This would be consistent with the reports of vesicular [4] or mitochondrial localisation of ABCC5 [22]. Reliable detection of ABCC5 is hindered by the lack of specific antibodies and a high sequence homology between ABCC5, ABCC11 and ABCC12 in humans, and between Abcc5 and Abcc12 in mice [367]. Possibly, the difficulty to detect ABCC5 *in situ* may be due to epitopes that are used to generate commercial antibodies are obscured in native ABCC5 or ABCC5 may be complexed with other proteins. It would be invaluable to create and validate bespoke antibodies against native ABCC5 in order to advance research into expression patterns of ABCC5 protein in intact tissue further. Moreover, only *ex vivo* transport assays utilising cell lines that overexpress ABCC5 confirmed the transport of a range of compounds, from cyclic nucleotides to various glutamate-conjugates, with K_m values ranging from µM to mM depending on the tested substrate [27, 31]. Therefore, there is a need to perform more sensitive radionucleotide transport assays using purified and reconstituted ABCC5 protein to validate against a functionally inactive ABCC5_K601A, K1233A

transporter, where the catalytic lysine residues in the NBDs are replaced by alanine residues to render the transporter inactive.

The mechanism underpinning the regulation of GLP-1 secretion by Abcc5 activity remains to be elucidated. However, here we report a possible link between downregulated Abcc5 expression and an increased level of GLP-1 secretion in *Abcc5*$^{-/-}$ mice and enhanced NMDA receptor activity. Pharmacological inhibition or knockdown of NMDA receptors in GLUTag cells increased GLP-1 release. It may be that NDMA receptor activity acts as a general hand brake to regulate GLP-1 secretion from L cells, and once blocked or downregulated it accelerates GLP-1 release. NMDA receptor subunits are expressed in human and mouse native L cells [57] . It is well established that EECs form direct connections with the nervous system via axon-like projections termed neuropods [183]. Innervated EECs take part in neuroepithelial circuits transducing the luminal nutrient information from the gut to the brain and feedback from the brain to the gut EECs [368]. This bidirectional communication has been reported to be dependent on the type of macronutrient sensed by EECs and the intestinal site of detection [369]. The primary intestinal cultures used in this study show that some primary L cells indeed develop neuropod-like structures. A natural extension of the work presented here would be to repeat the experiments done by Bohorquez *et al.*[183], including co-culture of gut epithelial cells with neuronal cells, and further investigate the role of NMDA receptors and glutamatergic signalling in the regulation of GLP-1 secretion using NMDAR inhibitors.

The limitations of the L cell models used in this study are also important to consider for the pH dependence of GLP-1 secretion. Native L cells are polarised with the microvilli-covered apical side facing the luminal content of the gut and making direct contact with nutrients, and being exposed to various intraluminal pH [139, 259], while the basolateral hormone-secreting side is facing the pH-controlled bloodstream [179]. It is uncertain if cultured in a 2D setting, primary L cells and GLUTag cells are representative of the apical or basolateral side as there is evidence

supporting both models. Knockout of apically expressed SGLT-1 in primary intestinal cultures [370] abolished the glucose-stimulated GLP-1 secretion [323], while inhibition of K_{ATP} channel expressed on the basolateral side triggered GLP-1 secretion from GLUTag cells and primary small intestine cultures [187, 189]. L cells in cell culture have unrestricted access to the nutrients on both sides, therefore it is difficult to discern if pH acts on the apical on the basolateral side of the L cells. Gut organoids may be a useful model to investigate the pH dependence of GLP-1 secretion in response to luminal or basolateral pH changes, as they are capable of forming a 'mini-lumen' and providing a polarized cell layer [371]. The pH-sensitive hormone release has been reported previously in various models of pancreatic β-cells, where acidic extracellular pH was shown to inhibit glucose-induced insulin secretion. The mechanism underlying the pH-dependent insulin release from pancreatic β-cells was proposed to involve glucose metabolism [279, 282]. Here, we show that pH-dependence of stimulated GLP-1 secretion is independent of the glucose-sensing mechanism in L cells, however, further studies are needed to explore the pH effect on the stimulus-secretion coupling of GLP-1 with different secretagogues. Nonetheless, our data suggest that pH affects the final steps of exocytosis, possibly the fusion of GLP-1 secretory granules with the outer membrane. This result will need to be confirmed with dedicated techniques such as measurements of membrane capacitance. L cells also co-express oxyntomodulin, GLP-1, GLP-2, PYY and in the distal colon INSL5 (insulin-like peptide 5) and these peptides were shown to be co-stored in the same vesicular pool as GLP-1 [372]. Although the focus of this study is GLP-1, it is possible that pH may also affect the secretion of other co-stored peptides.

Finally, data presented here demonstrated that although a well-studied field, the excitation-secretion coupling mechanisms of EECs are far from elucidated and that both glutamatergic signalling and pH can modulate GLP-1 secretion, which opens new possibilities for novel target discoveries in an attempt to enhance endogenous secretion of GLP-1.

Bibliography

1. Roden, M. and G.I. Shulman, *The integrative biology of type 2 diabetes.* Nature, 2019. **576**(7785): p. 51-60.
2. Khan, M.A.B., et al., *Epidemiology of Type 2 Diabetes - Global Burden of Disease and Forecasted Trends.* J Epidemiol Glob Health, 2020. **10**(1): p. 107-111.
3. Direk, K., et al., *ABCC5 transporter is a novel type 2 diabetes susceptibility gene in European and African American populations.* Ann Hum Genet, 2014. **78**(5): p. 333-44.
4. Cyranka, M., et al., *Abcc5 Knockout Mice Have Lower Fat Mass and Increased Levels of Circulating GLP-1.* Obesity (Silver Spring), 2019. **27**(8): p. 1292-1304.
5. Dean, M., A. Rzhetsky, and R. Allikmets, *The human ATP-binding cassette (ABC) transporter superfamily.* Genome Res, 2001. **11**(7): p. 1156-66.
6. Saier, M.H., Jr., *A functional-phylogenetic classification system for transmembrane solute transporters.* Microbiol Mol Biol Rev, 2000. **64**(2): p. 354-411.
7. Higgins, C.F. and K.J. Linton, *Structural biology. The xyz of ABC transporters.* Science, 2001. **293**(5536): p. 1782-4.
8. Oswald, C., I.B. Holland, and L. Schmitt, *The motor domains of ABC-transporters. What can structures tell us?* Naunyn Schmiedebergs Arch Pharmacol, 2006. **372**(6): p. 385-99.
9. Campbell, J.D., M.S. Sansom, and F.M. Ashcroft, *Potassium channel regulation.* EMBO Rep, 2003. **4**(11): p. 1038-42.
10. Li, H., et al., *Therapeutic approaches to CFTR dysfunction: From discovery to drug development.* J Cyst Fibros, 2018. **17**(2S): p. S14-S21.
11. Reid, G., et al., *The human multidrug resistance protein MRP4 functions as a prostaglandin efflux transporter and is inhibited by nonsteroidal antiinflammatory drugs.* Proc Natl Acad Sci U S A, 2003. **100**(16): p. 9244-9.
12. Cole, S.P., *Multidrug resistance protein 1 (MRP1, ABCC1), a "multitasking" ATP-binding cassette (ABC) transporter.* J Biol Chem, 2014. **289**(45): p. 30880-8.
13. Adamska, A., et al., *ABCC3 is a novel target for the treatment of pancreatic cancer.* Adv Biol Regul, 2019. **73**: p. 100634.
14. Shipp, L.E., et al., *ABCC5 is required for cAMP-mediated hindgut invagination in sea urchin embryos.* Development, 2015. **142**(20): p. 3537-48.
15. Dazert, P., et al., *Expression and localization of the multidrug resistance protein 5 (MRP5/ABCC5), a cellular export pump for cyclic nucleotides, in human heart.* Am J Pathol, 2003. **163**(4): p. 1567-77.
16. *The Human Protein Atlas*. Available from: https://www.proteinatlas.org/ENSG00000114770-ABCC5.
17. Meyer Zu Schwabedissen, H.E., et al., *Expression, localization, and function of MRP5 (ABCC5), a transporter for cyclic nucleotides, in human placenta and cultured human trophoblasts: effects of gestational age and cellular differentiation.* Am J Pathol, 2005. **166**(1): p. 39-48.
18. de Wolf, C.J., et al., *cGMP transport by vesicles from human and mouse erythrocytes.* FEBS J, 2007. **274**(2): p. 439-50.
19. McAleer, M.A., et al., *pABC11 (also known as MOAT-C and MRP5), a member of the ABC family of proteins, has anion transporter activity but does not confer multidrug resistance when overexpressed in human embryonic kidney 293 cells.* J Biol Chem, 1999. **274**(33): p. 23541-8.
20. Nies, A.T., et al., *Expression and immunolocalization of the multidrug resistance proteins, MRP1-MRP6 (ABCC1-ABCC6), in human brain.* Neuroscience, 2004. **129**(2): p. 349-60.
21. Bronger, H., et al., *ABCC drug efflux pumps and organic anion uptake transporters in human gliomas and the blood-tumor barrier.* Cancer Res, 2005. **65**(24): p. 11419-28.

22. Chambers, I.G., et al., *MRP5 and MRP9 play a concerted role in male reproduction and mitochondrial function.* Proc Natl Acad Sci U S A, 2022. **119**(6).
23. Wijnholds, J., et al., *Multidrug-resistance protein 5 is a multispecific organic anion transporter able to transport nucleotide analogs.* Proc Natl Acad Sci U S A, 2000. **97**(13): p. 7476-81.
24. Korolnek, T., et al., *Control of metazoan heme homeostasis by a conserved multidrug resistance protein.* Cell Metab, 2014. **19**(6): p. 1008-19.
25. Miyauchi, E., et al., *Quantitative Atlas of Cytochrome P450, UDP-Glucuronosyltransferase, and Transporter Proteins in Jejunum of Morbidly Obese Subjects.* Mol Pharm, 2016. **13**(8): p. 2631-40.
26. Ritter, C.A., et al., *Cellular export of drugs and signaling molecules by the ATP-binding cassette transporters MRP4 (ABCC4) and MRP5 (ABCC5).* Drug Metab Rev, 2005. **37**(1): p. 253-78.
27. Jedlitschky, G., B. Burchell, and D. Keppler, *The multidrug resistance protein 5 functions as an ATP-dependent export pump for cyclic nucleotides.* J Biol Chem, 2000. **275**(39): p. 30069-74.
28. Wielinga, P.R., et al., *Thiopurine metabolism and identification of the thiopurine metabolites transported by MRP4 and MRP5 overexpressed in human embryonic kidney cells.* Mol Pharmacol, 2002. **62**(6): p. 1321-31.
29. Long, Y., et al., *Molecular analysis, developmental function and heavy metal-induced expression of ABCC5 in zebrafish.* Comp Biochem Physiol B Biochem Mol Biol, 2011. **158**(1): p. 46-55.
30. Borst, P., C. de Wolf, and K. van de Wetering, *Multidrug resistance-associated proteins 3, 4, and 5.* Pflugers Arch, 2007. **453**(5): p. 661-73.
31. Jansen, R.S., et al., *ATP-binding Cassette Subfamily C Member 5 (ABCC5) Functions as an Efflux Transporter of Glutamate Conjugates and Analogs.* J Biol Chem, 2015. **290**(51): p. 30429-40.
32. Neale, J.H., T. Bzdega, and B. Wroblewska, *N-Acetylaspartylglutamate: the most abundant peptide neurotransmitter in the mammalian central nervous system.* J Neurochem, 2000. **75**(2): p. 443-52.
33. Lodder-Gadaczek, J., et al., *N-acetylaspartylglutamate synthetase II synthesizes N-acetylaspartylglutamylglutamate.* J Biol Chem, 2011. **286**(19): p. 16693-706.
34. Hamada-Kanazawa, M., et al., *beta-Citryl-L-glutamate acts as an iron carrier to activate aconitase activity.* Biol Pharm Bull, 2011. **34**(9): p. 1455-64.
35. Wielinga, P., et al., *The human multidrug resistance protein MRP5 transports folates and can mediate cellular resistance against antifolates.* Cancer Res, 2005. **65**(10): p. 4425-30.
36. Pouwels, P.J. and J. Frahm, *Differential distribution of NAA and NAAG in human brain as determined by quantitative localized proton MRS.* NMR Biomed, 1997. **10**(2): p. 73-8.
37. Neale, J.H. and T. Yamamoto, *N-acetylaspartylglutamate (NAAG) and glutamate carboxypeptidase II: An abundant peptide neurotransmitter-enzyme system with multiple clinical applications.* Prog Neurobiol, 2020. **184**: p. 101722.
38. Morland, C. and K. Nordengen, *N-Acetyl-Aspartyl-Glutamate in Brain Health and Disease.* Int J Mol Sci, 2022. **23**(3).
39. Zhong, C., et al., *NAAG peptidase inhibitor reduces acute neuronal degeneration and astrocyte damage following lateral fluid percussion TBI in rats.* J Neurotrauma, 2005. **22**(2): p. 266-76.
40. Jaarsma, D., L. Veenma-van der Duin, and J. Korf, *N-acetylaspartate and N-acetylaspartylglutamate levels in Alzheimer's disease post-mortem brain tissue.* J Neurol Sci, 1994. **127**(2): p. 230-3.
41. Li, K., et al., *The regulatory role of NAAG-mGluR3 signaling on cortical synaptic plasticity after hypoxic ischemia.* Cell Commun Signal, 2022. **20**(1): p. 55.
42. Wroblewska, B., et al., *N-acetylaspartylglutamate selectively activates mGluR3 receptors in transfected cells.* J Neurochem, 1997. **69**(1): p. 174-81.
43. Crupi, R., D. Impellizzeri, and S. Cuzzocrea, *Role of Metabotropic Glutamate Receptors in Neurological Disorders.* Front Mol Neurosci, 2019. **12**: p. 20.

44. Zollinger, M., et al., *Release of N-acetylaspartylglutamate on depolarization of rat brain slices.* J Neurochem, 1988. **51**(6): p. 1919-23.
45. Lodder-Gadaczek, J., V. Gieselmann, and M. Eckhardt, *Vesicular uptake of N-acetylaspartylglutamate is catalysed by sialin (SLC17A5).* Biochem J, 2013. **454**(1): p. 31-8.
46. Trombley, P.Q. and G.L. Westbrook, *Excitatory synaptic transmission in cultures of rat olfactory bulb.* J Neurophysiol, 1990. **64**(2): p. 598-606.
47. Sekiguchi, M., K. Wada, and R.J. Wenthold, *N-acetylaspartylglutamate acts as an agonist upon homomeric NMDA receptor (NMDAR1) expressed in Xenopus oocytes.* FEBS Lett, 1992. **311**(3): p. 285-9.
48. Losi, G., S. Vicini, and J. Neale, *NAAG fails to antagonize synaptic and extrasynaptic NMDA receptors in cerebellar granule neurons.* Neuropharmacology, 2004. **46**(4): p. 490-6.
49. Bergeron, R., et al., *NAAG reduces NMDA receptor current in CA1 hippocampal pyramidal neurons of acute slices and dissociated neurons.* Neuropsychopharmacology, 2005. **30**(1): p. 7-16.
50. Khacho, P., et al., *Differential effects of N-acetyl-aspartyl-glutamate on synaptic and extrasynaptic NMDA receptors are subunit- and pH-dependent in the CA1 region of the mouse hippocampus.* Neurobiol Dis, 2015. **82**: p. 580-592.
51. Evans, D.F., et al., *Measurement of gastrointestinal pH profiles in normal ambulant human subjects.* Gut, 1988. **29**(8): p. 1035-41.
52. Steenackers, N., et al., *Effect of obesity on gastrointestinal transit, pressure and pH using a wireless motility capsule.* Eur J Pharm Biopharm, 2021. **167**: p. 1-8.
53. *IMPC*. IMPC]. Available from: https://www.mousephenotype.org/data/genes/MGI:1351644.
54. Lee, Y.C., S.L. Asa, and D.J. Drucker, *Glucagon gene 5'-flanking sequences direct expression of simian virus 40 large T antigen to the intestine, producing carcinoma of the large bowel in transgenic mice.* J Biol Chem, 1992. **267**(15): p. 10705-8.
55. Goebel-Stengel, M., et al., *The importance of using the optimal plasticware and glassware in studies involving peptides.* Anal Biochem, 2011. **414**(1): p. 38-46.
56. Jameson, J.L., et al., *Endocrinology : adult & pediatric*. 2016, Elsevier/Saunders,: Philadelphia, PA. p. 1 online resource.
57. Cyranka, M., et al., *NMDA Receptor Antagonists Increase the Release of GLP-1 From Gut Endocrine Cells.* Front Pharmacol, 2022. **13**: p. 861311.
58. Kersten, K., et al., *Genetically engineered mouse models in oncology research and cancer medicine.* EMBO Mol Med, 2017. **9**(2): p. 137-153.
59. Brereton, M.F. and F.M. Ashcroft, *Mouse Models of beta-cell KATP Channel Dysfunction.* Drug Discov Today Dis Models, 2013. **10**(2): p. e101-e109.
60. Elder, G.A., M.A. Gama Sosa, and R. De Gasperi, *Transgenic mouse models of Alzheimer's disease.* Mt Sinai J Med, 2010. **77**(1): p. 69-81.
61. Wilke, M., et al., *Mouse models of cystic fibrosis: phenotypic analysis and research applications.* J Cyst Fibros, 2011. **10 Suppl 2**: p. S152-71.
62. Williams, S.M., J.L. Haines, and J.H. Moore, *The use of animal models in the study of complex disease: all else is never equal or why do so many human studies fail to replicate animal findings?* Bioessays, 2004. **26**(2): p. 170-9.
63. Perlman, R.L., *Mouse models of human disease: An evolutionary perspective.* Evol Med Public Health, 2016. **2016**(1): p. 170-6.
64. Fox, J.G., *The mouse in biomedical research*. 2nd ed. American College of Laboratory Animal Medicine series. 2007, Amsterdam ; Boston: Elsevier, AP. v. <2-4>.
65. Gurumurthy, C.B. and K.C.K. Lloyd, *Generating mouse models for biomedical research: technological advances.* Dis Model Mech, 2019. **12**(1).
66. Lloyd, K.C.K., et al., *The Deep Genome Project.* Genome Biol, 2020. **21**(1): p. 18.
67. Brown, S.D.M., et al., *High-throughput mouse phenomics for characterizing mammalian gene function.* Nat Rev Genet, 2018. **19**(6): p. 357-370.

68. Bucan, M. and T. Abel, *The mouse: genetics meets behaviour.* Nat Rev Genet, 2002. **3**(2): p. 114-23.
69. Powell, S.B., X. Zhou, and M.A. Geyer, *Prepulse inhibition and genetic mouse models of schizophrenia.* Behav Brain Res, 2009. **204**(2): p. 282-94.
70. Brody, S.A., et al., *Assessment of a prepulse inhibition deficit in a mutant mouse lacking mGlu5 receptors.* Mol Psychiatry, 2004. **9**(1): p. 35-41.
71. Nicoletti, F., et al., *Targeting mGlu Receptors for Optimization of Antipsychotic Activity and Disease-Modifying Effect in Schizophrenia.* Front Psychiatry, 2019. **10**: p. 49.
72. Ayalew, M., et al., *Convergent functional genomics of schizophrenia: from comprehensive understanding to genetic risk prediction.* Mol Psychiatry, 2012. **17**(9): p. 887-905.
73. Balan, S., et al., *Role of an Atypical Cadherin Gene, Cdh23 in Prepulse Inhibition, and Implication of CDH23 in Schizophrenia.* Schizophr Bull, 2021. **47**(4): p. 1190-1200.
74. Ison, J.R., et al., *Facilitation and inhibition of the acoustic startle reflex in the rat after a momentary increase in background noise level.* Behav Neurosci, 1997. **111**(6): p. 1335-52.
75. Willott, J.F., S. Carlson, and H. Chen, *Prepulse inhibition of the startle response in mice: relationship to hearing loss and auditory system plasticity.* Behav Neurosci, 1994. **108**(4): p. 703-13.
76. Hasenkamp, W., et al., *Heritability of acoustic startle magnitude, prepulse inhibition, and startle latency in schizophrenia and control families.* Psychiatry Res, 2010. **178**(2): p. 236-43.
77. Swerdlow, N.R., D.L. Braff, and M.A. Geyer, *Sensorimotor gating of the startle reflex: what we said 25 years ago, what has happened since then, and what comes next.* J Psychopharmacol, 2016. **30**(11): p. 1072-1081.
78. Turetsky, B.I., et al., *Neurophysiological endophenotypes of schizophrenia: the viability of selected candidate measures.* Schizophr Bull, 2007. **33**(1): p. 69-94.
79. Lauer, A.M., D. Behrens, and G. Klump, *Acoustic startle modification as a tool for evaluating auditory function of the mouse: Progress, pitfalls, and potential.* Neurosci Biobehav Rev, 2017. **77**: p. 194-208.
80. Freudenberg, F., et al., *Selective breeding for deficient sensorimotor gating is accompanied by increased perseveration in rats.* Neuroscience, 2007. **148**(3): p. 612-22.
81. Gomez-Nieto, R., S. Hormigo, and D.E. Lopez, *Prepulse Inhibition of the Auditory Startle Reflex Assessment as a Hallmark of Brainstem Sensorimotor Gating Mechanisms.* Brain Sci, 2020. **10**(9).
82. Weber, M., H.U. Schnitzler, and S. Schmid, *Synaptic plasticity in the acoustic startle pathway: the neuronal basis for short-term habituation?* Eur J Neurosci, 2002. **16**(7): p. 1325-32.
83. O'Leary, T.P., et al., *Reduced acoustic startle response and peripheral hearing loss in the 5xFAD mouse model of Alzheimer's disease.* Genes Brain Behav, 2017. **16**(5): p. 554-563.
84. Simons-Weidenmaier, N.S., et al., *Synaptic depression and short-term habituation are located in the sensory part of the mammalian startle pathway.* BMC Neurosci, 2006. **7**: p. 38.
85. Willott, J.F., et al., *Acoustic startle and prepulse inhibition in 40 inbred strains of mice.* Behav Neurosci, 2003. **117**(4): p. 716-27.
86. Ouagazzal, A.M., D. Reiss, and R. Romand, *Effects of age-related hearing loss on startle reflex and prepulse inhibition in mice on pure and mixed C57BL and 129 genetic background.* Behav Brain Res, 2006. **172**(2): p. 307-15.
87. Pilz, P.K. and H.U. Schnitzler, *Habituation and sensitization of the acoustic startle response in rats: amplitude, threshold, and latency measures.* Neurobiol Learn Mem, 1996. **66**(1): p. 67-79.
88. Braff, D.L. and M.A. Geyer, *Sensorimotor gating and schizophrenia. Human and animal model studies.* Arch Gen Psychiatry, 1990. **47**(2): p. 181-8.
89. Swerdlow, N.R., M.A. Geyer, and D.L. Braff, *Neural circuit regulation of prepulse inhibition of startle in the rat: current knowledge and future challenges.* Psychopharmacology (Berl), 2001. **156**(2-3): p. 194-215.

90. Li, L., et al., *Top-down modulation of prepulse inhibition of the startle reflex in humans and rats.* Neurosci Biobehav Rev, 2009. **33**(8): p. 1157-67.
91. Fendt, M., L. Li, and J.S. Yeomans, *Brain stem circuits mediating prepulse inhibition of the startle reflex.* Psychopharmacology (Berl), 2001. **156**(2-3): p. 216-24.
92. Yeomans, J.S., et al., *Midbrain pathways for prepulse inhibition and startle activation in rat.* Neuroscience, 2006. **142**(4): p. 921-9.
93. Carlson, S. and J.F. Willott, *Caudal pontine reticular formation of C57BL/6J mice: responses to startle stimuli, inhibition by tones, and plasticity.* J Neurophysiol, 1998. **79**(5): p. 2603-14.
94. Azzopardi, E., et al., *The Role of Cholinergic Midbrain Neurons in Startle and Prepulse Inhibition.* J Neurosci, 2018. **38**(41): p. 8798-8808.
95. Cano, J.C., W. Huang, and K. Fenelon, *The amygdala modulates prepulse inhibition of the auditory startle reflex through excitatory inputs to the caudal pontine reticular nucleus.* BMC Biol, 2021. **19**(1): p. 116.
96. Swerdlow, N.R., et al., *Realistic expectations of prepulse inhibition in translational models for schizophrenia research.* Psychopharmacology (Berl), 2008. **199**(3): p. 331-88.
97. Geyer, M.A., et al., *Pharmacological studies of prepulse inhibition models of sensorimotor gating deficits in schizophrenia: a decade in review.* Psychopharmacology (Berl), 2001. **156**(2-3): p. 117-54.
98. Ralph, R.J., et al., *Prepulse inhibition deficits and perseverative motor patterns in dopamine transporter knock-out mice: differential effects of D1 and D2 receptor antagonists.* J Neurosci, 2001. **21**(1): p. 305-13.
99. Aubert, L., D. Reiss, and A.M. Ouagazzal, *Auditory and visual prepulse inhibition in mice: parametric analysis and strain comparisons.* Genes Brain Behav, 2006. **5**(5): p. 423-31.
100. Ioannidou, C., G. Marsicano, and A. Busquets-Garcia, *Assessing Prepulse Inhibition of Startle in Mice.* Bio Protoc, 2018. **8**(7): p. e2789.
101. Plappert, C.F., P.K. Pilz, and H.U. Schnitzler, *Factors governing prepulse inhibition and prepulse facilitation of the acoustic startle response in mice.* Behav Brain Res, 2004. **152**(2): p. 403-12.
102. Hoffman, H.S. and J.L. Searle, *Acoustic and temporal factors in the evocation of startle.* J Acoust Soc Am, 1968. **43**(2): p. 269-82.
103. Ison, J.R., D.W. McAdam, and G.R. Hammond, *Latency and amplitude changes in the acoustic startle reflex of the rat produced by variation in auditory prestimulation.* Physiol Behav, 1973. **10**(6): p. 1035-9.
104. Mansbach, R.S. and M.A. Geyer, *Parametric determinants in pre-stimulus modification of acoustic startle: interaction with ketamine.* Psychopharmacology (Berl), 1991. **105**(2): p. 162-8.
105. Plappert, C.F., A.M. Rodenbucher, and P.K. Pilz, *Effects of sex and estrous cycle on modulation of the acoustic startle response in mice.* Physiol Behav, 2005. **84**(4): p. 585-94.
106. Charitidi, K., I. Meltser, and B. Canlon, *Estradiol treatment and hormonal fluctuations during the estrous cycle modulate the expression of estrogen receptors in the auditory system and the prepulse inhibition of acoustic startle response.* Endocrinology, 2012. **153**(9): p. 4412-21.
107. Kim, J.J. and M.W. Jung, *Neural circuits and mechanisms involved in Pavlovian fear conditioning: a critical review.* Neurosci Biobehav Rev, 2006. **30**(2): p. 188-202.
108. LeDoux, J.E., et al., *Disruption of auditory but not visual learning by destruction of intrinsic neurons in the rat medial geniculate body.* Brain Res, 1986. **371**(2): p. 395-9.
109. Medina, J.F., et al., *Parallels between cerebellum- and amygdala-dependent conditioning.* Nat Rev Neurosci, 2002. **3**(2): p. 122-31.
110. Sun, Y., H. Gooch, and P. Sah, *Fear conditioning and the basolateral amygdala.* F1000Res, 2020. **9**.
111. Malenka, R.C. and R.A. Nicoll, *Long-term potentiation--a decade of progress?* Science, 1999. **285**(5435): p. 1870-4.

112. Fanselow, M.S. and J.J. Kim, *Acquisition of contextual Pavlovian fear conditioning is blocked by application of an NMDA receptor antagonist D,L-2-amino-5-phosphonovaleric acid to the basolateral amygdala.* Behav Neurosci, 1994. **108**(1): p. 210-2.
113. Lee, H.J., et al., *Amygdalar nmda receptors are critical for the expression of multiple conditioned fear responses.* J Neurosci, 2001. **21**(11): p. 4116-24.
114. Stojic, J., H. Stohr, and B.H. Weber, *Three novel ABCC5 splice variants in human retina and their role as regulators of ABCC5 gene expression.* BMC Mol Biol, 2007. **8**: p. 42.
115. Steinpreis, R.E., *The behavioral and neurochemical effects of phencyclidine in humans and animals: some implications for modeling psychosis.* Behav Brain Res, 1996. **74**(1-2): p. 45-55.
116. Lazic, S.E., *Analytical strategies for the marble burying test: avoiding impossible predictions and invalid p-values.* BMC Res Notes, 2015. **8**: p. 141.
117. Wotjak, C.T., *Sound check, stage design and screen plot - how to increase the comparability of fear conditioning and fear extinction experiments.* Psychopharmacology (Berl), 2019. **236**(1): p. 33-48.
118. Carola, V., et al., *Evaluation of the elevated plus-maze and open-field tests for the assessment of anxiety-related behaviour in inbred mice.* Behav Brain Res, 2002. **134**(1-2): p. 49-57.
119. Deacon, R.M., *Digging and marble burying in mice: simple methods for in vivo identification of biological impacts.* Nat Protoc, 2006. **1**(1): p. 122-4.
120. Iscru, E., et al., *Sensorimotor enhancement in mouse mutants lacking the Purkinje cell-specific Gi/o modulator, Pcp2(L7).* Mol Cell Neurosci, 2009. **40**(1): p. 62-75.
121. Schrode, K.M., et al., *Central Compensation in Auditory Brainstem after Damaging Noise Exposure.* eNeuro, 2018. **5**(4).
122. Willott, J.F. and S. Carlson, *Modification of the acoustic startle response in hearing-impaired C57BL/6J mice: prepulse augmentation and prolongation of prepulse inhibition.* Behav Neurosci, 1995. **109**(3): p. 396-403.
123. Longenecker, R.J., et al., *Prepulse inhibition of the acoustic startle reflex vs. auditory brainstem response for hearing assessment.* Hear Res, 2016. **339**: p. 80-93.
124. Knight, R.T., D. Scabini, and D.L. Woods, *Prefrontal cortex gating of auditory transmission in humans.* Brain Res, 1989. **504**(2): p. 338-42.
125. Kantrowitz, J. and D.C. Javitt, *Glutamatergic transmission in schizophrenia: from basic research to clinical practice.* Curr Opin Psychiatry, 2012. **25**(2): p. 96-102.
126. Rowland, L.M., et al., *In vivo measurements of glutamate, GABA, and NAAG in schizophrenia.* Schizophr Bull, 2013. **39**(5): p. 1096-104.
127. Aleman, A., R.S. Kahn, and J.P. Selten, *Sex differences in the risk of schizophrenia: evidence from meta-analysis.* Arch Gen Psychiatry, 2003. **60**(6): p. 565-71.
128. Pilz, P.K., T.D. Carl, and C.F. Plappert, *Habituation of the acoustic and the tactile startle responses in mice: two independent sensory processes.* Behav Neurosci, 2004. **118**(5): p. 975-83.
129. Wehner, J.M. and R.A. Radcliffe, *Cued and contextual fear conditioning in mice.* Curr Protoc Neurosci, 2004. **Chapter 8**: p. Unit 8 5C.
130. Liu, I.Y., et al., *Brain-derived neurotrophic factor plays a critical role in contextual fear conditioning.* J Neurosci, 2004. **24**(36): p. 7958-63.
131. Phillips, R.G. and J.E. LeDoux, *Differential contribution of amygdala and hippocampus to cued and contextual fear conditioning.* Behav Neurosci, 1992. **106**(2): p. 274-85.
132. Huerta, P.T., et al., *Formation of temporal memory requires NMDA receptors within CA1 pyramidal neurons.* Neuron, 2000. **25**(2): p. 473-80.
133. Garthwaite, J., S.L. Charles, and R. Chess-Williams, *Endothelium-derived relaxing factor release on activation of NMDA receptors suggests role as intercellular messenger in the brain.* Nature, 1988. **336**(6197): p. 385-8.

134. Paul, C., et al., *Signaling through cGMP-dependent protein kinase I in the amygdala is critical for auditory-cued fear memory and long-term potentiation.* J Neurosci, 2008. **28**(52): p. 14202-12.
135. Farley, S.J., et al., *Reevaluating hippocampus-dependent learning in FVB/N mice.* Behav Neurosci, 2011. **125**(6): p. 871-8.
136. Eltokhi, A., B. Kurpiers, and C. Pitzer, *Behavioral tests assessing neuropsychiatric phenotypes in adolescent mice reveal strain- and sex-specific effects.* Sci Rep, 2020. **10**(1): p. 11263.
137. Sternini, C., L. Anselmi, and E. Rozengurt, *Enteroendocrine cells: a site of 'taste' in gastrointestinal chemosensing.* Curr Opin Endocrinol Diabetes Obes, 2008. **15**(1): p. 73-8.
138. Habib, A.M., et al., *Overlap of endocrine hormone expression in the mouse intestine revealed by transcriptional profiling and flow cytometry.* Endocrinology, 2012. **153**(7): p. 3054-65.
139. Gribble, F.M. and F. Reimann, *Enteroendocrine Cells: Chemosensors in the Intestinal Epithelium.* Annu Rev Physiol, 2016. **78**: p. 277-99.
140. Dockray, G.J., A. Varro, and R. Dimaline, *Gastric endocrine cells: gene expression, processing, and targeting of active products.* Physiol Rev, 1996. **76**(3): p. 767-98.
141. Lee, A.A. and C. Owyang, *Sugars, Sweet Taste Receptors, and Brain Responses.* Nutrients, 2017. **9**(7).
142. Engelstoft, M.S., et al., *Enteroendocrine cell types revisited.* Curr Opin Pharmacol, 2013. **13**(6): p. 912-21.
143. Gehart, H., et al., *Identification of Enteroendocrine Regulators by Real-Time Single-Cell Differentiation Mapping.* Cell, 2019. **176**(5): p. 1158-1173 e16.
144. Beumer, J., et al., *Enteroendocrine cells switch hormone expression along the crypt-to-villus BMP signalling gradient.* Nat Cell Biol, 2018. **20**(8): p. 909-916.
145. Eissele, R., et al., *Glucagon-like peptide-1 cells in the gastrointestinal tract and pancreas of rat, pig and man.* Eur J Clin Invest, 1992. **22**(4): p. 283-91.
146. Theodorakis, M.J., et al., *Human duodenal enteroendocrine cells: source of both incretin peptides, GLP-1 and GIP.* Am J Physiol Endocrinol Metab, 2006. **290**(3): p. E550-9.
147. Mortensen, K., et al., *GLP-1 and GIP are colocalized in a subset of endocrine cells in the small intestine.* Regul Pept, 2003. **114**(2-3): p. 189-96.
148. Roberts, G.P., et al., *Comparison of Human and Murine Enteroendocrine Cells by Transcriptomic and Peptidomic Profiling.* Diabetes, 2019. **68**(5): p. 1062-1072.
149. Habib, A.M., et al., *Co-localisation and secretion of glucagon-like peptide 1 and peptide YY from primary cultured human L cells.* Diabetologia, 2013. **56**(6): p. 1413-6.
150. Huang, W.K., et al., *Development of innovative tools for investigation of nutrient-gut interaction.* World J Gastroenterol, 2020. **26**(25): p. 3562-3576.
151. Goldspink, D.A., F. Reimann, and F.M. Gribble, *Models and Tools for Studying Enteroendocrine Cells.* Endocrinology, 2018. **159**(12): p. 3874-3884.
152. Psichas, A., et al., *Mixed Primary Cultures of Murine Small Intestine Intended for the Study of Gut Hormone Secretion and Live Cell Imaging of Enteroendocrine Cells.* J Vis Exp, 2017(122).
153. Goldspink, D.A., et al., *Labeling and Characterization of Human GLP-1-Secreting L-cells in Primary Ileal Organoid Culture.* Cell Rep, 2020. **31**(13): p. 107833.
154. Beumer, J., et al., *High-Resolution mRNA and Secretome Atlas of Human Enteroendocrine Cells.* Cell, 2020. **181**(6): p. 1291-1306 e19.
155. de Bruine, A.P., et al., *NCI-H716 cells as a model for endocrine differentiation in colorectal cancer.* Virchows Arch B Cell Pathol Incl Mol Pathol, 1992. **62**(5): p. 311-20.
156. Kuhre, R.E., et al., *Peptide production and secretion in GLUTag, NCI-H716, and STC-1 cells: a comparison to native L-cells.* J Mol Endocrinol, 2016. **56**(3): p. 201-11.
157. Drucker, D.J., *The biology of incretin hormones.* Cell Metab, 2006. **3**(3): p. 153-65.
158. Gray, S.M., et al., *Discordance between GLP-1R gene and protein expression in mouse pancreatic islet cells.* J Biol Chem, 2020. **295**(33): p. 11529-11541.

159. Nauck, M.A., et al., *Incretin effects of increasing glucose loads in man calculated from venous insulin and C-peptide responses.* J Clin Endocrinol Metab, 1986. **63**(2): p. 492-8.
160. Nauck, M., et al., *Reduced incretin effect in type 2 (non-insulin-dependent) diabetes.* Diabetologia, 1986. **29**(1): p. 46-52.
161. Muscelli, E., et al., *Separate impact of obesity and glucose tolerance on the incretin effect in normal subjects and type 2 diabetic patients.* Diabetes, 2008. **57**(5): p. 1340-8.
162. Knop, F.K., et al., *Impaired incretin effect and fasting hyperglucagonaemia characterizing type 2 diabetic subjects are early signs of dysmetabolism in obesity.* Diabetes Obes Metab, 2012. **14**(6): p. 500-10.
163. Nauck, M.A., et al., *Preserved incretin activity of glucagon-like peptide 1 [7-36 amide] but not of synthetic human gastric inhibitory polypeptide in patients with type-2 diabetes mellitus.* J Clin Invest, 1993. **91**(1): p. 301-7.
164. Vilsboll, T., et al., *Defective amplification of the late phase insulin response to glucose by GIP in obese Type II diabetic patients.* Diabetologia, 2002. **45**(8): p. 1111-9.
165. Wettergren, A., et al., *Truncated GLP-1 (proglucagon 78-107-amide) inhibits gastric and pancreatic functions in man.* Dig Dis Sci, 1993. **38**(4): p. 665-73.
166. Nauck, M.A., et al., *Glucagon-like peptide 1 inhibition of gastric emptying outweighs its insulinotropic effects in healthy humans.* Am J Physiol, 1997. **273**(5): p. E981-8.
167. Knop, F.K., et al., *Inappropriate suppression of glucagon during OGTT but not during isoglycaemic i.v. glucose infusion contributes to the reduced incretin effect in type 2 diabetes mellitus.* Diabetologia, 2007. **50**(4): p. 797-805.
168. Lundgren, J.R., et al., *Healthy Weight Loss Maintenance with Exercise, Liraglutide, or Both Combined.* N Engl J Med, 2021. **384**(18): p. 1719-1730.
169. Wilding, J.P.H., et al., *Once-Weekly Semaglutide in Adults with Overweight or Obesity.* N Engl J Med, 2021. **384**(11): p. 989-1002.
170. Chao, A.M., et al., *Semaglutide for the treatment of obesity.* Trends Cardiovasc Med, 2021.
171. Orskov, C., et al., *Tissue and plasma concentrations of amidated and glycine-extended glucagon-like peptide I in humans.* Diabetes, 1994. **43**(4): p. 535-9.
172. Deacon, C.F., et al., *Dipeptidyl peptidase IV resistant analogues of glucagon-like peptide-1 which have extended metabolic stability and improved biological activity.* Diabetologia, 1998. **41**(3): p. 271-8.
173. Deacon, C.F., *What do we know about the secretion and degradation of incretin hormones?* Regul Pept, 2005. **128**(2): p. 117-24.
174. Gupta, V. and S. Kalra, *Choosing a gliptin.* Indian J Endocrinol Metab, 2011. **15**(4): p. 298-308.
175. Nauck, M.A. and J.J. Meier, *The incretin effect in healthy individuals and those with type 2 diabetes: physiology, pathophysiology, and response to therapeutic interventions.* Lancet Diabetes Endocrinol, 2016. **4**(6): p. 525-36.
176. Vilsboll, T., et al., *Similar elimination rates of glucagon-like peptide-1 in obese type 2 diabetic patients and healthy subjects.* J Clin Endocrinol Metab, 2003. **88**(1): p. 220-4.
177. Kjems, L.L., et al., *The influence of GLP-1 on glucose-stimulated insulin secretion: effects on beta-cell sensitivity in type 2 and nondiabetic subjects.* Diabetes, 2003. **52**(2): p. 380-6.
178. Nauck, M.A., et al., *Normalization of fasting hyperglycaemia by exogenous glucagon-like peptide 1 (7-36 amide) in type 2 (non-insulin-dependent) diabetic patients.* Diabetologia, 1993. **36**(8): p. 741-4.
179. Liddle, R.A., *Interactions of Gut Endocrine Cells with Epithelium and Neurons.* Compr Physiol, 2018. **8**(3): p. 1019-1030.
180. Pais, R., F.M. Gribble, and F. Reimann, *Stimulation of incretin secreting cells.* Ther Adv Endocrinol Metab, 2016. **7**(1): p. 24-42.
181. Hjorne, A.P., I.M. Modvig, and J.J. Holst, *The Sensory Mechanisms of Nutrient-Induced GLP-1 Secretion.* Metabolites, 2022. **12**(5).

182. Gribble, F.M. and F. Reimann, *Signalling in the gut endocrine axis.* Physiol Behav, 2017. **176**: p. 183-188.
183. Bohorquez, D.V., et al., *Neuroepithelial circuit formed by innervation of sensory enteroendocrine cells.* J Clin Invest, 2015. **125**(2): p. 782-6.
184. Pan, X., S. Tao, and N. Tong, *Potential Therapeutic Targeting Neurotransmitter Receptors in Diabetes.* Front Endocrinol (Lausanne), 2022. **13**: p. 884549.
185. Bagger, J.I., et al., *Impaired regulation of the incretin effect in patients with type 2 diabetes.* J Clin Endocrinol Metab, 2011. **96**(3): p. 737-45.
186. Ashcroft, F.M., D.E. Harrison, and S.J. Ashcroft, *Glucose induces closure of single potassium channels in isolated rat pancreatic beta-cells.* Nature, 1984. **312**(5993): p. 446-8.
187. Gribble, F.M., et al., *A novel glucose-sensing mechanism contributing to glucagon-like peptide-1 secretion from the GLUTag cell line.* Diabetes, 2003. **52**(5): p. 1147-54.
188. Reimann, F. and F.M. Gribble, *Glucose-sensing in glucagon-like peptide-1-secreting cells.* Diabetes, 2002. **51**(9): p. 2757-63.
189. Reimann, F., et al., *Glucose sensing in L cells: a primary cell study.* Cell Metab, 2008. **8**(6): p. 532-9.
190. Sun, E.W., et al., *Mechanisms Controlling Glucose-Induced GLP-1 Secretion in Human Small Intestine.* Diabetes, 2017. **66**(8): p. 2144-2149.
191. Henquin, J.C., *Tolbutamide stimulation and inhibition of insulin release: studies of the underlying ionic mechanisms in isolated rat islets.* Diabetologia, 1980. **18**(2): p. 151-60.
192. Kuhre, R.E., et al., *Molecular mechanisms of glucose-stimulated GLP-1 secretion from perfused rat small intestine.* Diabetes, 2015. **64**(2): p. 370-82.
193. Stephens, J.W., et al., *Effects of short-term therapy with glibenclamide and repaglinide on incretin hormones and oxidative damage associated with postprandial hyperglycaemia in people with type 2 diabetes mellitus.* Diabetes Res Clin Pract, 2011. **94**(2): p. 199-206.
194. Guillam, M.T., et al., *Early diabetes and abnormal postnatal pancreatic islet development in mice lacking Glut-2.* Nat Genet, 1997. **17**(3): p. 327-30.
195. Cani, P.D., et al., *GLUT2 and the incretin receptors are involved in glucose-induced incretin secretion.* Mol Cell Endocrinol, 2007. **276**(1-2): p. 18-23.
196. Parker, H.E., et al., *Predominant role of active versus facilitative glucose transport for glucagon-like peptide-1 secretion.* Diabetologia, 2012. **55**(9): p. 2445-55.
197. Mace, O.J., M. Schindler, and S. Patel, *The regulation of K- and L-cell activity by GLUT2 and the calcium-sensing receptor CasR in rat small intestine.* J Physiol, 2012. **590**(12): p. 2917-36.
198. Gribble, F.M., *An absorbing sense of sweetness.* Diabetes, 2015. **64**(2): p. 338-40.
199. Reimann, F., G. Tolhurst, and F.M. Gribble, *G-protein-coupled receptors in intestinal chemosensation.* Cell Metab, 2012. **15**(4): p. 421-31.
200. Rao, M. and M.D. Gershon, *The bowel and beyond: the enteric nervous system in neurological disorders.* Nat Rev Gastroenterol Hepatol, 2016. **13**(9): p. 517-28.
201. Hansen, L., et al., *Neural regulation of glucagon-like peptide-1 secretion in pigs.* Am J Physiol Endocrinol Metab, 2004. **287**(5): p. E939-47.
202. Anini, Y. and P.L. Brubaker, *Muscarinic receptors control glucagon-like peptide 1 secretion by human endocrine L cells.* Endocrinology, 2003. **144**(7): p. 3244-50.
203. Anini, Y., T. Hansotia, and P.L. Brubaker, *Muscarinic receptors control postprandial release of glucagon-like peptide-1: in vivo and in vitro studies in rats.* Endocrinology, 2002. **143**(6): p. 2420-6.
204. Wang, D., et al., *alpha7 Nicotinic Acetylcholine Receptor Regulates the Function and Viability of L Cells.* Endocrinology, 2018. **159**(9): p. 3132-3142.
205. Zhou, Y. and N.C. Danbolt, *Glutamate as a neurotransmitter in the healthy brain.* J Neural Transm (Vienna), 2014. **121**(8): p. 799-817.
206. Tome, D., *The Roles of Dietary Glutamate in the Intestine.* Ann Nutr Metab, 2018. **73 Suppl 5**: p. 15-20.

207. Reimann, F., et al., *Glutamine potently stimulates glucagon-like peptide-1 secretion from GLUTag cells.* Diabetologia, 2004. **47**(9): p. 1592-601.
208. Modvig, I.M., et al., *Amino acids differ in their capacity to stimulate GLP-1 release from the perfused rat small intestine and stimulate secretion by different sensing mechanisms.* Am J Physiol Endocrinol Metab, 2021. **320**(5): p. E874-E885.
209. Tolhurst, G., et al., *Glutamine triggers and potentiates glucagon-like peptide-1 secretion by raising cytosolic Ca2+ and cAMP.* Endocrinology, 2011. **152**(2): p. 405-13.
210. Andersson, L.E., et al., *Glutamine-Elicited Secretion of Glucagon-Like Peptide 1 Is Governed by an Activated Glutamate Dehydrogenase.* Diabetes, 2018. **67**(3): p. 372-384.
211. Rogers, G.J., et al., *Electrical activity-triggered glucagon-like peptide-1 secretion from primary murine L-cells.* J Physiol, 2011. **589**(Pt 5): p. 1081-93.
212. Uehara, S., et al., *Vesicular storage and secretion of L-glutamate from glucagon-like peptide 1-secreting clonal intestinal L cells.* J Neurochem, 2006. **96**(2): p. 550-60.
213. Vyklicky, V., et al., *Structure, function, and pharmacology of NMDA receptor channels.* Physiol Res, 2014. **63**(Suppl 1): p. S191-203.
214. Hansen, K.B., et al., *Structure, Function, and Pharmacology of Glutamate Receptor Ion Channels.* Pharmacol Rev, 2021. **73**(4): p. 298-487.
215. Smothers, C.T. and J.J. Woodward, *Expression of glycine-activated diheteromeric NR1/NR3 receptors in human embryonic kidney 293 cells Is NR1 splice variant-dependent.* J Pharmacol Exp Ther, 2009. **331**(3): p. 975-84.
216. Grand, T., et al., *Unmasking GluN1/GluN3A excitatory glycine NMDA receptors.* Nat Commun, 2018. **9**(1): p. 4769.
217. Tovar, K.R. and G.L. Westbrook, *The incorporation of NMDA receptors with a distinct subunit composition at nascent hippocampal synapses in vitro.* J Neurosci, 1999. **19**(10): p. 4180-8.
218. Dumas, T.C., *Developmental regulation of cognitive abilities: modified composition of a molecular switch turns on associative learning.* Prog Neurobiol, 2005. **76**(3): p. 189-211.
219. Monyer, H., et al., *Developmental and regional expression in the rat brain and functional properties of four NMDA receptors.* Neuron, 1994. **12**(3): p. 529-40.
220. Paoletti, P., C. Bellone, and Q. Zhou, *NMDA receptor subunit diversity: impact on receptor properties, synaptic plasticity and disease.* Nat Rev Neurosci, 2013. **14**(6): p. 383-400.
221. Crawley, O., M.J. Conde-Dusman, and I. Perez-Otano, *GluN3A NMDA receptor subunits: more enigmatic than ever?* J Physiol, 2022. **600**(2): p. 261-276.
222. Chatterton, J.E., et al., *Excitatory glycine receptors containing the NR3 family of NMDA receptor subunits.* Nature, 2002. **415**(6873): p. 793-8.
223. Gribkova, E.D. and R. Gillette, *Role of NMDAR plasticity in a computational model of synaptic memory.* Sci Rep, 2021. **11**(1): p. 21182.
224. Luscher, C. and R.C. Malenka, *NMDA receptor-dependent long-term potentiation and long-term depression (LTP/LTD).* Cold Spring Harb Perspect Biol, 2012. **4**(6).
225. Pfisterer, U. and K. Khodosevich, *Neuronal survival in the brain: neuron type-specific mechanisms.* Cell Death Dis, 2017. **8**(3): p. e2643.
226. Seillier, C., et al., *Targeting NMDA Receptors at the Neurovascular Unit: Past and Future Treatments for Central Nervous System Diseases.* Int J Mol Sci, 2022. **23**(18).
227. Zhou, Q. and M. Sheng, *NMDA receptors in nervous system diseases.* Neuropharmacology, 2013. **74**: p. 69-75.
228. Welters, A., et al., *Need for Better Diabetes Treatment: The Therapeutic Potential of NMDA Receptor Antagonists.* Klin Padiatr, 2017. **229**(1): p. 14-20.
229. Bozic, M. and J.M. Valdivielso, *The potential of targeting NMDA receptors outside the CNS.* Expert Opin Ther Targets, 2015. **19**(3): p. 399-413.
230. Rivera-Villasenor, A., et al., *NMDA Receptor Hypofunction in the Aging-Associated Malfunction of Peripheral Tissue.* Front Physiol, 2021. **12**: p. 687121.

231. Golovynska, I., et al., *Peripheral N-methyl-D-aspartate receptor localization and role in gastric acid secretion regulation: immunofluorescence and pharmacological studies.* Sci Rep, 2018. **8**(1): p. 7445.
232. Parisi, E., et al., *N-methyl-D-aspartate receptors are expressed in rat parathyroid gland and regulate PTH secretion.* Am J Physiol Renal Physiol, 2009. **296**(6): p. F1291-6.
233. Marquard, J., et al., *Characterization of pancreatic NMDA receptors as possible drug targets for diabetes treatment.* Nat Med, 2015. **21**(4): p. 363-72.
234. Marquard, J., et al., *Effects of dextromethorphan as add-on to sitagliptin on blood glucose and serum insulin concentrations in individuals with type 2 diabetes mellitus: a randomized, placebo-controlled, double-blinded, multiple crossover, single-dose clinical trial.* Diabetes Obes Metab, 2016. **18**(1): p. 100-3.
235. Gresch, A. and M. Dufer, *Dextromethorphan and Dextrorphan Influence Insulin Secretion by Interacting with KATP and L-type Ca(2+) Channels in Pancreatic beta-Cells.* J Pharmacol Exp Ther, 2020. **375**(1): p. 10-20.
236. Hirayama, M. and M. Kuriyama, *MK-801 is cytotoxic to microglia in vitro and its cytotoxicity is attenuated by glutamate, other excitotoxic agents and atropine. Possible presence of glutamate receptor and muscarinic receptor on microglia.* Brain Res, 2001. **897**(1-2): p. 204-6.
237. Patneau, D.K. and M.L. Mayer, *Structure-activity relationships for amino acid transmitter candidates acting at N-methyl-D-aspartate and quisqualate receptors.* J Neurosci, 1990. **10**(7): p. 2385-99.
238. Gameiro, A., et al., *The neurotransmitters glycine and GABA stimulate glucagon-like peptide-1 release from the GLUTag cell line.* J Physiol, 2005. **569**(Pt 3): p. 761-72.
239. Brubaker, P.L., J. Schloos, and D.J. Drucker, *Regulation of glucagon-like peptide-1 synthesis and secretion in the GLUTag enteroendocrine cell line.* Endocrinology, 1998. **139**(10): p. 4108-14.
240. Muller, T.D., et al., *Glucagon-like peptide 1 (GLP-1).* Mol Metab, 2019. **30**: p. 72-130.
241. Amador, M. and J.A. Dani, *MK-801 inhibition of nicotinic acetylcholine receptor channels.* Synapse, 1991. **7**(3): p. 207-15.
242. Briggs, C.A. and D.G. McKenna, *Effect of MK-801 at the human alpha 7 nicotinic acetylcholine receptor.* Neuropharmacology, 1996. **35**(4): p. 407-14.
243. Wang, C.C., et al., *Profiling transcriptomes of human SH-SY5Y neuroblastoma cells exposed to maleic acid.* PeerJ, 2017. **5**: p. e3175.
244. Huettner, J.E. and B.P. Bean, *Block of N-methyl-D-aspartate-activated current by the anticonvulsant MK-801: selective binding to open channels.* Proc Natl Acad Sci U S A, 1988. **85**(4): p. 1307-11.
245. Foster, A.C. and E.H. Wong, *The novel anticonvulsant MK-801 binds to the activated state of the N-methyl-D-aspartate receptor in rat brain.* Br J Pharmacol, 1987. **91**(2): p. 403-9.
246. Reynolds, I.J. and R.J. Miller, *Multiple sites for the regulation of the N-methyl-D-aspartate receptor.* Mol Pharmacol, 1988. **33**(6): p. 581-4.
247. Lodge, D. and K.M. Johnson, *Noncompetitive excitatory amino acid receptor antagonists.* Trends Pharmacol Sci, 1990. **11**(2): p. 81-6.
248. Williams, K., *Extracellular Modulation of NMDA Receptors*, in *Biology of the NMDA Receptor*, A.M. Van Dongen, Editor. 2009: Boca Raton (FL).
249. Ransom, R.W. and N.L. Stec, *Cooperative modulation of [3H]MK-801 binding to the N-methyl-D-aspartate receptor-ion channel complex by L-glutamate, glycine, and polyamines.* J Neurochem, 1988. **51**(3): p. 830-6.
250. Costa, B.M., et al., *N-methyl-D-aspartate (NMDA) receptor NR2 subunit selectivity of a series of novel piperazine-2,3-dicarboxylate derivatives: preferential blockade of extrasynaptic NMDA receptors in the rat hippocampal CA3-CA1 synapse.* J Pharmacol Exp Ther, 2009. **331**(2): p. 618-26.

251. Morley, R.M., et al., *Synthesis and pharmacology of N1-substituted piperazine-2,3-dicarboxylic acid derivatives acting as NMDA receptor antagonists.* J Med Chem, 2005. **48**(7): p. 2627-37.
252. Rajani, V., A.S. Sengar, and M.W. Salter, *Tripartite signalling by NMDA receptors.* Mol Brain, 2020. **13**(1): p. 23.
253. Park, D.K., I.S. Stein, and K. Zito, *Ion flux-independent NMDA receptor signaling.* Neuropharmacology, 2022. **210**: p. 109019.
254. Nong, Y., et al., *Glycine binding primes NMDA receptor internalization.* Nature, 2003. **422**(6929): p. 302-7.
255. Li, H., et al., *Alternative splicing of GluN1 gates glycine site-dependent nonionotropic signaling by NMDAR receptors.* Proc Natl Acad Sci U S A, 2021. **118**(27).
256. Cummings, D.E. and J. Overduin, *Gastrointestinal regulation of food intake.* J Clin Invest, 2007. **117**(1): p. 13-23.
257. Murthy, S.N., et al., *Neurohormonal regulation of secretin secretion in canine duodenal mucosa in vitro.* Peptides, 1986. **7 Suppl 1**: p. 229-36.
258. Miedzybrodzka, E.L., et al., *Stimulation of motilin secretion by bile, free fatty acids, and acidification in human duodenal organoids.* Mol Metab, 2021. **54**: p. 101356.
259. Koziolek, M., et al., *Investigation of pH and Temperature Profiles in the GI Tract of Fasted Human Subjects Using the Intellicap((R)) System.* J Pharm Sci, 2015. **104**(9): p. 2855-63.
260. Zarate, N., et al., *Accurate localization of a fall in pH within the ileocecal region: validation using a dual-scintigraphic technique.* Am J Physiol Gastrointest Liver Physiol, 2010. **299**(6): p. G1276-86.
261. Maurer, J.M., et al., *Gastrointestinal pH and Transit Time Profiling in Healthy Volunteers Using the IntelliCap System Confirms Ileo-Colonic Release of ColoPulse Tablets.* PLoS One, 2015. **10**(7): p. e0129076.
262. Koziolek, M., et al., *Intragastric pH and pressure profiles after intake of the high-caloric, high-fat meal as used for food effect studies.* J Control Release, 2015. **220**(Pt A): p. 71-78.
263. McDougall, C.J., et al., *Colonic mucosal pH in humans.* Dig Dis Sci, 1993. **38**(3): p. 542-5.
264. Nugent, S.G., et al., *Intestinal luminal pH in inflammatory bowel disease: possible determinants and implications for therapy with aminosalicylates and other drugs.* Gut, 2001. **48**(4): p. 571-7.
265. Johansson, M.E., H. Sjovall, and G.C. Hansson, *The gastrointestinal mucus system in health and disease.* Nat Rev Gastroenterol Hepatol, 2013. **10**(6): p. 352-61.
266. McNeil, N.I., K.L. Ling, and J. Wager, *Mucosal surface pH of the large intestine of the rat and of normal and inflamed large intestine in man.* Gut, 1987. **28**(6): p. 707-13.
267. Khutoryanskiy, V.V., *Supramolecular materials: Longer and safer gastric residence.* Nat Mater, 2015. **14**(10): p. 963-4.
268. Newmark, H.L. and J.R. Lupton, *Determinants and consequences of colonic luminal pH: implications for colon cancer.* Nutr Cancer, 1990. **14**(3-4): p. 161-73.
269. Youngberg, C.A., et al., *Comparison of gastrointestinal pH in cystic fibrosis and healthy subjects.* Dig Dis Sci, 1987. **32**(5): p. 472-80.
270. Hillman, M., et al., *Reduced levels of active GLP-1 in patients with cystic fibrosis with and without diabetes mellitus.* J Cyst Fibros, 2012. **11**(2): p. 144-9.
271. Gelfond, D., et al., *Impact of CFTR Modulation on Intestinal pH, Motility, and Clinical Outcomes in Patients With Cystic Fibrosis and the G551D Mutation.* Clin Transl Gastroenterol, 2017. **8**(3): p. e81.
272. Gribble, F.M., C.L. Meek, and F. Reimann, *Targeted intestinal delivery of incretin secretagogues-towards new diabetes and obesity therapies.* Peptides, 2018. **100**: p. 68-74.
273. Larraufie, P., et al., *Important Role of the GLP-1 Axis for Glucose Homeostasis after Bariatric Surgery.* Cell Rep, 2019. **26**(6): p. 1399-1408 e6.
274. Smith, A., B. Henriksen, and A. Cohen, *Pharmacokinetic considerations in Roux-en-Y gastric bypass patients.* Am J Health Syst Pharm, 2011. **68**(23): p. 2241-7.

275. Ladebo, L., et al., *Gastrointestinal pH, Motility Patterns, and Transit Times After Roux-en-Y Gastric Bypass.* Obes Surg, 2021. **31**(6): p. 2632-2640.
276. Baekdal, T.A., et al., *Effect of Various Dosing Conditions on the Pharmacokinetics of Oral Semaglutide, a Human Glucagon-Like Peptide-1 Analogue in a Tablet Formulation.* Diabetes Ther, 2021. **12**(7): p. 1915-1927.
277. Smith, J.S. and C.S. Pace, *Modification of glucose-induced insulin release by alteration of pH.* Diabetes, 1983. **32**(1): p. 61-6.
278. Ohta, M., et al., *Relationships between energy level and insulin secretion in isolated rat islets of Langerhans. A study at various pH values.* Biochem Pharmacol, 1991. **42**(3): p. 593-8.
279. Hutton, J.C., et al., *The stimulus-secretion coupling of glucose-induced insulin release. XLII. Effects of extracellular pH on insulin release: their dependency on nutrient concentration.* Horm Metab Res, 1980. **12**(7): p. 294-9.
280. Rebolledo, O.R. and J.J. Gagliardino, *Glucagon and insulin secretion during acid-base alterations.* Acta Diabetol Lat, 1983. **20**(3): p. 211-20.
281. Proks, P., M. Takano, and F.M. Ashcroft, *Effects of intracellular pH on ATP-sensitive K+ channels in mouse pancreatic beta-cells.* J Physiol, 1994. **475**(1): p. 33-44.
282. Malaisse, W.J., A. Herchuelz, and A. Sener, *The possible significance of intracellular pH in insulin release.* Life Sci, 1980. **26**(17): p. 1367-71.
283. Juntti-Berggren, L., et al., *Intracellular pH and the stimulus-secretion coupling in insulin-producing RINm5F cells.* Biochem J, 1992. **287 (Pt 1)**(Pt 1): p. 59-66.
284. Gunawardana, S.C., et al., *Nutrient-stimulated insulin secretion in mouse islets is critically dependent on intracellular pH.* BMC Endocr Disord, 2004. **4**(1): p. 1.
285. Deisl, C., G. Albano, and D.G. Fuster, *Role of Na/H exchange in insulin secretion by islet cells.* Curr Opin Nephrol Hypertens, 2014. **23**(4): p. 406-10.
286. Juntti-Berggren, L., et al., *Glucose-induced increase in cytoplasmic pH in pancreatic beta-cells is mediated by Na+/H+ exchange, an effect not dependent on protein kinase C.* J Biol Chem, 1991. **266**(35): p. 23537-41.
287. Omar-Hmeadi, M. and O. Idevall-Hagren, *Insulin granule biogenesis and exocytosis.* Cell Mol Life Sci, 2021. **78**(5): p. 1957-1970.
288. Barg, S., et al., *Priming of insulin granules for exocytosis by granular Cl(-) uptake and acidification.* J Cell Sci, 2001. **114**(Pt 11): p. 2145-54.
289. Simpson, A.K., et al., *Cyclic AMP triggers glucagon-like peptide-1 secretion from the GLUTag enteroendocrine cell line.* Diabetologia, 2007. **50**(10): p. 2181-9.
290. Varndell, I.M., et al., *Localization of glucagon-like peptide (GLP) immunoreactants in human gut and pancreas using light and electron microscopic immunocytochemistry.* J Histochem Cytochem, 1985. **33**(10): p. 1080-6.
291. Wheeler, S.E., et al., *The SNARE Protein Syntaxin-1a Plays an Essential Role in Biphasic Exocytosis of the Incretin Hormone Glucagon-Like Peptide 1.* Diabetes, 2017. **66**(9): p. 2327-2338.
292. Takahashi, N., et al., *Sequential exocytosis of insulin granules is associated with redistribution of SNAP25.* J Cell Biol, 2004. **165**(2): p. 255-62.
293. Li, S.K., et al., *Role of vesicle-associated membrane protein 2 in exocytosis of glucagon-like peptide-1 from the murine intestinal L cell.* Diabetologia, 2014. **57**(4): p. 809-18.
294. Gustavsson, N., et al., *Synaptotagmin-7 as a positive regulator of glucose-induced glucagon-like peptide-1 secretion in mice.* Diabetologia, 2011. **54**(7): p. 1824-30.
295. Michl, J., K.C. Park, and P. Swietach, *Evidence-based guidelines for controlling pH in mammalian live-cell culture systems.* Commun Biol, 2019. **2**: p. 144.
296. Orlowski, J. and S. Grinstein, *Diversity of the mammalian sodium/proton exchanger SLC9 gene family.* Pflugers Arch, 2004. **447**(5): p. 549-65.
297. Alper, S.L. and A.K. Sharma, *The SLC26 gene family of anion transporters and channels.* Mol Aspects Med, 2013. **34**(2-3): p. 494-515.

298. Boron, W.F., *Regulation of intracellular pH.* Adv Physiol Educ, 2004. **28**(1-4): p. 160-79.
299. Thomas, R.C., *Cell growth factors. Bicarbonate and pHi response.* Nature, 1989. **337**(6208): p. 601.
300. Swietach, P., *What is pH regulation, and why do cancer cells need it?* Cancer Metastasis Rev, 2019. **38**(1-2): p. 5-15.
301. Thomas, R.C. and R.W. Meech, *Hydrogen ion currents and intracellular pH in depolarized voltage-clamped snail neurones.* Nature, 1982. **299**(5886): p. 826-8.
302. Pang, H., J. Li, and S.J. Li, *Role of the voltage-gated proton channel Hv1 in insulin secretion, glucose homeostasis, and obesity.* J Physiol Biochem, 2022. **78**(3): p. 593-601.
303. Paroutis, P., N. Touret, and S. Grinstein, *The pH of the secretory pathway: measurement, determinants, and regulation.* Physiology (Bethesda), 2004. **19**: p. 207-15.
304. Poea-Guyon, S., et al., *The V-ATPase membrane domain is a sensor of granular pH that controls the exocytotic machinery.* J Cell Biol, 2013. **203**(2): p. 283-98.
305. Tucker, J.D., S. Dhanvantari, and P.L. Brubaker, *Proglucagon processing in islet and intestinal cell lines.* Regul Pept, 1996. **62**(1): p. 29-35.
306. Ramzy, A., A. Asadi, and T.J. Kieffer, *Revisiting Proinsulin Processing: Evidence That Human beta-Cells Process Proinsulin With Prohormone Convertase (PC) 1/3 but Not PC2.* Diabetes, 2020. **69**(7): p. 1451-1462.
307. Duhamel, M., et al., *The proprotein convertase PC1/3 regulates TLR9 trafficking and the associated signaling pathways.* Sci Rep, 2016. **6**: p. 19360.
308. Dikeakos, J.D., et al., *PC1/3, PC2 and PC5/6A are targeted to dense core secretory granules by a common mechanism.* FEBS J, 2007. **274**(16): p. 4094-102.
309. Dillon, S.L., et al., *Propeptides are sufficient to regulate organelle-specific pH-dependent activation of furin and proprotein convertase 1/3.* J Mol Biol, 2012. **423**(1): p. 47-62.
310. Zhou, Y. and I. Lindberg, *Enzymatic properties of carboxyl-terminally truncated prohormone convertase 1 (PC1/SPC3) and evidence for autocatalytic conversion.* J Biol Chem, 1994. **269**(28): p. 18408-13.
311. Rufaut, N.W., et al., *Purification and characterization of the candidate prohormone-processing enzyme SPC3 produced in a mouse L cell line.* J Biol Chem, 1993. **268**(27): p. 20291-8.
312. Boudreault, A., et al., *Molecular characterization, enzymatic analysis, and purification of murine proprotein convertase-1/3 (PC1/PC3) secreted from recombinant baculovirus-infected insect cells.* Protein Expr Purif, 1998. **14**(3): p. 353-66.
313. Zhou, Y. and I. Lindberg, *Purification and characterization of the prohormone convertase PC1(PC3).* J Biol Chem, 1993. **268**(8): p. 5615-23.
314. Sehlin, J., *Interrelationship between chloride fluxes in pancreatic islets and insulin release.* Am J Physiol, 1978. **235**(5): p. E501-8.
315. Somers, G., et al., *The stimulus-secretion coupling of glucose-induced insulin release. XLV. The anion-osmotic hypothesis for exocytosis.* Pflugers Arch, 1980. **388**(3): p. 249-53.
316. Li, D.Q., et al., *Suppression of sulfonylurea- and glucose-induced insulin secretion in vitro and in vivo in mice lacking the chloride transport protein ClC-3.* Cell Metab, 2009. **10**(4): p. 309-15.
317. Deriy, L.V., et al., *The granular chloride channel ClC-3 is permissive for insulin secretion.* Cell Metab, 2009. **10**(4): p. 316-23.
318. Jentsch, T.J., et al., *ClC-3--a granular anion transporter involved in insulin secretion?* Cell Metab, 2010. **12**(4): p. 307-308.
319. Maritzen, T., et al., *Role of the vesicular chloride transporter ClC-3 in neuroendocrine tissue.* J Neurosci, 2008. **28**(42): p. 10587-98.
320. Kinard, T.A. and L.S. Satin, *An ATP-sensitive Cl- channel current that is activated by cell swelling, cAMP, and glyburide in insulin-secreting cells.* Diabetes, 1995. **44**(12): p. 1461-6.
321. Best, L., H.E. Miley, and A.P. Yates, *Activation of an anion conductance and beta-cell depolarization during hypotonically induced insulin release.* Exp Physiol, 1996. **81**(6): p. 927-33.

322. Kang, C., et al., *SWELL1 is a glucose sensor regulating beta-cell excitability and systemic glycaemia.* Nat Commun, 2018. **9**(1): p. 367.
323. Gorboulev, V., et al., *Na(+)-D-glucose cotransporter SGLT1 is pivotal for intestinal glucose absorption and glucose-dependent incretin secretion.* Diabetes, 2012. **61**(1): p. 187-96.
324. Reimann, F., et al., *Characterization and functional role of voltage gated cation conductances in the glucagon-like peptide-1 secreting GLUTag cell line.* J Physiol, 2005. **563**(Pt 1): p. 161-75.
325. Diez-Sampedro, A., et al., *Glycoside binding and translocation in Na(+)-dependent glucose cotransporters: comparison of SGLT1 and SGLT3.* J Membr Biol, 2000. **176**(2): p. 111-7.
326. Hirayama, B.A., D.D. Loo, and E.M. Wright, *Protons drive sugar transport through the Na+/glucose cotransporter (SGLT1).* J Biol Chem, 1994. **269**(34): p. 21407-10.
327. Holst, J.J. and N.J. Wewer Albrechtsen, *Methods and Guidelines for Measurement of Glucagon in Plasma.* Int J Mol Sci, 2019. **20**(21).
328. Nishi, T. and M. Forgac, *The vacuolar (H+)-ATPases--nature's most versatile proton pumps.* Nat Rev Mol Cell Biol, 2002. **3**(2): p. 94-103.
329. Breton, S. and D. Brown, *Regulation of luminal acidification by the V-ATPase.* Physiology (Bethesda), 2013. **28**(5): p. 318-29.
330. Wang, R., et al., *Molecular basis of V-ATPase inhibition by bafilomycin A1.* Nat Commun, 2021. **12**(1): p. 1782.
331. Bowman, E.J., A. Siebers, and K. Altendorf, *Bafilomycins: a class of inhibitors of membrane ATPases from microorganisms, animal cells, and plant cells.* Proc Natl Acad Sci U S A, 1988. **85**(21): p. 7972-6.
332. Adam, J., et al., *Fumarate Hydratase Deletion in Pancreatic beta Cells Leads to Progressive Diabetes.* Cell Rep, 2017. **20**(13): p. 3135-3148.
333. Wongdee, K., et al., *Factors inhibiting intestinal calcium absorption: hormones and luminal factors that prevent excessive calcium uptake.* J Physiol Sci, 2019. **69**(5): p. 683-696.
334. Pentafragka, C., et al., *The impact of food intake on the luminal environment and performance of oral drug products with a view to in vitro and in silico simulations: a PEARRL review.* J Pharm Pharmacol, 2019. **71**(4): p. 557-580.
335. Mace, O.J., B. Tehan, and F. Marshall, *Pharmacology and physiology of gastrointestinal enteroendocrine cells.* Pharmacol Res Perspect, 2015. **3**(4): p. e00155.
336. Kellett, G.L., *Alternative perspective on intestinal calcium absorption: proposed complementary actions of Ca(v)1.3 and TRPV6.* Nutr Rev, 2011. **69**(7): p. 347-70.
337. Han, G.A., et al., *Munc18-1 domain-1 controls vesicle docking and secretion by interacting with syntaxin-1 and chaperoning it to the plasma membrane.* Mol Biol Cell, 2011. **22**(21): p. 4134-49.
338. Nausch, I., R. Mentlein, and E. Heymann, *The degradation of bioactive peptides and proteins by dipeptidyl peptidase IV from human placenta.* Biol Chem Hoppe Seyler, 1990. **371**(11): p. 1113-8.
339. Kuhre, R.E., et al., *GLP-1 amidation efficiency along the length of the intestine in mice, rats and pigs and in GLP-1 secreting cell lines.* Peptides, 2014. **55**: p. 52-7.
340. Milgram, S.L., R.E. Mains, and B.A. Eipper, *COOH-terminal signals mediate the trafficking of a peptide processing enzyme in endocrine cells.* J Cell Biol, 1993. **121**(1): p. 23-36.
341. Eipper, B.A., et al., *Peptidyl-alpha-hydroxyglycine alpha-amidating lyase. Purification, characterization, and expression.* J Biol Chem, 1991. **266**(12): p. 7827-33.
342. Hayashi, Y., et al., *Effects of bafilomycin A1, a vacuolar type H+ ATPase inhibitor, on the thermosensitivity of a human pancreatic cancer cell line.* Int J Hyperthermia, 2006. **22**(4): p. 275-85.
343. Zhdanov, A.V., R.I. Dmitriev, and D.B. Papkovsky, *Bafilomycin A1 activates respiration of neuronal cells via uncoupling associated with flickering depolarization of mitochondria.* Cell Mol Life Sci, 2011. **68**(5): p. 903-17.

344. Song, Q., et al., *The emerging roles of vacuolar-type ATPase-dependent Lysosomal acidification in neurodegenerative diseases.* Transl Neurodegener, 2020. **9**(1): p. 17.
345. Rhodes, C.J., et al., *Stimulation by ATP of proinsulin to insulin conversion in isolated rat pancreatic islet secretory granules. Association with the ATP-dependent proton pump.* J Biol Chem, 1987. **262**(22): p. 10712-7.
346. Yoshimori, T., et al., *Bafilomycin A1, a specific inhibitor of vacuolar-type H(+)-ATPase, inhibits acidification and protein degradation in lysosomes of cultured cells.* J Biol Chem, 1991. **266**(26): p. 17707-12.
347. Shao, E. and M. Forgac, *Involvement of the nonhomologous region of subunit A of the yeast V-ATPase in coupling and in vivo dissociation.* J Biol Chem, 2004. **279**(47): p. 48663-70.
348. Dechant, R., et al., *Cytosolic pH is a second messenger for glucose and regulates the PKA pathway through V-ATPase.* EMBO J, 2010. **29**(15): p. 2515-26.
349. Diakov, T.T. and P.M. Kane, *Regulation of vacuolar proton-translocating ATPase activity and assembly by extracellular pH.* J Biol Chem, 2010. **285**(31): p. 23771-8.
350. Bodzeta, A., M. Kahms, and J. Klingauf, *The Presynaptic v-ATPase Reversibly Disassembles and Thereby Modulates Exocytosis but Is Not Part of the Fusion Machinery.* Cell Rep, 2017. **20**(6): p. 1348-1359.
351. Rienecker, K.D.A., R.G. Poston, and R.N. Saha, *Merits and Limitations of Studying Neuronal Depolarization-Dependent Processes Using Elevated External Potassium.* ASN Neuro, 2020. **12**: p. 1759091420974807.
352. Friedlander, R.S., et al., *Role of phosphodiesterase and adenylate cyclase isozymes in murine colonic glucagon-like peptide 1 secreting cells.* Br J Pharmacol, 2011. **163**(2): p. 261-71.
353. Chen, X.H., I. Bezprozvanny, and R.W. Tsien, *Molecular basis of proton block of L-type Ca2+ channels.* J Gen Physiol, 1996. **108**(5): p. 363-74.
354. Saegusa, N., et al., *Influence of pH on Ca(2)(+) current and its control of electrical and Ca(2)(+) signaling in ventricular myocytes.* J Gen Physiol, 2011. **138**(5): p. 537-59.
355. Sabatini, P.V., T. Speckmann, and F.C. Lynn, *Friend and foe: beta-cell Ca(2+) signaling and the development of diabetes.* Mol Metab, 2019. **21**: p. 1-12.
356. Pace, C.S., J.T. Tarvin, and J.S. Smith, *Stimulus-secretion coupling in beta-cells: modulation by pH.* Am J Physiol, 1983. **244**(1): p. E3-18.
357. B. Ramos-Molina, I.L., J.R. Peinado, *Regulated Proteolysis of Signaling Molecules: The Proprotein Convertases*. Encyclopedia of Cell Biology. 2016: Academic Press.
358. Muller, L. and I. Lindberg, *The cell biology of the prohormone convertases PC1 and PC2.* Prog Nucleic Acid Res Mol Biol, 1999. **63**: p. 69-108.
359. Ryu, J.K., R. Jahn, and T.Y. Yoon, *Review: Progresses in understanding N-ethylmaleimide sensitive factor (NSF) mediated disassembly of SNARE complexes.* Biopolymers, 2016. **105**(8): p. 518-31.
360. Otter-Nilsson, M., et al., *Cytosolic ATPases, p97 and NSF, are sufficient to mediate rapid membrane fusion.* EMBO J, 1999. **18**(8): p. 2074-83.
361. Rituper, B., et al., *High-resolution membrane capacitance measurements for the study of exocytosis and endocytosis.* Nat Protoc, 2013. **8**(6): p. 1169-83.
362. Mei, Y.Y., D.C. Wu, and N. Zhou, *Astrocytic Regulation of Glutamate Transmission in Schizophrenia.* Front Psychiatry, 2018. **9**: p. 544.
363. *Mouse Brain Atlas*. Available from: https://mouse.brain-map.org/experiment/show/69236628.
364. Zhang, T., et al., *Generation of excitatory and inhibitory neurons from common progenitors via Notch signaling in the cerebellum.* Cell Rep, 2021. **35**(10): p. 109208.
365. Zhang, W., et al., *Suppression of Glutamate Carboxypeptidase II Ameliorates Neuronal Apoptosis from Ischemic Brain Injury.* J Stroke Cerebrovasc Dis, 2016. **25**(7): p. 1599-1605.

366. Olszewski, R.T., et al., *NAAG peptidase inhibition reduces locomotor activity and some stereotypes in the PCP model of schizophrenia via group II mGluR.* J Neurochem, 2004. **89**(4): p. 876-85.
367. Tammur, J., et al., *Two new genes from the human ATP-binding cassette transporter superfamily, ABCC11 and ABCC12, tandemly duplicated on chromosome 16q12.* Gene, 2001. **273**(1): p. 89-96.
368. Latorre, R., et al., *Enteroendocrine cells: a review of their role in brain-gut communication.* Neurogastroenterol Motil, 2016. **28**(5): p. 620-30.
369. Goldstein, N., et al., *Hypothalamic detection of macronutrients via multiple gut-brain pathways.* Cell Metab, 2021. **33**(3): p. 676-687 e5.
370. Suzuki, T., et al., *The apical localization of SGLT1 glucose transporter is determined by the short amino acid sequence in its N-terminal domain.* Eur J Cell Biol, 2001. **80**(12): p. 765-74.
371. Sato, T. and H. Clevers, *Growing self-organizing mini-guts from a single intestinal stem cell: mechanism and applications.* Science, 2013. **340**(6137): p. 1190-4.
372. Billing, L.J., et al., *Co-storage and release of insulin-like peptide-5, glucagon-like peptide-1 and peptideYY from murine and human colonic enteroendocrine cells.* Mol Metab, 2018. **16**: p. 65-75.